Studying the Fluorescence Emission Properties of 1,2,3 Triazine based Fluorophores in Polymer Thin Films.

Muhammad Zakarul Islam, MSc.

Thesis presented for the degree of PhD
of the National University of Ireland, Galway

Submitted September, 2016

School of Chemistry
National University of Ireland, Galway

Supervisor: Prof. Alan G Ryder

Abstract

The application of thin polymeric films for medical purposes is growing very fast. Two of the most important uses of thin polymer films are drug coatings for controlled release and tissue engineering. Thermoresponsive polymers are extensively used in this field [1-3]. These polymer thin films are complex in geometry and water uptake into thin films (during manufacturing or aging) may change their physicochemical properties limiting their application. One challenge for the use of soft thermoresponsive polymers as thin films in regulated medical devices and drug delivery systems is their accurate characterisation on surfaces. A non-contact, non-destructive, method is required for the *in situ* analysis of polymer thin films. Spectroscopic techniques, both vibrational (*i.e.* IR, Raman) and electronic excitation (UV-Visible, Fluorescence spectroscopy) have received much attention for the analysis of polymer thin films. Among them fluorescence spectroscopy has received considerable interest due to its high sensitivity and non-destructive nature [4]. The use of fluorescence spectroscopy as a potential tool for the rapid, *in situ*, and routine analysis of polymer film characterization was investigated in this thesis.

In order to justify the use of 1,2,3- triazine (Tr) fluorophores for the development of fluorescence based methods for thickness measurements (of thermoresponsive polymer thin films), we then investigated the photophysical properties of Tr doped poly N-(isopropyl acrylamide), PNIPAm (Tr-PNIPAm) thin films. Three derivatives such as 5-methoxycarbonyl-5-(N-phenylformimidoyl)-2,4,6-triphenyl-2,5-dihydro-1,2,3-triazine (pTr), hydrolysed form of pTr (hTr), and keto form of triazine (kpTr) were used for this study. These Tr fluorophores are hydrophobic and their overall emission is complex and composed of three emitting conformers. They have a large Stokes shift, and their absorption and emission properties are unaffected by changing the nature of the solvents [5-7]. We incorporated these fluorophores into a thermoresponsive polymer (*e.g.* PNIPAm) and investigated the effect of humidity on emission properties. Here we controlled the polymer environment using a controlled humidity chamber and analysed the emission properties of the fluorophores using both steady-state (S-S) and time-resolved fluorescence (TRF) measurements. The hydrophobic nature of Tr fluorophores governs its photophysical properties. The pTr doped PNIPAm (pTr-PNIPAm) thin film shows excellent stability and was insensitive to changes of microenvironment (*i.e.* humidity, temperature). The S-S emission properties showed only minor changes and the variation in the lifetime measurement was due to refractive index (RI) changes of the polymer matrix. Most

significantly, pTr-PNIPAm thin film also showed unique photostability compared to the other triazine fluorophores studies.

In addition, a series of Tr fluorophores doped polyvinyl alcohol, PVA (Tr-PVA) thin films were also fabricated and studied to explore the photophysical properties in another hydrophilic polymer. Unfortunately, the presence of anionic impurities in PVA (traces amount of sodium/methyl acetate) effects anion-induced quenching leading to a large decrease in emission intensity.

Acknowledgements

First of all, I would like to express my gratitude to my supervisor Dr Alan G Ryder for his continuous support, patience, and expertise and taking the time to read my thesis many times. I am feeling proud to be a member of your talented group. I will always value the friendship you have shown to me and all lessons I have learnt from being your student.

It's also my immense pleasure to express my gratitude to Dr Kevin Buckley for his time, effort and valuable suggestions during my thesis writing. I would also like give a special thanks to all the members of NBL research group over the time I have been in Galway for providing a friendly atmosphere and for useful discussions on my work. During this journey, I was given the opportunity to experience multicultural environments and improving my knowledge and skills in conducting innovative research within nanoscale groups. Besides all the scientific and professional acquirements within the PhD, I feel honoured to have shared ideas, thoughts, laughs, tears travels and my life with everyone that has been part of it.

I will always cherish the moment we have spent together and I will keep in memory all the professors, colleagues, friends, family places, cultures that have all contributed to the person I am today. You all made me feel home and so very special.

Thank you to my family and friends specially my parents for their love and support over the course of my degree. Specially thanks goes to my wife Ansara Noori for her infinite patience and bringing up my little mum (baby Juwairya) alone in Australia. Her love, patience, and encouragement make me finish the thesis. I also miss this type of conversation with my baby in skype. "Papa: I want to play with you baby". Juwairya: "papa, you can't play because you are in Ireland".

List of Abbreviations

Abbreviations	Definition
3HC	3-hydroxychromon
3HF	3- hydroxyflavones
AMPN	N-allyl-4-(4’-methyl-piperazinyl)-1,8-naphthalimide
BFE	5,6-benzo-4'-diethylamino-3-hydroxyflavone
CAM	Contact angle method
CCVJ	9-(2-carboxy-2-cyano) vinyljulolidine
Coumarin 151	7-amino-4-trifluoromethyl-1, 2-benzopyrone
Coumarin 152	7-N.N-dimethylamino-4-trifluoromethyl-1, 2-benzopyrone
CST	Critical solution temperature
DCVJ	9-(dicyanovinyl)-julolidine
D-D interaction	Dye dye interaction
DMABN	4,4-dimethylaminobenzonitrile
ESIPT	Excited State Intramolecular Proton Transfer
ETS	Excited triplet state
FCS	Fluorescence correlation spectroscopy
FE	4'-diethylamino 3-hydroxyflavone
FL	Fluorescein
FL-PVA film	Fluorescein doped poly vinyl alcohol (PVA) film
FRET	Förster resonance energy transfer
FTIR	Fourier transform infrared spectroscopy
FWHM	Full width at half maximum
HOMO	Highest Occupied Molecular Orbital
HPTS	8-Hydroxy-1,3,6-pyrenetrisulfonic acid trisodium salt
hTr	5-methoxycarbonyl-5-H-2,4,6-triphenyl-2,5-dihydro-1,2,3-triazine
hTr-PNIPAm	hTr doped PNIPAm
hTr-PVA	hTr doped PVA
IC	Internal conversion
ICT	Intramolecular charge transfer

IR	Infrared Spectroscopy
IRF	Instrument response functions
ISC	Intersystem crossing
IVR	Intramolecular vibrational relaxation
kpTr	5-propan-one-5-(N-phenylformimidoyl)-2,4,6-triphenyl-2,5-dihydro-1,2,3-triazine
kpTr-PNIPAm	kpTr doped PNIPAm
LCST	Lower critical solution temperature
LUMO	Lowest Unoccupied Molecular Orbital
MEC	4-methyl-7-(2,3-expoxypropoxy) coumarin
MFE	4'-diethylamino-3-hydroxy-7 methoxyflavone
MW	Molecular weight
NIPAm	N-isopropylacrylamide
NIR	Near infrared Spectroscopy
NR	Nile red
NtBA	N-tert-butylacrylamide
PDEAAm	poly (N, N-diethylacrylamide)
PDMAPS-MA	poly (2-dimethyl (methacryloxyethyl) ammonium propane sulfonate
PDMAPS-MAM	poly (3-(N-(3-methacrylamidopropyl)-N, N-dimethyl) ammonium propane sulfonate
PLA	Polylactic acid
PMAm	poly(methylacrylamide)
PMMA	polymethylmethacrylate
PNAGA	poly(N-acryloylglycynamide)
PNIPAm	Poly N- (isopropyl acrylamide)
PRODAN	6-propionyl-2-(dimethylamino) napthalene
PS	Poly styrene
pTr	5-methoxycarbonyl-5-(N-phenylformimidoyl)-2,4,6-triphenyl-2,5-dihydro-1,2,3-triazine
pTr-PNIPAm	pTr doped PNIPAm
pTr-PS	pTr doped PS
pTr-PVA	pTr doped PVA

PVA	Poly vinyl alcohol
PVC	Polyvinyl chloride
PVP	Polyvinylpyrrolidone
RET	Resonance Energy Transfer
RI	Refractive Index
S-S	Steady state
T_g	Glass transition temperature
T_m	Melting temperature
TAPP	Meso-5,10,15,20-tert-(-4-allyloxyphenyl)porphyrin
TCSPC	Time correlated single photon counting
TICT	Twisted intramolecular charge transfer
TNS	2,6-p-toluidinonaphthalene sulfonate
TRF	Time resolved fluorescence
Tr-polymer	Triazine doped polymer
UCST	Upper critical solution temperature

Table of contents

Chapter 1 : Introduction

1.1. Fluorescence

Any process (chemical or physical) triggered by the interaction of matter with electromagnetic radiation is known as a photophysical process. Generally, these processes can be categorised into four different types: 1) Absorption, 2) Radiative deactivation (Photoluminescence), 3) Non-radiative deactivation, and 4) scattering of radiation *i.e.* Rayleigh, Raman, Mie, and Tyndall scattering [8]. Molecular luminescence is a process where light is emitted from electronically excited states of molecules. Since they have a common mode of excitation (*i.e.* exciting an electron from the ground state to a higher level after absorbing a photon of light), fluorescence, phosphorescence and delayed fluorescence are referred to collectively as photoluminescence. Fluorescence is a process, in which the molecules are first promoted to an electronically excited state by photon absorption and then return to the ground state by re-emission of photons with lower energy, and all states have the same spin multiplicity [9, 10].

1.2. Absorption of light: Electronic excitation

Two types of molecular orbitals are central to absorption and fluorescence spectroscopies, namely the Highest Occupied Molecular Orbital (HOMO) and the Lowest Unoccupied Molecular Orbital (LUMO) [11]. An electron in the HOMO can be promoted to the LUMO by absorption of quanta of energy. If this energy is supplied by light, then to bring a molecule into the excited state, a photon requires the energy equal to the energy difference between the excited state and the ground state which can be expressed as:

$$\Delta E = h\nu = hc/\lambda = E_e - E_g \qquad \text{Equation 1.1}$$

where h is Planck's constant (= 6.626 x 10^{-34} J.s), c is the velocity of light and ν is the frequency and λ is the wavelength. E_e is the energy of the excited state and E_g is the energy of the ground state. Generally, electronic transitions for most molecules are observed in the UV- NIR spectral range.

Usually, in the HOMO, neutral organic molecules have a pair of electrons with opposite spin and the spin multiplicity ($M_s = 2S + 1 = 1$) is referred to as a singlet state.

If the ground and the excited states have the same spin multiplicity then the labelling convention is S_0 for the ground, and S_1, S_2, S_3... for the excited state is used. In some excited states with one electron in the HOMO and one in the LUMO, the electrons can have the same spin multiplicity *i.e.* S = ½ + ½ = 1. Hence the multiplicity becomes M = 2(1) + 1 = 3 and the state is called a triplet state. According to Hund's Rule a triplet state has lower energy than the corresponding singlet state [11, 12].

Electronic transitions (*e.g.* $S_0 \rightarrow S_1$) occur at a much faster rate ($\sim 10^{-15}$s) than molecular vibrations ($\sim 10^{-11}$s); thus electrons are likely to have completed their transitions before any structural change can occur in a molecule. This is known as the **Franck-Condon principle** [8, 11-13].

Every electronic state also has attendant vibrational and rotational energy states, and the spacing between the two adjacent vibrational levels decreases with increasing vibrational quantum number. Electronic transitions are accompanied by vibrational transitions and these vibronic transitions determine the appearance of the absorption and emission spectra [12].

1.3. Principles of fluorescence spectroscopy:

At ambient temperature, according to the Boltzmann distribution, almost all molecules in a system are in the lowest electronic and vibrational states. After absorbing an appropriate amount of energy, the molecule is promoted from the ground state to one of the upper excited electronic states S_1 or S_2 (or sometimes S_3, depending on the absorbed energy). This is the vertical transition and takes place within a time frame of 10^{-15}s, which is too short to execute any displacement of the nuclei. During the following 10^{-13} to 10^{-11} seconds, the excited molecule rapidly relaxes to the lowest vibrational energy level of the singlet excited state S_1 through vibrational relaxation and sometimes by internal conversion if the transition is from the excited state S_2 [11, 13]. Depending on the structure of the molecule and its interaction with the environment, the fluorophore may remain in this lowest vibrational energy state (*i.e.* S_1, singlet state) for a few tens of picoseconds to a few hundred nanoseconds before either relaxing to the ground state non-radiatively or relaxing to the ground state with the emission of a photon of light (radiative decay), or undergoing intersystem crossing

to the triplet state T_1 [11]. The Jablonski diagram (Figure 1.1) illustrates these various processes.

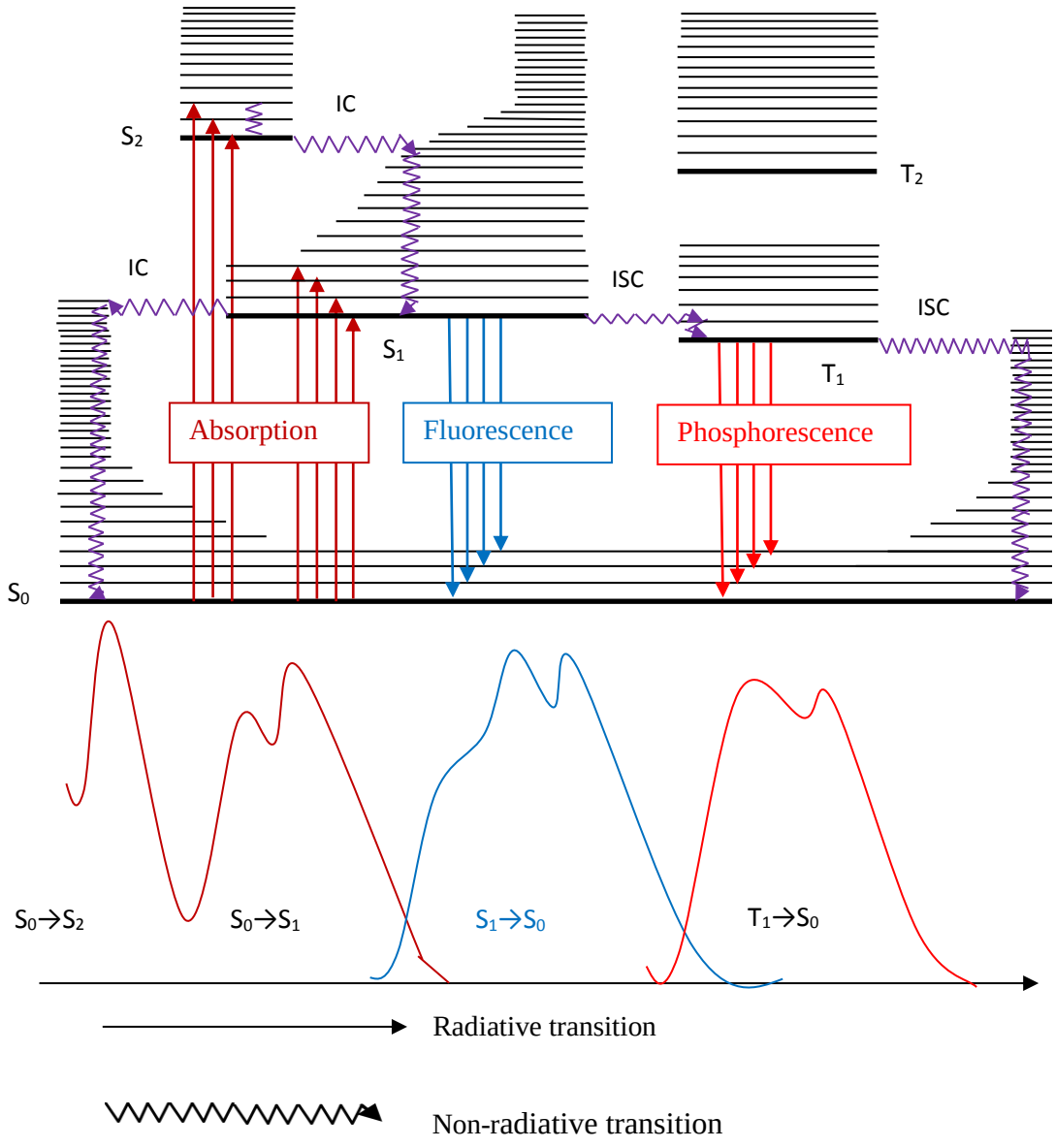

Figure 1.1: A modified Jablonski diagram to illustrate the principles behind fluorescence spectroscopy. Figure describes the photon absorption and emission among different vibrational levels of the singlet ground state, the excited singlet state (S_1, S_2...) and also the triplet state. It also shows the different radiative and non-radiative pathways for releasing energy to return back to the ground state. Reproduced from ref. [11].

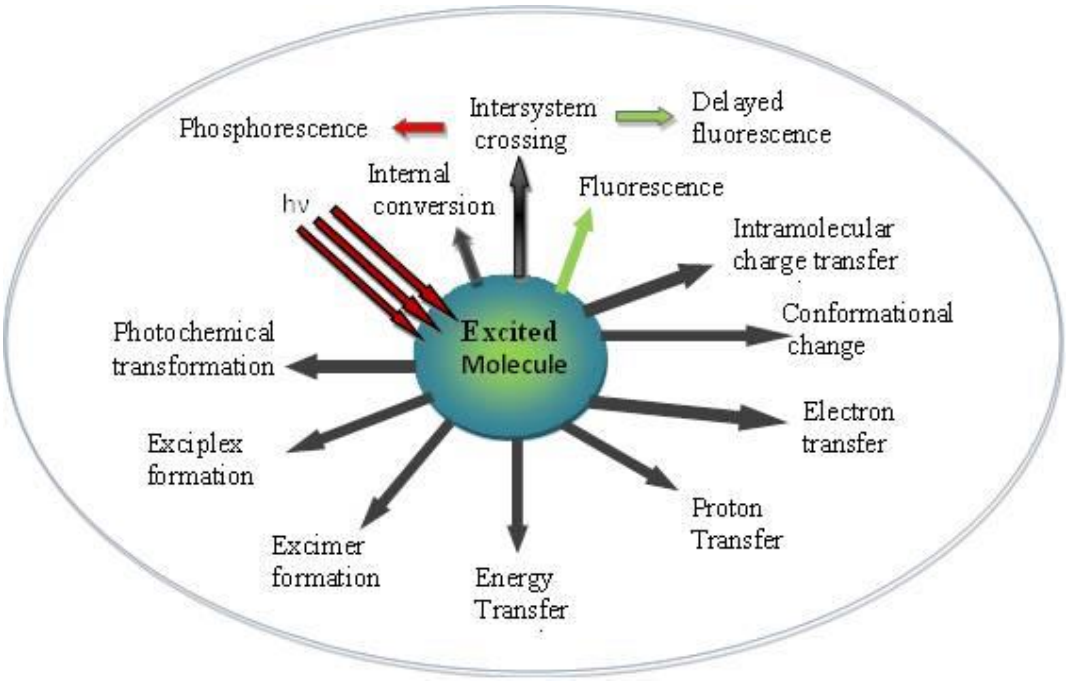

Figure 1.2: Illustration of possible de-excitation pathways (radiative and non-radiative) of excited state molecules. Reproduced from ref. [11].

In addition, there are other non-radiative pathways where the excited state can interact with its environment *i.e.* quenching, Förster resonance energy transfer (FRET) and the possibility of interaction in the excited state with other molecules may also be responsible for de-excitation *i.e.* electron transfer, excimer or exciplex formation shown in Figure 1.2.

1.4. Important features of fluorescence spectroscopy

1.4.1. Internal conversion (IC)

Internal conversion is a non-radiative transition between two electronic states of the same spin multiplicity [11]. The rate of IC is a function of the energy difference between the states (ΔE). As ΔE gets smaller the rate of IC increases as described by the energy gap law which states that the rate of non-radiative transition generally increases exponentially with the decrease of energy gap between the two electronic states [14].

1.4.2. Intersystem crossing (ISC)

Based on the selection rule for optical absorption, transitions between the same spin multiplicity (*i.e.* singlet-singlet) is favourable whereas those involving different

multiplicity (*i.e.* singlet-triplet) are forbidden [12]. However, transitions involving spin conversion may occur when there is an interaction between the orbital angular momentum and the spin orbital momentum of a molecule (*i.e.* spin orbital coupling) [15]. ISC is a type of conversion where a triplet state is formed from the appropriate excited singlet state via an isoenergetic radiationless process. The probability of ISC occurring is dependent on the corresponding singlet and triplet states. If a molecule has the transition type $n \rightarrow \pi^*$ for $S_0 \rightarrow S_1$ transition, then ISC is often favoured [11]. The probability of ISC is increased, if a molecule contains heavy or paramagnetic atoms [16, 17]. For example, the triplet state transition via ISC for rhodamine and cyanine dyes has been reported to increase in the presence of divalent manganese which also causes fluorescence intensity fluctuations and enhancement of photobleaching [15].

From a triplet state, the excited molecules can either non-radiatively return to the ground state or via a radiative process known as **phosphorescence**. Phosphorescence has a considerably longer lifetime (from milliseconds to seconds) because it is a forbidden process and emission is red shifted compared to fluorescence due to there being a lower energy for the lowest vibrational state of T_1 compared to that of S_1 [11]. Since the transition from S_1 to T_1 is relatively slow occurring between 10^{-10} to 10^{-8} s, there is much more time for the excited molecule to interact with solvent molecules. As a consequence, de-excitation favours non-radiative means (*i.e.* vibrational relaxation) to return to the ground state. For this reason phosphorescence is more often observed/studied at low temperatures and in rigid systems (*e.g.* in a polymer matrix).

Another route for relaxation from the triplet state is by reverse ISC to S_1 and this can occur when the lifetime of the triplet state is long enough and the energy gap between the T_1 and S_1 state is very small. This emission (radiative transition from $S_1 \rightarrow S_0$) obtained from this state is known as **delayed fluorescence** [11, 18, 19]. It is also called *E-type* delayed fluorescence since it was first observed in eosin. It has the same emission spectra as the normal ($S_1 \rightarrow S_0$) fluorescence but has a longer lifetime, because the population of the excited state originates from a long-lived triplet state [11]. There is another type of delayed fluorescence known as *P-type* delayed fluorescence (since it was first noticed in pyrene molecule). It is usually observed when

the collision between two molecules in the T_1 state provides sufficient energy to allow one of them to return back to the S_1 state and which thus leads to a *P-type* delayed fluorescence.

1.4.3. Fluorescence lifetime and quantum yield

The fluorescence lifetime (τ) can be defined as the average amount of time a fluorophore stays in the excited state before returning to the ground state. It is a very important parameter as it also determines the time available for the excited molecules to interact with its microenvironment. It is important to mention that the lifetime of a fluorophore is a statistical average value of the time spent in the excited state and not all the molecules will emit a photon at exactly $t = \tau$. For a single exponential decay, about 63% of the total molecules present have emitted a photon by a time delay equal to lifetime and 37% is decayed at $t > \tau$ [13].

Excited fluorophores can be deactivated by two pathways: radiative or non-radiative (Figure 1.3). So, the lifetime of a fluorophore can be expressed as:

$$\tau = \frac{1}{k_r + k_{nr}} \qquad \text{Equation 1.2}$$

where k_r is the rate constant for radiative deactivation and k_{nr} is the overall non radiative rate (the sum of the rate constant of internal conversion, intersystem crossing and quenching etc.). The lifetime τ depends on the fluorophore environment, pH, viscosity of the medium, refractive index (will be discussed in section 1.8) and interaction with other molecules present in the systems (*e.g.* collision or energy transfer).

The quantum yield (Φ_F) is also an important property of a fluorophore. It can be defined as the ratio: numbers of photons emitted (N_{em}) over the numbers of photons absorbed (N_{abs}). It can be expressed as:

$$\Phi_F = \frac{N_{em}}{N_{abs}} \qquad \text{Equation 1.3}$$

It can be alternatively expressed using the radiative and non-radiative decay rates:

$$\Phi_F = \frac{k_r}{k_r + k_{nr}} \qquad \text{Equation 1.4}$$

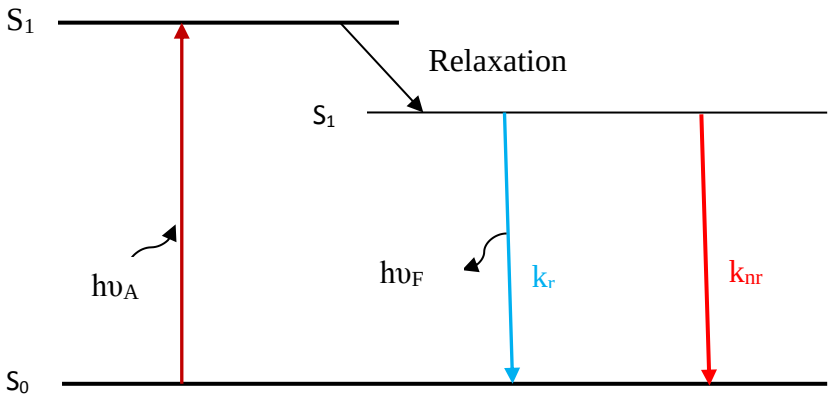

Figure 1.3: A very simplified form of Jablonski diagram to illustrate the fluorescence lifetime and quantum yield where S_0 and S_1 are the singlet electronic state. Here individual relaxation processes leading to relaxed S_1 state are not considered for simplicity. After absorption of appropriate amount of energy, the molecule is electronically excited from S_0 to S_1. Losing some of the energy by relaxation, the excited molecules then return to the ground state by two means (*i.e.* radiative and non-radiative) with the rate of k_r and k_{nr}. Reproduced from ref. [13].

When the non-radiative decay rate is much smaller than that of the radiative *i.e.* $k_{nr} << k_r$, then the quantum yield will be close to unity. However, it is important to note that Φ_F is always less than unity due to energy losses by vibrational relaxation.

Φ_F can be also expressed by considering the absence of non-radiative decay as:

$$\Phi_F = \frac{\tau_s}{\tau_r} \qquad \text{Equation 1.5}$$

where τ_S is the excited state (S_1) lifetime and τ_r is the radiative lifetime (preferred to known as a natural lifetime) of a molecule [11].

Bringing the lifetime term from Equation 1.2 into Equation 1.4 yields,

$$\tau = \frac{\Phi_F}{k_r} \qquad \text{Equation 1.6}$$

1.4.4. Stokes shift

The Stokes shift (shown in Figure 1.4) is defined as the separation between the position of the first absorption band maximum and the emission band maximum (expressed as a wavenumber/wavelength) [11]. It measures the loss in energy due to the multitude of excited state processes and interactions with the fluorophore environment.

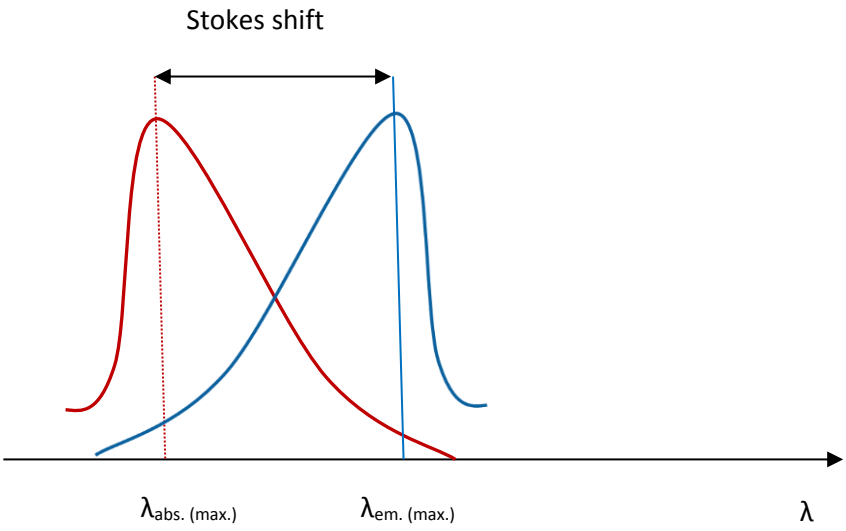

Figure 1.4: Stokes shift, the difference between the position of absorption band maximum and emission band maximum of a fluorophore. Reproduced from [11].

The Stokes shift is an important fluorescence parameter as it provides valuable information about the excited state of a molecule. It can be sensitive to solvent polarity, if there is a significant change in dipole moment between the excited state and the ground state of a fluorophore molecule. So, one can use the change in Stokes shift for measuring the polarity of a medium by using an appropriate polarity sensing probe (which will be discussed in section 1.8).

1.4.5. Quenching

Apart from photobleaching (section 1.4.9), fluorescence emission intensity can be decreased by a variety of other mechanisms, which are collectively known as quenching. Molecular oxygen, heavy atoms (*e.g.* halides), amines and electron-deficient molecules (acrylamide) are common examples of fluorescence quenchers. The possible molecular interactions which cause quenching are energy transfer, proton transfer, and the formation of ground state complexes (known as static quenching) [13]. Quenching can be investigated by measuring the changes in emission intensity and lifetime as a function of quencher concentration using steady- state and the time resolved measurements respectively.

1.4.5.1. Collisional quenching

Dynamic (or collisional) quenching can be defined as the decrease of fluorescence intensity or lifetime by the collision of the excited state fluorophore with

other molecules present in the system. This quenching is usually observed in situations where the excited molecules and the quencher are free to diffuse and interact each other. This is common in solution samples [12].

The energy of the excited state (A^*) of a molecule can be lost as heat as a result of collision with the quencher Q and presented as following:

$$A^* (S_1) + Q (S_0) \rightarrow A (S_0) + Q (S_0)$$

The quantum yield of a fluorophore in the presence of quencher (Φ_q) is expressed by:

$$\Phi_q = \frac{k_r}{k_r + k_{nr} + k_q [Q]} = \frac{k_r}{1/\tau + k_q [Q]} = \frac{k_r \tau}{1 + k_q \tau [Q]} \quad \text{Equation 1.7}$$

where k_q is the bimolecular quenching constant, [Q] is the concentration of quencher.

Using Equation 1.6 we can write

$$\frac{\Phi_F}{\Phi_q} = 1 + k_q \tau [Q] \quad \text{Equation 1.8}$$

Equation 1.8 is the well-known Stern-Volmer equation. Both fluorescence lifetime and the intensity are proportionally related to quantum yield, so Equation 1.8 can be written as

$$\frac{I_0}{I} = \frac{\tau_0}{\tau} = 1 + k_q \tau_0 [Q] = 1 + K_{SV}[Q] \quad \text{Equation 1.9}$$

where I_0 and I are the fluorescence intensities in the absence and presence of quencher respectively, τ_0 and τ are the fluorescence lifetime in the absence and presence of quencher respectively. The term K_{SV} is known as the Stern-Volmer quenching constant and is a measure of the sensitivity of a fluorophore to a quencher.

1.4.5.2. Static quenching

Most commonly, static quenching can be described by either of two models; the sphere of effective quenching or the formation of ground state non-fluorescent complex.

Sphere of effective quenching: In solid matrices or viscous media where molecular concentrations are very high, a quencher Q can often be located inside the sphere of effective quenching (alternatively known as active sphere or quenching sphere) of the excited molecules M^* (Figure 1.5a), quenching may then occur according to Perrin model. The Perrin model stated that, quenching is supposed to be happen when the quencher molecules are situated inside the active sphere of M^*. On the other hand, M is totally unaffected when the quencher Q is situated outside the active sphere. Therefore, even though the intensity of fluorophore is decreased by this mechanism, the excited state lifetime will be unchanged.

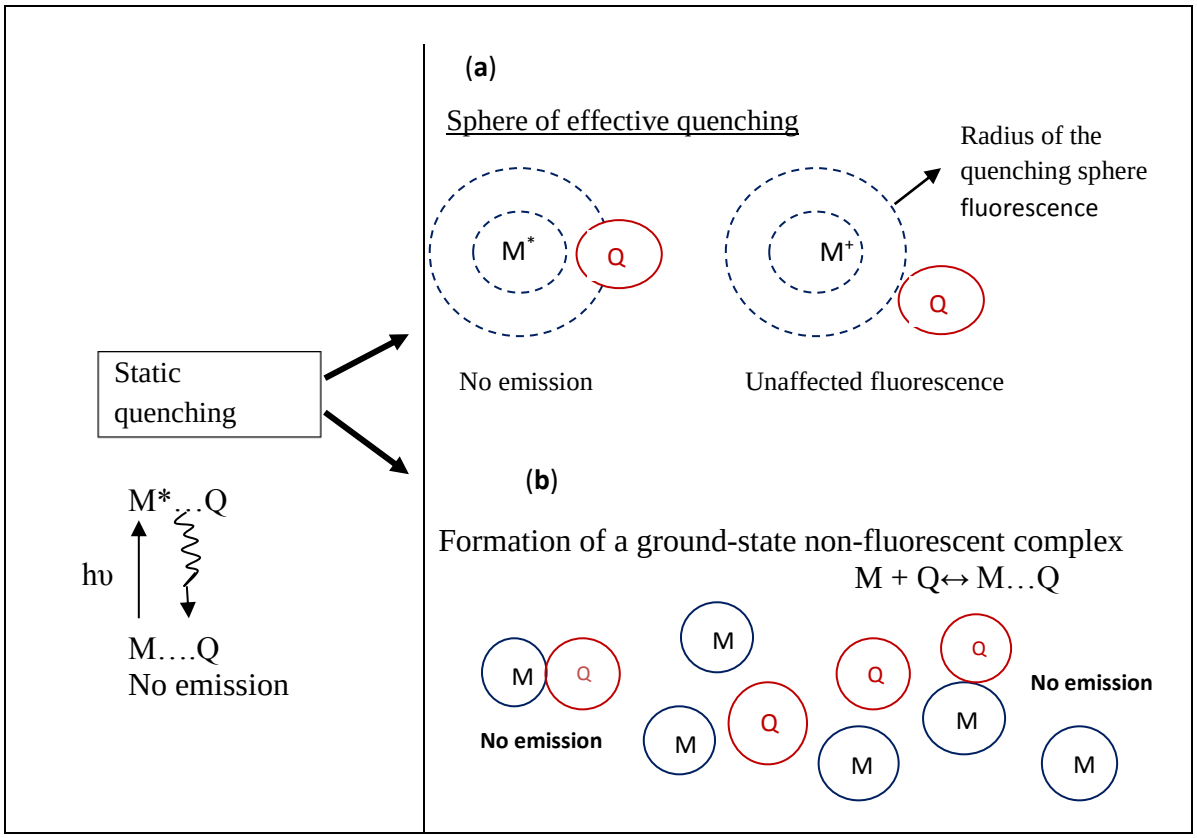

Figure 1.5: The different mechanisms for static quenching. One mechanism is: the quenchers are located inside the effective diameter of spheres and thus leading to static quenching (a) and the formation of ground complexes with the quenchers is another mechanism for static quenching (b). Reproduced from ref. [11].

Formation of a ground state non-fluorescent complex: Quenching may also happen by ground state non-fluorescent complex formation (Figure 1.5b). When these complexes absorb light, immediately it returns to the ground state without emitting a photon. In this case, the stability constant for the complex can be expressed as:

$$K_S = \frac{[M \ldots Q]}{[M][Q]}$$

Total concentration according to mass conservation

$$[M]_0 = [M] + [M \ldots Q]$$

So the fraction of un-complexed fluorophores is:

$$\frac{M}{M_0} = \frac{1}{1 + K_S[Q]} \qquad \text{Equation 1.10}$$

The above equation can be written as (in the case of a dilute solution)

$$\frac{I_0}{I} = 1 + K_S[Q] \qquad \text{Equation 1.11}$$

So one can get a linear relationship in the Stern-Volmer plot for intensity; however there is no change in lifetime for static quenching processes.

1.4.5.3. Comparison of Static quenching and dynamic quenching

One can note from the Equation 1.9 and Equation 1.11 that sometimes there can be a linear dependence between the I_0/I and [Q] for both static and dynamic quenching. So, the two mechanisms cannot be distinguished on the basis of intensity measurements alone. They can however be differentiated by their differing dependence on temperature or preferably by lifetime measurements.

Generally, in dynamic quenching, the lifetime of a fluorophore is reduced along with the reduction of intensity; whilst, lifetime is unaltered in the case of static quenching. So, in static quenching, only the reduction of the concentration of emitting fluorophores is observed by the formation of ground –state non-fluorescent complex, where the $\frac{\tau_0}{\tau}$ ratio is equal to one [12]. In dynamic quenching the ratio $\frac{I_0}{I}$ is usually proportional to $\frac{\tau_0}{\tau}$ whilst, in static quenching these two ratios is not equal (*i.e.* $\frac{I_0}{I} \neq \frac{\tau_0}{\tau}$).

In addition, at higher temperature there will be a faster diffusion and thus a higher rate of collisional quenching. This higher temperature also facilitates the dissociation of weakly bound ground complexes and decreases the amount of static quenching (Figure 1.6). Static quenching is favoured over collisional quenching when the media is rigid and where diffusion is either greatly reduced or absent [20].

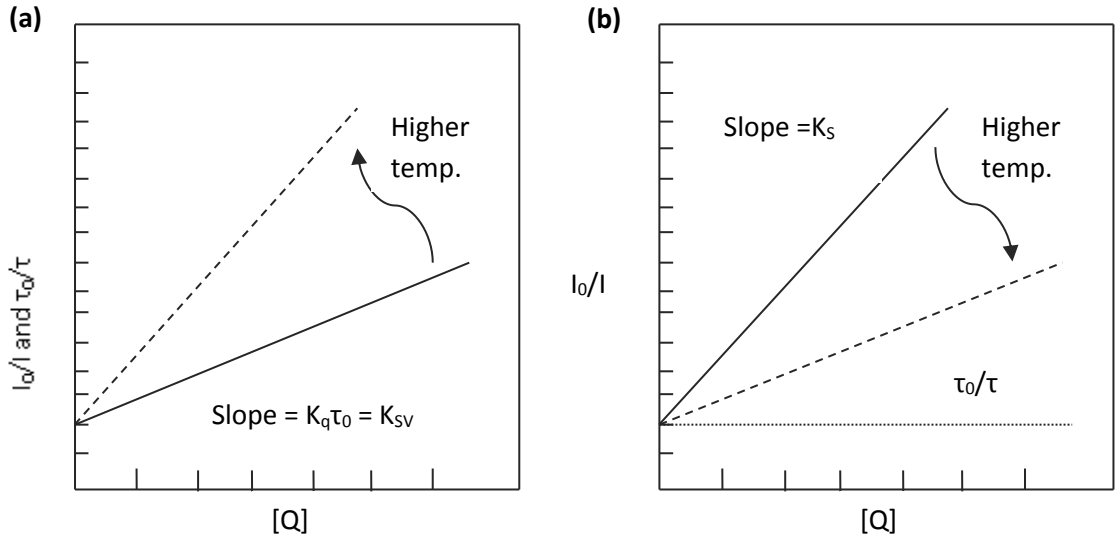

Figure 1.6: (a) Plot showing collisional quenching where slope of the straight line is increased by the increase of temperature because at the higher temperature, the molecules move faster. The variation of intensity and lifetime of the molecules generally maintains same trend. (b) Figure showing static quenching where the quenching constant is decreased with the increase of temperature and the ratio of lifetime with and without the quencher is unaffected by static quenching. Reproduced from ref. [13].

1.4.5.4. Combined static and dynamic quenching:

It i**s** often the case that fluorophores can be quenched by both collisional and static mechanism in a single sample. This situation can be described by combining the Equation 1.9 and Equation 1.11:

$$\frac{I_0}{I} = (1 + K_{SV}[Q])(1 + K_S[Q]) \qquad \text{Equation 1.12}$$

The Equation 1.12 is a second order in terms of quencher concentration. Therefore, in the presence of both dynamic and static quenching for same fluorophore, one can get an upward deviation (concave to the y-axis) from the linear Stern-Volmer plot (Figure 1.7a) when the intensity ratio vs quencher concentration is plotted.

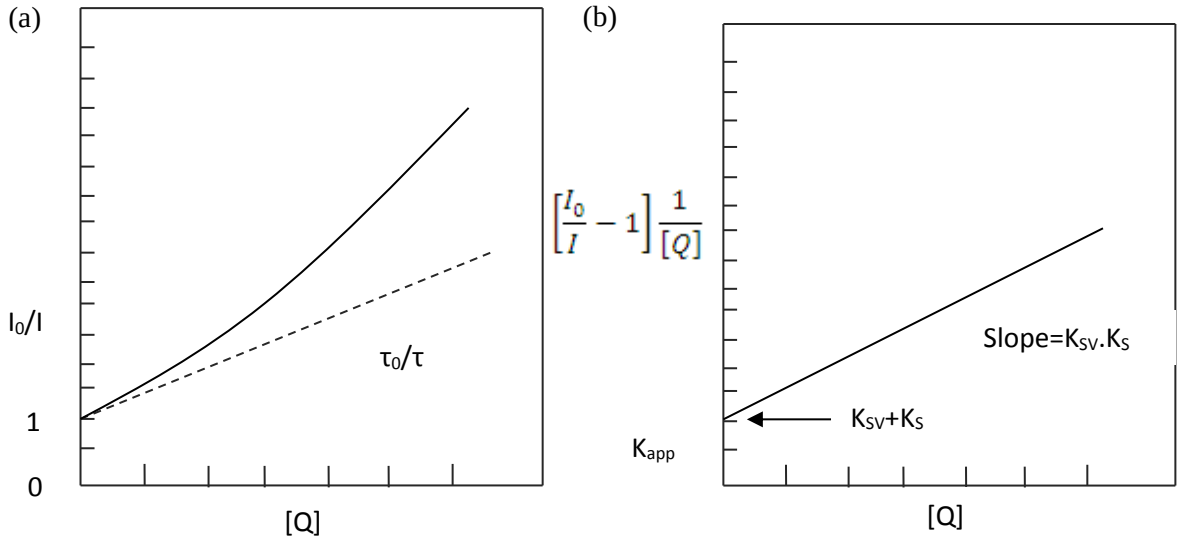

Figure 1.7: Schematic presentation of static and dynamic quenching where (a) represent the deviation from linear behaviour of lifetime and intensity to upward curvature due to the presence of static and dynamic quenching, both in same condition and (b) represent the slope and intercept of combined equation in the presence of both static and dynamic quenching. Reproduced from ref. [13].

The contribution of dynamic quenching can be measured by using $\frac{\tau_0}{\tau} = 1 + K_{SV}[Q]$, when lifetime data are available. On the other hand, in absence of lifetime data one could graphically separate the K_{SV} and K_S by modifying the Equation 1.12

$$\frac{I_0}{I} = 1 + (K_{SV} + K_S)[Q]) + K_{SV}K_S[Q]^2$$

$$K_{app} = \left[\frac{I_0}{I} - 1\right]\frac{1}{[Q]} = (K_{SV} + K_S) + K_{SV}K_S[Q] \qquad \text{Equation 1.13}$$

Where K_{app} is the apparent quenching constant. A plot of K_{app} versus $[Q]$ will be a straight line where $K_{SV} + K_S$ is the slope and $K_{SV}K_S$ is the intercept (Figure 1.7b)

1.4.6. Förster Resonance Energy Transfer (FRET)

FRET (Figure 1.8) is non-radiative energy transfer from an excited donor fluorophore (D) to a nearby chromophore, the acceptor (A) and is a very important technique due to its distance dependency [21, 22]. FRET is a process where the excited dipole of donor fluorophore initiates the excitation of a dipole of an acceptor molecule and, eventually, the donor get deactivated and the acceptor becomes excited [12].

The requirements below must be fulfilled for FRET to occur [23]

1. The donor emission spectrum must overlap with the acceptor absorption spectrum. The degree of spectral overlap is a determinant of the efficiency of FRET.
2. The donor and acceptor molecules must be close to each other (<100Å)
3. The orientation of the transition dipole moments of the donor and acceptor should be approximately parallel to each other.

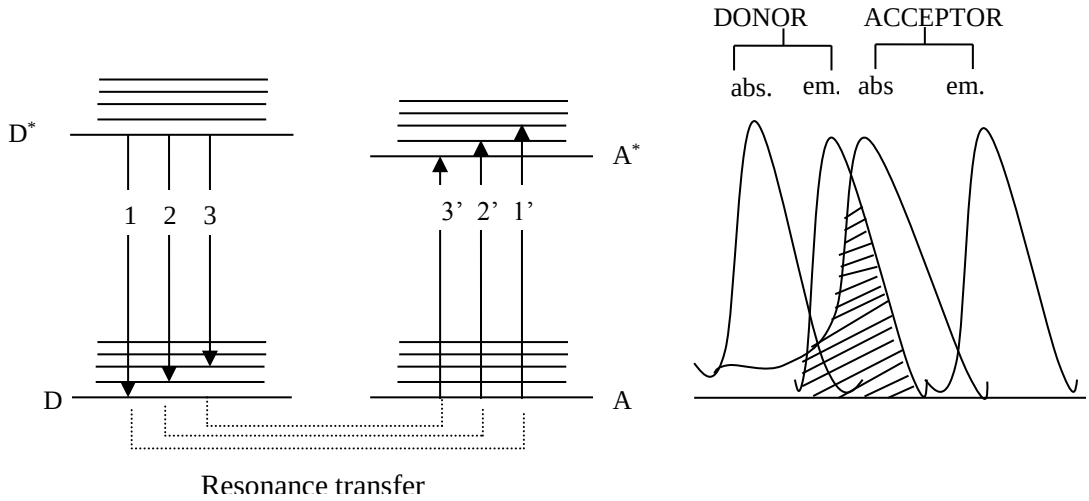

Figure 1.8: Non-radiative energy transfer from the donor molecule to the acceptor molecule and also showing the overlap of emission spectra of donor probes and absorption spectra of acceptors. Reproduced from [11].

The rate of energy transfer from a donor to an acceptor can be expressed by the following equation:

$$k_T(r) = \frac{1}{\tau_D}\left(\frac{R_0}{r}\right)^6 \qquad \text{Equation 1.14}$$

where r is the distance between the donor and the acceptor and the τ_D is the lifetime of the donor in the absence of acceptor. R_0 is the Förster distance which can be defined as the distance at which the efficiency of FRET is 50% *i.e.* one half of the donor molecules decay by energy transfer and other half decay by usual radiative and non-radiative means. It can be seen from Equation 1.14 that FRET is strongly dependant on the distance, which is inversely proportional to the sixth power of r. So that, it can be used as a spectroscopic ruler for the measurement of small distances between the two points in a protein *e.g.* the unfolding of protein [13].

The theory of Resonance Energy Transfer (RET) can be better understood by considering a single donor and acceptor separated by a distance r. By considering the classical and quantum mechanics, the rate of energy transfer in this case can be expressed by:

$$k_T(r) = \frac{\Phi_D \kappa^2}{\tau_D r^6}\left(\frac{9000(\ln 10)}{128\pi^5 N n^4}\right)\int_0^\infty F_D(\lambda)\varepsilon_A(\lambda)\lambda^4 d\lambda \qquad \text{Equation 1.15}$$

Where, Φ_D is the quantum yield of donor in the absence of acceptor, κ^2 is the relative orientation factor in space of the transition dipoles of the donor and acceptor. The value of κ^2 is usually in the range of 0 – 4 depending on the molecular orientation. When the dipoles are oriented perpendicular to each other the value is 0 and will be 4 when the dipoles are collinear (head–to–tail). However κ^2 = 2/3 is often used by averaging all possible angles for freely rotating donor and acceptor molecules [15]. τ_D is the lifetime of donor in the absence of acceptor, N is Avogadro's number, n is the RI of the medium, $F_D(\lambda)$ is the normalized donor fluorescence spectrum in the wavelength range λ to $\lambda+\Delta\lambda$, and $\varepsilon_A(\lambda)$ is the wavelength dependence molar extinction co-efficient of the acceptor.

At Förster distance R_0, the transfer rate is equal to the decay rate of the donor in the absence of acceptor *i.e.* $k_T(r) = \tau_D^{-1}$. So, from Equation 1.14 and Equation 1.15 it can be written [13]:

$$R_0^6 = \frac{9000(\ln 10)\Phi_D \kappa^2}{128\pi^5 N n^4}\int_0^\infty F_D(\lambda)\varepsilon_A(\lambda)\lambda^4 d\lambda \qquad \text{Equation 1.16}$$

The integral part in the right hand of Equation 1.15 or Equation 1.16 is known as the spectral overlap integral $J(\lambda)$ and expresses the degree of spectral overlap between the donor emission and the acceptor absorption. The Equation 1.16 then can be rewritten as:

$$R_0 = 0.211[\kappa^2 n^{-4}\Phi_D J(\lambda)]^{1/6} \quad \text{(in Å)} \qquad \text{Equation 1.17}$$

Where unit of $J(\lambda)$ is $M^{-1}cm^{-1}(nm)^4$.

1.4.7. Molecular structure of fluorophores and fluorescence properties

The vast majority of fluorophores are aromatic compounds. Generally, the extent of π conjugation determines the absorption and fluorescence emission spectra and quantum yield. The aromatic hydrocarbons in which $\pi \rightarrow \pi^*$ transitions are the lowest-lying, generally can be characterized by high absorption coefficients and quantum yields. However, if there is an involvement of a heteroatom in the π electron system, the $n \rightarrow \pi^*$ transitions could be the lowest-lying, and will have a lower absorption coefficient (at least 10^2 times lower, compared to a $\pi \rightarrow \pi^*$ transition). This leads to a much slower radiative process which cannot compete with the dominant non-radiative processes and, thus, a lower quantum yield will be the consequence [11]. As an example, acridine shows very low fluorescence quantum yields in the vapour phase, aprotic, non-hydrogen bonding, and hydrocarbon solvents. The $n \rightarrow \pi^*$ state could be the lowest S_1 state in the vapour and aprotic solvents and giving rise to a weak radiation process which will ultimately result in low fluorescence [11].

Conformational flexibility may also increase the rate of non-radiative decay for a fluorophore. For example, the quantum yield of toluene and *t*-butyl benzene is 0.14 and 0.032, respectively, which is due to the significant side-chain vibration in the latter [14]. The incorporation of heavy atoms in aromatic compounds increases the probability of ISC and lowering the quantum yield. This effect is known as internal heavy atom effect. This heavy atom effect would be small where i) the fluorophore has such a large fluorescence quantum yield that fluorescence de-excitation dominates all other de-excitation pathways; ii) the quantum yield is so low that an increase in efficiency of ISC will be relatively very small; or iii) if there is no triplet state energetically close to the singlet state for ISC [11].

In general, electron donating groups (-OH, -OR, $-NH_2$, -NHR, $-NR_2$) substitution in an aromatic ring increases the molar absorption coefficient and causes shifts of both absorption and emission spectra. The spectra obtained from this substitution are usually broad compared to the parent aromatic hydrocarbons (e.g. 1– and 2-naphthol compared to naphthalene).

Fluorophores containing both electron donating (*i.e.* $–NH_2$, $–NMe_2$, $–CH_3O$) and electron acceptor groups (*i.e.* >C=O, -CN) can undergo excitation accompanied

by a large increase in dipole moment which leads to the formation of an **intramolecular charge transfer (ICT)** state. In this case, the excited state (Franck-Condon state/locally excited state, LE) of this fluorophore will be not in equilibrium with the surrounding solvent molecules, particularly with polar solvents. Following excitation, the solvent molecules have to reorient themselves around the excited molecule, leading to a relaxed state with a minimum energy. According to Kasha's rule, emission is generated from the lowest excited energy state. Hence, a red shifted emission is observed in polar solvent. The extent of this red shift is dependent on the polarity of the solvents. Generally, the more polar the solvent the greater the red-shift.

Sometimes, relaxation during the ICT state is accompanied by the internal rotation of a group within the fluorophore and a **twisted intramolecular charge transfer** state (TICT) is the consequence [11, 13]. The emission from the TICT state is of longer wavelengths *i.e.* red shifted. An example of a molecule showing TICT is 4,4-dimethylaminobenzonitrile (DMABN). The mechanism for forming a TICT state is: in the excited state, the donor part *i.e.* dimethylamino of the initially planar molecule rotates around the amino-phenyl bond which is accompanied by a charge separation between the donor and acceptor groups of DMABN. In polar solvents, this twisted conformer can be stabilized by solvent reorientation. Therefore, photon emission from this TICT state will be red shifted. When a molecule has several possibilities for internal rotation (*e.g.* the molecule having anilino moiety) in the excited state, the interpretation of photophysics in terms of TICT becomes difficult (example:4-dicyanomethylene-2-methyl-6-p-dimethylamino-styryl-4H-pyran, DCM) [11]. The fluorescence properties of these TICT susceptible molecules are strongly dependent on medium viscosity and polarity. Therefore, this group of molecules has been studied to sense the microscopic environments (more details will be presented in Section 1.9).

1.4.8. Temperature and fluorescence

The fluorescence quantum yield and lifetime are generally decreased with an increase of temperature because many non-radiative processes are related to thermal motion. The collision between the excited molecules and the solvent molecules, intramolecular vibration, and rotation etc. increase with temperature [11]. In addition, temperature dependent non-radiative transitions $S_1 \rightarrow S_0$ (IC) or $S_1 \rightarrow T$ (ISC) can occur

if the upper vibrational levels of S_1 undergo a different mechanism for non-radiative transition compared to the v = 0 level. A common mechanism of this type is thermally activated $S_1 \rightarrow T_n$ ISC [24], where $n \neq 1$. For example, temperature dependant ISC of $S_1 \rightarrow T_2$ has been reported for certain anthracene derivatives [14]. The rate constant for ISC from S_1 to the triplet state (K_{ST}) of 9,10-dibromoanthracene may be expressed by $K_{ST} = \sim 10^{12} \exp[-E_a/RT]$ where activation energy, E_a = ~4.5 kcal/mole. A large energy gap between S_1 and T_1 leads to an unfavourable Franck-Condon factor which thus slows the direct $S_1 \rightarrow T_1$ ISC process. The T_2 lies in ~ 4–5 kcal/mole above the S_1 and the E_a is ~4.5 kcal/mole. Therefore, instead of populating the upper vibrational level of T_1, the T_2 is being populated by $S_1 \rightarrow T_2$ ISC process.

Wang *et al.* studied the temperature effect on the fluorescence properties of a 4-methyl-7-(2,3-epoxypropoxy) coumarin (MEC) doped PVA polymeric film matrix [25]. They did the experiment over a 273-333 K (Figure 1.9a) temperature range and reported that fluorescence intensity and quantum yield decreased with the increase in temperature. A good linear correlation between K_{IC} and 1/T was also reported within 273–323 K temperature range for a fluorescein fluorophore in aqueous solution which had a $K_{IC} = 2.0 \times 10^{11} \exp[(- 5.5 \text{ kcal/mol})/RT]\ s^{-1}$, where k_{IC} stands for the IC rate constant. They explained these temperature dependant fluorescence properties by the photophysical and photochemical dye properties. The fluorescence intensity of MEC bearing PVA is mainly controlled by a radiationless temperature dependant process. Temperature increases collision between molecules and thus quenching of fluorescence intensity. Thermally activated ISC is also responsible for decreasing the quantum yield of fluorescence.

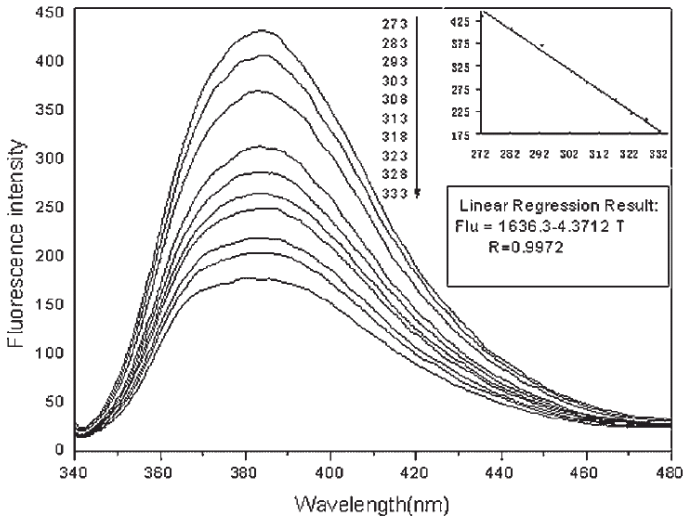

Figure 1.9: (a) Decrease of fluorescence intensity of 4-methyl-7-(2,3-epoxypropoxy) coumarin bearing PVA polymeric film matrix as a function of temperature where λ_{ex} =323 nm. The linear relation between fluorescence intensity over the temperature range 273–333K is shown in inset. Adapted from ref. [25].

A temperature dependant increase of fluorescence intensity is also sometimes observed (generally at high concentration of fluorophore) for fluorophore containing films where the polymer relaxation process induces molecular motion in the fluorophores. For example, fluorescein in PVA matrix (at a concentration of 0.1% w/w) shows an increase of intensity at a certain range of temperature [26]. This increase in intensity started at 260–270 K and increased up to 315 K. The behaviour can be explained by the fact that the segmental motion of non H-bonded –OH group of PVA during relaxation is comparable with the diameter of fluorescein. Therefore the molecular motion of fluorescein is induced by the segmental movement of PVA chain which thus minimize the self-quenching (self-quenching is produced by the interaction between neighbour dye molecules or the dimer formation) and an increase in fluorescence intensity is the consequence.

1.4.9. Photobleaching

Bleaching refers to the irreversible conversion of a fluorophore or particle into a non-fluorescent entity. In most cases, this process is photoinduced (and called photobleaching) which ultimately causes the loss of emission or absorption intensity. This is a common phenomenon for fluorophores and ultimately limits practically all fluorescence techniques which may require high sensitivity, high signal rate *i.e.* all

imaging techniques of fluorescence, single molecule fluorescence, fluorescence correlation spectroscopy (FCS) [15].

There are a number of chemical pathways by which a fluorophore is going to permanently photobleach. These reactions usually occur when fluorophores are in the singlet or triplet excited state. There are three types of photobleaching processes [27]:

Unimolecular: The fluorophore molecules are photochemically fragmented to produce radical or ions (*e.g.* homo– or heterolytic dissociation reactions). This dissociation pathway is important for the fluorescent aromatic amino acids tyrosine and tryptophan [28].

Multiphoton photolysis: The fluorescence techniques, where high irradiance is used (*i.e.* Single Molecule Detection or Fluorescence Confocal microscopy) generally there has a greater probability of multiphoton absorption. It thus leads to a high probability of photobleaching reaction due to the population of higher excited electronic states. In polar solvents (e.g. water), a subsequent heterolytic dissociation of fluorophore (M) forming a radical ion pair ($M^{+}e^{-}$) from a higher excited state is specially favoured. The two-photon excitation and the consequence higher excited singlet or triplet state ($^{(1,3)}M_{n}$) can be achived by the following:

1. A successive absorption of photon via an intermediate state (either first excited singlet or triplet).

$$^{1}M_{0} \xrightarrow{h\nu} {}^{(1,3)}M_{1} \xrightarrow{h\nu} {}^{(1,3)}M_{n} \rightarrow (M^{+}e^{-}) \qquad \text{Equation 1.18}$$

2. A simultaneous absorption of two photon via a virtual state.

$$^{1}M_{0} \xrightarrow{2h\nu} {}^{1}M_{n} \rightarrow (M^{+}e^{-}) \qquad \text{Equation 1.19}$$

Where the superscript indicates singlet (^{1}) or triplet (^{3}) state and subscript denotes the respective electronis state (*e.g.* 0 for ground, 1 for first and n for higher). For more details, the author would suggest ref. [27].

Bimolecular reaction: This type of reaction covers different photoinduced reactions proceeding via the formation of an encounter complex. It can usually takes place either from the first excited singlet or triplet state and several types of chemical

reaction involving energy transfer, electron transfer, proton transfer, and addition reaction can subsequently take place by the following:

$$^{(1,3)}M_1 + R \rightarrow X + Y \quad \text{or} \quad ^{(1,3)}M_1 + R \rightarrow Z \qquad \text{Equation 1.20}$$

Where, *R* is the solvent molecule, an added reactant (such as proton donor, quencher etc.), an impurities, another dye molecule or atmospheric oxygen.

One possible pathway for photobleaching from the first excited singlet state is: when there has been a large increase in dipole moment during electronic excitation, a greater degree of interaction with the micro-environment could occur and some of this would be irreversible and responsible for photobleaching.

On the other hand, photobleaching from the excited triplet state, (ETS) can occur by several reaction pathways [29]. Once an ETS is formed from the singlet state, it may be depopulated by two pathways. Firstly and more importantly, the reaction of ETS with oxygen from the environment [30]. This reaction may involve electron/energy transfers from ETS to molecular oxygen. The electron transfer produces superoxide radical (O_2^-) and a cationic non-fluorescent state. On the other hand, energy transfer from ETS to molecular oxygen ($T^* + {}^3O_2 \rightarrow S + {}^1O_2$) produces a reactive singlet oxygen. This singlet oxygen is very reactive and immediately reacts with exposed group of fluorophores and produces irreversible non-fluorescent product [31]. And secondly, a fluorophore in the ETS itself is very reactive (triplet state has two unpaired electrons, which can act as a radical) and undergoes several irreversible reactions *e.g.* triplet quenching, electron transfer between two ETS, reaction between ETS and ground state fluorophore.

Photobleaching can also be observed in an inert atmosphere where no oxygen is present. The mechanism involves the reaction between the triplet state of a fluorophore and the matrix molecules or impurities present in the local environment. This type of non-oxygen mediated photobleaching was reported by several authors for fluorescein [30, 32-34].

Since photobleaching generally involves some form of chemical reaction and thus activation energy, it means that photobleaching is temperature dependant. Usually the photobleaching rate increases with temperature [35] because of the increase of

reaction rates responsible for photobleaching. In addition, additional reaction pathways could be activated at higher temperature leading to greater photobleaching.

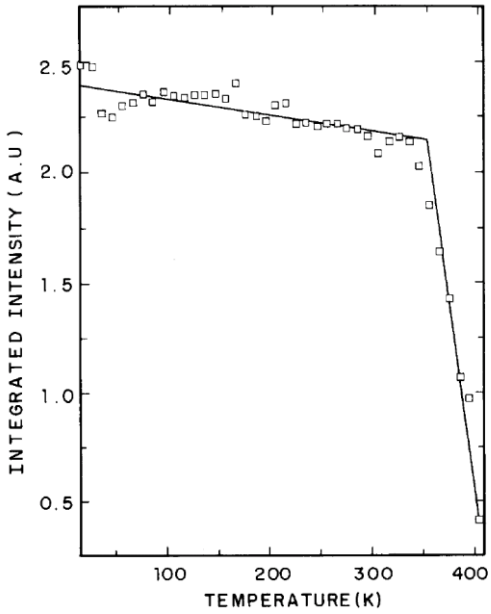

Figure 1.10: Integrated fluorescence intensity of FL doped PVA film as a function of temperature. The fluorescence intensity decreased with temperature and at T_g of PVA there was a sharp drop in intensity. Adapted from kind permission [36].

The temperature dependant photobleaching process in a polymer matrix is also dependent on the polymer glass transition temperature[1], T_g. For example, Dibbern-Brunelli *et al.* reported the temperature dependent photobleaching of fluorescein (FL) doped into 87% - 89% hydrolysed poly vinyl alcohol (PVA) film (FL-PVA) cast on a glass plate. The integrated emission intensity of FL-PVA decreased as a function of temperature. There was a clear inflexion in the plot observed at 350 K (Figure 1.10) which is the T_g of PVA. And after that a sharp decrease in intensity was measured which was associated with the increased mobility of polymer chains which caused quenching.

To the author's knowledge, most of the photobleaching kinetics of fluorophores in polymer thin films systems have been described in literature are fluorophores of xanthene groups (specially fluorescein in PVA polymer matrices) [26, 30, 37]. This photobleaching kinetics in polymer matrix generally can be described by using two models: B model and exponential model. From B model one could get

[1] Will be discussed in section 1.7

information about the decay constant of reaction and photobleaching quantum yield[2] (for more details see [30, 38]). On the other hand, the probability of a fluorophore surviving a certain number of excitation cycles before being photobleached is usually exponentially distributed. The exponential model represents the decrease of fluorescence intensity over time and is used to determine the rate constant and activation energy of the active photobleaching reaction.

The fitting of experimental photobleaching data to a specific exponential function depends on the fluorophore environments *e.g.* fluorophore concentration, temperature etc. For example, photobleaching of 0.1% fluorescein in PVA is mono-exponentially fitted above the T_g of PVA whereas bi-exponentially fitted at temperatures below the T_g (77 °C) [26]. The possible reason for this bi-exponential relationship is the existence of two different domains below the T_g in PVA. One region contains isolated fluorophores and is responsible for the lower rate of photobleaching. And the other contains closely located fluorophores (separated by Förster radii or less) which allow dye-dye (D-D) interaction between two neighbouring molecules and this is responsible for the faster rate of bleaching. They also concluded that this faster process involved triplet- triplet and triplet-ground state fluorophore interactions [26]. However, above the T_g, these two domains are equalized and work as a homogeneous viscous medium. The kinetics of photobleaching then can be described by the single exponential function at above T_g [39, 40].

1.4.10. Anisotropy

When a fluorophore is excited by polarized light, its emission may also be polarized. The degree of polarization can be expressed as its anisotropy. In homogeneous solutions, fluorophores usually have random transition dipole orientations in the ground state. When they are excited by linearly polarized light, the molecules which have an absorption transition moment (M_A) aligned with the electric vector of the incident light (E) will be preferentially excited. The excitation probability is proportionally related to the square scalar product of M_A and E, *i.e.* $\cos^2\theta_A$, in which θ_A is the angle between E and M_A [11]. Therefore, it will be a maximum when E is

[2] The quantum yield of photobleaching is the ratio between the number of molecules which have been photobleached and the total number of photon absorbed at the same time intervals.

oriented parallel to M_A of the fluorophore and will be the minimum at a perpendicular orientation.

Mathematically, this phenomenon of fluorescence anisotropy can be expressed either by Equation 1.21 or Equation 1.22 (for polarization) respectively.

$$r = \frac{I_{II} - I_{\perp}}{I_{II} + 2I_{\perp}} \qquad \text{Equation 1.21}$$

where r is the emission anisotropy, $I_{\perp}$ is the component of emission intensity when the emission polarizer is directed perpendicular to the excitation light and I_{II} is the emission intensity when the emission polarizer is parallel to the excitation.

As a polarization ratio/degree of polarization

$$P = \frac{I_{II} - I_{\perp}}{I_{II} + I_{\perp}} \qquad \text{Equation 1.22}$$

Since the difference of the emission component, *i.e.*$(I_{II} - I_{\perp})$ is normalised by the total emission intensity, the anisotropy value is dimensionless. Usually, in most cases, anisotropy (exception, *i.e.* study of radiative transfer) is preferred over polarization due to its simplicity in theoretical expression.

Anisotropy and polarization can be related by the following equation:

$$r = \frac{2P}{3 - P} \qquad \text{Equation 1.23}$$

The r value is directly related with the segmental mobility of macromolecules or better the rotational correlation time. Basically, anisotropy increases with molecular size (rotational correlation) and increasing viscosity. Hence this process is used to investigate the size and shape of the macromolecules and the viscosity/rigidity of the medium [13].

Fang *et al.* studied the conformational behaviour of PNIPAm by labelling it with acenaphthylene dye [41]. They also studied the effect of addition of urea into PNIPAm solution at its phase transition temperature by using fluorescence anisotropy. Below PNIPAm's LCST (Lower Critical Solution Temperature[3]), addition of urea has very little effect on anisotropy which is due to the coil structure of PNIPAm. However

[3] Will be discussed in section 1.7

above 31 °C, the r values changes differently with or without urea addition. Without urea, the PNIPAm structure is compact above the LCST and the corresponding anisotropy is high. The presence of urea, however, disrupts the intra-molecular H-bonding in PNIPAm causing a looser, less compact structure, as evidence by the lower anisotropy.

1.5. Measurement of fluorescence

Fluorescence measurements can be broadly classified into steady-state (most common) and time-resolved measurements [42].

1.5.1. Steady-state (S-S) measurements

In **steady-state measurements** the sample is illuminated by a constant beam of light and the emission or excitation spectrum is recorded by a spectrometer [43]. Usually, steady state spectra are collected under equilibrium conditions when all of the vibrational and solvent induced relaxations of the excited species are completed and the rate of excitation and emission under constant illumination are equal. The fluorescence emission spectrum is the wavelength distribution of the fluorescence intensity, measured at a single fixed excitation wavelength, and is usually plotted using either a wavenumber (cm^{-1}) or wavelength (nm) scale. The fluorescence intensity (I_F) of a single isolated fluorophore can be described by the following equation

$$I_F = \Phi_F I_0 (1 - e^{-\varepsilon l c}) \qquad \text{Equation 1.24}$$

Where Φ_F is the fluorescence quantum yield, I_0 is the incident light, ε is the molar extinction coefficient, l is the optical path length and c is the concentration of fluorophore [44].

A simple conventional spectrofluorometer is presented in Figure 1.11. The light source is generally a high-pressure xenon lamp which can provide a wide range of light wavelengths *i.e.* from ~250 nm to the infrared. The light from the xenon lamp is separated by an excitation monochromator into various wavelengths. The fluorescence spectrum is usually collected at right angles to the incident light and detected after passing through an emission monochromator by a photomultiplier. The output is usually presented in graphical form and stored digitally. Automatic scanning of wavelength is generally done by the monochromators which are computer controlled.

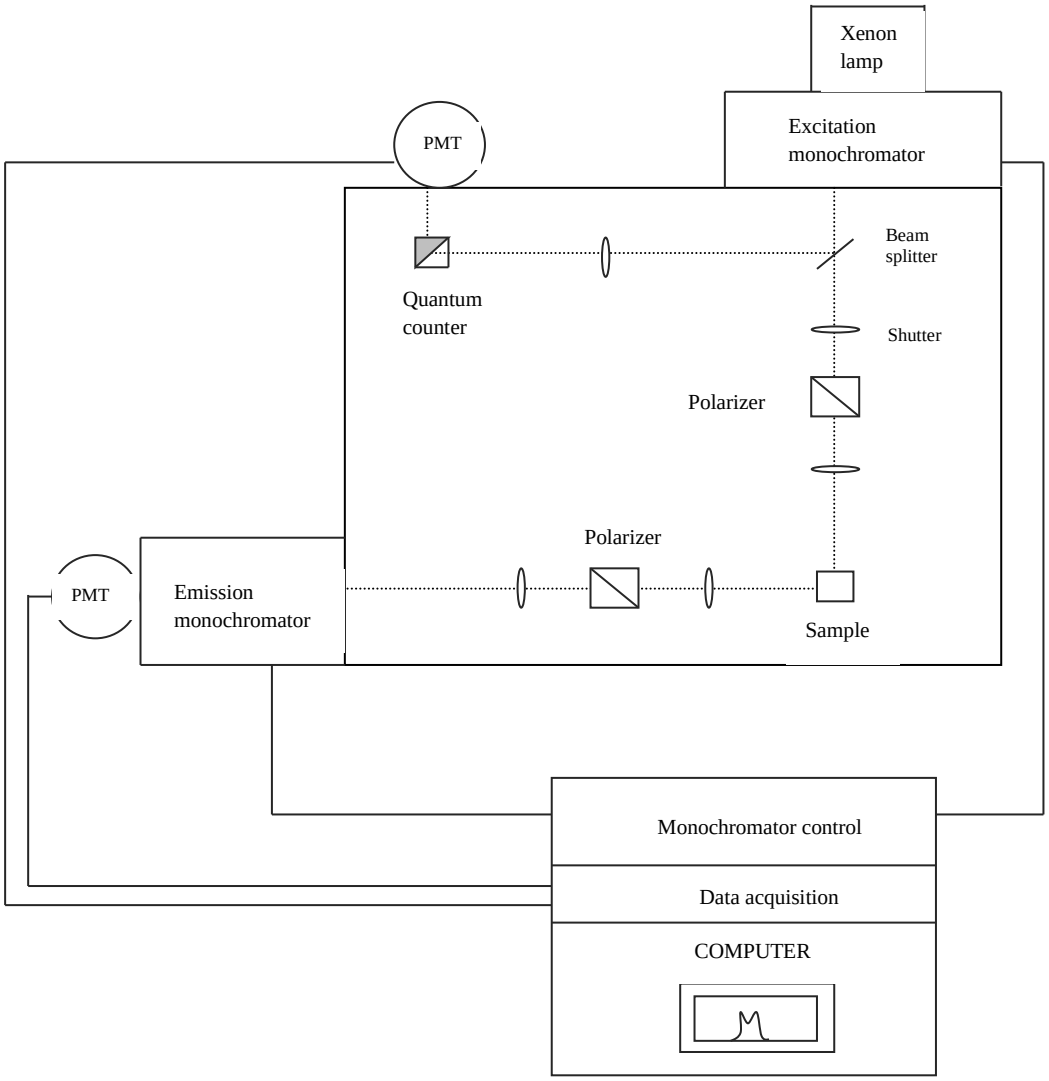

Figure 1.11: A schematic representation of a general purpose spectrofluorometer. After selecting the required wavelength by an excitation monochromator, the excitation light is split into two fractions: one part is passes through the reference channel and other fraction is passes through the sample. Finally the emission intensity is measures as a function of wavelength. In figure PMT is refers to the photomultiplier tube. Reproduced from ref. [11].

The optical module contains beam splitter, shutter, polarizer (if necessary), and sample holder. The purpose of the shutters is to eliminate the exciting light or to close off the emission channel. The beam splitter consisted of a quartz slide which can reflect a portion (~4%) of the incident light into a quantum counter or a photo diode. This quantum counter or a photodiode is used for measuring corrected excitation spectra. Polarizers can also be included on the excitation and emission light paths. Often the polarizers are removable and inserted only for the measurement of anisotropy.

1.5.2. Time-resolved fluorescence (TRF) measurements

The other types of fluorescence measurement are **time-resolved measurements** and one iteration is where the sample is excited by a pulse of light. This pulse is generally shorter than the decay time of the samples. TRF is most often used to measure intensity and anisotropy decay data.

The relationship between S-S and time-resolved measurements, is basically that the S-S observation is an average of time resolved phenomena over the intensity decay of the samples. For example, the intensity decay of a fluorophore with a single decay time (τ) can be expressed as:

$$I_{(t)} = I_0 e^{\frac{-t}{\tau}} \qquad \text{Equation 1.25}$$

where I_0 is the intensity at time t =0.

The relationship between steady state intensity (I_{ss}) and fluorescence decay time can be expressed by the following:

$$I_{ss} = \int_0^\infty I_0 \, e^{\frac{-t}{\tau}} dt = I_0 \tau \qquad \text{Equation 1.26}$$

I_0 is dependent on excitation light intensity, molar absorptivity of the fluorophore at the excitation wavelength, concentration, and quantum yield.

However in the case of mixture of fluorophores, or a fluorophore which has more than one decay component and cannot be described by single exponential decay law, then the intensity decay may be fitted by multi-exponential decay law:

$$I(t) = \sum_{i=0}^{n} \alpha_i \, e^{-t/\tau_i} \qquad \text{Equation 1.27}$$

where α_i is a pre-exponential factor which represent the amplitude of components, τ_i is the lifetime of each component, and n is the number of components [13].

There are two primary measurement methods for fluorescence lifetime. One is based on the time domain while the other is based on the frequency domain. In time domain method the fluorophores are excited by a pulse of light whose temporal width is as short as possible and preferably much shorter compared with the decay time of a fluorophore. The time dependant intensity drop is then measured after the excitation

pulse and the decay time is calculated from the slope of a plot of log I (t) versus t, and is defined as the time at which the intensity has decayed to 1/e of the original value (Figure 1.12). One of the most widely used methods for lifetime measurements are Time correlated single photon counting, TCSPC (time domain measurement; see Appendix I for more details about the measurement methods).

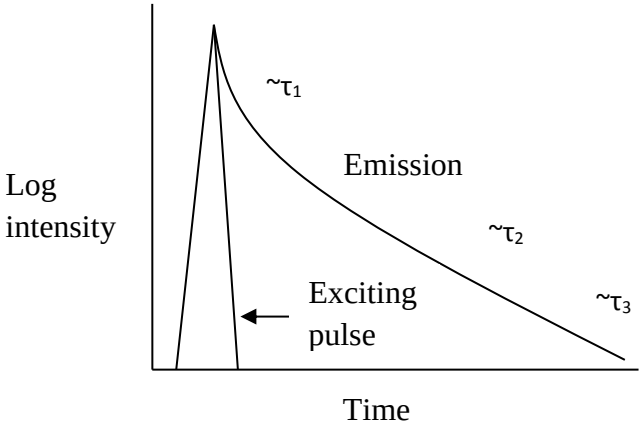

Figure 1.12: Time resolved decay curve of 3 components in a system, where τ_1, τ_2, and τ_3 represent the lifetime of each component. Reproduced from [13].

In the frequency domain/phase modulation method, the sample is excited by a sinusoidally modulated light; usually a sine wave (but could also be a square wave). The resultant fluorescence emission occurs at the same frequency as the excitation. Due to the time delay between absorption and emission, phase shifting and demodulation is observed in the emission [13, 45]. The lifetime can then be determined by analysis of the phase shift or demodulation of the emission light [13].

1.5.2.1. Average lifetime:

In many cases, the measured fluorescence decay does not correspond to a mono-exponential decay, either because: a) a single fluorophore exists in multiple species / environment (*e.g.* conformational changes during excitation) or b) more than one fluorophore in the system (*e.g.* crude oil, [46]) being studied. In this situation, the average lifetime is often used for easier interpretation. The two common average lifetimes (intensity weighted and amplitude weighted) describe different photophysical situations [47].

For the analysis of a single fluorophore having a multi-exponential decay curve, the intensity based average lifetime (known as intensity weighted average lifetime) is commonly used and can be expressed by:

$$\langle\tau\rangle_f = \frac{\alpha_1\tau_1^2 + \alpha_2\tau_2^2 + \alpha_n\tau_n^2}{\alpha_1\tau_1 + \alpha_2\tau_2 + \alpha_n\tau_n} = f_1\tau_1 + f_2\tau_2 + f_n\tau_n = \sum_{i=1}^{n} f_i\tau_i \qquad \text{Equation 1.28}$$

where f_i is the fractional contribution of the i^{th} component. Hence, this fractional contribution of each decay component is measured from τ_i and α_I value by the following equation:

$$f_i = \frac{\alpha_i\tau_i}{\sum_{i=1}^{n}\alpha_i\tau_i} \qquad \text{Equation 1.29}$$

Since each decay time is weighted by the total intensity (Equation 1.29), the average lifetime is termed the intensity weighted average lifetime.

Alternatively, for the analysis of samples with multiple fluorophores one should use an amplitude based lifetime which can be expressed by:

$$\langle\tau\rangle_a = \frac{\sum_{i=1}^{n}\alpha_i\tau_i}{\sum_{i=1}^{n}\alpha_i}$$

where α_i is the fractional amplitude and can be expressed as:

$$\alpha_i = \frac{\alpha_i}{\sum_{i=1}^{n}\alpha_i}$$

But we know $\sum_{i=1}^{n}\alpha_i = 1$, so the amplitude average lifetime is:

$$\langle\tau\rangle_a = \sum_{i=1}^{n}\alpha_i\tau_i \qquad \text{Equation 1.30}$$

1.6. Optical constants related to fluorescence properties

Fluorescence properties (*i.e.* emission intensity, fluorescence decay time) are dependent on a variety of factors apart from the structure and chemical, physical properties of the environment. Several physical properties (*i.e.* dielectric constant, electrical conductivity, refractive index) etc. also have an impact. One of the most

important optical properties is refractive index, RI (*n*), which is the ratio between the velocity of light in the vacuum (c) and the velocity of its in a medium (*v*):

$$n = \frac{c}{v} \qquad \text{Equation 1.31}$$

We know from the Maxwell's equation, the velocity of light in vacuum is $\frac{1}{\sqrt{\varepsilon_0 \mu_0}}$, where ε_0 and μ_0 are the permittivity (8.854×10^{-12} $C^2N^{-1}m^{-2}$) and permeability ($4\pi \times 10^{-7}$ $kg.m.C^{-2}$) of free space respectively. However in matter the velocity will be reduced and can be expressed as $v = \frac{1}{\sqrt{\varepsilon.\mu}}$. So the refractive index

$$n = \frac{c}{v} = \sqrt{\frac{\varepsilon.\mu}{\varepsilon_0 \mu_0}} \qquad \text{Equation 1.32}$$

Or, it can be clearly alternatively expressed by the Maxwell's equation for refractive index

$$n = \sqrt{\varepsilon_r \mu_r} \qquad \text{Equation 1.33}$$

where ε_r is the relative permittivity or dielectric constant of the medium and μ_r is the relative permeability.

1.6.1. Fluorescence lifetime as a function of RI

It is now well established that the radiative lifetime or the natural lifetime of a fluorophore is a function of refractive index of the medium. This relationship is represented by the Strickler-Berg equation which describes the relationship between the absorption and emission spectra to the radiative lifetime as follows:

$$k_r = \frac{1}{\tau_0} = 2.88 \times 10^{-9} n^2 \frac{\int I(v)dv}{\int I(v)v^{-3}dv} \int \frac{\varepsilon(v)}{v} dv \qquad \text{Equation 1.34}$$

Where τ_0 is the natural lifetime, n is the refractive index, I is the emission intensity, ε is the extinction coefficient, and v is the frequency of the transition in wavenumbers [48]. In an ideal case *i.e.* negligible Stokes shift and a perfect mirror image relationship between absorption and emission, the equation can be simplified to:

$$k_r = \frac{1}{\tau_0} = 2.88 \times 10^{-9} n^2 \langle \vartheta \rangle_{av}^2 \int \varepsilon(\vartheta)\, d\vartheta \qquad \text{Equation 1.35}$$

$\langle\vartheta\rangle_{av}$ is the average wave number corresponding to the 0-0 transition. The integral part of the above equation can be expressed as oscillator strength (f) where $f = 4.32 \times 10^{-9} \int \varepsilon(\vartheta)\, d\vartheta$. Now the equation can be written as:

$$k_r = 0.668 n^2 \langle\vartheta\rangle_{av}^2 f \qquad \text{Equation 1.36}$$

From the equation it can be predicted that the fluorescence lifetime of a fluorophore should be inversely related to the square of the medium refractive index, and thus will vary significantly with emission wavelength.

Several studies have shown the applicability of the three equations above. In the case of allowed transitions for fluorophores, the oscillator strength is almost same for all solvents. Hence, k_r is directly related to the square of the RI [49-52]. This relationship is important for the calculation of RI and the polarizability[4].

1.7. Polymers

Polymer is derived from two Greek words 'poly' meaning many and 'meros' meaning parts. Hence a polymer is a substance, which has long sequence of low molar mass base-units linked to each other by primary bonds (usually covalent) [53]. A polymer is a term synonymous with macromolecules that have long chains and large molecular weights. When polymers are formed from few monomer units, the resulting low molecular weight polymer is known as an oligomer. If the monomer molecule is A and –A- is the repeating/ base unit, then chemically the polymers can be represented as

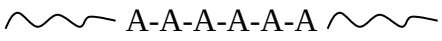

or

The process, by which the polymers are formed is called polymerization and the number of repeating units, 'n' (an integer), and called the degree of polymerization [53]. Polymers formed from the same monomers are called homopolymers whereas copolymers are those where two or more monomers are incorporated.

[4] Polarizability is the ability of relative charge distribution of a molecule and which resulted from the distortion its original shape by an external electric field. It is related to the refractive index by $P = (n^2-1)/(n^2+2)$

Natural polymers such as shellac, amber, wool, silk have been used for millennia whereas most synthetic polymers have been mostly developed since the start of the 20th century [54]. Bakelite, the first truly synthetic polymer was developed by Belgian-born chemist Leo-Baekeland in the early 1900s. The 1930s is considered as the birth of polymer science and the following 20 years saw an enormous development in polymer chemistry and the first commercial production was started for a large number of polymers *e.g.* polystyrene, nylon 6.6, polyethylene, polyvinyl chloride etc.

Polymers have diverse physical and chemical properties (*e.g.* can have high strength, conducting properties, biocompatible, biodegradable, highly corrosion resistance *etc.*). More importantly these properties are tuneable as well, for specific needs by modifying the chemical structure.

At room temperature, different amorphous polymers can have two distinctly different mechanical properties. For example, some amorphous polymers are hard and rigid glasslike materials *e.g.* polystyrene (PS), polyvinyl chloride (PVC) and some others are soft and rubbery *e.g.* polyisoprene, polybutadiene. When glasslike amorphous polymers are heated, the kinetic energy of the constituent molecules is increased and the polymers may be able to vibrate slightly, however up to a certain temperature, the segmental motion in which portions of the molecule wiggle around will remain locked. At a certain temperature, the polymer loses its glasslike properties and transforms into a rubber–like state. The temperature at which the change from the glassy state to rubbery state and vice versa (for rubbery amorphous polymer) takes place is known as the glass transition temperature T_g [55-57]. This transition is accompanied by a greater rotational freedom and segmental motion of constituent units, whereas the entire chain as a whole is at rest. On further heating, the whole chain begins to start moving and the temperature at which this begins is the melting temperature, T_m. Several factors can affect the T_g value of a polymer. One of the important aspects is the chemical structure, for example, if the polymer contains a bulky group in the polymer backbone, that may restrict rotational freedom, then a higher T_g is the consequence. Branching in polymer chains also cause an increase in T_g. Sometimes, polymer polarity influences T_g, which is due to more dipole-dipole interaction. For example, PVC has T_g at 81 °C wheras PVA it occurs at 85 °C. Molecular weight also has an effect on T_g because the higher the molecular weight the

in fewer chain end present and this leads to a lower free volume. For example the T_g of PS is 40 °C for an average molecular weight (MW) of 3000, but 100 °C for an average of MW 300,000 [56].

Biocompatibility and biodegradability are important characteristics of polymers. A polymer will be considered as biocompatible, if it allows the biological organism to function without any complications such as allergic reaction or other adverse side effects.

The use of both hydrophilic and hydrophobic polymers in biomedical science is widespread. In order to accommodate various functional demands, polymeric materials with desired physical, chemical, biological, biomechanical and degradation properties must be selected. Hence, research into the modification of existing polymers and research into the development of new polymeric materials for biomedical applications (*e.g.* tissue engineering, controlled drug delivery systems, implantation to the human body as foreign materials, dentistry, etc.) are growing very fast [58]. For biomedical applications, polymers are often classified according to their interaction with water: hydrophilic for those that interacts strongly, whilst hydrophobic refers to disliking water. However, there is no clear scale for hydrophilic/hydrophobic, rather it is a relative scale, and can be subjective.

1.7.1. Hydrophobic polymers

Hydrophobic means water fearing *i.e.* does not like water. A solid surface is generally regarded as being hydrophobic, when the surfaces are not wetted by water. Hydrophobicity is mainly dependent on the chemical structure of the material. If a polymer is formed entirely from hydrocarbons, they are usually hydrophobic. Some examples of the most hydrophobic polymers are polyethylene, polystyrene, polyvinyl chloride (PVC), polytetrafluoroethylene, and polydimethylsiloxane [59]. For example, PVC has very low water absorption properties; only about 0.048-0.08% water is absorbed when immersed in water at 23 °C for 24 h. Polytetrafluoroethylene absorbs only 0.005% water as measured by ASTM D570 method [60].

1.7.1.1. Polystyrene (PS)

PS is a polymer of covalently bound units of styrene monomer and was first commercialized by Dow in 1938. It is a high molecular weight linear polymer that is usually amorphous in nature. Its physical properties are mainly dependant on its MW

and the presence of additives. For example, high molecular weight PS is actually tougher and stronger. Small amounts of specific additives can be used to enhance the physical properties of PS. For example, in order to improve its mechanical properties, PS generally contains polybutadiene which is incorporated into PS matrix by block copolymerization.

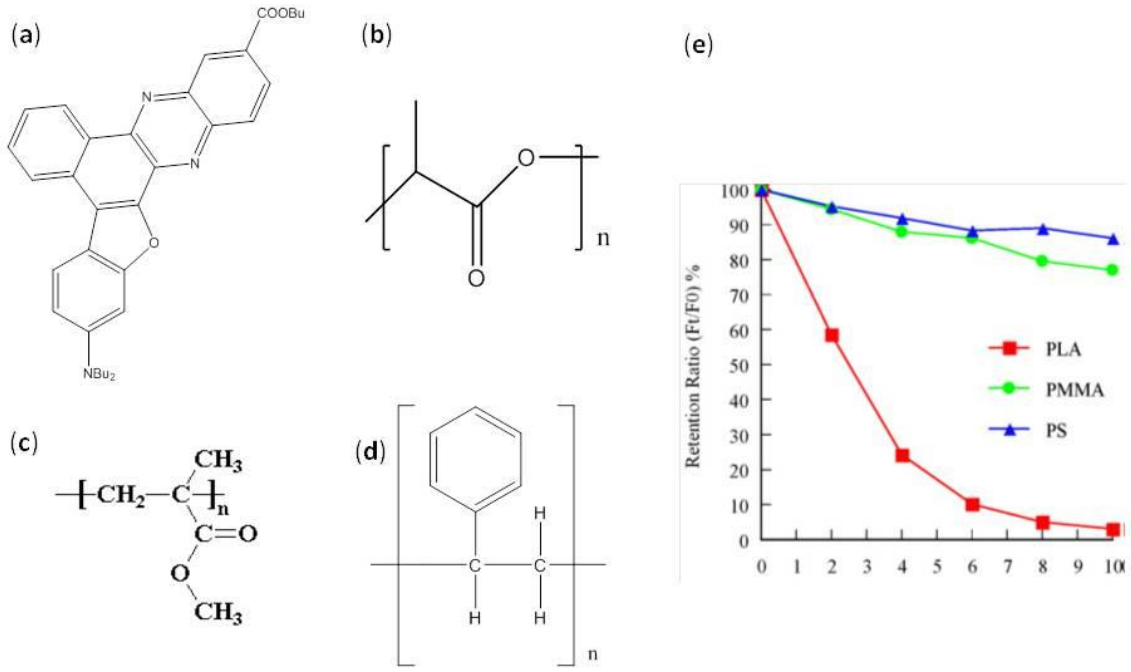

Figure 1.13: Structure of polycyclicphenazine-type D-π-A fluorophore (a), PLA (b), PMMA (c), and PS (d). The plot showing the comparative photostability study of polycyclicphenazine-type D-π-A doped different polymer films (e). Adapted from ref. [61].

Generally PS is a hard, rigid and transparent thermoplastic but when heated above its T_g it turns into a form that flows and can be easily used for moulding and extrusion. It has good electrical insulation properties *i.e.* very low electrical permittivity. Its dielectric constant[5] is 2.49-2.55 for amorphous PS and 2.61 for crystalline PS. The dielectric constant decreases with increasing temperature [62]. PS has a high RI (~1.59) compared to other polymers because of the high polarizability of the phenyl groups [60]. PS films can absorb 0.05% water at 50% RH (at 23 °C) temperature [60].

[5] Dielectric constant is known as the relative permittivity of a medium which is defined by the ratio of the electric field strength in vacuum to that of the given medium. Physically it means the ability of polarization by a material in an applied field of a given strength.

Ooyama *et al.* have studied the photophysics of a novel polycyclicphenazine-type D-π-A fluorophores by doping it into PS, polylactic acid (PLA), and polymethylmethacrylate (PMMA) polymer films [61]. The absorption properties of polycyclicphenazine-type D-π-A were not changed when incorporated into the polymer; however the emission properties were changed as a function of the polymer di-electric constant. They further reported that the fluorophore had a higher quantum yield doped into PS compared to PMMA and PLA. They also studied the photostability of fluorophore doped polymer thin films (100 µm) by irradiation with 300-800 nm light and presented the photostability as a retention ratio[6] (Figure 1.13e). The fluorophore doped PS and PMMA show higher photostability compared to PLA (the reason behind that was not described).

1.7.2. Hydrophilic polymers

Hydrophilic polymers are a group of polymers that exhibit strong interaction with water and can be characterized by either solubility in, or compatibility with water [63]. The presence of oxygen (in functional groups) can often be linked to their hydrophilicity. Oxygen having a lone pair of electrons, and being electronegative is good at forming H-bonds. Therefore, if oxygen is available for H-bonding to water in a polymer it will determine the degree of hydrophilicity. This can be either be an increasing ability to absorb water or a propensity to dissolve in water. Some hydrophilic polymers contain nitrogen atoms which have two lone pair electrons and also form inter-polymer H-bonds. Some examples of hydrophilic polymers are acrylic (acrylamides and acrylates) polymers, amine functional polymers, vinyl acids, and vinyl alcohols.

1.7.2.1. Polyvinylpyrrolidone (PVP)

PVP is a water soluble, linear non-ionic polymer and is produced from monomer N-vinylpyrrolidone. It has good film forming properties, and the cast films are hard, glossy and transparent. PVP films allow the permeation of oxygen and have high water absorption properties. The amount of water absorption by PVP polymer films is about 33% of its relative humidity [64]. The RI of PVP films at 25 °C is 1.53.

[6] Retention ratio $=F_t/F_0$, where F_t is the fluorescence intensity at time t and F_0 is the intensity at time t=0

Industrial application includes: increase the strength of paper in paper industries, used as a binder in pharmaceutical industries, as a lubricant in some eye drops etc.

Sen *et al.* studied the solvation dynamics of 2,6-p-toluidinonaphthalene sulfonate (TNS) in PVP solution (in water) by using S-S and TRF techniques [65]. TNS is generally sensitive to formation of ICT state in water environment and thus a reduction in fluorescence intensity. However, they found a large increase of emission intensity when it was measured in concentrated PVP solutions. This is attributed to PVP shielding TNS from the bulk water, thus suppressions of non-radiative ICT. For this reason the TNS emission intensity as well as quantum yield increases with increasing PVP concentration in aqueous solution (Figure 1.14).

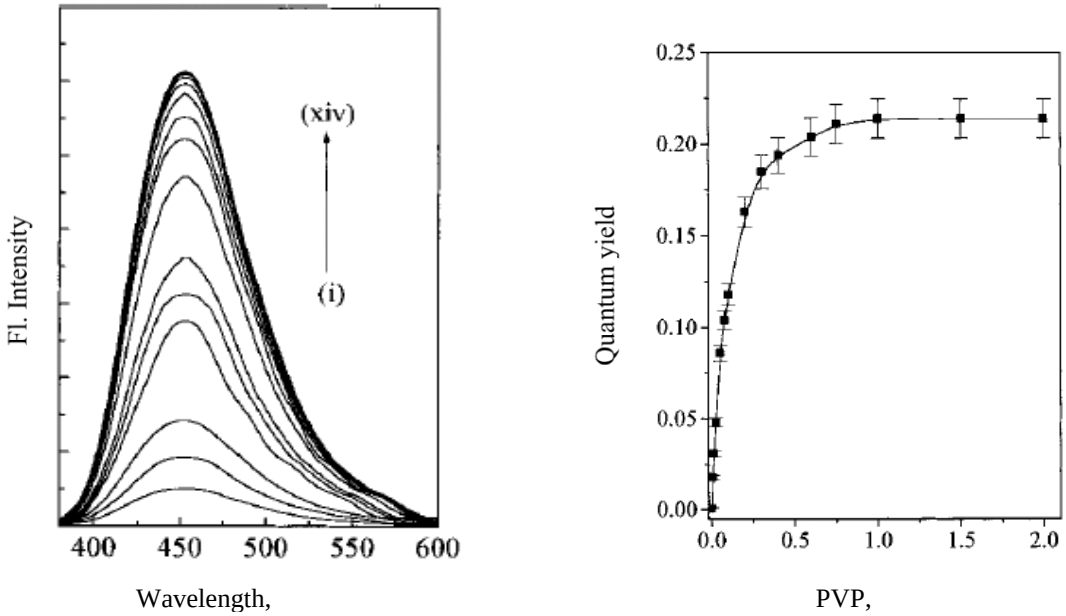

Figure 1.14: Fluorescence steady state emission properties (a) and quantum yield (b) of TNS in different concentration of PVP 0.006, 0.012, 0.025, 0.05, 0.075, 0.10, 0.20, 0.30, 0.40, 0.60, 0.75, 1.0, 1.5, and 2.0 wt%. Adopted from kind permission from ref [65].

1.7.2.2. Poly vinyl alcohol (PVA):

PVA is a water soluble polyhydroxy polymer and was first prepared from polyvinyl acetate in 1924 by Herrmann and Haehnel [66]. It is hydrophilic in nature, semicrystaline, thermally, and chemically stable polymer [67]. It's ability to crystallize is the most important parameter that controls the solubility and sensitivity to water, tensile strength and thermoplastic properties [68]. It has excellent chemical resistance, optical and physical properties, and good film forming capability which makes it a

versatile polymer with many uses [25, 69, 70]. It exhibits a high degree of swelling[7], and its nontoxic and biocompatible properties make it suitable for application as a hydrogel in controlled release carrier of drugs [71-73].

Like many other synthetic polymers, PVA cannot be prepared from its monomer (vinyl alcohol) due to its unstable nature causing it to form a tautomer[8] of acetaldehyde. Hence, PVA is produced, first by the polymerization of vinyl acetate to poly vinyl acetate (PVAc), which is then followed by hydrolysis to PVA (Figure 1.15). The hydrolysis does not go to completion; in essence PVA is always a mixture of copolymers of PVA and PVAc (partially hydrolysed PVA contains the residual acetate group).

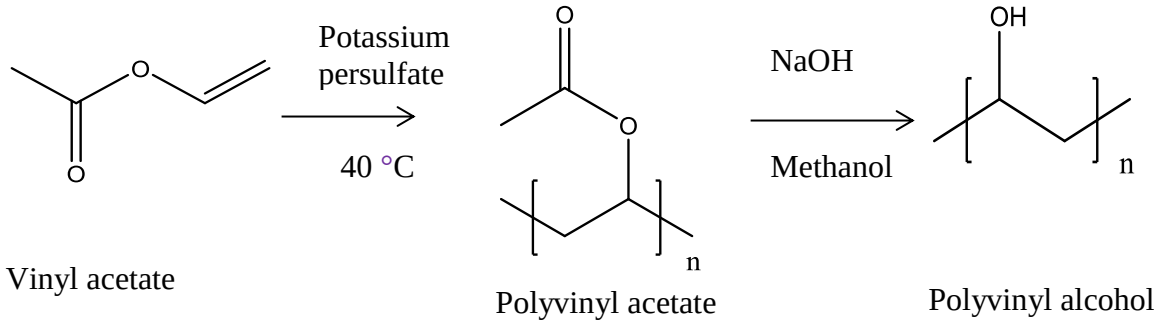

Figure 1.15: One most widely used methods for the production of PVA. Reproduced from [74]

PVA films and water

PVA can be employed in several different ways depending on the application. PVA (pure PVA or PVA blended with other polymers) thin films are often encountered on medical devices and as coating a drugs [75, 76]. In this physical form, the interactions with water need to be considered. Water absorption into hydrophilic polymers such as PVA influences the polymer's physicochemical properties. This water adsorption into polymer films depends on intermolecular forces *i.e.* electrostatic, directional, and inductive forces as well as the H-bond forces between the functional

[7] The extent to which, a polymer can swell rather than dissolve, when they are come into contact with a solvent. It is a measure of crosslinking/3D structure of corresponding polymer, i.e. a highly cross linked polymer has weaker swelling ability.

[8]A tautomer is one type of constitutional isomer, where two forms of a molecule are readily interconvertible by intramolecular migration of an atom/a group and exist in equilibrium.

groups in the polymers and absorbed water molecules [77]. Water absorption causes hydrophilic polymers to swell and elevates the mobility of individual polymer chains.

Due to the chemical and physical interaction between hydrophilic polymers and water, the behaviour of water is changed when absorbed into the polymer. This absorbed water has different thermodynamic properties compared to bulk liquid phase. For example, the absorbed water molecules in hydrophilic polymers are generally not crystallized at 0 °C. Based on the thermodynamic properties changes for water, three states of water may be present in hydrophilic polymer matrices [78, 79]. Type 1 possesses similar thermal phase transitions as bulk water and is known as 'free water'. Type 2 is known as the 'freezable bound water' which possesses a shifted thermal phase transition compared to bulk water (usually lower than 0 °C). Type 3 is called 'non-freezing water 'and does not crystallizes over a certain range of temperature (even when the swollen sample is cooled down to -100 °C). This odd behaviour can be explained by the confinement of water molecules in the polymer matrix or when there has been a strong interactions between the water molecules and the polymer. All three forms of water have been observed in PVA films [80].

Ping *et al*. [81] studied the presence of different water states in PVA films and tried to correlate with the extent of interaction with the –OH group of PVA. They first made the films and injected predetermined amounts of water and then incubated for 24 h at 303 K to attain equilibration in a tightly sealed environment. They used a differential scanning calorimeter[9] with a cooling system to measure the phase transition of water, and FTIR to see the interaction of polar sites in the polymer with the absorbed water. At the initial stage of water absorption, only the non-freezable water was present. Incoming water molecules were bound with the polymer –OH groups and no water was present in a freezable state. The maximum quantity of non-freezable bound water was a characteristic property of the polymer and for PVA, it was 25 wt% water content (Figure 1.16). They further added that, there were two types of H-bond present in water exposed polymer systems, one was directly attached to the

[9]Differential scanning calorimeter is a tool for thermal analysis. It works generally by the principle of measuring the amount of heat absorbed or released during a transition such as melts, phase change, glass transition, and curing.

polar group of polymers and water, and other were the water molecules included in the second hydration shell.

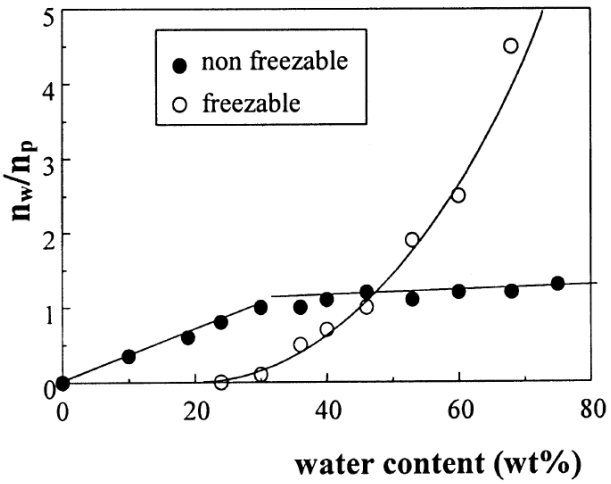

Figure 1.16: The variation of freezable and non-freezable bound water as a function of absorbed water content in PVA films. Where, the n_w/n_p is molar ratio of freezable and non-freezable bound water. Only the non-freezable bound water is present in PVA films up to ~25% water content which is due to the formation of H-bond between the incoming water and –OH groups of PVA. Adapted from ref. [81].

Tamai *et al*. studied the interaction between polymers and water by performing molecular dynamics simulations of hydrogel models of PVA and PNIPAm at different % water [82]. At different % content of water in a hydrogel, they categorized the water molecules (based on their position) into three types within the polymer hydrogel system:

1) those around the hydrophilic groups (-OH, -O-, and -CONH),

2) those around the hydrophobic groups (=CH-, $-CH_2$, $-CH_3$) and

3) those in the bulk region *i.e.* inside the polymer.

The number of water molecules present in the different regions depends on polymer structure as well as the wt% water in the system. For example, at 25% water (wt%) and at 300 K, about 5 times more (compared to hydrophobic) water molecules are present in the hydrophilic part of PVA, whereas in PNIPAm the number of water molecules are almost same both in hydrophilic and hydrophobic part (*e.g.* 111.7, 23.4, and 14.9 were the number of water molecules in hydrophilic, hydrophobic and bulk region respectively for PVA, whereas this number was 71.7, 71.0, 7.3 in hydrophilic, hydrophobic and bulk region respectively for PNIPAm).

Hou and Higgins studied the dynamics of the Nile red (NR) fluorophore in PVA thin films surface (a few hundred nm thickness) as a function of ambient relative humidity by single molecule studies [83]. They acquired the single molecule images using a scanning confocal microscope. The NR images were bright round spots at low humidity and it started to change to predominantly streaks from around 75% RH which thus sharply increases the amplitude and frequency of time-dependant signal fluctuations for NR single molecules. At lower humidity, PVA films provide a relatively rigid environment (due to their intermolecular H-bonding) for NR. However, this H-bonding is readily broken with the incorporation of water into the films at higher humidity. At 78% RH, an appreciable amount of water is adsorbed onto the PVA film surface and penetrated as well into the film and thus the film becomes swollen. As a result, the PVA films provide a more fluid environment around the NR molecule. This increase in NR mobility was quantified using the single molecule detection method.

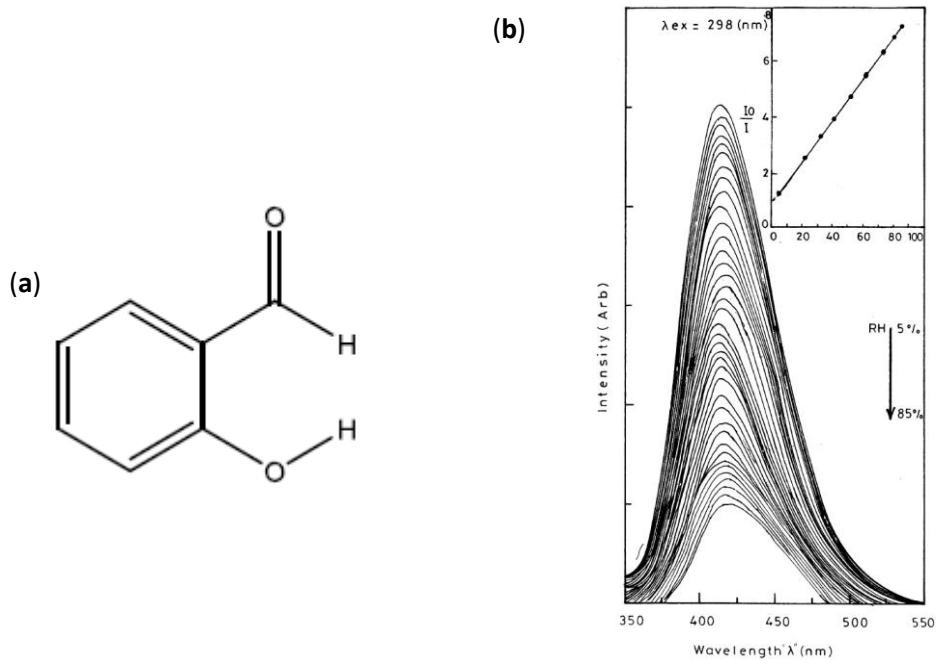

Figure 1.17: The structure of SA dye (a). (b) The intensity drop of SA dye doped PVA film as a function of RH. The inset plot is the Stern-Volmer derivation where I_0 is the fluorescence intensity in the absence of quencher *i.e.* water and I is the fluorescence intensity in the presence of quencher (at different humidity) [84].

Mishra *et al*. studied the photophysical behaviour of salicylic acid (SA) doped PVA films by S-S and TRF measurements as they explored the possibility of using SA doped PVA films as a sensor for humidity [84]. Upon exposure to moisture, the SA doped PVA film did not show any significant changes in the shape of the absorption

or emission bands, but the fluorescence intensity decreased due to water absorption (Figure 1.17). These drops in intensity were due to 1) water-induced quenching of SA fluorescence and 2) the decrease of SA concentration due to water absorption by the PVA films. The absorbed water forms H-bonds with SA in the excited state and when there is sufficient water absorption, transfer of a proton (from water) to the phenolate oxygen occurred and the fluorescence intensity was quenched as a consequence. Additionally, with the increase in absorbed water, the volume of the PVA matrices was increased which decreased SA concentration and thus drop in intensity.

1.7.3. Smart polymers

A polymer which can change properties (*e.g.* surface characteristics, shape, solubility etc.) dramatically with a small variation of its microenvironment (*i.e*. pH, temperature, ionic strength, electric or magnetic field, light and or chemical and biological stimuli), is known variously as smart/intelligent/stimuli responsive/environmental sensitive polymer. One type of a smart polymer changes its water-interaction behaviour in response to a stimulus such as temperature *i.e.* a polymer can change from hydrophilic to hydrophobic (or vice versa). These properties make them suitable for use in drug delivery, gene delivery, tissue engineering, and biosensors [85-96].

There are three main classes of smart polymers [94, 97, 98] according to their physical form (Figure 1.18):

i. **Linear free chains in solution.** Polymers of this kind undergo reversible chain collapse, when an external stimulus is applied. These type of polymers need to maintain a delicate balance between hydrophilic and hydrophobic components in their structure for phase transition to occur.

ii. **Chain absorbed or surface grafted form.** When a specific external stimulus is changed, this type of polymer reversibly adsorbs or collapses on a surface and respectively transforms the interface from hydrophilic to hydrophobic.

iii. **Covalently cross-linked reversible and physical gels.** These types of smart hydrogel can be either a microscopic or macroscopic network and on which swelling or shrinking behaviour is environmentally triggered.

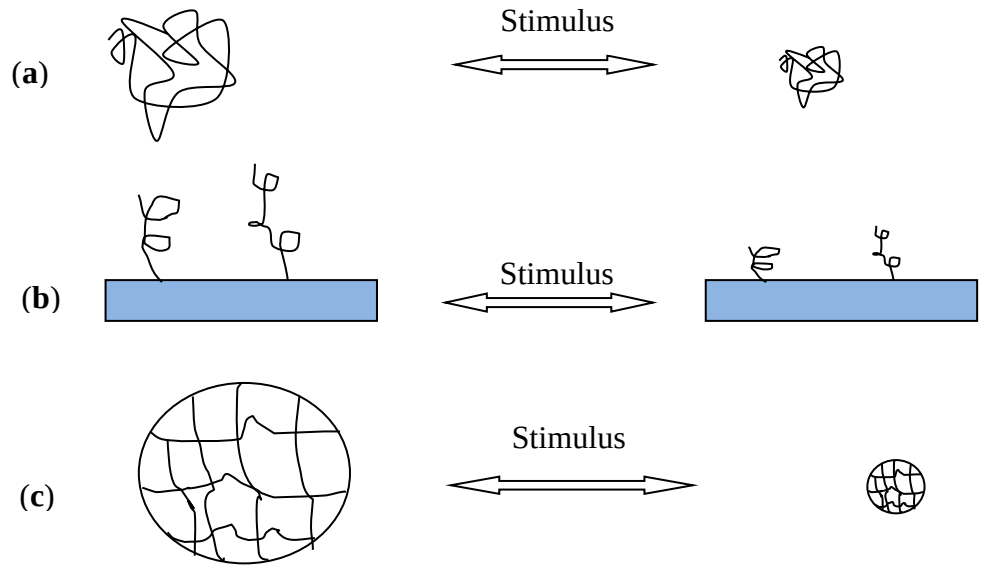

Figure 1.18: Three different types of smart polymers according to their physical form. Where (a) Linear free chains in solutions, (b) Chain absorbed or surface grafted form and (c) Covalently cross-linked reversible and physical gels. Reproduced from [99].

The choice of smart polymers for biomedical applications (*e.g.* locally controlled release of drugs) is mainly dependent on the physiological conditions (external stimulus) in the human body. For example, the human body shows variation on pH in the gastrointestinal tract and some specific areas *i.e.* tumour cell or sub-cellular compartments [100]. The temperature also plays a vital role for the choice of smart polymers in biomedical applications. Therefore, pH and temperature sensitive smart polymers are generally favoured in biomedical applications and the latter one is the most widely studied among the stimuli responsive polymers [4].

1.7.3.1. Thermoresponsive polymers and phase transition

This type of polymer undergoes conformational changes in response to temperature and exhibit a critical solution temperature (CST). In a temperature-composition phase diagram, the CST is the specific temperature where the distinction between two co-existent phases vanishes. There are two main types of thermoresponsive polymers; one group exhibits a lower critical solution temperature (LCST) whilst the other exhibits an upper critical solution temperature (UCST), Figure 1.19. Polymers that possess a LCST are soluble in a solvent (*e.g.* water) below the transition temperature. The solution will become insoluble just above the LCST [101] and phase separation will occur (Figure 1.19). Examples of polymers having a LCST

are poly (N-isopropylacrylamide), (PNIPAm) and poly (N, N-diethylacrylamide) (PDEAAm) [102, 103].

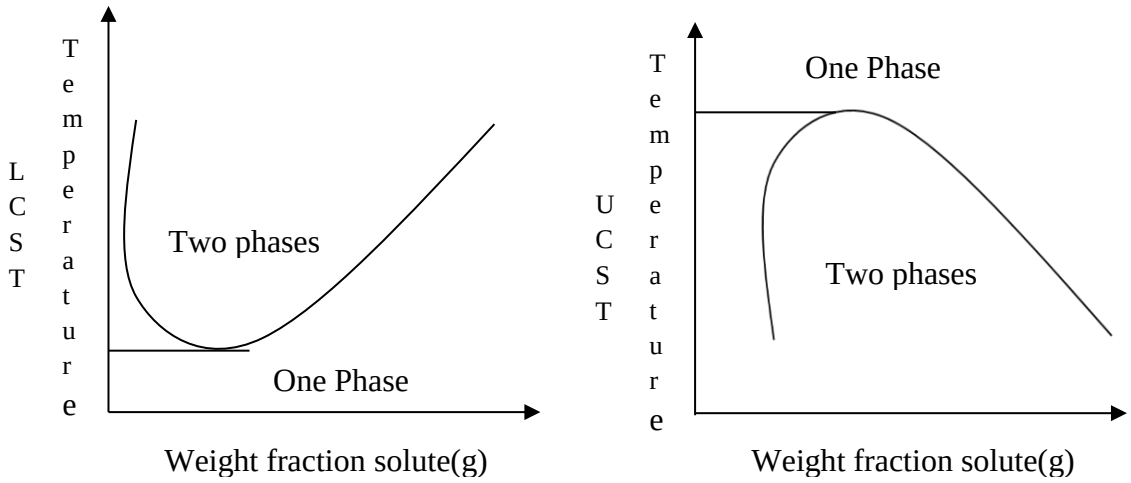

Figure 1.19: Temperature-concentration plots showing phase separation of LCST and UCST polymers. Polymers having a LCST exhibit two phase above the LCST and one phase below the LCST, whilst a polymer with a UCST exhibits one phase above the UCST whilst two phase below the UCST in solution. Reproduced from ref. [104] .

On the other hand, polymers whose solubility is increased with an increase in temperature have an UCST. Therefore, this type of polymer shows a clear homogeneous solution above the UCST and becomes biphasic below the UCST. In comparison to the frequently observed LCST, the UCST behaviour of polymers in water is rare. This behaviour originates from either a strong polymer-polymer interaction (*i.e.* electrostatic interactions) or solvent-solvent interaction (*e.g.* interaction between water-organic solvent mixtures) rather than a weak polymer solvent interaction [105]. In addition, UCST can occur when the solvent properties are changed upon heat treatment *e.g.* such as for non-ideal alcohol-water mixtures (decrease in polarity upon heating). For example, based on this phenomenon poly (2-oxazoline) have been reported to show a UCST phase transition in alcohol-water mixtures over a wide temperature range, 0 – 100 °C. The most well-known polymer-polymer interaction/ electrostatic interaction based UCST polymers (in water) are the poly (betaine)s, a type of zwitterionic polymer. Some examples are poly (2-dimethyl (methacryloxyethyl) ammonium propane sulfonate (PDMAPS-MA) and poly (3-(N-(3-methacrylamidopropyl)-N, N-dimethyl) ammonium propane sulfonate (PDMAPS-MAM). When there are no ionic impurities in the polymer (*e.g.* by the partial hydrolysis of the side chains) the primary amide groups in the side chain of the

polymers can induce UCST behaviour based on inter-polymer H-bonding interactions. Some common examples of this type of polymers are poly(methylacrylamide) (PMAm), poly(N-acryloylglycinamide) (PNAGA), poly(acrylamide) with hydrophobic co-monomers [105].

PNIPAm. PNIPAm is a thermoresponsive polymer and is probably the most widely studied [4, 102, 106-111]. It is soluble both in water and ethanol separately but insoluble in a mixture of water and EtOH. In other words the PNIPAm polymer may be precipitated out/phase separate below the LCST (Figure 1.20) [101, 102]. H.G. Schild explains that this is due to the complexation of water with EtOH is more preferable than polymer-EtOH complexation.

In solution the physiochemical properties of PNIPAm depend on polymer-polymer and solvent-polymer interactions. It displays a reversible temperature-dependent solubility behaviour *i.e.* it is water soluble at the temperatures below 32 °C but is insoluble and undergoes a phase separation at the temperatures above 32 °C (Figure 1.20) [112]. Below the LCST, it exists in a coil like form but when the temperature is raised to above the LCST, it converts to a globule form and forced its solution water from the matrix. By using this important phenomenon researchers have studied its potential use in tissue engineering [113, 114] and controlled drug delivery system [115, 116].

PNIPAm has a carbon backbone which contains both hydrophilic (carboxylic, amide) and hydrophobic moieties (isopropyl group). Below the LCST, the water-polymer interaction is stronger than the polymer-polymer interaction and thus PNIPAm remains soluble in water. The solvation of PNIPAm with water is driven by the enthalpic gain from strong H-bonding between the amide group of PNIPAm and water molecules [103, 117] which generates the coil structure.

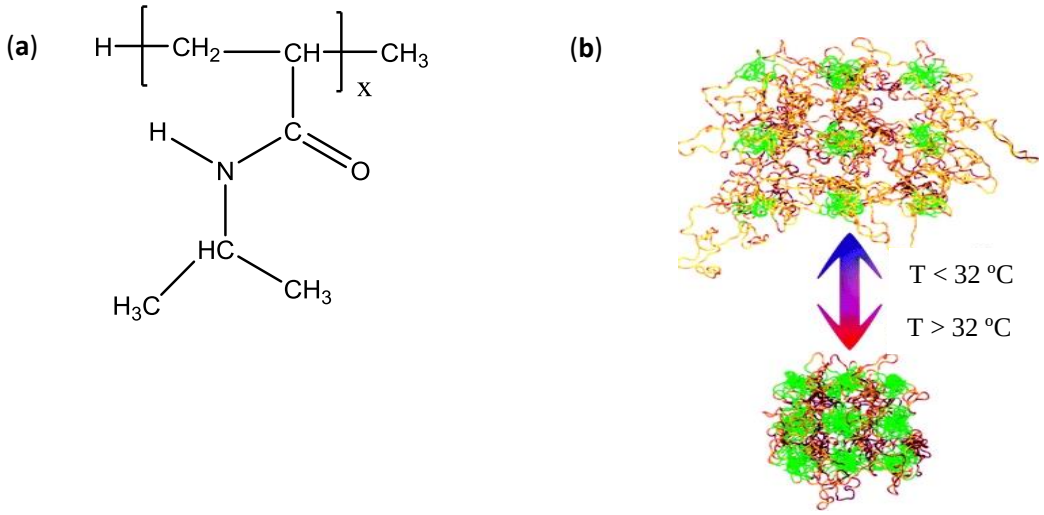

Figure 1.20: The structure of PNIPAm (a). The phase change of PNIPAm at below and above the LCST (b). Taken from ref. [118].

However, above the LCST, H-bonding between water and polymer is hindered, leading to increased intra- and inter-polymer H-bonding. As a consequence, the hydrophobic interactions within the polymers dominate the system, and eventually a globular structure is formed. In a different way we can say that at temperatures above the LCST, intramolecular hydrogen bonding between carboxylic and amide groups begins to dominate due to the interruption of H-bonding of these groups with water. Thus at the LCST, PNIPAm undergoes a sharp and reversible coil-to-globule transition from a hydrophilic to a more hydrophobic state [102, 119-124].

1.8. Thermoresponsive polymer thin films and their characterization

The use of thermoresponsive polymers as micrometer thin films (<100) has biomedical applications such as for local drug delivery [1, 2], cell sheet engineering [3], microfluidic devices [125-128], bioadhesion mediators [128, 129], and bioactuators [130-132]. If one uses the polymer as a thin film then one needs to know not only the thickness of the film but the physicochemical nature of the polymer. One of the most common methods employed for characterizing polymer thin films is the contact angle method (CAM). CAM is widely used to quantify the degree of hydrophobicity for material surfaces. Ingress of moisture into thin polymer systems is a common phenomenon which can significantly alter the physicochemical properties when they are used in biomedical applications [133]. For example, PNIPAm thin films can absorb significant amounts of water from the surrounding microenvironment above and below the LCST [4]. This water infiltration may considerably alter the

physico-chemical properties of the polymer, which in turn will have adverse effects on the final intended function of the polymers for example, in the case of drug delivery it can affect: drug elution rate, long term storage, device efficacy etc. [134]. In some medical devices, there are complex and small surface geometrics present over which thin films are deposited. In such cases *in-situ* CAM are not always possible. Thus optical spectroscopy could be the better approach for physicochemical characterization of polymer thin films.

1.8.1. Optical spectroscopy

Optical spectroscopy is a versatile tool for investigating polymer characteristics such as the chemical structure and orientation of molecular units of polymers, electronic and vibronic excitations, and relaxations of polymer chains, optical constants such as absorption coefficient & RI [135, 136], and changes in physicochemical properties of polymer due to micro-environmental changes [4]. The most important optical spectroscopies are vibrational and electronic spectroscopies. Vibrational spectroscopies like near infrared (NIR), Fourier transform infrared (FTIR) and Raman are often used for physicochemical analysis of thin polymer films. Electronic spectroscopies like UV-vis absorption or fluorescence spectroscopy can also be used, but in these cases one also often needs to use a probe molecule that is sensitive to changes in polymer properties. In a condensed polymer system (*e.g.* thin film), multiple factors (*i.e.* polarity, pH, temperature, H-bond and many more) may influence the system at the same time. All three may result in changes in absorption/emission properties (*e.g.* changes in intensity, shift of absorption/emission spectra, anisotropy and or fluorescence lifetime). Due to the high sensitivity and selectivity of probes to their microenvironment, non-destructive nature, and short response time of the techniques, electronic spectroscopies have been become popular for investigating condensed polymer matrixes [4]. One can easily get access to information about physicochemical changes via UV-visible spectroscopy with the use of suitable indicators, the method is known as solvatochromism.

1.8.1.1. Solvatochromism

Changing solvent polarity can affect the position, intensity, and shape of absorption and/or emission bands. This effect is known as solvatochromism. Generally, a hypsochromic/blue shift corresponds to negative solvatochromism and a

bathochromic/red shift corresponds to positive solvatochromism with the increase in solvent polarity. This solvatochromism is caused by the differential solvation of the ground and the first excited state of the chromophore/fluorophore. Negative solvatochromism (hypsochromic/blue) is observed, when the ground state of a molecule is more stabilized by solvation than the first excited state of the molecule [137]. On the other hand, if there is a better stabilization of the excited state compared to the ground state with increasing solvent polarity, then positive solvatochromism occurs (Bathochromic/red shift).

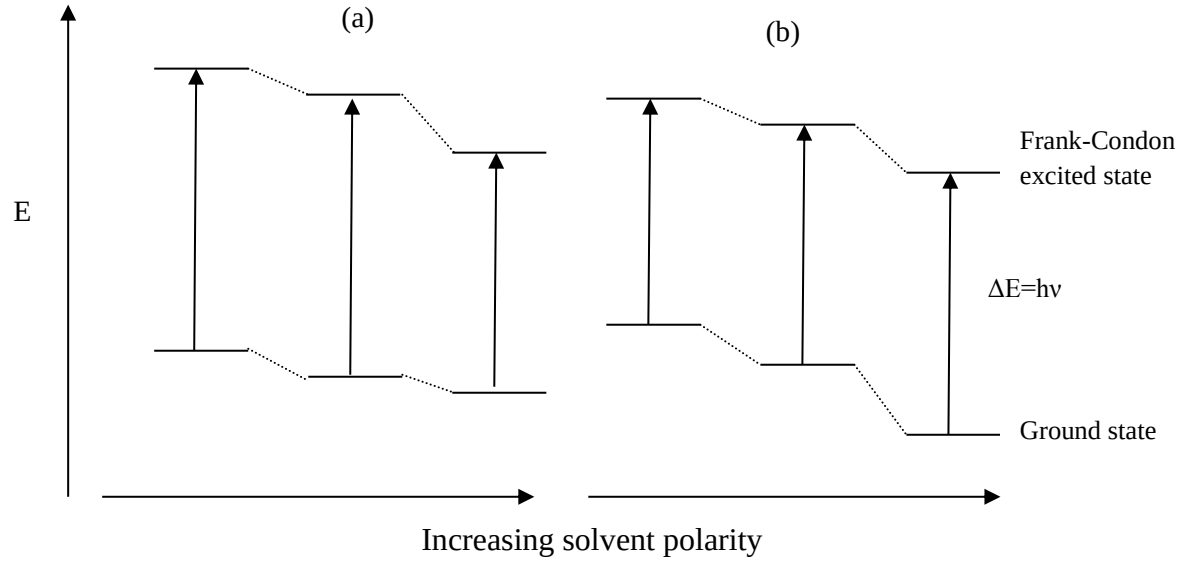

Figure 1.21: Schematic presentation of solvent polarity effect on the electronic transition energy of dipolar solutes. Where (a) shows positive solvatochromism (bathochromic/red shift) which means the transition energy is shifted to lower enrgy *i.e.* longer wavelength with increase of solvent polarity and (b) shows the negative solvatochromism (hypsochromic/blue shift) which means the transition energy is shifted to higher energy *i.e.* shorter wavelength with increase of solvent polarity. Reproduced from ref. [138].

The physical basis for this solvatochromism is the strength of the intermolecular solute (*e.g.* chromophore)/solvent interaction *(i.e.* electrostatic force such as dipole-dipole interaction) in the equilibrium ground state and Franck-Condon excited state. In general, molecules which display large changes in permanent dipole moment between ground and excited state tend to show strong solvatochromism. If the solute dipole moment is increased during electronic excitation, a more polar solvent will better stabilize the excited state than the ground state. So the energy difference between the equilibrium ground state and the excited state will be decreased, positive solvatochromism is the consequence (Figure 1.21a). And in the case of a decrease of

solute dipole moment during electronic excitation negative solvatochromism results (Figure 1.21b). Apart from the changing of dipole moment upon excitation, the magnitude and type of solvatochromism is also affected by the ability of a solute molecule to donate/accept H-bond to or from the surrounding solvent molecules in its ground and Franck- Condon excited state [139, 140].

There are several empirical scales for measuring solvent polarity, including the Z scale of Kosower [141], the π^* scale of Kamlet, Abboud and Taft [142], the π^*_{azo} scale of Buncel *et al*. [143] and the $E_T(30)$ scale of Dimroth and Reichardt [144]. The Py (or pyrene) scale of Dong and Winnik [145] is also important. These solvatochromic methods are generally robust and often used to investigate solvent systems but can also be used for polymer thin film characterization.

Szczupak *et al.* studied hydrogen bond donor/acceptor properties for a series of thermoresponsive N-isopropylacrylamide/N-tert-butylacrylamide (NIPAm/NtBA) co-polymer films using different solvatochromic parameters such as $E_T(30)$, α, β, π* with a variety of solvatochromic probes. $E_T(30)$, α, and π* values decreased with the increase in hydrophobic NtBA fraction but β was relatively unchanged (Figure 1.22). Finally, it was reported that there is a good correlation between experimental $E_T(30)$ and independently determined α, β, π* [146] (Figure 1.22). Matsuguchi *et al.* also reported a linear relationship between E_T (30) and α, β, π* during investigation of water sorption in the poly-(ethylene oxide) film.

Although solvatochromism is able to give accurate information about changing microenvironments in polymer thin films, the high concentration requirement (typical weight ratios of fluorophore : polymer is 1: (36-20) [77]) for many applications is a disadvantage, which could be solved by using fluorescence spectroscopy which is potentially much more sensitive (typical weight ratios of 1900-2230 to 1, [134]).

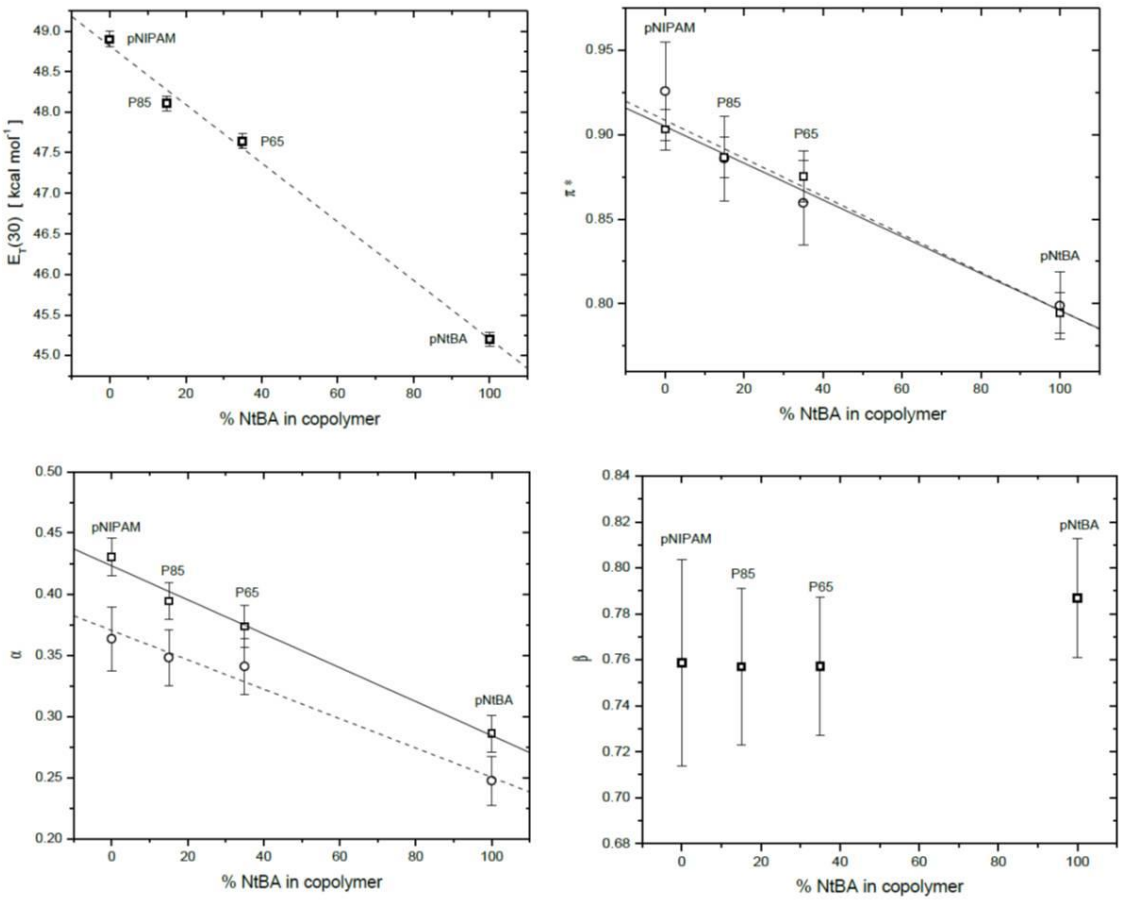

Figure 1.22: Plot showing the correlation of $E_T(30)$ with other parameters of solvatochromism such as α, β, π* of thin film prepared from poly(NIPAm –co- NtBA) with increasing %NtBA fraction. Where P85 is a co-polymer in which the fraction of PNIPAm is 85% and NtBA is 15%. Taken from ref. [146].

1.8.1.2. Fluorescence spectroscopy as a tool for measuring water ingress

Fluorescence spectroscopy is a very powerful tool to monitor microscopic environmental changes in the polymer systems/ polymer thin films because of its high sensitivity and selectivity, high speed measurements and non-destructive nature [147]. The surrounding microenvironment can be responsible for changes in the absorption/emission intensity, shifting of band position, anisotropy and fluorescence lifetime [13, 148, 149].

Mainly there are three types of fluorescent probe systems used in polymer science [8] 1) Some polymers contain intrinsic fluorophores within their structure [150]. 2) At the end/middle of the polymerization process a fluorophore can be introduced into the system by a covalent bond [151, 152]. 3) Fluorophores can be doped or inserted into the polymer systems without the formation of covalent bonds

(*e.g.* salicylic acid doped PVA [84]). Category 2 and 3 are known as external probes. Fluorophores doped into polymer thin films were used in the present study.

1.9. Fluorophores: polymer film analysis

The choice of fluorophore often depends on the specific photo-physical/physicochemical parameter that needs to be measured. There are probes sensitive to polarity, viscosity, ion concentration etc. For some applications however e.g. thin film thickness, probes are required which are insensitive to small fluctuations in probe microenvironments.

1.9.1. Polarity assessment fluorophores

One of the most common fluorophores used for polarity assessment is pyrene. The relative changes in intensities of various forbidden vibronic bands of pyrene are due to vibronic coupling between the first and the second excited singlet state. This

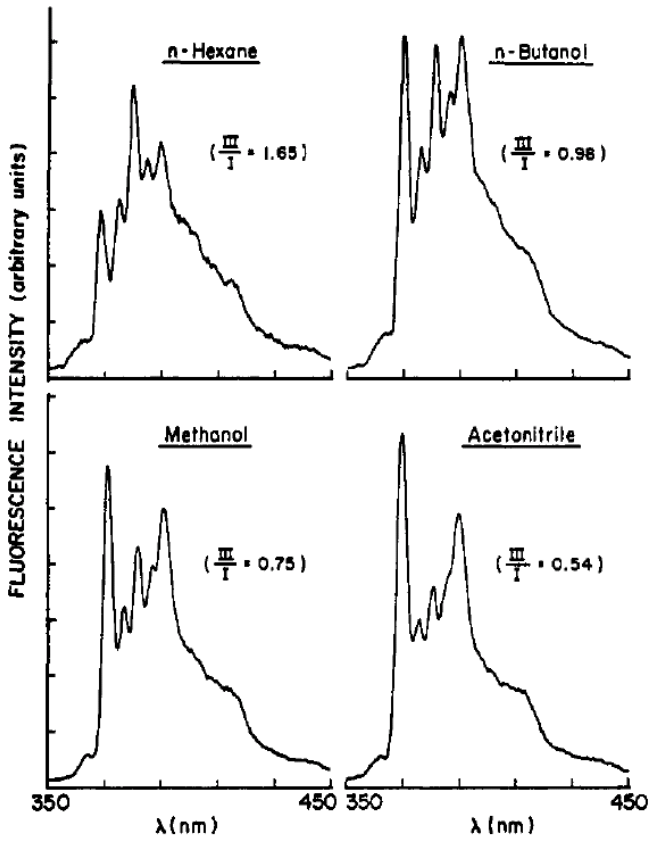

Figure 1.23: Vibronic band intensities of pyrene in different polarity solvent where $\lambda_{ex.}$ = 310nm. Taken from ref [153].

relative change of intensities is sensitive to polarity. The polarity of the pyrene environment may be correlated with the ratio of the fluorescence intensities of the third and first vibronic bands. Dong and Winnik developed the Py scale for solvent polarity, it is insensitive to H-bonding ability of protic solvent [11, 153]. This value can be easily determined with good precision over a wide range *i.e*. from 0.41 in the gas phase and 1.95 for DMSO (Figure 1.23).

Szczupak *et al*. investigated the polarity of co-polymer film (NIPAm-co-NtBA) by using pyrene as a polarity probe [146]. They found a reduction of polarity as the I_I/I_{III} ratio is reduced with the increase of NtBA fraction in the co-polymers (Figure 1.24). However, they found a poor correlation of pyrene ratio with other solvatochromic parameters. This was due to ignoring very significant H-bonding effects, as only dipole-induced-dipole interaction was accounted for in the Py scale.

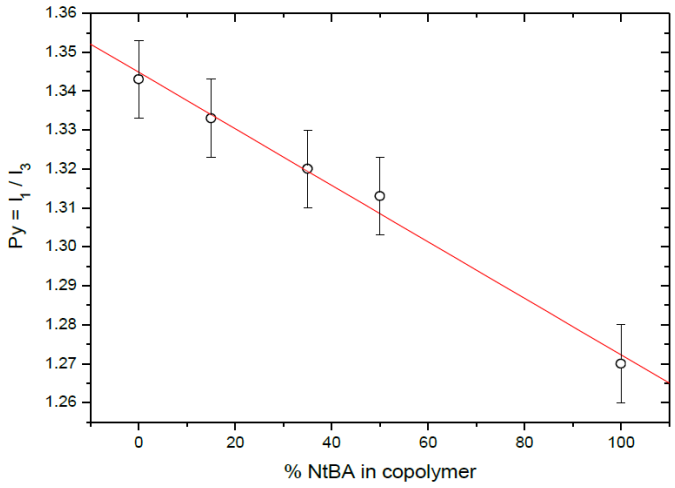

Figure 1.24: Variation of Py scale with % NtBA in copolymer at 20 °C. Taken from ref [134].

The fluorescence properties of pyrene were not greatly affected by the physiochemical changes that occur at the LCST of the co-polymer and showed only a linear decrease in I_1/I_3 ratio over the temperature range from 20 °C to 40 °C (Figure 1.24). This decreased I_1/I_3 ratio from 1.345 to 1.285 over that temperature range was in stark contrast to the magnitude of change (1.79 to 1.38) reported for PNIPAm in solution. This was due to there being no distinct aqueous phase, so most of the pyrene fluorophores were dispersed throughout the hydrophobic domain of the polymer and therefore there is much less change in emission properties. Based on this discussion,

they concluded that, pyrene was not a suitable fluorophore for studying water ingress in polymer thin films.

PRODAN and its derivatives

PRODAN (6-propionyl-2-(dimethylamino) naphthalene) was first synthesized by Weber and Farris in 1979 [154]. It is a useful fluorescent probe for assessing micropolarity. It has an electron donating dimethylamino group and electron withdrawing propionyl group positioned at maximum distance from the amino group. Transfer of an electron from the donor to the acceptor, produces a substantial excited state dipole moment which is very sensitive to polarity. It shows strong shifts in absorption and emission bands with the change of micro-environment. The emission band is strongly red shifted with the increase of polarity and H-bond donor ability. For example, the emission maximum of PRODAN is shifted from 401 nm to 531 nm after changing the solvent from cyclohexane to water (Figure 1.25). Therefore, PRODAN and its derivative are important for studying the polarity of various biological and chemical systems [155-161].

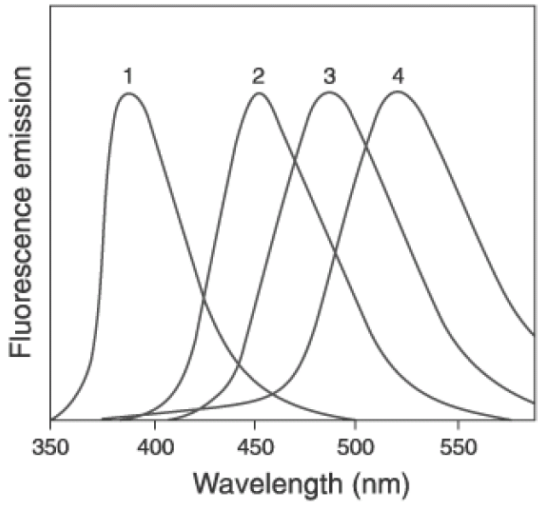

Figure 1.25: Normalised fluorescence spectra of PRODAN in (1) cyclohexane (2) dimethylformamide (3) ethanol and (4) water excited at 345 nm. Taken from ref. [162]

Coumarin and its derivatives

The benzo-α-pyrones commonly known as coumarin, consist of fused pyrone and benzene rings (Figure 1.26). It is widely distributed in nature and was first isolated in 1820. Due to its distinctive odour coumarin has been used as a food additive and perfume ingredient since the late 1800s [163]. Among groups of coumarin dyes, 7-

amino coumarin was of special interest due to having a high quantum yield, a substantial change in dipole moment during excitation, and a relatively large Stokes shift. The emission spectra of these coumarins show a high degree of sensitivity to the local environment *i.e.* polarity and viscosity [164].

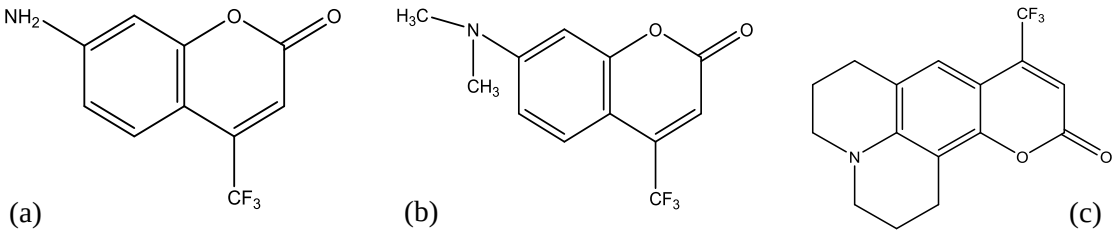

Figure 1.26: Structure of Coumarin derivatives (a) Coumarin 151, (b) Coumarin 152 and (c) Coumarin 153.

Jones *et al.* [165] reported the solvatochromic effects of some 4–trifluoromethyl substituted 7–aminocoumarin derivatives. These derivatives show a strong red-shifted emission with increasing solvent polarity. This photophysical property is attributed mainly to an emission from an ICT state and a non-radiative decay pathway which involves the rotation of the 7–amine functionality to form a TICT state. Thus an enhanced non-radiative decay rate is observed in polar solvents. This is the reason for the solvatochromism of 7–aminocoumarin derivatives in different polar solvents. They reported in further work [166] that the H-bonding between the coumarin and the solvent molecules is the main factor controlling the formation of the TICT state. They also observed a good correlation between the wavelengths of maximum intensity with the π^* scale and H-bonding parameters.

1.9.2. Viscosity sensing fluorophores

The fluorophores which show viscosity-dependant quantum yields are usually known as molecular rotors. Chemically, molecular rotors are a group of fluorophores which exhibit TICT based emission and de-excitation is non-radiative from the TICT state [167]. Generally, the emission band position, shape, intensity of these TICT based probes is dependent on molecular mobility, solvation, and polarity of the micro-environment. Therefore, this class of probe can be used for viscosity/polarity sensing of micro-environments. For example: 9-(dicyanovinyl)-julolidine (DCVJ), 9-(2-carboxy-2-cyano) vinyljulolidine (CCVJ), PRODAN etc.

The TICT formation rate is decreased with an increase in viscosity of the environment generally leading to an increase in emission intensity with viscosity [168]. For example, DCVJ forms a TICT state by photo-induced electron transfer from the julolidine nitrogen to one of the nitrile groups with subsequent intramolecular rotation around the julolidine vinyl group. This intramolecular rotation is dependent on the molecular free volume of solvent (*i.e.* viscosity). The microenvironment having a lower free volume (higher viscosity) leads to inhibit the rotation and thus shifted the radiative relaxation to higher rates (compared to higher free volume solvents *i.e.* lower viscosity). As a consequence, the fluorescence intensity increases as the viscosity of the medium increases.

1.9.3. pH sensing fluorophores

The fluorophores for sensing ions are widely employed in a variety of field such as biological probes, molecular devices, and environmental sensors [169]. Among these, fluorescent pH sensors got much interest due to their higher sensitivity and selectivity in bioanalytical chemistry, cellular biology for measuring intracellular pH, and medicine science for measuring pH or pCO_2 in blood [170-172]. A large variety of fluorescent pH sensors have been successfully developed and most of these sensors are based on fluorescent intensity changes as a function of H^+ concentration. Unfortunately, the determination accuracy is frequently compromised by the instrumental condition and external interference such as source instability, photobleaching, drifts in the optoelectronic set up etc. Although lifetime based pH sensitive fluorophores are preferable (due to not being effected by the above mentioned limitation), their complexity restricts their adoption and work is underway to develop a ratiometric fluorophore whose dual band emission are sensitive to pH [173].

Niu *et al.* have reported a ratiometric fluorescence sensor based on two fluorophores [173]. They used two pH sensitive fluorophores named N-allyl-4-(4'-methyl-piperazinyl)-1,8-naphthalimide (AMPN) and meso-5,10,15,20-tert-(-4-allyloxyphenyl) porphyrin (TAPP) which were copolymerized with a blend of polymers (*i.e.* acrylamide, hydroxyethyl methacrylate and triethylene glycol dimethacrylate) on a silanized glass surface. TAPP showed a strong fluorescence at neutral pH and a strong decrease in emission intensity as the pH dropped. Whereas, AMPN shows no appreciable changes within the acidic region (below the pH 5).

Therefore TAPP works as a reference at neutral pH range and AMPN is used as a reference in the acidic region. They monitored the pH of a buffer solution by measuring the ratio of their respective fluorescence intensities. They also showed that the sensor is reproducible and accurate across a wide pH range (1.5 to 9).

1.9.4. Water ingress sensing fluorophores

One drawback of simple, single-band fluorophores is that emission intensities can fluctuate due to a variety of factors that are not related to the factor of interest (excitation source instability, local concentration of fluorophores, concentration variation, and photobleaching). This may lead to inaccurate measurements particularly in viscous or rigid polymers [148, 174-176]. When a fluorophore gives two or more emission bands, generally all will be equally affected by the above factors and therefore using ratiometric measurements, the problem can be minimized [174-176]. These ratiometric probes whose emission bands are sensitive to environmental factors have clear advantages [177, 178] such as: 1) the fluorescence data are independent on instrumental factors (*e.g.* illumination stability) or on fluorophore concentration [179-182], and 2) the dual band probes may be considered as a multiparametric because of the possibility to record a number of spectroscopic variables which are differentially sensitive to different kinds of interactions with microenvironments [183-186].

Dual band fluorescence is often caused, when a molecule can undergo Excited State Intramolecular Proton Transfer (ESIPT) of a hydroxyl proton to carbonyl oxygen/ from amino proton to pyridinic nitrogen. The photo-tautomer (T*) produced by the ESIPT reaction shows different structural and electronic conformation compared to the corresponding normal (N^*) excited form (Figure 1.27)

Among the various compounds that exhibit ESIPT, only 3-hydroxychromone (3HC) and their derivatives 3-hydroxyflavones (3HF) display solvent dependant dual emission [179, 182, 187-193]. The most studied ESIPT system is 3HF [194-225] for which the first dual band fluorophore was observed by Sengupta and Kasha [216]. However, this fluorophore has some limitations such as: 1) it has absorption in the ultraviolet (λ_{max} = 343 nm in EtOH), 2) it has a low quantum yield (φ =0.024 in EtOH), and 3) its N^* band has a low relative intensity compared to the T^* band in most media

[226]. Therefore, this parent fluorophore needs to be chemically modified which may adjust its response to a specific range of solvent polarities and may switch off the sensitivity to hydrogen bonding [185, 226-229]. It is also possible to increase water solubility through charged substituents such as sulfonic or carboxylic acids, and photostability can be increased by blocking reactive positions and sterically reducing probe reactivity by introducing bulky groups [230].

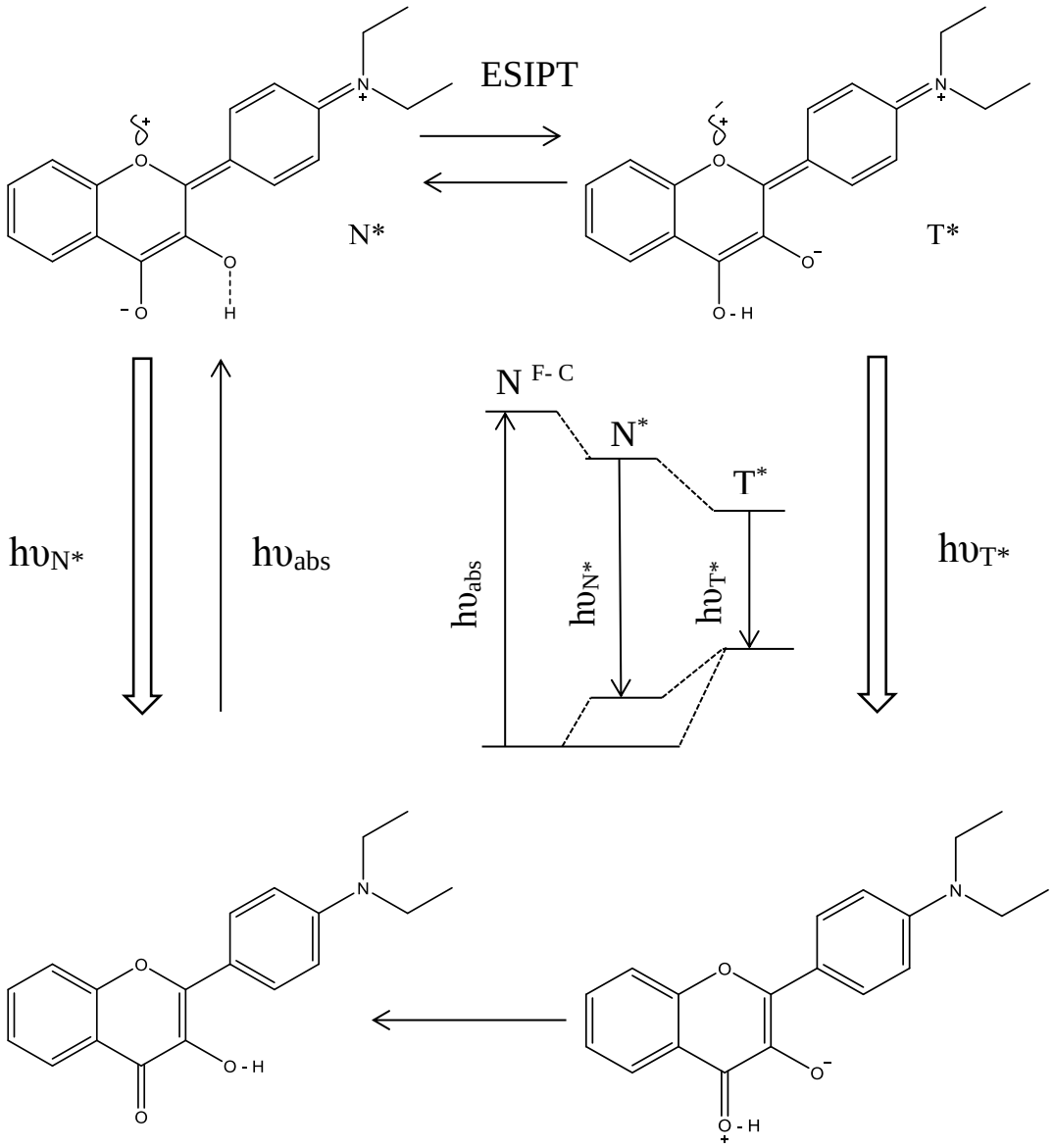

Figure 1.27: Schematic of the photophysical processes of 4'-diethylamino-3-hydroxyflavone (FE) resulting in two emission bands. Reproduced from ref. [184].

One such modification is an attachment of donor dialkylamino group at the 4' position of 3HF (Figure 1.28) which gives a larger excited state dipole moment in the normal form, giving rise to a charge transfer character for the normal fluorescence [231-234]. So that the N^* band relative intensity becomes stronger and it is now well resolved even in non-polar aprotic solvents. N^* band position and intensity are dependent on solvent polarity but the T^* band is less sensitive to solvent polarity due to a smaller dipole moment changes during its formation [231, 232, 234-238].

Morris *et al.* studied the water adsorption characteristics of FE, MFE, and BFE dyes doped PNIPAm thin film by using a controlled relative humidity chamber [4]. It was reported that all of these hydroxyflavone derivatives were sensitive to changes in the microenvironment. The fluorescence properties (intensity, band position, band width) changed significantly with increasing %RH. Water adsorption at higher %RH caused a dramatic increase in the micro-polarity which was manifested by an increase in the polarity assessment parameter (intensity ratio (log (I_N^*/I_T^*)) with increasing %RH (Figure 1.29).

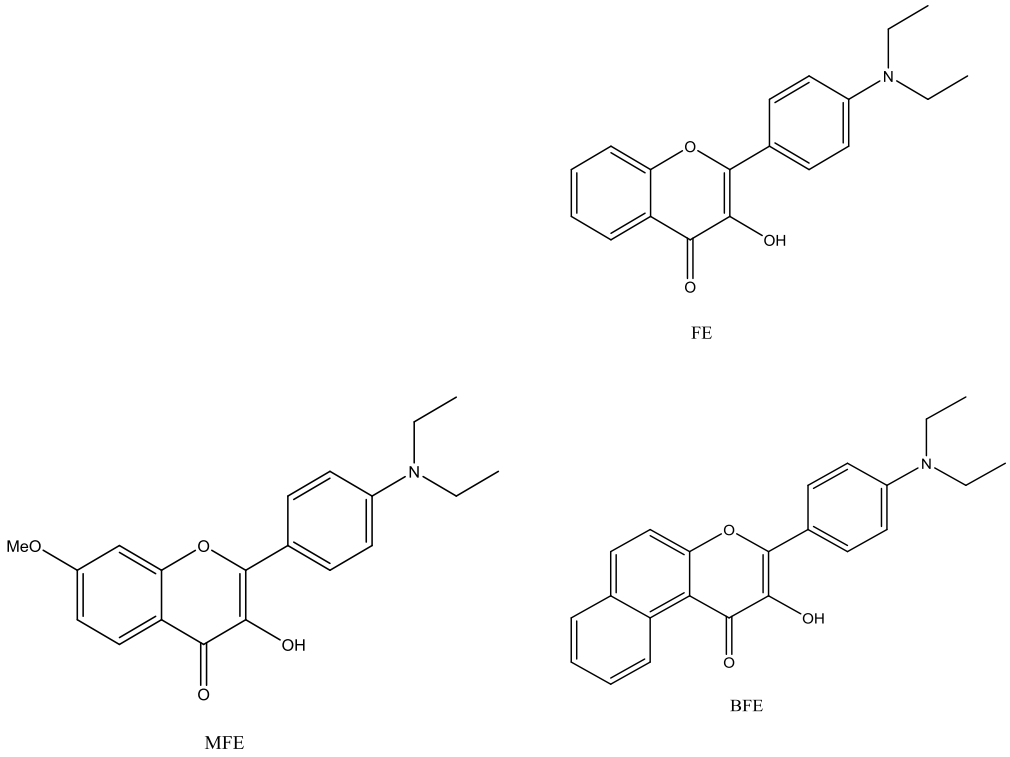

Figure 1.28: Some structural modification of 4'-dialkylamino-substituted 3-hydroxyflavone derivatives. (a) 4'-diethylamino 3-hydroxyflavone (FE) (b) 5,6-benzo-4'-diethylamino-3-hydroxyflavone(BFE) (c) 4'-diethylamino-3-hydroxy-7methoxyflavone (MFE) [226, 229]

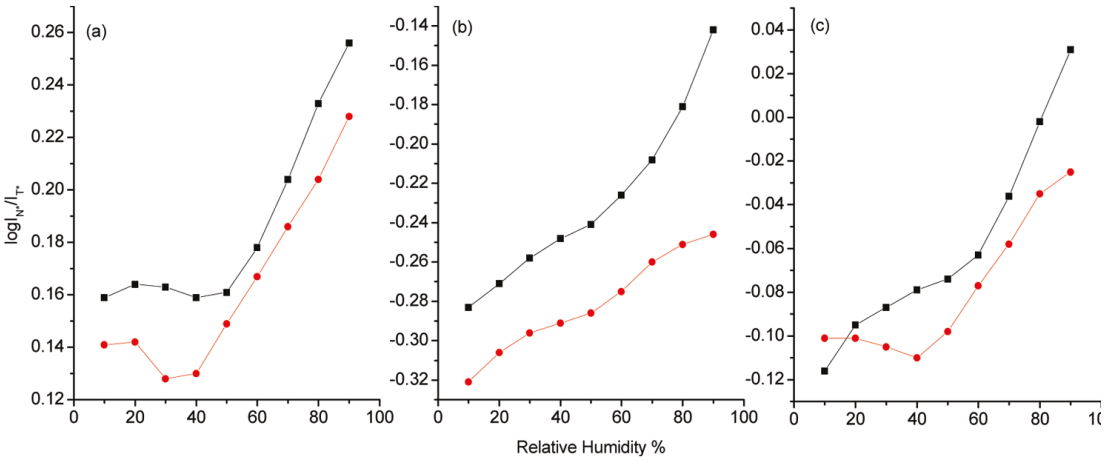

Figure 1.29: Plot showing the log ratio with increasing %RH of PNIPAm films doped with (a) FE, (b) BFE and (c) MFE both at 25 ˚C (─)and 37 ˚C (─). Taken from ref. [4]

They also reported a two phase hydration process where, first in the relatively dry domain (*i.e.* at relatively lower humidity<50%RH), water molecules accumulate in the polymer matrix and bind with the hydrophilic parts of polymer chain such as N-H and C=O. As water absorption increased further, in the second phase of hydration (>50%RH), the additional adsorbed water is associated with the primary hydration shell's water leading to form a loosely bound water domain within the polymer. This was then significantly affect the polarity parameter log (I_N^*/I_T^*) (Figure 1.29). These 3-HF fluorophores were reported as being good determinants of physicochemical changes arising from changes to the local microenvironment [239].

1.9.5. Polymer film thickness measurement

Film thickness plays an important role in the controlled release of drugs. For example, drug load is a function of thickness, and may also affect the drug release rate. Therefore thickness measurement during manufacturing of thin film coatings is important [240]. At the NBL there has extensive work already been done for developing a robust fluorescence method for characterization of physicochemical properties *i.e.* polarity, H-bond ability of polymer thin films which has great importance in controlled drug release coating [4, 134]. The fluorophores used for the previous studies have allowed the tracking of moisture ingress into polymer films. However, the fluorophores were not sufficiently photostable [239] for imaging

applications which is the next step in developing a robust analytical method for *in-situ* polymer characterisation. Photostable imaging probes are needed:

1. To accurately measure film thickness by correlating emission intensity with local polymer concentration and
2. To look at polymer movement on surfaces during various processes like drying etc.

So, fluorescent probes are required that are both sensitive to some environmental factors (*e.g.* water) and/or are yet very photostable to allow for imaging based diagnostics. Hence, 2, 5 di hydro 1, 2, 3 Tr series fluorophores have been explored in this thesis.

1.9.5.1. Novel Tr fluorophores

Due to low stability, fluorophores containing 1, 2, 3 triazine rings have been the least studied. These triazine based fluorophores have a complex emission, comprised of three emission bands (however in previous publication showed only two emission band, since they used naïve band fitting [5]) and a relatively long and complex lifetime. For example, 5-methoxycarbonyl-5-(N-phenylformimidoyl)-2,4,6-triphenyl-2,5-dihydro-1,2,3-triazine has a large Stokes shift of ~120 nm at 400 nm excitation and ~200 nm with 317 nm excitation (Figure 1.30).

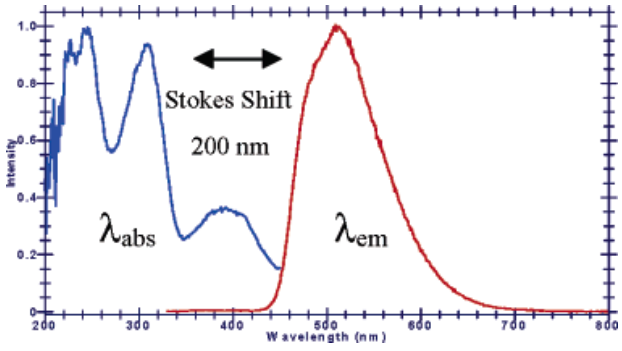

Figure 1.30: Normalised excitation and emission spectra of pTr in MeOH [5].

The 2,5-Dihydro-1,2,3-triazine derivatives were prepared in NUI Maynooth by the research team of Dr. John Stephens using methods previously described [5]. Three Tr derivatives (*e.g.* 5-methoxycarbonyl-5-(N-phenylformimidoyl)-2,4,6-triphenyl-2,5-dihydro-1,2,3-triazine (pTr), 5-methoxycarbonyl-5-H-2,4,6-triphenyl-2,5-dihydro-1,2,3-triazine (hTr) and 5-propan-one-5-(N-phenylformimidoyl)-2,4,6-

triphenyl-2,5-dihydro-1,2,3-triazine (kpTr)) have been investigated in this thesis and are shown in Figure 1.31.

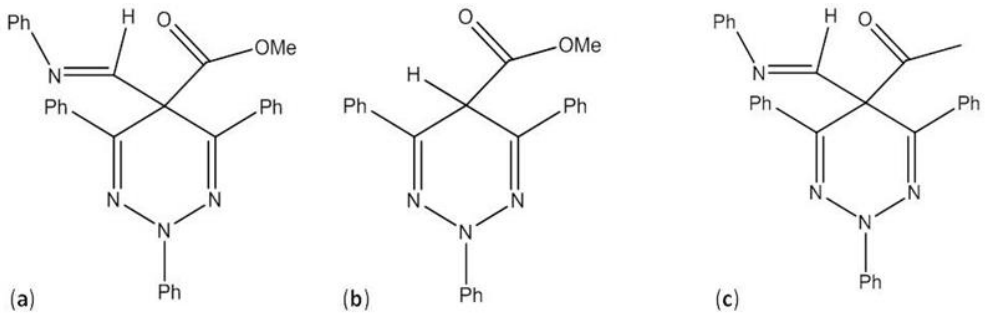

Figure 1.31: Structural form of Tr fluorophores used in this research where (a) pTr, (b) hTr, and (c) kpTr.

According to Dean St. Mart *et al.* [6], the complex fluorescence emission of Tr fluorophores contains three emission bands, which correspond to emission from three conformers, designated as g0, g1, and g2, and each conformer corresponds to an energy minimum for S_0, S_1, and S_2 states, respectively (Figure 1.32). By using the planarity of the dihydro-triazine ring as a motif, following three structural forms (*e.g.* g0, g1, and g2) of Tr can be considered to form:

1. g0: Through the Tr ring, a pseudo-plane of symmetry is formed. The triazine ring is in an envelope conformation with equatorial ester and axial imine (Figure 1.32a).
2. g1: A pseudo-C_2 axis of symmetry is formed where the Tr ring is in a flat conformation with a co-planar N-2 phenyl and twisted C-4 and C-6 phenyl (Figure 1.32b).
3. g2: A total C_s symmetry is formed where the Tr ring is in an envelope conformation with axial ester and equatorial imine (Figure 1.32c).

Additionally, all the geometric forms are vibrationally (but not thermally) accessible in the ground state S_0 due to the relatively low energy differences.

A model has been proposed for the emission of Tr fluorophores at 400 nm excitation (also proposed an emission model at λ_{ex} = 300 nm). Excitation at 400 nm: S_0 (g0) to S_1 (g0) transition is believed to occur for pTr fluorophore. Since, the S_1 (g0)

excited state is very close to that of the S_1 (g1) and S_1 (g2) excited state, a significant overlap of the vibronic states and high rates of IC is expected. Thus, three transitions from these three excited states (*i.e.* S_1 (g0), S_1 (g1), and S_1 (g2)) to the ground state are responsible for the three emission bands (Figure 1.33). The source and pathways for three emission bands (at 400 nm excitation) are the following:

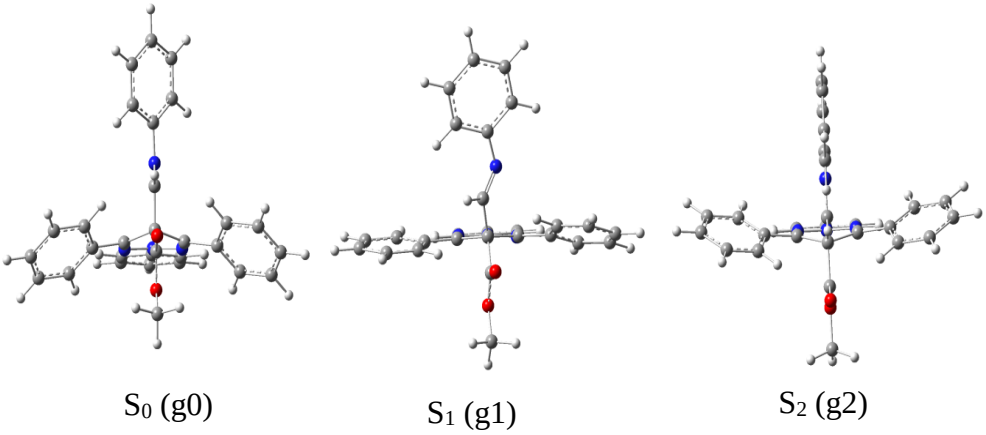

Figure 1.32: The structure of three states (S_0 (g0), S_1 (g1), and S_2 (g2)) with the rear view through the triazine ring. Adapted from ref. [6].

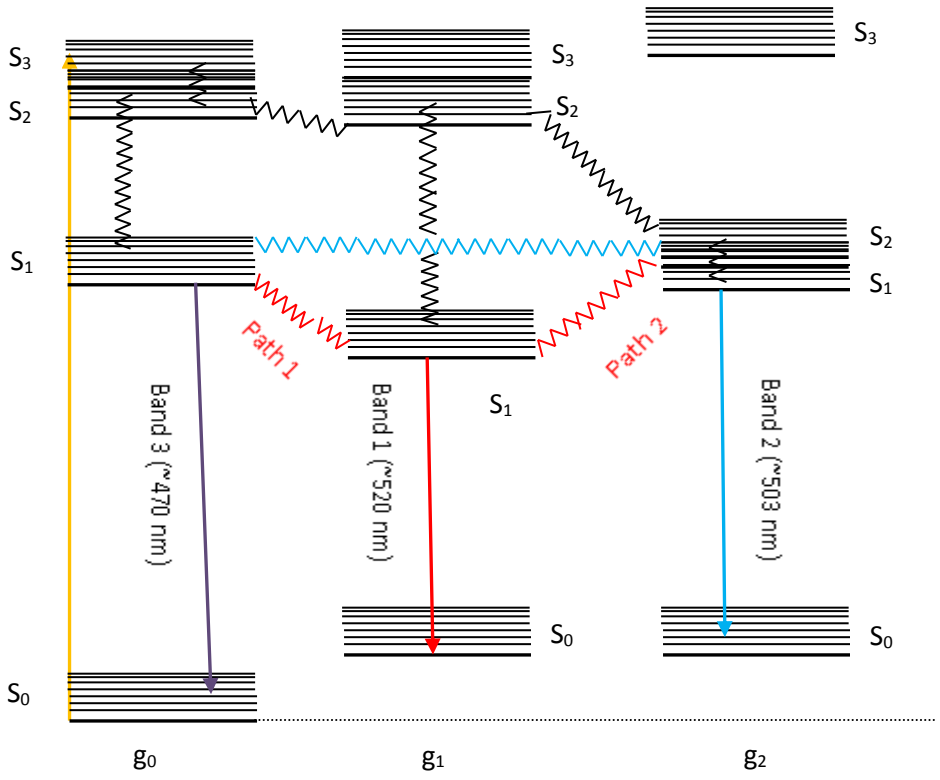

Figure 1.33: A schematic presentation of the source of three emission bands for 1, 2, 3 Tr fluorophores. Due to three conformation of Tr fluorophore, three transition is observed from the excited singlet state. Band 1, Band 2 and Band 3 are the consequence of $S_{1\rightarrow0}$ (g1) transition, $S_{1\rightarrow0}$ (g2), and $S_{1\rightarrow0}$ (g0) transition respectively. Reproduced from ref. [6].

1. Emission due to the $S_{1\rightarrow0}$ (g0) transition, denoted Band 3, is positioned at~ 470 nm (at shortest wavelength) with ~12% relative area.
2. Emission due to the $S_{1\rightarrow0}$ (g1) transition, denoted Band 1, is positioned at ~540 nm (~41% population). Two pathways may produce this transition. First, IC directly from the S_1 (g0) to lowest vibrational energy level of S_1 (g1) state, followed by radiative decay to the ground state. Second, the molecules in the S_1 (g2) state can IC to S_1 (g1) state. Emission of a photon may then follow.

3. Emission due to the $S_{1\rightarrow0}$ (g2) transition, denoted Band 2, is the most populated (~47%) and occurs at ~503 nm.

They also undertook a comprehensive study (synthesis, absorption and emission properties) of the different derivatives of Tr fluorophores by using UV absorption, steady state and time resolved fluorescence spectroscopy [7]. The photophysics of these Tr derivatives were relatively unaffected by changing the solvent polarity.

Table 1.1: Fluorescence lifetime data for pTr in MeOH at different emission wavelengths using 405 nm excitation wavelength. Where τ_i represents the individual lifetime components and $\langle\tau\rangle_f$ is the intensity weighted average lifetime. Collected from ref. [5].

Wavelengths	solvent	A_1 (%)	τ_1	A_2 (%)	τ_2	A_3 (%)	τ_3	$\chi2$	$\langle\tau\rangle_f$
470 nm		4.3	11.2	89.3	4.0	6.4	1.1	1.34	4.09
490 nm		16.0	10.7	78.9	4.0	5.1	0.9	1.40	4.89
520 nm	MeOH	28.5	11.6	67.4	4.0	4.1	0.8	1.40	6.05
540 nm		35.6	11.8	60.6	4.0	3.8	0.8	1.46	6.65
570 nm		42.9	12.0	53.6	4.0	3.5	0.8	1.68	7.36

The Tr fluorophore's decay curve usually consists of three lifetime components which are called as short lived component (τ_3), medium component (τ_2), and long lived component (τ_1). These triazine series fluorophores also show a large change in lifetime as a function of wavelength and some of the lifetime data for pTr in MeOH is presented on Table 1.1.

Replacing the imine phenyl group by a H in C-5 carbon of Tr ring (*e.g.* hTr), a major difference was observed in the absorption bands, where the 310 nm band is red shifted and a broad absorption band is observed at ~390 nm. This also affects the quantum yield of hTr *e.g.* quantum yield is 0.2 and 0.79 (in toluene) for hTr and pTr respectively at 400 nm excitation and also the energy state of the emission (emission spectrum is positioned at higher energy (~480 nm) compared to pTr (520 nm)). However, it does not show any significant changes in absorption or emission band position with changing the solvent polarity compared to the parent pTr.

A remarkable shortening of lifetime is observed for hTr compared to the parent pTr which is supposed to due to significantly shortening of the long lifetime component. For example, τ_1 is only 4.14 ns at 470 nm in acetonitrile, whereas 10.59 ns at 470 nm in chloroform for pTr [241].

Substitution of the ester by a ketone group significantly changes the dipole moment in the excited state and thus affects the energy of transition. For example, the emission from kpTr is red shifted compared to pTr. This also affects the intensity weighted average lifetime. The average lifetime of pTr in propylene carbonate is 6.87 ns at 470 nm, whereas it is 13.95 ns for kpTr in ethyl acetate at 490 nm.

1.10. Aims of thesis

The key aim of this thesis was to investigate the suitability of three 1, 2, 3 triazine based fluorophores for the analysis of polymer thin films. We wanted to:

1. Determine their sensitivity to water ingress.
2. Assess how they changed with different polymer types (PS, PNIPAm, PVA)
3. Measure their photostability under different conditions to see if they could be used as imaging probes.
4. See, if they are better as S-S or TRF based probe sensors.
5. Understand in detail the factors that affected the photophysics of Tr emission in polymer.

Chapter 2 : Materials and Experimental Procedure

In this section, the techniques and procedures of the photophysical studies of Tr fluorophores (both in polymer thin films and solution) used throughout this body of work will be described. Firstly, the sample preparation for Tr fluorophore doped polymer (Tr-polymer) thin films will be described followed by the instrumental set up of the fiber optic-based home-built spectrometer for steady-state and time- resolved measurements. Secondly, this section will also include a description of the procedures used for data analysis of steady state and lifetime measurements. Finally, the experimental procedure for the photostability studies of Tr fluorophores doped in polymer thin films, and the theory/basis for the experimental techniques used to study the interaction of Tr fluorophores with different hydrophilic polymer solutions (in water) will be discussed.

2.1. Materials and reagents

All the fluorescent 2,5-dihydro-1,2,3-triazine derivatives were supplied by the research team of Dr. John Stephens (NUI Maynooth) and used as received. PVA (98% hydrolysed average molecular weight 13000-23000), PNIPAm (average molecular weight 20000-25000), PS and Polyvinylpyrrolidone, PVP were purchased from Sigma-Aldrich, USA and used as received. The polymers were stored without any specific precautions (*i.e.* under controlled humidity) at room temperature. Solvents were spectroscopic grade and purchased from Sigma-Aldrich and used as received.

2.2. Thin film Preparation

Polymer thin films were prepared on quartz slides (12 mm × 45 mm × 1.5 mm, Lightpath Optical Ltd, UK). The reusable quartz slides were first washed at least three times with millipore water followed by acetone and ethanol, before a final rinse with water. The substrates were then dried in an oven at 70 °C prior to use. The Tr fluorophore stock solutions could not be prepared directly by mixing with EtOH (the fluorophores were very hydrophobic). We first prepared a 1 mL dichloromethane solution of the Tr (e.g. pTr: 0.0075 g), this was then slowly evaporated under reduced pressure to near dryness before being taken up in 15 mL of spectroscopic grade EtOH (solution concentration was 1.058×10^{-3}M). The stock solution was then aliquotted

into smaller volumes (7.5×10^{-5} M for PNIPAm or PS and 3.75×10^{-4} M for PVA) and stored at –70°C prior to use.

2.2.1. PNIPAm and PVP thin films

The required quantity for making a 5% w/w solution (in EtOH) of PNIPAm/PVP was measured out using a microbalance and then 1 mL of the Tr fluorophore (7.5×10^{-5} M, in ethanol) solution was added. The solution was then stored in the dark overnight, to allow for proper dissolution prior to film casting. To prepare a 10 µm thick film 138 µL (see Appendix II for details of the calculation) of the polymer-fluorophore solution was cast onto the quartz slide. Immediately, afterwards the samples were placed under reduced pressure in a vacuum desiccator to aid solvent removal overnight [242-244]. The final drying stage for all the polymer thin films involved transferring the films into an oven at 70 °C for 3 days prior to measurement. The 3-day drying period was found to be necessary because with a shorter 2-day drying time (at 70 °C), the spectral measurements were found to be not very reproducible (described in Chapter 3). An image of dry pTr doped PNIPAm (pTr-PNIPAm) thin films is shown in Figure 2.1 showing the distribution of fluorophores. The thicknesses of films were confirmed by a micrometer gauge. A blank quartz substrate was measured first followed by post film casting and drying of the films. A total of 25 measurements were taken at different locations across the sample. The five measurements which deviated (>±0.001 mm) from the highest repeating value were discarded and the mean of remaining twenty measurements was calculated. A film thickness of 10 µm was confirmed.

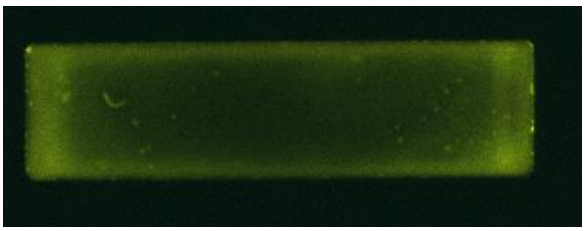

Figure 2.1: An image of a pTr-PNIPAm thin film prepared on a quartz substrate casting from 7.5×10^{-5} M pTr/ PNIPAm (5% w/w) solution. The image was taken using a Fluo-S™ MultiImager (Bio-Rad) after final drying of the thin films in oven at 70 °C for 3 days.

Average measured thickness of film + substrate = 1.264 mm (n = number of measurements = 20)

Measured thickness of blank substrate = 1.254 mm (n = number of measurements = 10)

Thickness of film =0.01 mm = 10 µm

2.2.2. PVA thin films

PVA thin films required a different preparation method. PVA is only sparingly soluble in ethanol, so the polymer solutions were prepared (5% w/w) in hot water (70 °C) first and then doped with the fluorophore solution. 200 µL of the pTr solution (3.75×10^{-4} M in EtOH) was injected into 0.8 mL of the PVA solution (in water) and the final concentration of the pTr fluorophore was 7.5×10^{-5} M. As hTr has a low quantum yield, a more concentrated solution compared to pTr was used (4.0×10^{-4} M). 200 µL of this solution was injected into 0.8 mL PVA solution (in water) yielding a final concentration 8.0×10^{-5} M. The 20 µm thick PVA thin films were prepared immediately after mixing of PVA and Tr solution since there was a possibility for interaction/reaction with water due to the acidic nature of PVA solution (in water) [66]. The thin films were cast onto quartz substrates using 284 µL (see Appendix for details of the calculation) of the relevant probe-PVA solutions for producing 20 µm thick films. This was then dried overnight under reduced pressure. Films were then transferred to an oven for 3 days at 70 °C to complete the drying process. The film thickness was confirmed by a micrometer by the same process used for PNIPAm thin films.

2.2.3. PS thin films

Since PS does not usually dissolve in EtOH, the pTr-PS thin films were prepared from PS (5% w/w)/pTr (7.5×10^{-5} M) in dichloromethane, DCM solution. First 1mL of a 7.5×10^{-5} M pTr solution in EtOH was placed in a glass vial and evaporated to dryness in a vacuum desiccator. The dry pTr fluorophore was then dissolved in 1mL of a 5% (w/w) PS solution in DCM. Thorough mixing was achieved using a vortex. The procedure used to prepare the pTr-PNIPAm thin films was followed again here. However the volume required in this case was 81 µL; see

Appendix II for details of the calculation. The film thickness was confirmed by using a micrometer.

2.2.4. The Tr fluorophores concentration in polymer films

It was considered an uniform distribution of Tr fluorophores throughout the polymer thin films to determine the Tr fluorophores concentration in corresponding polymer films as %w/w. The calculated concentration of Tr fluorophores in polymer films (for calculation see Appendix II) are presented in Table 2.1 for further discussion in the following humidity-induced changes in Tr-polymer thin films photophysics.

Table 2.1: The concentration of Tr in different polymer thin films.

Polymer	Tr Fluorophores		
	pTr (% w/w)	hTr (% w/w)	kpTr (% w/w)
PS	0.05	-	-
PVP	0.09	-	-
PNIPAm	0.09	0.07	0.08
PVA	0.09	0.077	-

2.3. Instrumentations

The polymer thin films were placed in a VGI2000M controlled humidity chamber, (Surface Measurement Systems Ltd. UK). Spectroscopic data were collected over the 10 to 90% RH range. The humidity was increased at 10% intervals for steady-state and 20% for time resolved measurements. The VGI2000M is shown in Figure 2.2a. The humidity chamber (Figure 2.2b) was designed to hold a standard microscope slide and has double glazed windows on the top and bottom for allowing transmission or reflected sample illumination and prevent moisture condensation during operation above or below ambient temperatures. There is a stainless steel sample head inside the chamber which acts as a humidity generation reservoir and ensures uniform temperature distribution and stable sample humidity. This is governed by circulating water through a series of channels in the head using a thermoelectric heating and cooling stage to maintain the desired temperature [4].

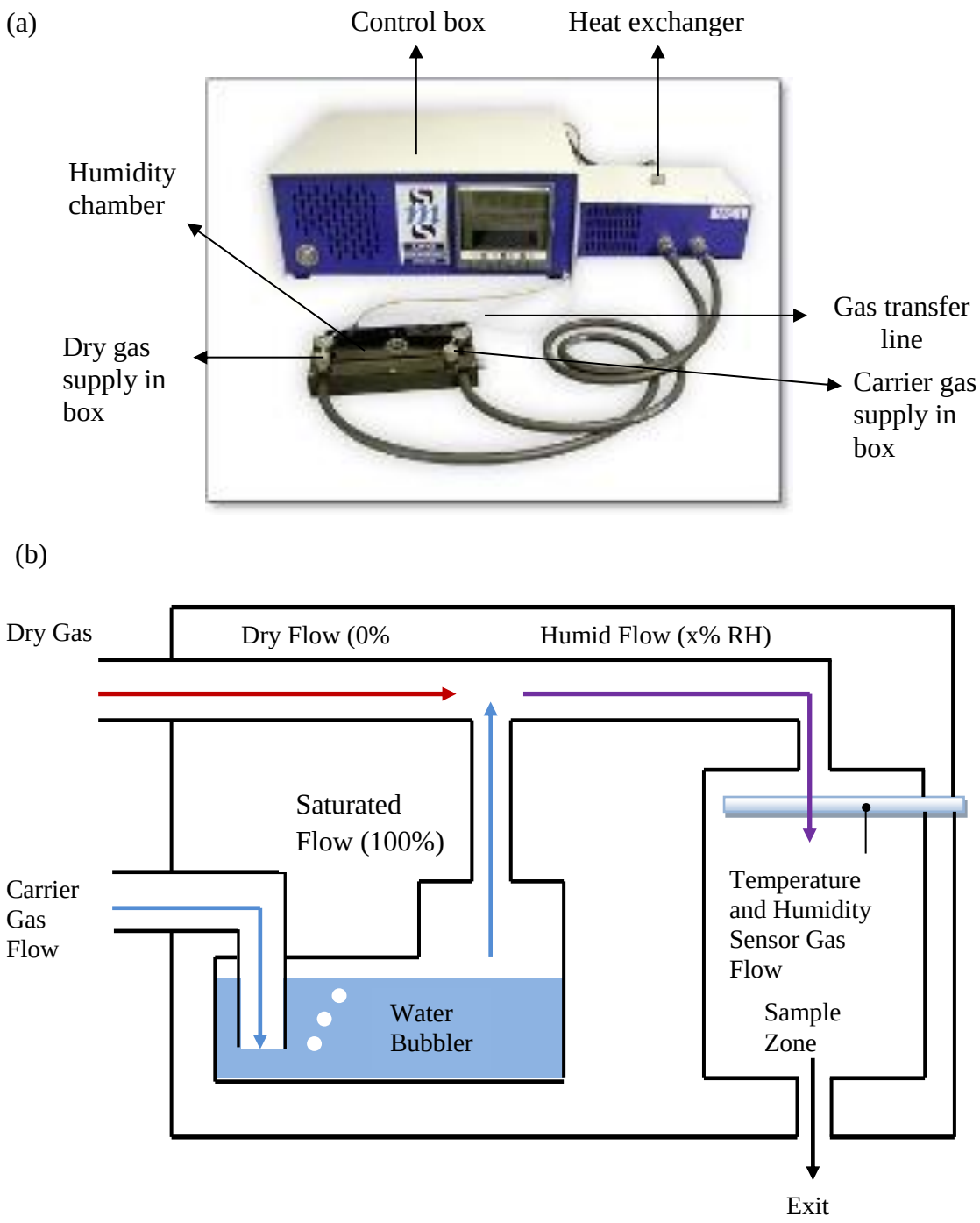

Figure 2.2: (a) VGI2000M controlled humidity instrument. (b) Generation of isothermal humidity within the chamber. A precise humidity level is generated within the chamber by mixing water saturated nitrogen gas with dry nitrogen gas in the appropriate proportion controlled by computer software.

A set humidity can be maintained by proper mixing of water saturated N_2 gas with an appropriate proportion of dry N_2 under computer control. The system has a digital controller which enables manual control and measurement of humidity. Instant feedback of temperature and humidity is obtained by the temperature and humidity sensor placed in the sample region. Figure 2.2b shows the schematic presentation of humidity generation in the chamber.

2.3.1 Steady-state measurements

Steady-state emission spectra were collected using an in-house assembled fibre-optic based system which was previously described [4]. Briefly it consisted of a 405 nm pulsed laser diode excitation source (PicoQuant) coupled into the central fibre of a fibre-optic reflection probe (Ocean Optics) which has one illumination and six read fibres bundle (all 400 µm diameter). The probe was used to couple the excitation light down into and fluorescence emission out of the humidity chamber.

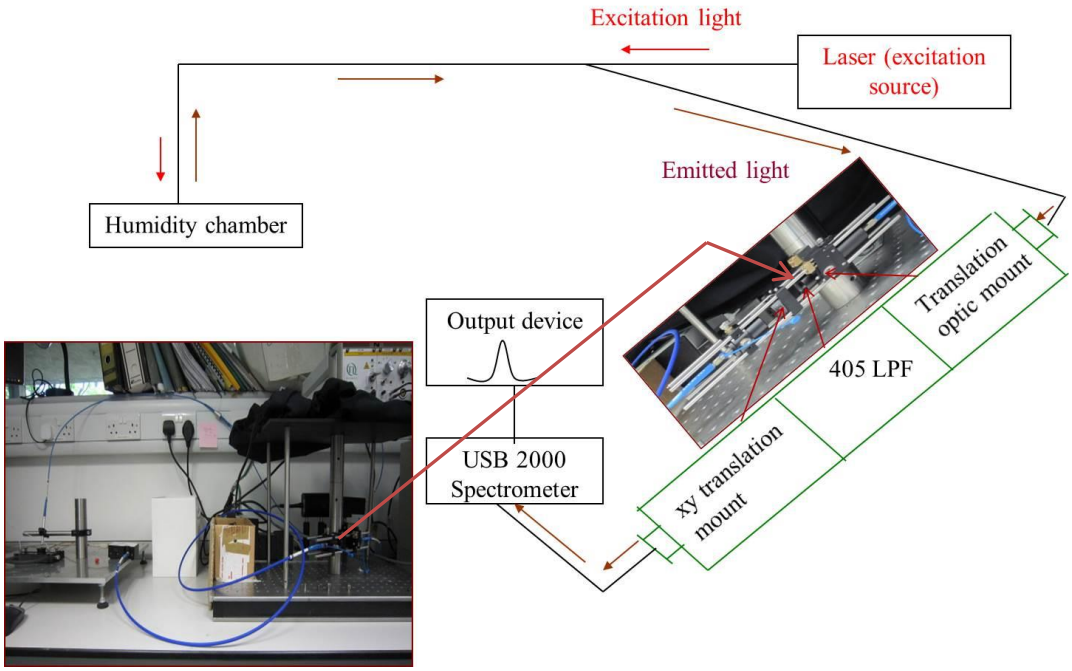

Figure 2.3: Schematic presentation of steady state measurements system. The excitation light from 405 nm laser is first passes through the central fiber and incident into the sample placed in the humidity chamber. The emission light is then collected through an in house assembly comprising of 430 nm long pass filter (LPF), xy translation mount into the USB spectrometer. The emission spectra are then recorded in the output device.

The resulting emission light was passed through a home built assembly (comprising of focusing optics and a 430 nm long pass filter) into a 1000 µm diameter

optical fibre connected to a USB miniature spectrometer (USB2000, Ocean Optics). The USB spectrometer is connected to a computer and the steady state spectra were collected by using OOIBase32 (version 2) software. The spot size on the samples from this fibre-optic arrangement was ~1 mm and the maximum light power delivered was ~ 10 microwatt (measured by a laser power meter, THORLABS PM100). The schematic diagram for our home built spectrometer is shown in Figure 2.3.

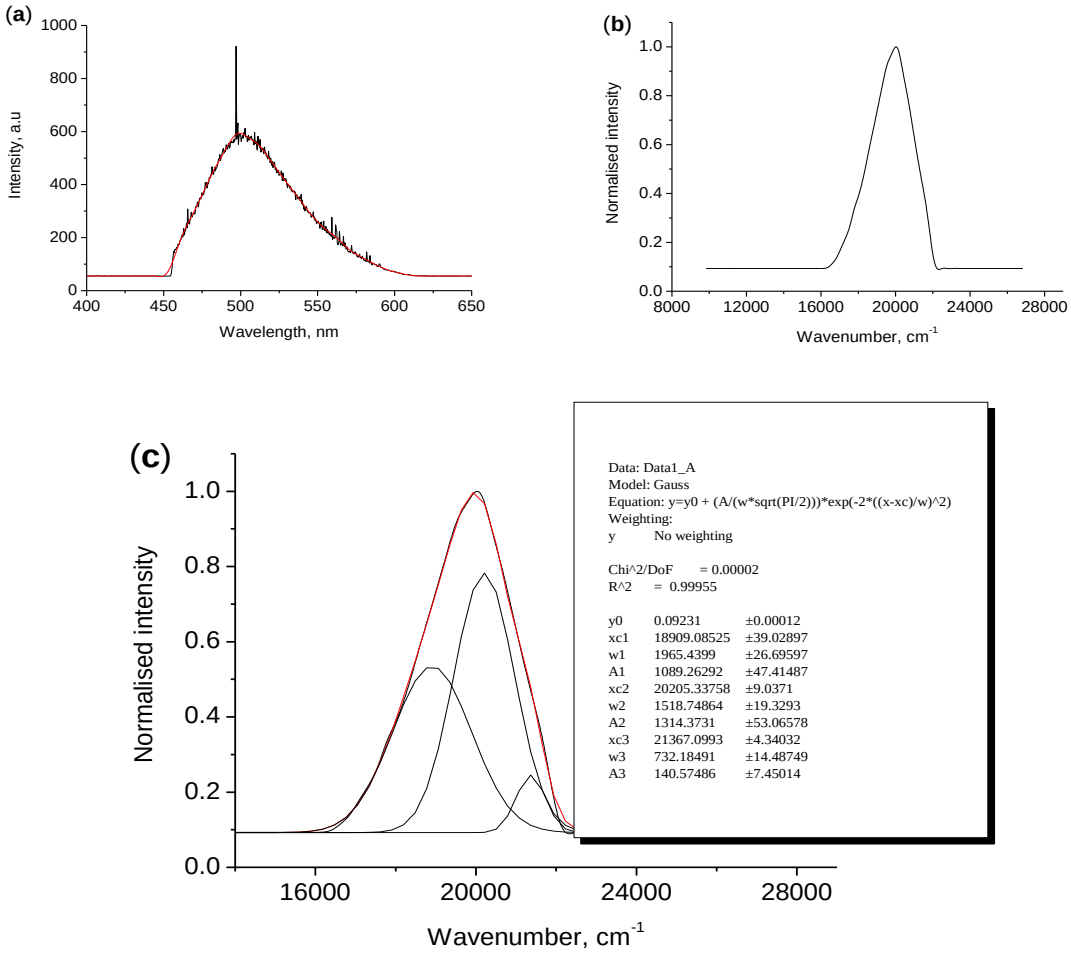

Figure 2.4: The step by step data analysis procedure for the steady state emission spectra. First wavelength vs overall emission spectra were plotted from where the emission intensity maximum values were collected (a). Secondly, the wavelength was converted into wavenumber and a smoothed wavenumber vs normalised intensity was plotted for Gaussian 3 bands fit (b) the best fit was determined by the r^2 (as close to unity) and the lowest χ^2 value. The intensity (as % relative band area), bandwidth and band position were then collected from the analysis (c). The inset data shows the area (as A), FWHM (as W) and band position (as C) of each individual emission transition of pTr-PNIPAm thin films.

The emission spectra were then converted to a wavenumber scale, smoothed, baseline corrected and normalised (to the band of maximum intensity) prior to being fitted to 3 band Gaussian fit by using Origin software (Origin version 7.0, Origin Lab Corporation, Northampton, MA). Fit quality was determined according to $\chi 2$ (as low as possible) and r^2 values (as closest to unity). The relative areas of the individual bands, full width at half maximum (FWHM), and band position were obtained from the fit models (Figure 2.4).

Accuracy of fitting

The quality of each individual fit was assessed on the basis of r^2 and χ^2 values in conjunction with the residual trace. However for comparison between samples we also needed to determine the inter-sample fit variance. To do this, 15 different S-S spectra of pTr-PNIPAm thin films (dry condition) were chosen randomly. In each case, a three-band Gaussian fit was carried out and assessed for maximum accuracy of fitting. Values of relative error were calculated for the band area, FWHM, and band position of each fitted band. All relative errors were then averaged and the SD was determined in each case. The range of relative error was finally determined for the band area, FWHM, and band position for each emission conformer (Figure 2.5).

It can be seen from Figure 2.5 that the band position was the most accurate; (± 0.3% relative error). The relative band areas (populations) of each conformer were least accurate and the average relative errors were ± 7%, ±8%, and ±13% for g1, g2 and g0 conformers respectively. So, any changes within ±7% in % band area of each emission conformer can be described as an intrinsic fitting error. The average relative errors of FWHM of each conformer were ±2%, ±4%, and ±2% for g1, g2 and g0 conformers respectively. Therefore, it also can be concluded that any changes within ±2% in FWHM could be described as being within the fitting error.

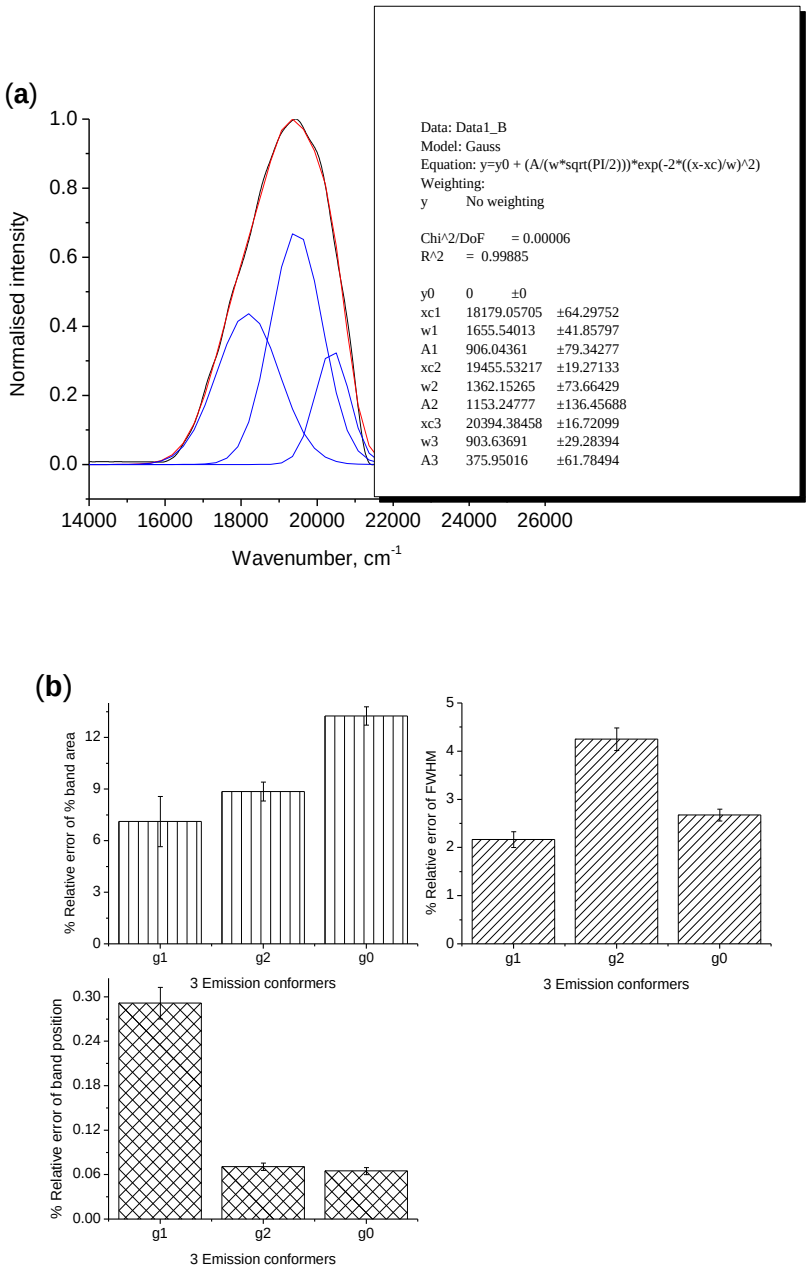

Figure 2.5: (a) A sample emission spectra fitted to 3 bands Gaussian fit from where the % relative error of each emission parameter was calculated. (b) Plot shows the average of % relative error calculated from 15 different emission spectra of Tr-polymer thin films.

2.3.2. Lifetime measurements

The same fiber optic reflection probe (R 400-7, UV-vis, Ocean Optics) for steady state measurements was used also for lifetime measurements to couple the excitation light into and the fluorescence emission out of the chamber. The excitation light from a pulsed 405 nm PicoQuant laser diode was guided through a central fiber

of the optical probe was passed into the samples and the fluorescence emission collected by the probe passes into an in-house assembled TCSPC system (Figure 2.6)

The system consists of a manually controlled monochromator (Sciencetech, Canada, model 9030) with a photon counting PMT detector (model H5783, Hamamatsu). Data collection was controlled by a TimeHarp 100 TCSPC system. The instrument response functions (IRF) were collected once for each set of experiments by collecting the scattered light from a blank dry quartz slide which was placed in the humidity chamber.

The sample placed in the humidity chamber was excited with a pulse of light and the time is measured between the excitation pulse and the observed photon and stored in a histogram to generate a decay curve. The fluorescence emission wavelength was selected manually on the monochromator and lifetime data were collected at 5 wavelengths: 470, 490, 520, 540 and 570 nm the same as for the previous studies by Butler *et al.* [5].

The lifetime data for the Tr fluorophores doped polymer thin films were collected at different %RH. The samples were kept for one hour at each level of humidity in the humidity chamber to allow the sample to equilibrate and measurements were performed at 25 and 37 °C.

Generally a minimum of 10k, 20k, and 30k counts in the channel of maximum intensity are recommended for accurate fitting of single, double, and tri exponential decay curve respectively. However, due to the lower efficiency of our home built TCSPC system, usually a longer accumulation time was required for the collection of 20k or 30k counts, and within this time, a fraction of fluorophores may be photobleached. Therefore, for every decay curve recorded, the data was accumulated, until the channel at maximum intensity had reached an intensity of at least 10k counts.

The decay curve was then analysed by loading the curve into FluoFit (version 3.1, PicoQuant). The results were extracted from a multi-exponential decay model:

$$I(t) = \sum_{i=1}^{n} \alpha_i \, exp\left(-\frac{t}{\tau_i}\right) \qquad \text{Equation 2.1}$$

Where τ_i is the decay time and $\propto_i$ is the pre-exponential factor (amplitude) of the individual components and $\sum \alpha_i = 1$. And the contribution of individual component in the steady state intensity can be expressed as:

$$f_i = \frac{\alpha_i \tau_i}{\sum_j \alpha_j \tau_j} \qquad \text{Equation 2.2}$$

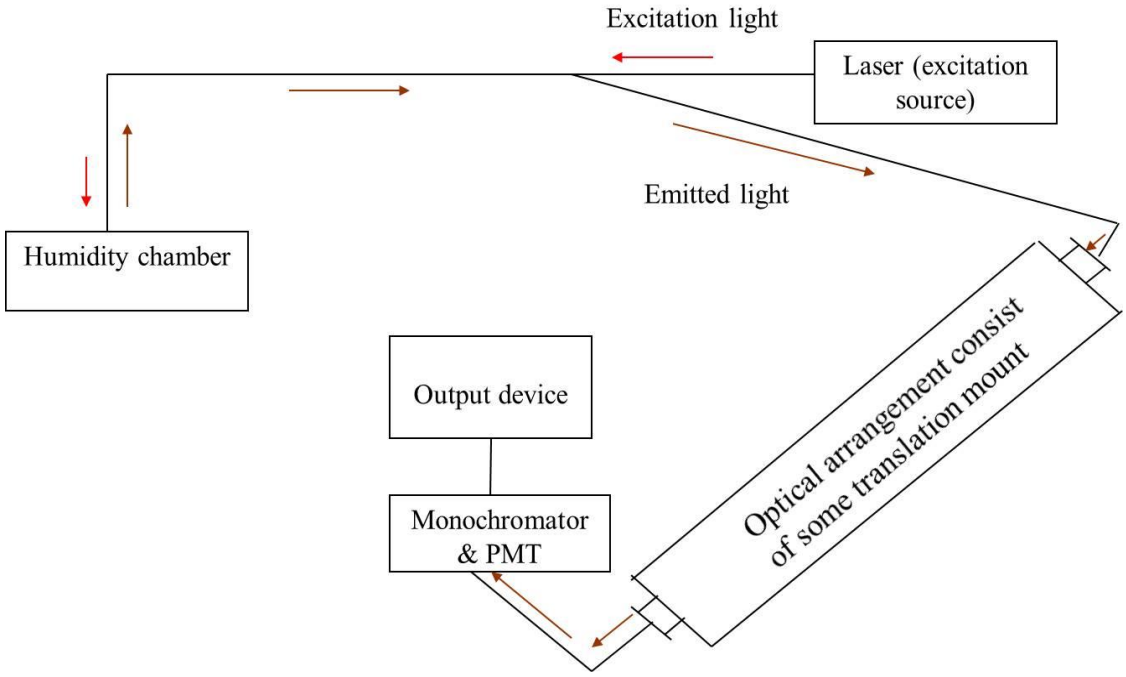

Figure 2.6: Schematic presentation of lifetime instrumentation. The excitation light from the 405 nm laser is guided through the central fiber into the sample placed in humidity chamber and the fluorescence emission is collected by an in house assembled TCSPC system.

The quality of fits was assessed by the $\chi 2$ value and the quality of the residuals trace *i.e.* symmetry about zero. Fitting with $\chi 2$ value not more than 1.2 was taken as acceptable. The standard deviation and error data were calculated by support plane error analysis. For every lifetime analysis, we calculated the intensity weighted average lifetime and reported three individual lifetime components (τ_1, τ_2, and τ_3) with their fractional amplitude (α_1, α_2, and α_3).

2.4. Photostability study

The aim of this experiment was to assess the photostability of the Tr fluorophores in thin polymer films. The same experimental set up described in Section 2.3.1. was used for photostability study. A spot on a sample of each Tr-polymer thin

film placed in the humidity chamber was continuously irradiated using 405 nm laser light (10 µwatt, 1 mm spot size) for ~4 hours at 50% RH. The emission spectra were recorded after every 10 mins. Before collecting emission spectra, the Tr doped polymer thin films were kept at a pre-set temperature and humidity (50%) in the chamber for 1 hour to ensure equilibration. The spectra were then analysed by curve fitting the spectra with the same method as described in Section 2.3.1. The photostability of Tr-polymer thin films were then presented as a fraction not photobleached versus time (in minute). The fraction not photobleached is calculated by the following equation

Fraction not photobleached = $(I_t / I_0) \times 100$

Where I_t is the fluorescence emission intensity maximum at time t

And I_0 is the emission intensity maximum at time 0.

2.5. Tr fluorophores photophysics: a solution study

Along with the Tr fluorophore's photophysical study (humidity-induced) in polymer thin films, the changes in photophysical properties when the Tr fluorophore was transferred from normal solution to polymer solution (or incorporation of thin films from its polymer solution) was also investigated. This study involved UV-vis, fluorescence and lifetime measurement of Tr fluorophore in different media.

The UV-vis absorption spectra were recorded with a Shimadzu UV-1601, the spectrometer was controlled and data viewed using the instrument software (UVProbe). Fluorescence emission spectra were collected using LS-50B (Perkin-Elmer) fluorescence spectrometer. All measurements were made using quartz cuvettes with pathlengths of 10.0 mm × 2.0 mm and the experiments were made at 25 °C.

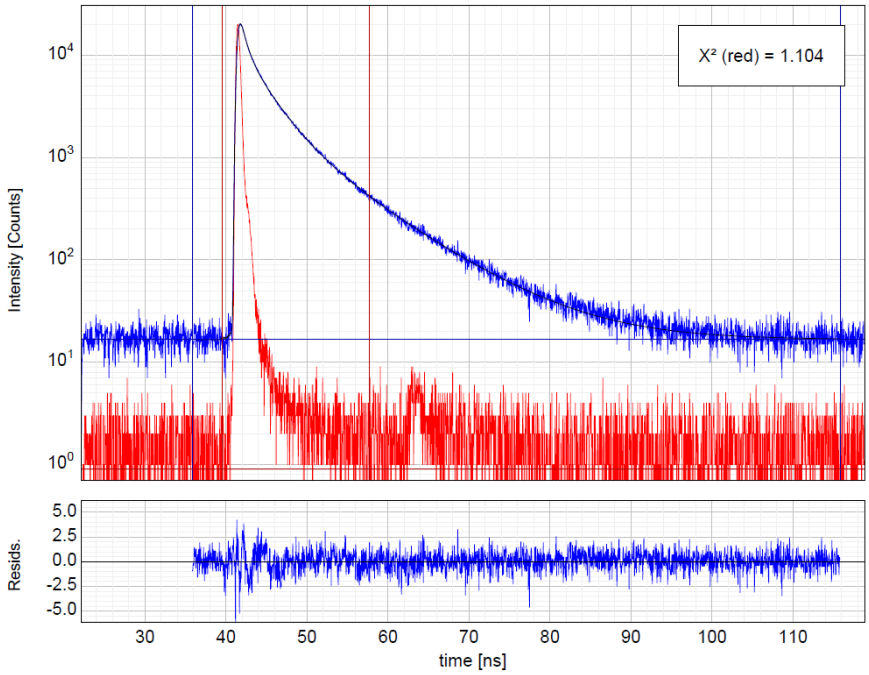

PicoQuant FluoFit 12/05/2015

Parameter	Value	Conf. Lower	Conf. Upper	Conf. Estimation
A_1 [Cnts]	380.89	-5.49	+5.49	Fitting
τ_1 [ns]	8.1596	-0.0698	+0.0698	Fitting
A_2 [Cnts]	1515.2	-18.1	+18.1	Fitting
τ_2 [ns]	2.8386	-0.0280	+0.0280	Fitting
A_3 [Cnts]	2714.9	-63.7	+63.7	Fitting
τ_3 [ns]	0.6206	-0.0152	+0.0152	Fitting
Bkgr. Dec [Cnts]	16.63	-1.03	+1.03	Fitting
Bkgr. IRF [Cnts]	0.90	-1.74	+1.74	Fitting
Shift IRF [ns]	0.14066	-0.00415	+0.00415	Fitting
A Scat [Cnts]	62410	-3540	+3540	Fitting
Period Rep [ns]	0.03508	-0.00215	+0.00215	Fitting

Average Lifetime:

$\tau_{Av.1}$=4.2462 ns (intensity weighted)

$\tau_{Av.2}$=1.9722 ns (amplitude weighted)

Fractional Intensities of the Positive Decay Components:

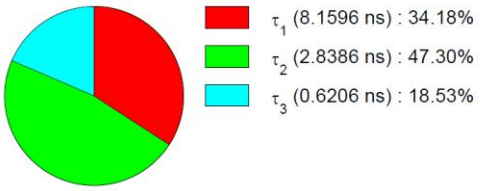

Figure 2.7 : A snapshot of lifetime data analysis by Fluofit software of TCSPC system for pTr (1×10^{-5}M) doped PNIPAm polymer (5% w/w) solution in water at 470 nm emission wavelength and λ_{ex} was 405 nm. The decay curves were fitted as a multi-exponential decay model and the intensity weighted average lifetime$\langle\tau\rangle$, three individual lifetime components (τ_1, τ_2, and τ_3) and fractional amplitude (α_1, α_2, and α_3) were collected from the analysis. The fitting were judged by $\chi 2$ value and a usually below 1.2 value was taken as acceptable. The lifetime was reported up to two decimal places.

Lifetime measurements of fluorophore doped polymer solutions were carried using the TimeHarp 200 (PicoQuant) TCSPC system using 405 nm excitation and the same emission wavelengths as previously described. IRF data was collected by using diluted (in water) 1 drop Ludox (AS-40 colloidal silica, 40 wt % suspensions in water (Sigma Aldrich)) in a cuvette for each set of experiments. For validation of the instrument 1×10^{-6} M HPTS (8-Hydroxy-1,3,6-pyrenetrisulfonic acid trisodium salt) was used. Decay curves were collected at room temperature. For every decay curve recorded, data was accumulated, until the channel at maximum intensity had reached an intensity of at least 20 k counts. Data analysis was performed by FluoFit (version: 4.5, PicoQuant) software (Figure 2.7) and the procedure was the same as previous described in section 2.3.2.

2.6. Optimization of some experimental parameters

Before assessing the humidity effects on spectral properties (in the following chapters) of the Tr fluorophores in different polymer thin films, we first optimized some experimental conditions *e.g.* drying time of Tr-polymer thin films for getting reproducible result, system equilibration time after absorbing water at specific %RH, and the effect of film thickness on the emission properties of Tr fluorophores.

2.6.1. Drying time of polymer thin films

A precise method of drying the polymer thin films was vital for producing reproducible results because should any residual water remains in the thin polymer matrices it may interfere with the fluorescence measurements. Hence, before conducting any experiments it was necessary to ensure that the films were completely dry. Previous studies in our lab [4] showed that several days of drying between two consecutive measurements were required for FE dye doped PNIPAm (FE-PNIPAm) thin films. They analysed the intensity ratio of two emission bands of FE-PNIPAm thin films as a function of humidity after drying the films for 48 hours and 84 hours. It was found that drying at 70 °C for 84 hours was required for the production of dry films reproducibility. To verify if a similar drying time was required for these pTr-PNIPAm systems the following experiments was undertaken. Two 10 µm thick pTr-PNIPAm films were prepared and then dried for 48 and 72 hours respectively. Each film was then placed in the humidity chamber and the emission data recorded at 25 °C

from 10- 90% RH. The experiment was repeated three times and the data plotted (Figure 2.8)

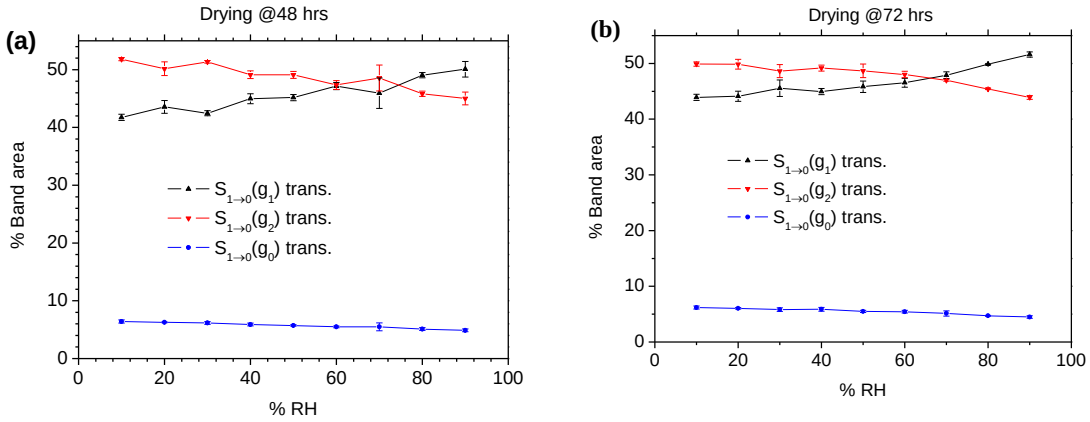

Figure 2.8: Plot of variation of % band area with increasing humidity for pTr-PNIPAm thin films at 25 °C after 48 hours (a) and 72 hours of drying (b). Each sample was equilibrated for one hour at each %RH set point prior to measurement. Error bar represents the standard deviation (S.D.) from the average of 3 replicate measurements.

It is clear from Figure 2.8 that the films which were dried for 72 hours yielded more reproducible results (Table 2.2). It is the % band area that is the most sensitive to film variation, and most of the variation involves the transition of the g1 and g2 conformers. As the pTr-PNIPAm films were obviously much less sensitive to water and drying compared to the FE-PNIPAm [4], it was not considered worthwhile to extend the films drying time any further.

Table 2.2: Average standard deviation of the variation of % band area as an effect of humidity for different excited state of pTr - PNIPAm thin films (10 µm) after 48 hours and 72 hours drying the film in oven at 70 °C. SD were calculated from the average of three replicate measurements.

Transition	Average SD	
	48 hours drying	72 hours drying
$S_{1\to0}$ (g_1) transition	± 0.95 %	± 0.71 %
$S_{1\to0}$ (g_2) transition	± 0.84 %	± 0.60 %
$S_{1\to0}$ (g_0) transition	± 0.25 %	± 0.25 %

2.6.2. Equilibration time at each humidity

The emission properties of fluorophores in liquid solvents can be measured easily and correlated with the physicochemical properties of the solvent since the sample is usually homogeneous [185, 226, 229]. It is more complex in polymer thin films. For humidity experiments, the thin films should have sufficient time to equilibrate with the environment at every specific humidity level. This equilibration time (the time required to extract the maximum amount of water from the chamber environment and diffuse throughout the polymers and establish equilibrium) is dependent on the polymer, water content of the films, temperature, and %RH. To obtain reproducible fluorescence emission data, it is necessary to allow a sufficiently long equilibration time for water to either fully diffuse in or out of the films.

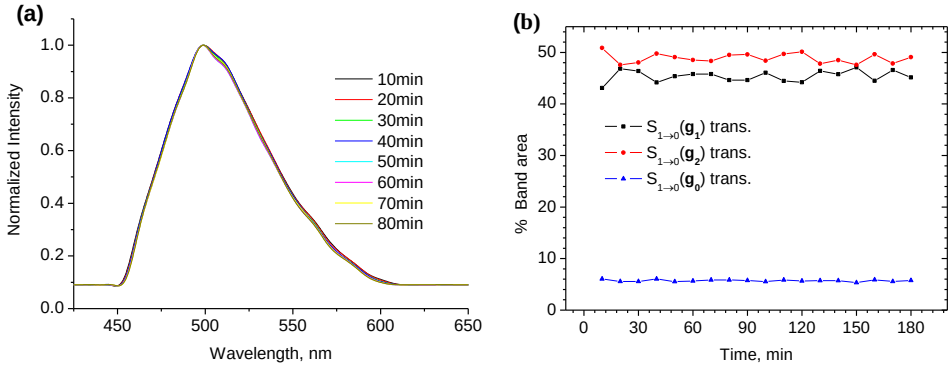

Figure 2.9: Plot showing the equilibration time for pTr-PNIPAm thin films at 50% RH where (a) smoothed normalized emission spectra with time (b) % band area variation with time. The humidity was set at 50%RH and the λ_{max} was 405 nm.

To determine the optimal equilibration time for the pTr-PNIPAm thin films system we took a film and placed it in the chamber. The sample was kept at 50% RH and data collected every 10 minutes for 180 minutes. Analysis of the data showed that there was very little spectral changes (Figure 2.9a) over this time. The band fitting (Figure 2.9b) showed some variation in the g1/g2 conformers but it was not time dependant and was more likely due to the intrinsic fit error. Therefore, from this experiment, and the fact that the much more water sensitive FE-PNIPAm system required 60 minutes, [4] we decided to use a standard 60 minutes equilibration time throughout.

2.6.3. Effect of film thickness on S-S emission properties of Tr

For the 10 µm thick Tr-PVA films, emission intensity was generally very low and thus long accumulation times (~25-40 min) were required to collect accurate data for lifetime analysis. This required time was longer at longer emission wavelength. For example, usually it was ~40 min. at 570 nm emission wavelength. This longer accumulation time causes photobleaching which could generate misleading results. To get a stronger emission required a higher concentration of fluorophores but we did not want to increase concentration, so the only alternative was to increase film thickness. However the thicker films affect the following things that will affect S-S measurements:

1. Might take longer for water to diffuse into film, so required longer equilibration.
2. More fluorophore in excitation volume increases the signal. This is the consequence of less noise and better quality fit.
3. Less scatter from quartz substrate and less noise.
4. Aggregation of fluorophore which may affect the S-S or lifetime measurements

To examine the effect of film thickness (within 10-20 µm) on S-S emission properties, first two pTr-PNIPAm thin films of 10 µm and 20 µm thick were prepared. The effect of humidity on S-S properties for both films were then studied and the most informative properties *i.e.* relative population of each emission conformer was plotted against humidity to see is there any variation in S-S emission properties when we varied the film thickness from 10- 20 µm.

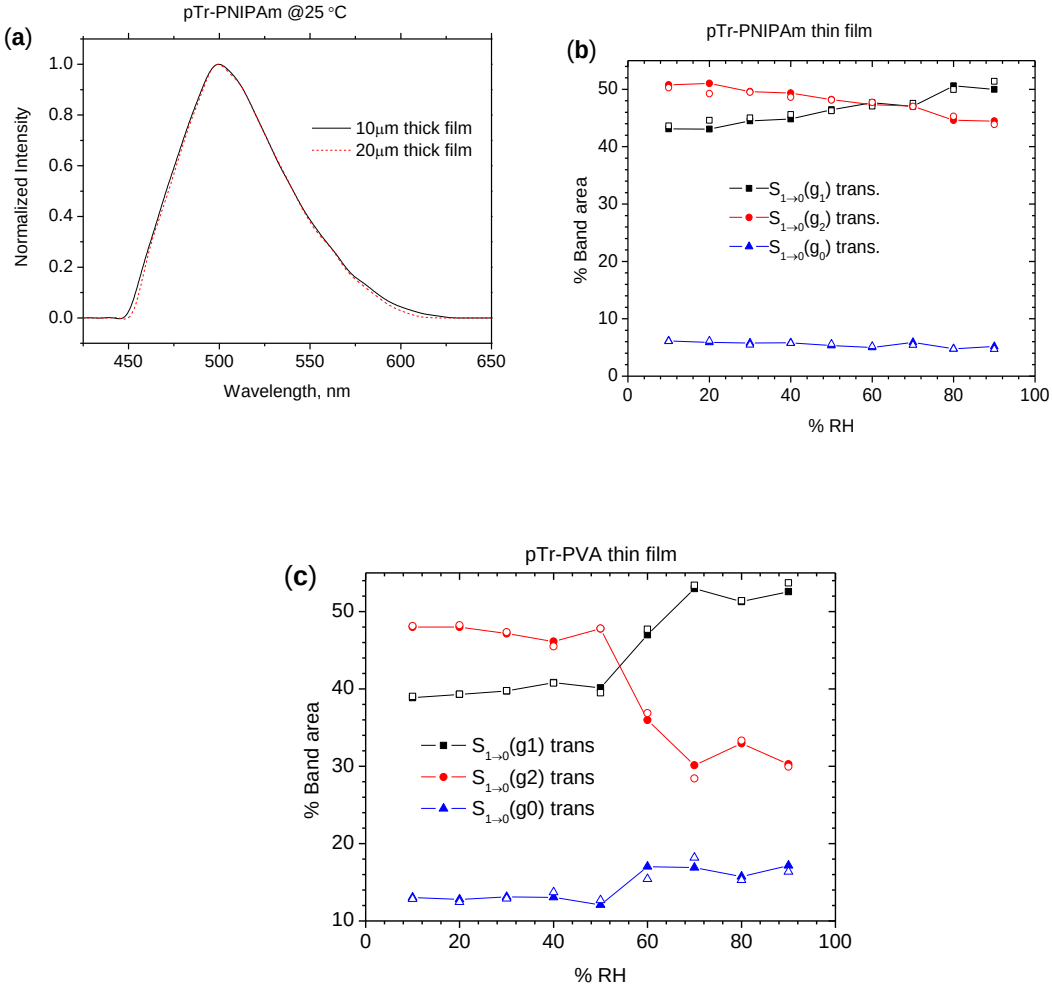

Figure 2.10: (a) Overlay emission spectra of pTr-PNIPAm thin films for 10 and 20 μm thick films. Plot represents the variation of % band area of pTr fluorophore doped into PNIPAm (b) and PVA (c) thin films (10 and 20 μm) as a function of humidity at 25 °C, where symbol represents the thickness of films, solid (10 μm) and open (20 μm). Samples were kept one hour prior to the spectral measurements for equilibration and humidity were varied from 10% - 90%.

The S-S emission properties remain relatively unchanged even upon increasing the films thickness from 10 to 20 μm both for PNIPAm and PVA thin films. The very small variations in relative population of three emission conformer were all within the intrinsic fit error (Figure 2.10 b/c). The emission were not shifted (Figure 2.10 a) which indicated that no aggregation of fluorophores within this range of thickness. For our investigation, 10 μm thick films for PS/PVP/PNIPAm and 20 μm for PVA were used throughout.

Chapter 3 : pTr in PS thin films: analysis of RI effects

3.1. Introduction

In this chapter the correlation between the variation in fluorescence lifetime of Tr-polymer thin films and the RI of the microenvironment will be investigated. The photophysical analysis of Tr fluorophores in hydrophilic and hydrophobic polymers, and the variation of the emission properties in a hydrophobic polymer (PS) as a function of humidity will be discussed. The hydrophobic nature of PS, would suggests that PS thin films should absorb very low amounts of water as humidity increases. To examine the correlation between the RI of the microenvironment and the average lifetime of Tr fluorophores, $\langle\tau\rangle_f$ was first measured for pTr doped PS and PVP thin films at a range of emission wavelength from 467 nm to 568 nm and then the RI data corresponding to the emission wavelengths were collected from literature [245].

3.2. Correlation of lifetime of Tr-polymer thin films with emission wavelengths and RI

The dependence of the fluorescence decay rate of fluorophores on the local micro-environments *i.e.* polarity [166, 246], temperature [166] and RI [48, 247, 248] is well established. The relationship between fluorescence lifetime and RI of the medium can be described by the well-known Strickler-Berg equation where the radiative decay rate is proportional to the square of the RI (Equation 1.37) when there is a mirror image relationship between the absorption and fluorescence. The exponent of RI dependence in the Strickler-Berg equation remains a subject of debate and several studies have attempted to investigate it [247]. The validation of the Strickler-Berg equation will not be discussed here; instead the correlation between emission lifetimes at various wavelengths with RI will be studied.

Two polymers (PS and PVP), for which RI data [245] were available, over the pTr emission range were selected to investigate the correlation between RI and lifetime. pTr doped thin films of both polymers were prepared and the lifetimes measured as previously described.

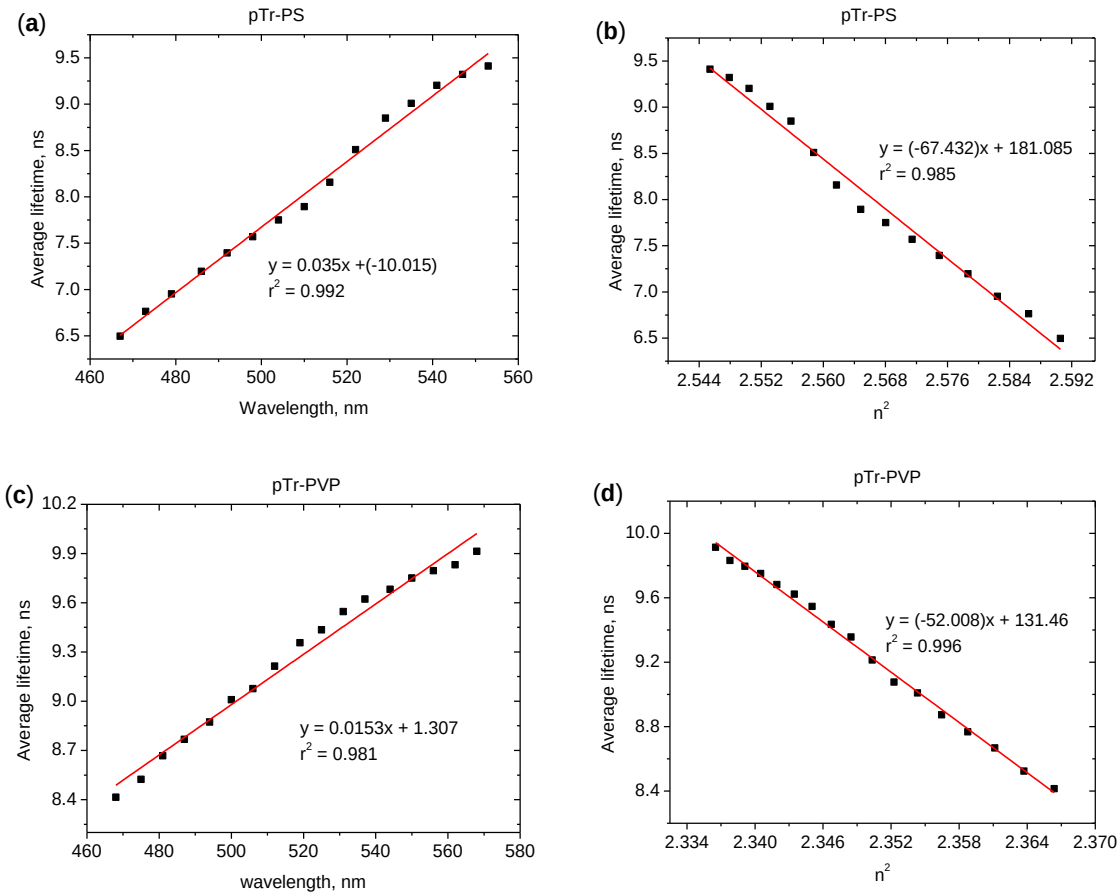

Figure 3.1: Plots showing the relationship between the average lifetime, $\langle\tau\rangle_f$ of pTr-polymer thin films and the emission wavelengths & RI of the thin films. The $\langle\tau\rangle_f$ vs emission wavelength is presented on (a) pTr-PS/(c) pTr-PVP thin films, and the $\langle\tau\rangle_f$ vs square of RI of the medium is presented on (b) pTr-PS/(d) pTr-PVP thin films. The $\langle\tau\rangle_f$ data of pTr doped PS and PVP thin films at different emission wavelengths were collected at 20 °C.

The $\langle\tau\rangle_f$ for pTr-PS and pTr-PVP thin films as a function of emission wavelength and n^2 are presented in Figure 3.1. An approximately linear relationship between lifetime and the emission wavelength was observed in both cases (Figure 3.1a/c). When n^2 of the PS and PVP polymers was plotted against the lifetimes for the pTr doped film (Figure 3.1b/d) we again obtained a near linear relationship. Interestingly, however, the small deviations from linearity match the emission band changes. This was due to the fact that each band represents a different emitting state and thus each will have a slightly different dependence on RI.

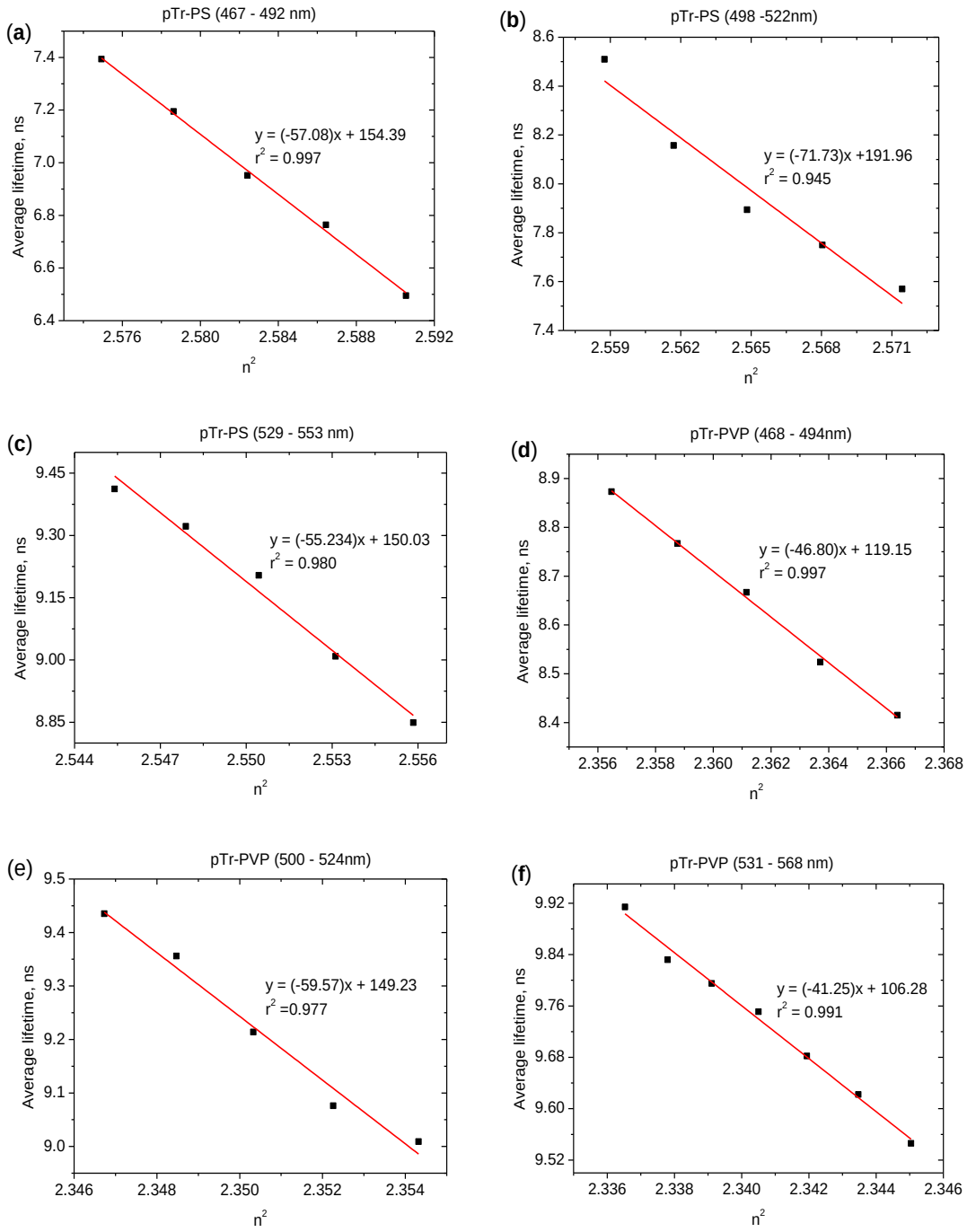

Figure 3.2: Plots showing the relationship between the average lifetime, $\langle\tau\rangle_f$ of pTr-PS and pTr-PVP thin films and the RI of polymer matrix in three prescribed regions of emission wavelength. Where, for pTr-PS, the three regions are: (a) 467 - 492 nm, (b) 498 - 522 nm, (c) 529 - 553 nm and for PVP: (d) 467 - 494 nm, (e) 500 - 524 nm, and (f) 531 - 568 nm. Data were collected at 20 °C.

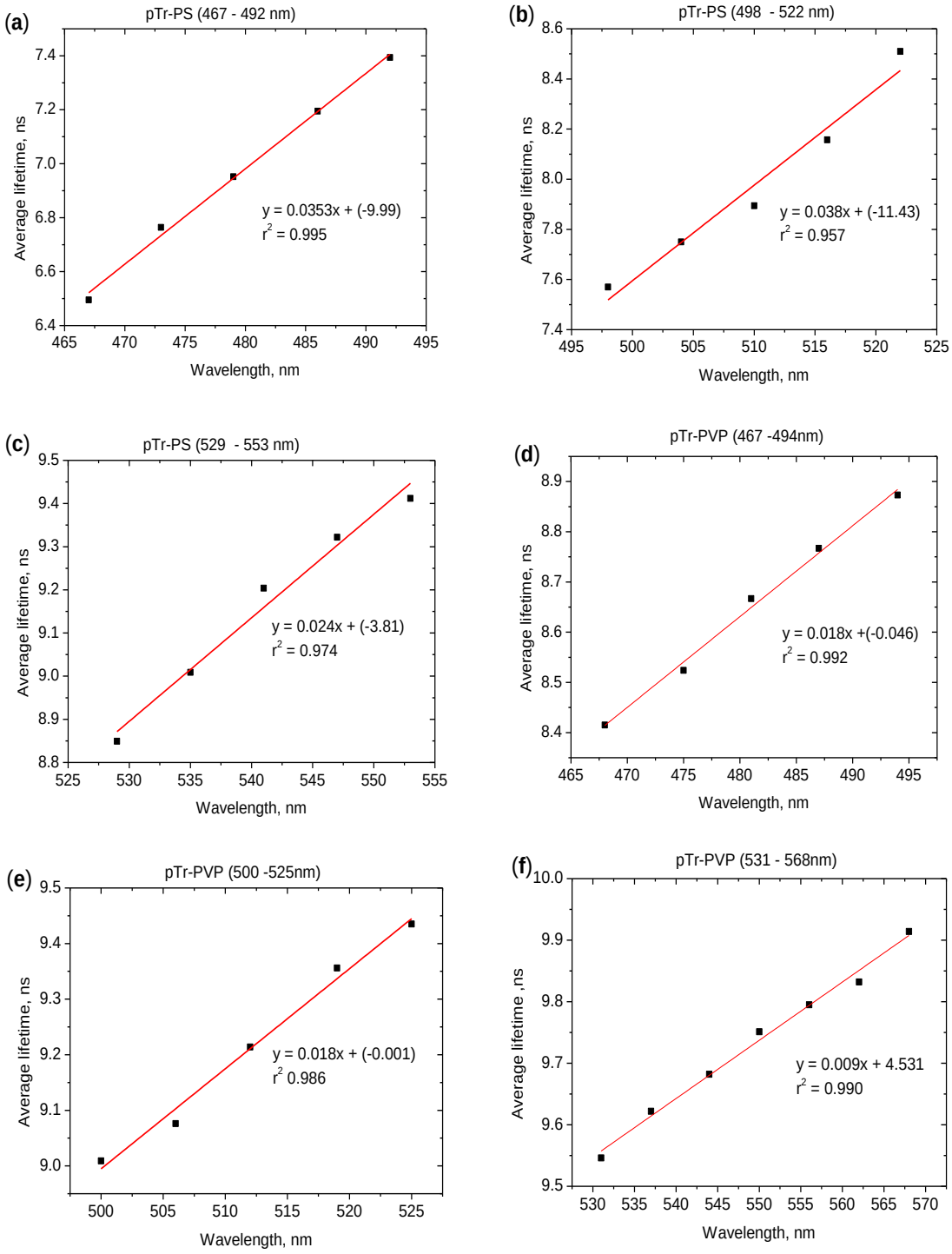

Figure 3.3: Plots showing the relationship between the average lifetime, $\langle\tau\rangle_f$ of pTr-PS and pTr-PVP thin films and the emission wavelengths at three prescribed regions. Where, for PTr-PS, the three regions are: (a) 467 - 492 nm, (b) 498 - 522 nm, (c) 529 - 553 nm, and for PVP: (d) 467 - 494 nm, (e) 500 - 524 nm, and (f) 531 - 568 nm. Data were collected at 20 °C.

To see if the lifetime dependence on RI was more linear over the individual bands, we replotted over three shorter wavelengths ranges corresponding to the centre band e.g. 465–495 nm, 496–525 nm, and 526–570 nm (Figure 3.2 and Figure 3.3).

For the first and third region an almost linear relationship was observed between the lifetime and n^2 of the medium (Figure 3.2 a/c/d/f). An approximately linear relationship (r^2 >0.98) for the first and third region was also observed between the lifetime of pTr doped PS/PVP thin films and the emission wavelength (Figure 3.3a/c/d/f). However, for the 496–525 nm region, there was a slight deviation from the linearity (r^2>0.94) (Figure 3.2 b/e and Figure 3.3 b/e). This was due to the overlap of the second emission band (*i.e.* $S_{1\rightarrow0}$ (g2) transition) with the other two emission bands ($S_{1\rightarrow0}$ (g1) transition and $S_{1\rightarrow0}$ (g0) transitions). Therefore, it is concluded that the wavelength dependent effect on lifetime is primarily a RI effect. The dependence was also slightly influenced by the different emitting species as evidence by the slightly different fit slopes (Figure 3.2 and Figure 3.3).

3.3. Study the photophysics of pTr in hydrophobic PS: a solution and thin film study

The steady-state emission properties of pTr were virtually unchanged when it was in a pure solvent solution, in a PS solution (in DCM) or when it was incorporated into thin films. The absorption (Figure 3.4a/c) and emission spectra (Figure 3.4b) were relatively unchanged when pTr was transferred from pure DCM solution into PS (solution) which indicates the absence of any kind of interaction in the ground state or in the excited state.

The fluorescence emission spectra were normalised and then band-fitted (Table 3.2) and in each case three distinct emission bands were obtained. The bands originated from the three different excited state conformers: $S_{1\rightarrow0}$ (g0) (Band 3), $S_{1\rightarrow0}$ (g1) (Band 1) and $S_{1\rightarrow0}$ (g2) (Band 2) transition. When the emission parameters (% band area, FWHM, band position) (Table 3.2) were analysed in more detail, again no significant changes were observed for pTr in DCM compared to a DCM/PS solution.

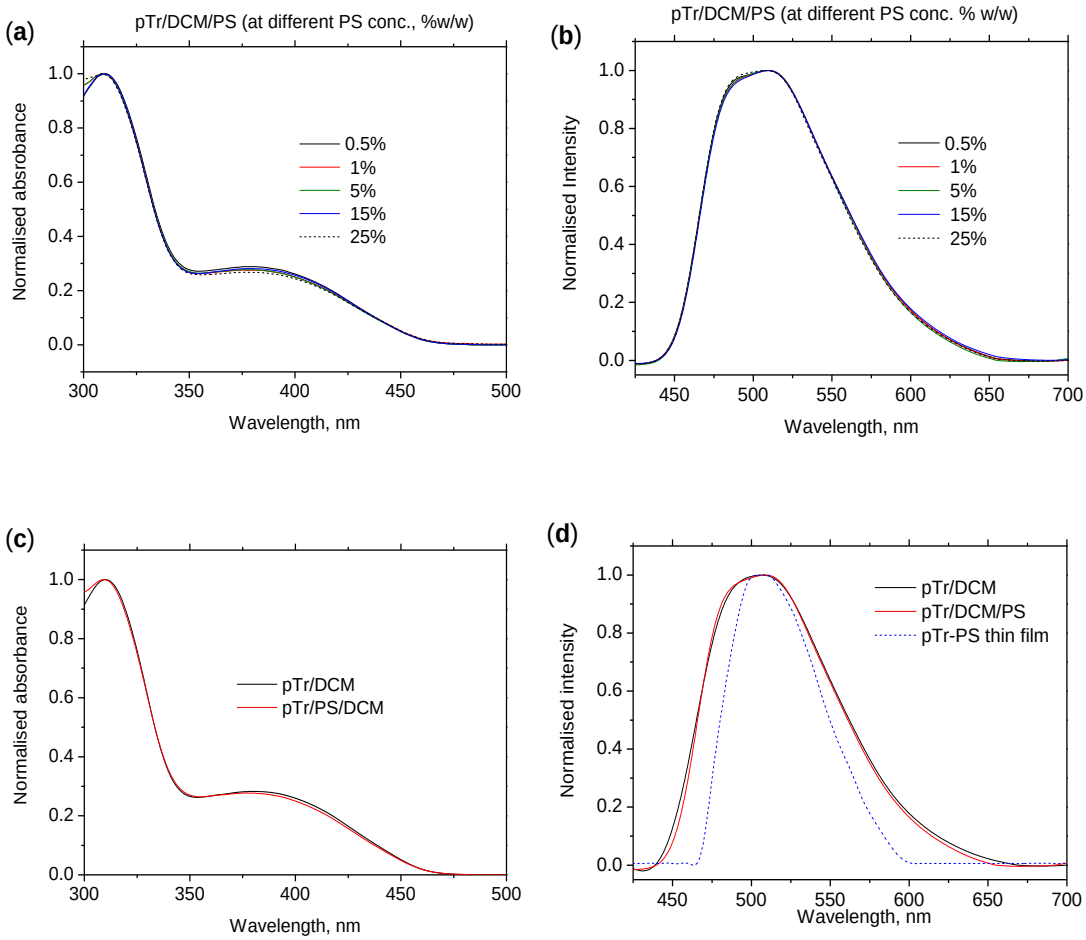

Figure 3.4: Plot of smoothed and normalised absorption (a), and emission (b) spectra of pTr doped into different concentration (%w/w) of PS polymer. (c) Plot of comparative normalised absorbance spectra of pTr, when it was doped into pure solvent, DCM and DCM/ PS (5% w/w) solution, (d) Comparative normalised emission spectra of pTr in pure DCM, DCM/PS (5% w/w) solution and in thin film. The concentration of pTr in solution was 7.5×10^{-5} M, λ_{ex} was 405 nm, and temperature was 25 °C.

Table 3.1: The intensity weighted average lifetime variation of pTr (1×10^{-5} M) in DCM solutions with different PS (%w/w) concentrations at room temperature and using 405 nm excitation. Only a single set of measurements made.

% PS	Intensity weighted average lifetime, ns				
	470 nm	490 nm	520 nm	540 nm	570 nm
0.5%	6.60	7.43	9.26	10.10	10.99
1%	6.61	7.49	9.41	10.27	11.21
5%	6.63	7.42	9.42	10.16	11.08
15%	6.25	7.43	9.14	9.99	10.87
25%	6.66	7.42	9.03	9.88	10.83

Table 3.2: Summary of the emission properties of pTr in pure solvent (DCM), in DCM/PS solution, and in thin films. The concentration of pTr in solutions was 7×10^{-5} M and PS was 5% w/w. All data acquired using 405 nm excitation and at 25 °C.

pTr in diff. media	Overall band position	Transition for 3 emission bands	Emission properties		
			% Band area	FWHM (cm^{-1})	Band position (nm)
pTr/DCM	509 nm	$S_{1\rightarrow0}$ (g1) trans.	36 ± 0.82	3098 ± 7.89	544 ± 0.58
		$S_{1\rightarrow0}$ (g2) trans.	47 ± 0.95	2219 ± 8.28	508 ± 0.69
		$S_{1\rightarrow0}$ (g0) trans.	16 ± 0.87	1296 ± 5.56	477 ± 0.61
pTr/PS/ DCM	509 nm	$S_{1\rightarrow0}$ (g1) trans.	35 ± 0.77	3139 ± 9.29	543 ± 0.88
		$S_{1\rightarrow0}$ (g2) trans.	49 ± 1.53	2251 ± 5.56	509 ± 0.92
		$S_{1\rightarrow0}$ (g0) trans.	14 ± 0.59	1248 ± 3.74	477 ± 0.75
pTr-PS thin films	508 nm	$S_{1\rightarrow0}$ (g1) trans.	45 ± 0.76	2253 ± 5.8	542 ± 0.20
		$S_{1\rightarrow0}$ (g2) trans.	52 ± 0.84	1607 ± 13.8	508 ± 0.09
		$S_{1\rightarrow0}$ (g0) trans.	04 ± 0.15	741 ± 8.4	475 ± 0.23

The small changes which were observed could be accounted for by the dilution effect. The FWHM of every band in the thin films were however only significantly reduced compared to DCM or DCM/PS which indicate that the pTr was located in a more restricted environment [61]. The lifetime data for pTr in DCM/PS solutions (Table 3.1) also suggest very small changes.

3.3.1. Effect of humidity on S-S properties in thin films

We expected that because PS is very hydrophobic that the degree of water absorption would be low (0.05% water absorption at 50% RH and 23 °C [62]) and thus the effect on pTr emission should be negligible when PS films were subjected to varying humidity. If this was to be the case, then the pTr-PS films could be used as a control to validate the humidity experiments[10].

[10] PS is very hydrophobic and thus has negligible water absorption. Any changes in pTr-PS thin film's emission properties were reasonably due to photobleaching rather than water effect. So, the humidity-induced photophysical properties of pTr doped hydrophilic polymer thin films could be corrected to get the only water-induced effect.

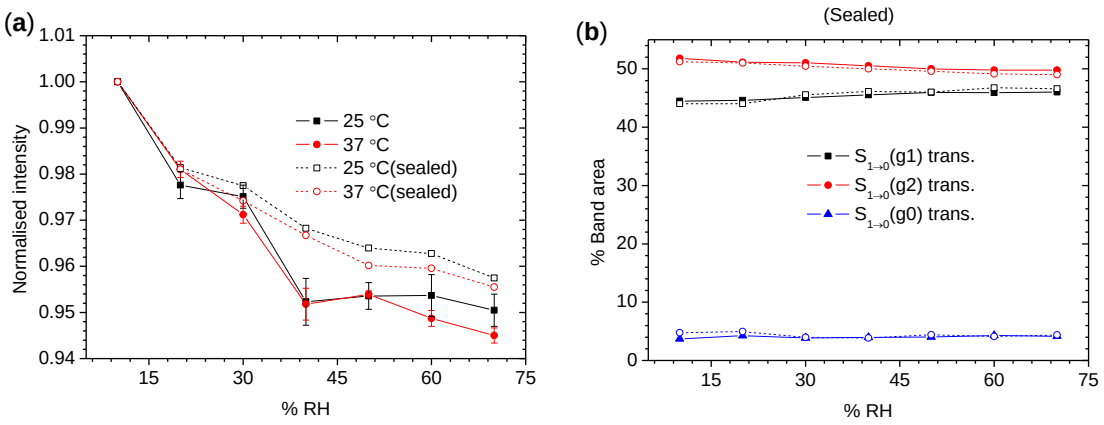

Figure 3.5: (a) Plot of changes in overall emission intensity (normalised to 10% RH) for Mylar sealed and open sample. Since, the accumulation of water droplet was observed in the humidity chamber window at ≥70%RH and at 37 °C, the intensity drop of pTr-PS thin films is presented up to 70% RH both for 25 and 37 °C. (b) Plot of changes in % band area (most sensitive emission parameter) for Mylar wrapped films study at both 25 and 37 °C. Symbols designate the measurement temperatures, solid (at 25 ° C) and open (at 37 ° C). For bandwidth and band position changes for wrapped films see Appendix III.

When exposed to changing humidity, small changes in the emission properties of pTr were observed *e.g.* a small drop (~ 5%) in intensity both at 25 and 37 °C up to 70% RH (Figure 3.5a), but the spectral shape was virtually unchanged (see Appendix III). Figure 3.6a shows that neither temperature nor %RH had a major effect on the individual band areas. Likewise, humidity-induced no significant changes in FWHM (Figure 3.6b) and band position (Figure 3.6c) were observed which indicate that there were no major changes in the energies either in the excited state or in the micro-heterogeneity.

This small overall intensity drop and changes in relative population of the g1 and g2 emission states could be due to photobleaching or water-induced quenching. As very small amount of water is absorbed (0.05%) by the PS films [60], one could expect minimal water induced quenching of fluorescence intensity.

To find out whether water infiltration was causing fluorescence quenching or any other changes in emission properties, the dry PS thin films were sealed by wrapping them in thin Mylar films and the same humidity variation S-S experiment was repeated. Plotting the changes in overall intensity as a function of humidity (Figure 3.5a), no significant difference (compared to wet film) in the Mylar wrapped

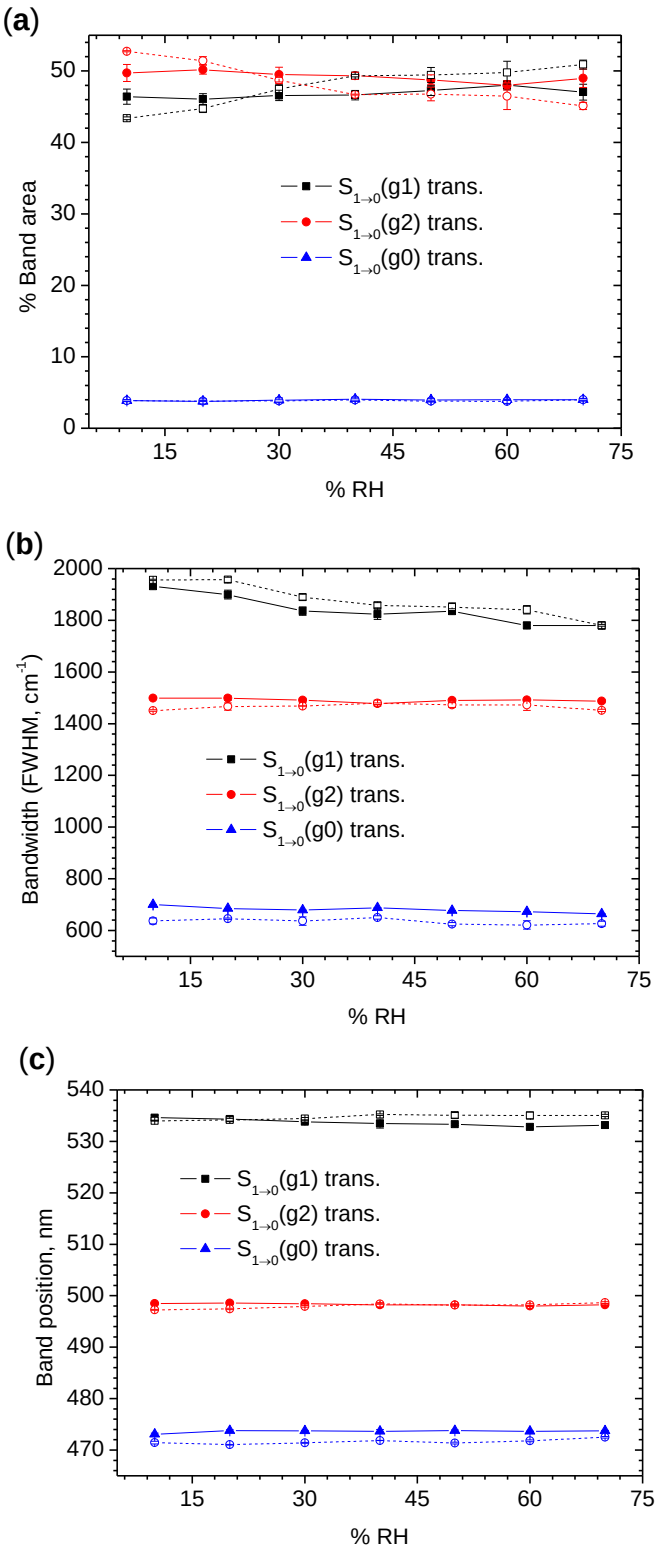

Figure 3.6: Plot of changes in (a) % band area, (b) bandwidth (FWHM, cm^{-1}), and (c) band position with increasing % RH for the pTr-PS thin films. Symbol designates the measurement temperature, solid (at 25 °C) and open (at 37 °C). For every case, error bar represents the SD from the average of three replicate measurements.

films were observed both at 25 and 37 °C. Again, no major changes in emission properties were observed, when band fitted for Mylar wrapped film emission spectra (Figure 3.5b). This would suggest that humidity-induced changes (Figure 3.5a) in emission intensity of pTr-PS thin films were due to photobleaching which might cause a small change in the relative populations of the g1 and g2 conformers.

Overall the changes in S-S emission properties of pTr in PS thin films were minimal and were relatively insensitive to changes in humidity. To gain a better insight into the pTr-PS humidity-induced photophysics, the effect of humidity on lifetime were then collected.

3.3.2. Lifetime at different emission wavelengths

The fluorescence lifetimes of pTr-PS thin films were measured at various emission wavelengths, and at 25/37 °C. All the lifetime decay data were fitted to a three exponential term. The humidity-induced changes in intensity weighted average lifetime (Figure 3.7), and individual fractional amplitudes and lifetimes, are shown in Figure 3.9. The three lifetime components were:

1. The longest lifetime component, τ_1 (fractional amplitude is α_1) was associated with Band 1 (*i.e.* $S_{1\rightarrow0}$ (g1) transition)
2. The medium lifetime component, τ_2 (α_2) was associated with Band 2 (*i.e.* $S_{1\rightarrow0}$ (g2) transition)
3. The shortest lifetime component, τ_3 (α_3) was associated with Band 3, (*i.e.* $S_{1\rightarrow0}$ (g0) transition)

Plotting the %RH humidity versus average lifetime of pTr-PS thin films at four different emission wavelengths (*i.e.* 470 nm, 490 nm, 520 nm, 540 nm), showed almost no variation at either 25 °C or 37 °C (Figure 3.7 a/b). The individual lifetime components also showed very little humidity-induced changes (Figure 3.9).

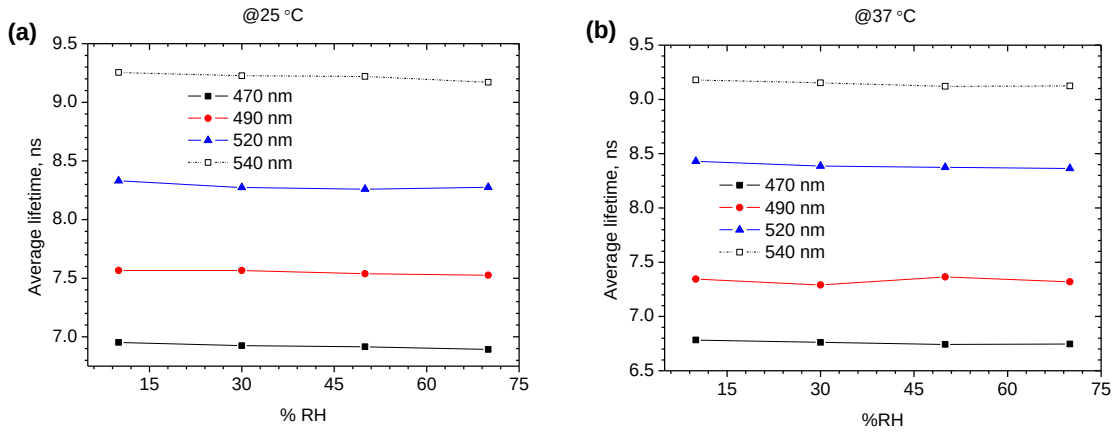

Figure 3.7: Plot showing the effect of humidity on the average lifetime, $\langle\tau\rangle_f$ of pTr-PS thin films at 25 °C (a)/37 °C (b) (at different emission wavelengths).

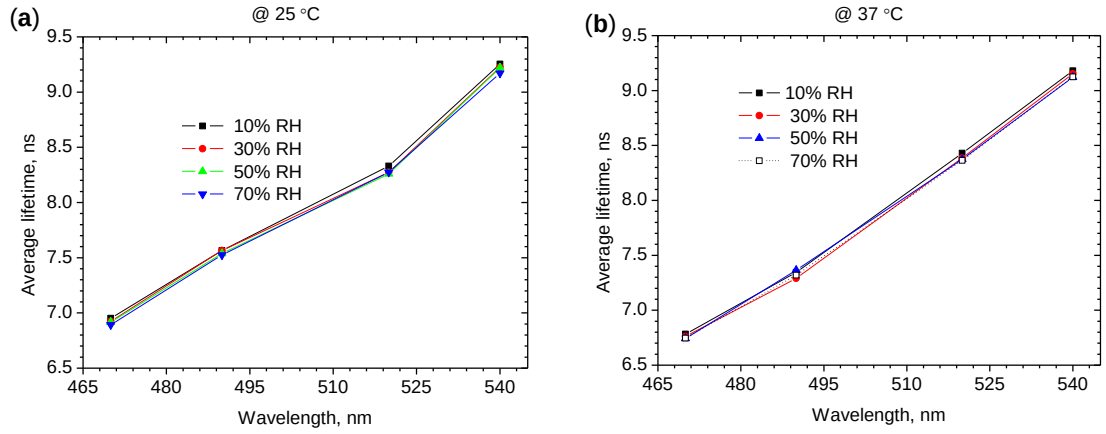

Figure 3.8: Plot showing the changes of average lifetime, $\langle\tau\rangle_f$ of pTr-PS thin films as a function of emission wavelengths at 25 °C (a) and 37 °C (b).

The small variation noted (~<1%) were within the error of the average lifetime fitting process. If the previous plot (Figure 3.5 a) showing a drop in intensity with increasing relative humidity had been due to a water-based quenching process then the lifetime data suggests that it could only be a static quenching process. However, we have already shown with the Mylar wrapped samples that the intensity drop is most likely due to photobleaching.

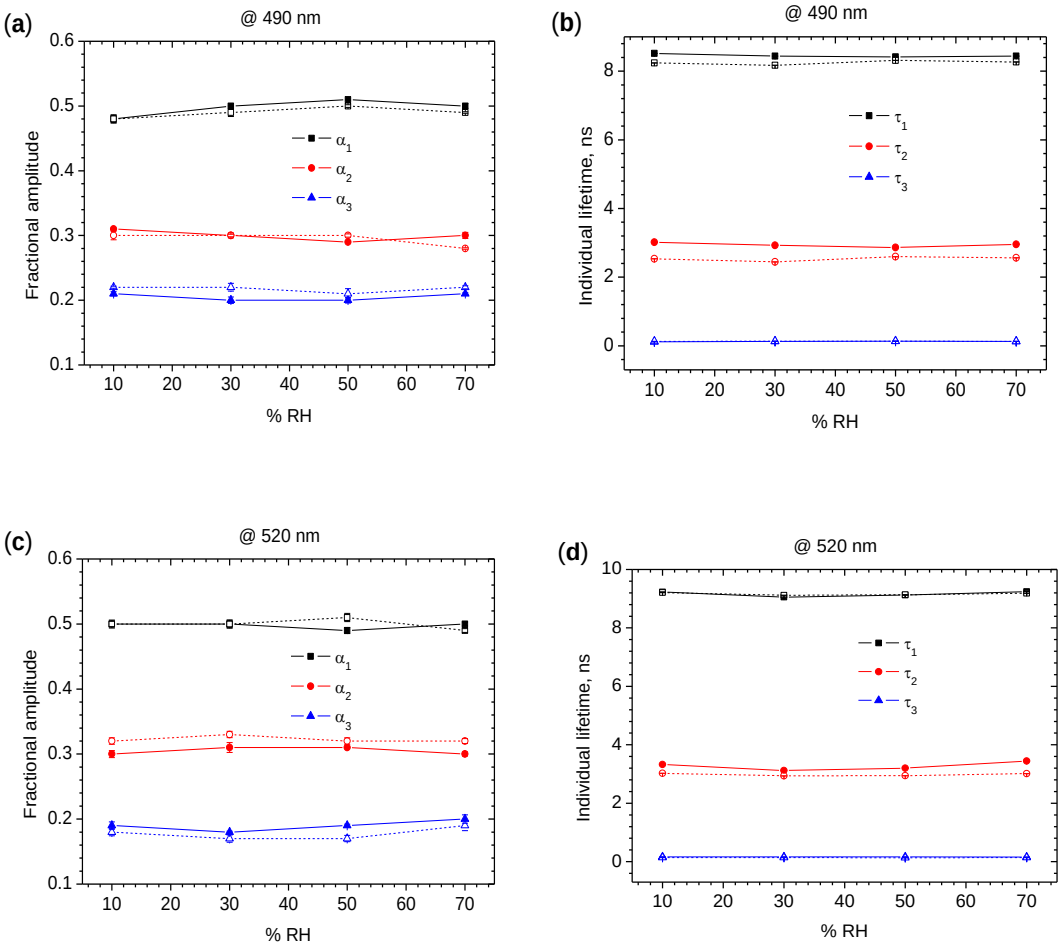

Figure 3.9: Plot of fractional amplitude and individual lifetime versus increasing humidity for a pTr-PS thin film at 25 and 37 °C at 490 and 520 nm emission wavelengths. All data were fitted to a tri-exponential model. Where αi = fractional amplitudes/pre-exponential factors. Amplitudes have been normalised such that Σ|αi| = 1.Errors calculated using support plane analysis. The individual lifetime and fractional amplitude for 470 nm and 540 nm see the Appendix III.

At any specific humidity, when we looked at $\langle\tau\rangle_f$, the lifetime increased with λ_{em} (Figure 3.8). For example, at 10% RH and at 25 °C, the lifetime of pTr-PS thin films were 6.95, 7.56, 8.33, and 9.25 ns at 470, 490, 520, and 540 nm emission wavelength respectively. This increase of average lifetime with emission wavelength was purely an RI issue and has already been described in Section 3.2.

3.3.3. Photostability study

When the overall emission intensity drop (as a fraction not photobleached) vs time of illumination of excitation light were plotted (Figure 3.10), a relatively small drop was observed after 4 hours of continuous illumination with 405 nm excitation

light (at 50% RH). No major changes in the other emission properties (bandwidth, FWHM, and band position) were observed both at 25 and 37 °C indicating that all conformers were equally affected (Figure 3.12).

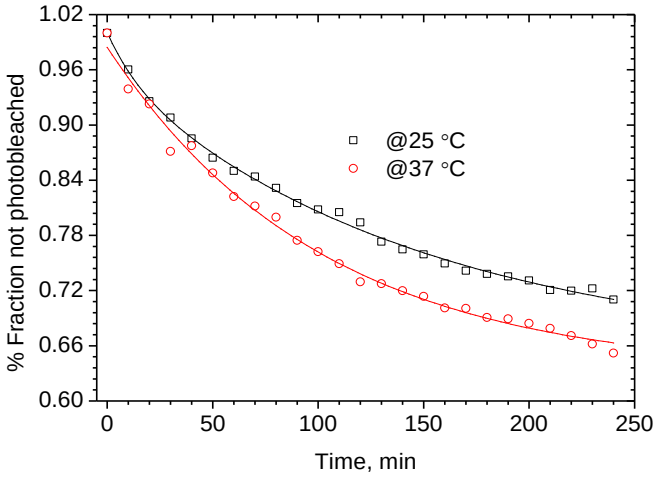

Figure 3.10: The photodegradation of pTr-PS thin films as a fraction not photobleached vs time both at 25 and 37 °C. The mono-exponential fitting equation at 25 °C was y = 0.305 exp(-x/108.92) + 0.68, r^2 = 0.993 and at 37 °C was y = 0.35 exp(-x/101.01) + 0.63, r^2 = 0.993. The film was continuously irradiated by 405 nm light over 4 hours where the power of incident light was 10 µW, the spot size was 1 mm, and the humidity was 50%.

The small photobleaching drop of pTr intensity (Figure 3.10) was not expected by water-induced H-bonding interaction with pTr and its absence was confirmed by the unchanged overall emission (see Appendix III). Since the photobleaching study was performed in a controlled humidity chamber, it was also very obvious that an O_2 driven photobleaching mechanism was absent in this system.

One possible reason for this intensity drop was: the changes in dipole moment during excitation might be somehow responsible for a photoinduced bi-molecular reaction with incoming highly polar water molecules leading to an irreversible photobleaching.

To ascertain the homogeneity of the pTr domain or where the pTr was located (during photobleaching) in PS thin films, the photobleaching curve was then fitted to various exponential models. This investigation was sought for whether mono-exponential or bi-exponential decay rate best describes the photobleaching. The behaviour of the photobleaching curve of pTr in PS films (both at 25 and 37 °C) was

captured well by a mono-exponential fit (by statistical analysis *i.e.* r^2, χ^2, and residual analysis, Figure 3.11, and Table 3.3). The mono-exponential decay indicates that the fluorophore is in a homogeneous environment and that a single process is responsible for photobleaching.

Table 3.3: Different statistical parameters from the decay kinetic model of photobleaching process of pTr-PS thin films at 25 and 37 °C

Parameter	Temperature			
	25 °C		37 °C	
	Mono-exponential	Bi-exponential	Mono-exponential	Bi-exponential
R^2	0.993	0.996	0.993	0.994
χ^2	4.20E–5	2.08E–5	6.41E–5	4.86E–5
$\sqrt{(\sum \text{Residual}^2)}$	9.25E–4	4.16E–4	0.0014	9.69E–4

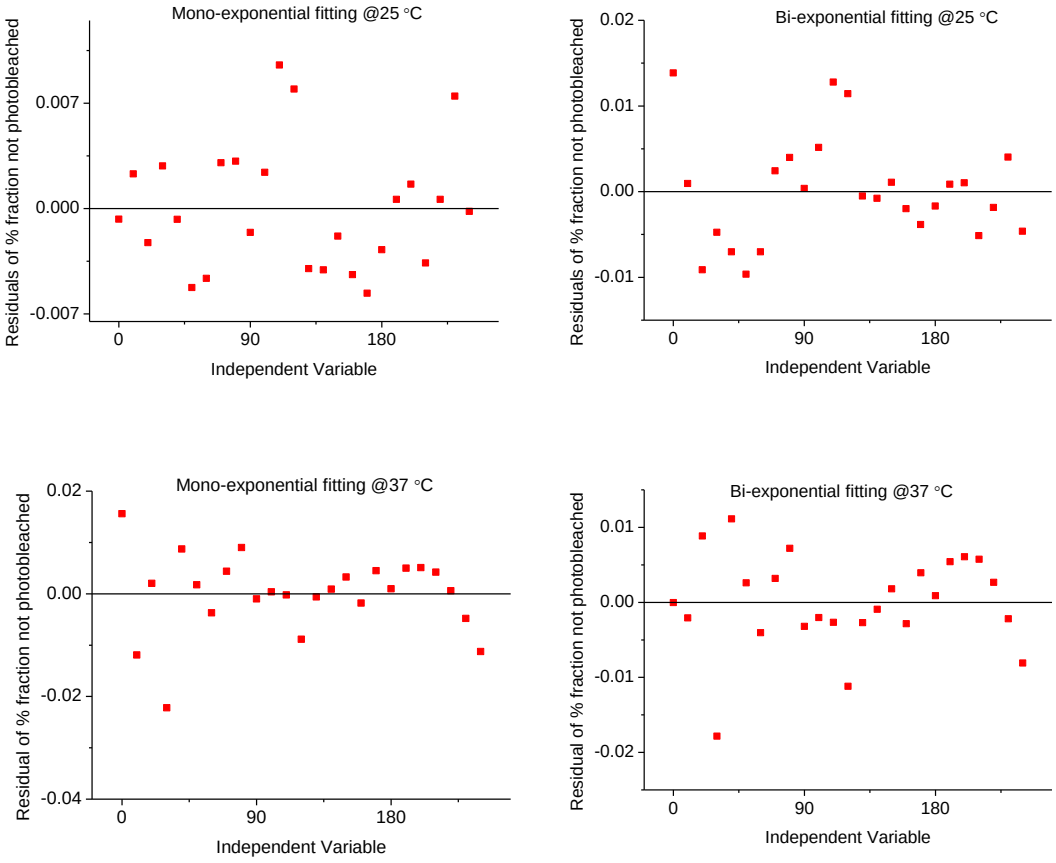

Figure 3.11: Plot of comparative residual from different decay kinetic model (mono and bi-exponential) of pTr-PS thin film's photobleaching curve both at 25 and 37 °C.

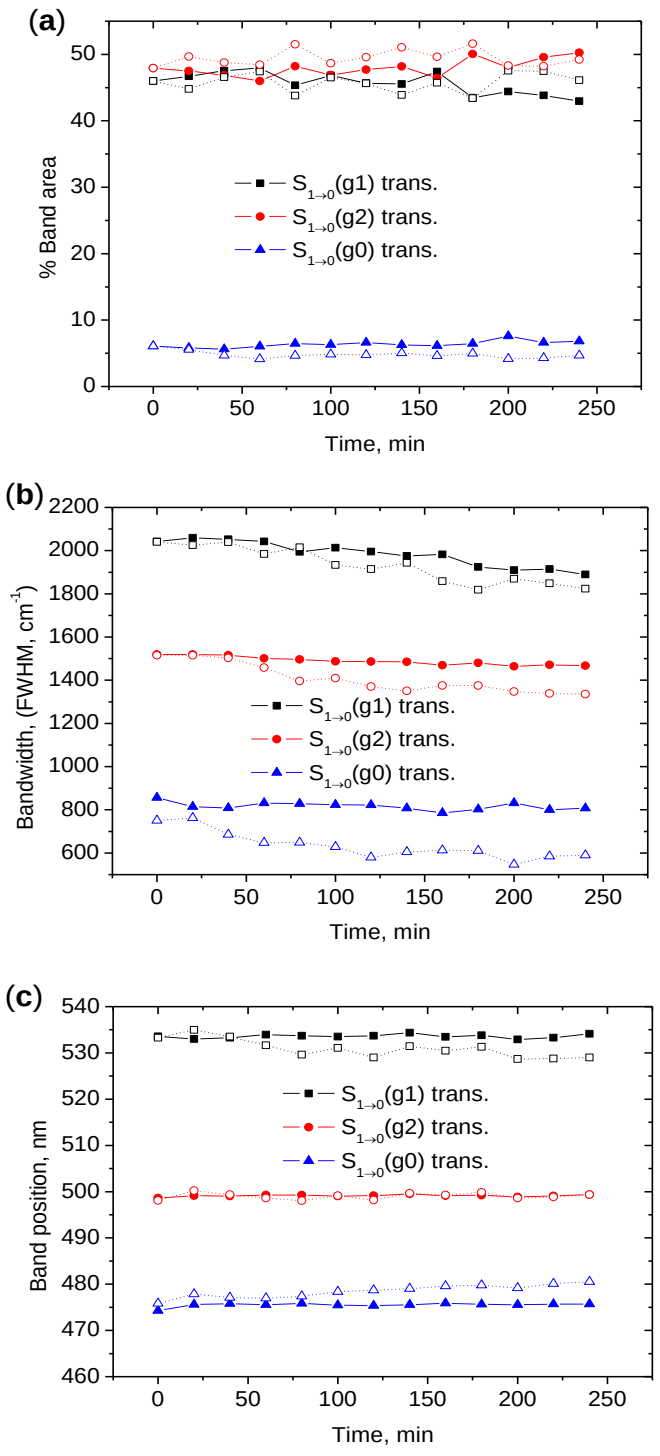

Figure 3.12: Photobleaching effect on emission properties of pTr-PS thin films, where plot of changes in % band area (a), bandwidth (FWHM, cm^{-1}) (b), and band position (c). Symbol designates the measurement temperature, solid (25 °C) open (37 °C). The humidity was 50 % and λ_{ex} was 405 nm.

The rate constant and the pre-exponential factor were slightly larger at 37 than 25 °C and thus a slight higher degree of photobleaching at 37 °C in Figure 3.10.

3.4. Conclusions

The main observation of this chapter was:

1) The wavelength-dependent increase in lifetime of pTr in PS thin films was found to be due only to the changing of RI.

2) When incorporated into PS thin films the pTr emission properties were found to be largely insensitive to changing humidity, which probably indicated that water was not being absorbed into the films and that any drop in intensity with illumination was due to photobleaching.

3) The photobleaching of pTr-PS thin films was found to be relatively small. The photobleaching curve was fitted to a mono-exponential function which indicated pTr was located in a homogeneous environment at 25 and 37 °C.

Chapter 4 : Effect of humidity on the emission properties of pTr in PNIPAm thin films.

The photophysical properties of pTr incorporated into thermoresponsive PNIPAm thin films were investigated. Experiments were designed to observe changes in the emission properties of pTr-PNIPAm thin films as a function of humidity below the LCST (*e.g.* at 25 °C), and above the LCST (*e.g.* at 37 °C) of PNIPAm.

4.1. pTr fluorophore: a solution study

The pTr fluorophore was hydrophobic but was relatively soluble in EtOH and the absorption (Figure 4.1a) and emission (Figure 4.1b) spectra in EtOH and EtOH-PNIPAm (5% w/w PNIPAm) solutions show some interesting features. First, there were significant differences in the absorption spectra and second, in the EtOH-PNIPAm solutions we observed a significant change in emission intensity, spectral profile and a blue shift (Figure 4.1c). The hypsochromic shift, and change in band shape were very significant as it indicated that there was some form of hydrophobic-hydrophobic interaction between pTr and the PNIPAm coils in solution.

The FWHM of all bands were very significantly reduced in the EtOH-PNIPAm solutions compared to EtOH (Table 4.1) indicative of some form of interaction. There was a further large decrease in bandwidth once incorporated in the polymer thin film, which is typical of being located in a more restricted environment [61]. There were also very significant changes in fluorescence lifetime as the proportion of PNIPAm increased (Table 4.2).

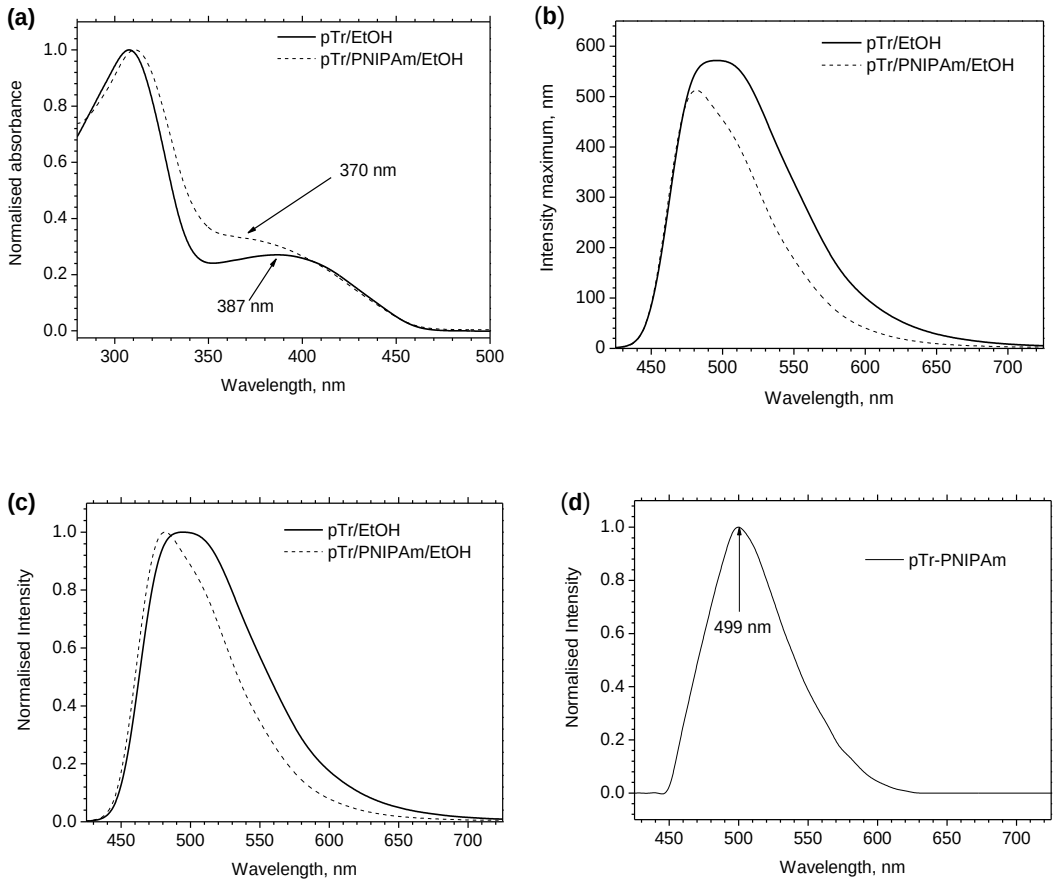

Figure 4.1: (a) Normalised absorption spectra of pTr in EtOH and PNIPAm/EtOH solutions. For pTr the first absorption band was at 308/309 nm. (b) Smoothed fluorescence emission spectra of pTr /EtOH and PNIPAm /pTr/EtOH. (c) Normalised emission spectra of pTr/EtOH and PNIPAm/pTr/EtOH. The concentration of pTr was 7×10^{-5} M. and PNIPAm was 5% w/w. (d) Normalised emission spectra of pTr-PNIPAm thin films at room temperature. All data acquired using 405 nm excitation and at 25 °C.

The hypsochromic shift observed for pTr when either incorporated into polymer thin or interacting with PNIPAm in solution was indicative of a significant physicochemical change in probe environment. The fact that the difference was very small between the EtOH/PNIPAm solutions and thin films indicates that the hydrophobic-hydrophobic interaction was strong in solution. This shift was unlikely to be solely caused by changes in dielectric constant (ε) as the change from ethanol (24.55) to PNIPAm below the LCST (63) was similar in magnitude to the difference in ε for PNIPAm above and below the LCST [249, 250] where we observed no hypsochromic shift (Figure 4.3c).

Table 4.1: Steady state emission properties for the pTr fluorophores in EtOH, EtOH/PNIPAm solutions, and dry PNIPAm thin films (all at 25 °C). All data acquired using 405 nm excitation.

pTr in diff. media	Transitions for 3 emission bands	Emission properties		
		% Band area	FWHM (cm^{-1})	Band position (nm)
pTr/EtOH	Band 1, $S_{1\rightarrow0}$ (g1)	36 ± 1.53	3092 ± 9.29	540 ± 2.08
	Band 2, $S_{1\rightarrow0}$ (g2)	49 ± 1.53	2187 ± 31.0	504 ± 1.52
	Band 3, $S_{1\rightarrow0}$ (g0)	15 ± 1.53	1252 ± 15.4	474 ± 1.15
pTr/EtOH/ PNIPAm	Band 1, $S_{1\rightarrow0}$ (g1)	34 ± 1.52	2894 ± 14.5	527 ± 2.08
	Band 2, $S_{1\rightarrow0}$ (g2)	43 ± 0.57	1962 ± 12.9	495 ± 1.52
	Band 3, $S_{1\rightarrow0}$ (g0)	23 ± 2.08	1210 ± 14.1	471 ± 1.15
pTr-PNIPAm thin films (dry)	Band 1, $S_{1\rightarrow0}$ (g1)	44 ± 1.15	2102 ± 35.1	527 ± 0.57
	Band 2, $S_{1\rightarrow0}$ (g2)	50 ± 2.00	1541 ± 17.5	495 ± 1.00
	Band 3, $S_{1\rightarrow0}$ (g0)	06 ± 0.57	818 ± 5.29	466 ± 1.15

Table 4.2: The intensity weighted average lifetime variation of pTr (1×10^{-5} M) in EtOH solutions with different PNIPAm (%w/w) concentrations at room temperature and using 405 nm excitation. Only a single set of measurements made.

% PNIPAm	Intensity weighted average lifetime (ns)				
	470 nm	490 nm	520 nm	540 nm	570 nm
0.5%	3.14	3.48	4.08	4.38	4.82
1%	2.77	2.79	2.81	2.83	2.88
2%	2.79	2.83	2.87	2.94	3.02
5%	2.78	2.80	2.84	2.87	2.92
10%	2.84	2.84	2.87	2.89	2.91
15%	2.94	2.95	2.96	2.97	2.98
20%	2.74	2.78	2.82	2.82	2.88
25%	2.66	2.79	2.83	2.85	2.95
$\Delta\langle\tau\rangle_f$	0.48	0.70	1.56	1.53	1.87

Taking the Lippert-Mataga equation (as an approximation) and using approximate RI values of 1.37 (EtOH) and 1.495 (PNIPAm) it was seen that the dominant factor affecting the Stokes shift was indeed RI [13, 251]. The calculated orientation polarizabilities for the two environments were 0.2856 (EtOH) and 0.2622

(PNIPAm) (See Appendix IV for more details). This was the root cause of the hypsochromic shift (and was backed up by lifetime data, *vide infra*), and the predicted shifts were 0.2856A for EtOH and 0.2622A for PNIPAm where $A=\frac{2}{hc}\left(\frac{(\mu_E-\mu_G)^2}{a^3}\right)$. Since this over predicts the observed hypsochromic shift by a significant margin (assuming the ground and excited state dipole moments were the same in EtOH and PNIPAm) then this also suggests that there was a significant change in cavity radius (a) for pTr. The small size of the observed shift would suggest that the cavity has decreased in size and this would tally with a strong hydrophobic interaction between PNIPAm and the probe.

Before assessing the humidity induced emission property changes of the Tr-PNIPAm thin films, an attempt was made to measure the water absorption of the film; this was done because water absorption will contribute to changes in micro-polarity of the system.

4.2. Mass of water absorption

The mass of water uptake by the Tr-PNIPAm thin films (as a percentage) as a function of humidity after each set of S-S experiment was determined by a simple procedure. The dry thin films on quartz slides were first weighed prior to starting the S-S fluorescence measurements. Successively, the humidity levels were increased by 10% and at each humidity level the samples were equilibrated for 1 hour in the humidity chamber. After completing data collection, the films were re-weighed immediately and the difference in weight between the dry and wet films was calculated to determine the amount of water absorbed. The range of RH examined was 10 - 90%.

For the 10 μm thick films, the total water absorption was 11.5±0.7 (original dry wt %) at 25 °C, and 4.3±0.3 (original dry wt %) at 37 °C. SD was calculated from the average of three replicate measurements.

4.3. Steady state (S-S) properties: a humidity study

It has been previously shown that PNIPAm films behave differently above and below the LCST and that water infiltration can have a dramatic effect on the emission properties of encapsulated fluorophores [4]. However, in the present experiments pTr displayed very little change in S-S emission as humidity increased and water was

absorbed. Only a slight decrease in overall emission intensity (Figure 4.2) was observed while there was a small change involved the band areas related to the population of g1/g2 conformers (Figure 4.3a) and temperature did not have a very significant effect. The spectral shape was relatively unchanged (Figure A.IV.1 and Table A.IV.1) and the FWHM of three bands varied only a little at both 25 °C and 37 °C (Figure 4.3b). This indicated that there was no major change in the energies of the excited states or the micro-heterogeneity.

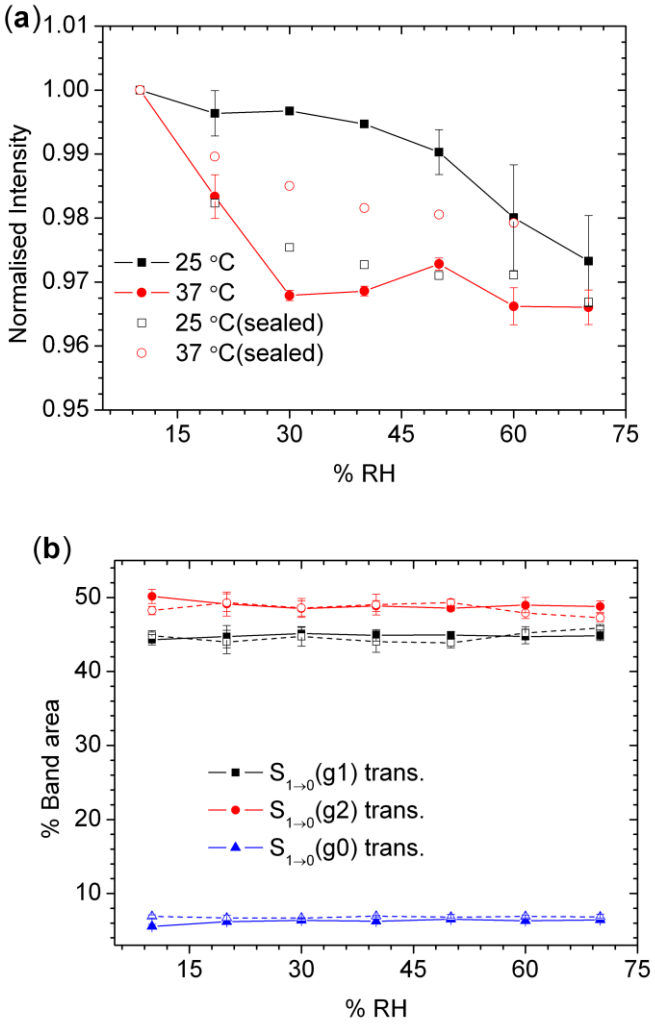

Figure 4.2: (a) Plot showing the humidity induced drop in overall emission intensity of pTr-PNIPAm thin films (wet and Mylar wrapped) both at 25 °C, and 37 °C, where intensity maximum at different humidities was normalised to 10% RH. (b) Plot of changes in % band areas for Mylar wrapped films as an effect of humidity (for changes in FWHM and band position see Appendix IV). The $\lambda_{ex.}$ was 405 nm. Since, the accumulation of water droplets were observed in the humidity chamber window at ≥70%RH and at 37 °C, the intensity drop of pTr-PNIPAm thin films is presented up to 70% RH both for 25 and 37 °C. The thickness of the films was 10 µm.

These small changes in the overall fluorescence intensity could be due to two factors, photobleaching and/or water-induced quenching. To try and discriminate which was the most dominant we prepared some pTr-PNIPAm films, sealed them in Mylar, and then placed in the chamber and repeated the humidity experiment. The data (Figure 4.2a) showed that there was no significant difference in intensity at 25 and 37 °C compared to that observed for the pTr containing films exposed to water, and crucially there was also no significant changes in the relative band areas at either temperature (Figure 4.2b). This indicates that photobleaching was the dominant factor affecting emission intensity in both dry and wet films, as the intensity decrease was the same. In the wet films however, there was also a significant change in the relative populations of g1 and g2 which (Figure 4.3a) must be due only to the presence of water.

It is clear from Figure 4.3 that the relative population of the g0 emission conformer was relatively unchanged, while a gradual increase in emission from the g1 conformer and a decrease in g2 emission were observed. For example, when the humidity was increased from 10-70% at 25 °C, the relative population of S_1 (g1) excited state appeared to increase by 4% for pTr. As there were no observable band shifts (Figure 4.3c) can ascribe these changes to changing populations of the S_1 (g1) and S_1 (g2) emitting states.

The changes in relative band intensity with relative humidity was fitted to a linear function and for the bands associated with g1 and g2 near linear relationships ($r^2 > 0.95$) were observed (Table 4.3). The fact that the slopes were opposite in the sign and almost the same magnitude indicates that this was a linked process. For the g0 related band the slope was nearly zero which indicates it's not really affected by the presence of water.

Table 4.3: Linear fit of changes in relative population of the three excited states, S_1 (g1), S_1 (g2), and S_1 (g0) of pTr- PNIPAm thin films as a function of humidity.

Tr	Transition	25 °C			37 °C		
		Slope	**Intercept**	**r^2**	**Slope**	**intercept**	**r^2**
pTr	$S_{1\rightarrow0}$(g1) trans.	0.08±0.06	42.02±0.25	0.97	0.11±0.02	40.87±0.67	0.95
	$S_{1\rightarrow0}$(g2) trans.	-0.06±0.04	51.50±0.16	0.98	-0.10±0.01	52.91±0.60	0.95
	$S_{1\rightarrow0}$(g0) trans	-0.01±0.03	6.47±0.13	0.87	-0.02±0.02	6.26±0.09	0.96

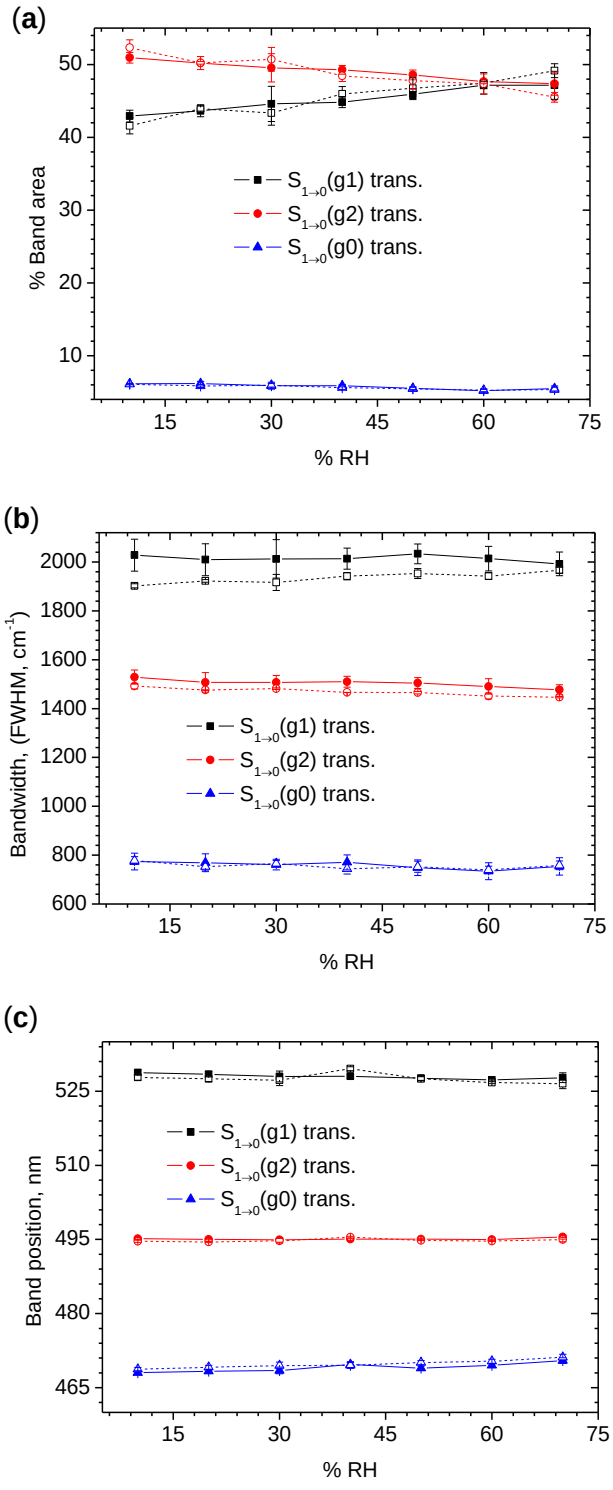

Figure 4.3: Plot of variation of (a) % band area, (b) bandwidth (FWHM, cm^{-1}), and (c) band position with increasing % RH for the pTr-PNIPAm thin films. Symbol designates the measurement temperature, solid (at 25 °C) open (at 37 °C). For every case, error bars represent the SD from the average of three replicate measurements.

The changes in the relative populations of g1 and g2 as observed by the relative changes in band area were driven by a combination of the excited state energies and dipole moments. For g2, the calculated values are 23759 cm^{-1}/4.51 μD whereas for g1 the corresponding values are 20523 cm^{-1}/4.69 μD [6]. Therefore, as water was absorbed, the matrix polarity was increased favouring the g1 conformer, the energy drop from g2 to g1 is also favourable, facilitating intramolecular vibrational relaxation (IVR) into g1.

What was also interesting here was that the two-step hydration process was not observed from the pTr emission which had clearly occurred with the emission of the 3-HF fluorophores in PNIPAm thin films and PNIPAm-NtBA copolymers [4]. With the 3-HF fluorophores most of the fluorescence variation was due to H-bonding and polarity changes [4, 134], and it was inferred that during water uptake the water first solvated the polymer generating a strongly hydrogen bound layer with the hydrophilic elements of the polymer chain (N–H and C=O groups), and then a second hydration layer was formed which had a greater effect on the 3-HF emission. This model was supported by the molecular dynamic studies of PNIPAm by Tamai [82].

Water uptake in bulk PNIPAm is significant with ~8% of its dry weight in water being absorbed at 20 °C with 90% RH and this should be greater once the polymer was prepared as a thin film. Above the LCST at 40 °C, in the bulk material, gravimetric analysis indicated that no water was absorbed [252] but it has been shown in ref. [4] (by changes in the fluorescence emission of 3-Hydroxyflavone (3-HF) fluorophores) and above in Section 4.2 (by gravimetric measurements) that above the LCST a significant amount of water was absorbed by high surface area thin films.

Table 4.4: The total changes of emission properties of pTr-PNIPAm thin films as a function of humidity up to 70% (the + and – sign indicates the increase and decrease of value respectively). Where A_1, A_2, A_3 are the relative population; W_1, W_2, and W_3 are the bandwidth (FWHM); and BP_1, BP_2, and BP_3 are the band position of S_1 (g1), S_1 (g2) and S_1 (g0) excited states respectively.

Tr	Temp.	Area (%)			FWHM (cm^{-1})			Band position, nm		
		ΔA_1	ΔA_2	ΔA_3	ΔW_1	ΔW_2	ΔW_3	ΔBP_1	ΔBP_2	ΔBP_3
pTr	25 °C	+4	- 3	-1	+14	-39	-40	-1	Const.	+2
	37 °C	+6	-5	-1	+46	-40	-39	-1	Const.	+2

Overall the changes in S-S emission properties were very small, and the pTr seems to be largely insensitive to the changing environment in PNIPAm (Table 4.4). There was a small red shift in the shortest wavelength band of ~ 2 nm up to 70% RH which may indicate that this conformer was slightly more sensitive to the environmental change. This holds with the computational modelling for this fluorophore [241] where the calculated dipole moment for the S_1(g0) state was considerably higher (6.25 μ(D)) than for the other two S_1 states (4.69 and 4.51 $\mu(D)$ for g1 and g2 respectively) so one might expect at least some increased interaction. However, the effect is the same above and below the LCST, despite the fact that the dielectric constant, ε, of the PNIPAm environment will have decreased from 63 (at 15 °C) to 17 (at 40 °C) according to Iwai *et al* [253]. They estimated these ε values for PNIPAm hydrogels based on fluorescence measurements made using a covalently linked 9-(4-N,N-dimethylaminophenyl) phenanthrene fluorophore which exhibited a strong intramolecular charge-transfer (ICT) fluorescence.

Since the S-S emission changes for the pTr in PNIPAm films were very small and there was some uncertainty over the cause of the small changes observed we collected detailed fluorescence lifetime data above and below the LCST at different %RH to try and better understand the emission properties.

4.4. Lifetime at different emission wavelengths

In Chapter 3 it was shown that for pTr, the change in lifetime with wavelength was an RI effect. In PNIPAm, a similar behaviour was observed (Figure 4.6) indicating that the same effect was occurring. The changes in RI with humidity were responsible for the increase of lifetime at 25 °C (Figure 4.5a) and decreases at 37 °C (Figure 4.5b). The pTr's average lifetime was much shorter in PNIPAm thin films (compared to PS) which were the effect of less rigid environment.

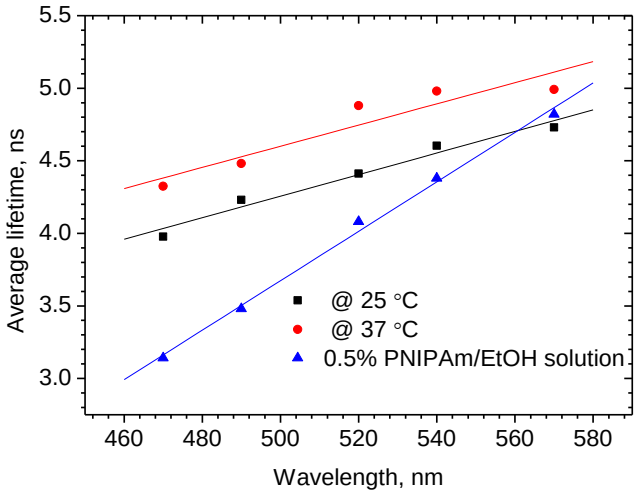

Figure 4.4: Plots of pTr intensity weighted average lifetime $\langle\tau\rangle_f$ vs. emission wavelengths at 25/37 °C for relatively dry PNIPAm films (10% RH) and a 0.5% w/w EtOH-PNIPAm solution. The data were linearly fitted and the fitted equation are @ 25 °C, y = 0.007x + 0.54, r^2 =0.98, @ 37 °C, y = 0.007x + 0.95, r^2 = 0.94, and @ 0.5% PNIPAm solution, y = 0.017x +(-4.84), r^2 = 0.99. The data were acquired at 405 nm excitation.

Under relatively dry conditions (10% RH), (Figure 4.4) the lifetime was slightly longer above the LCST and this indicates that the PNIPAm thin films must be less dense, with a lower RI, as there were no significant changes in the S-S emission Figure 4.3. Since these films were dried over three days, we were reasonably certain that in both cases all the water of hydration was eliminated and that the pTr was reporting only the change in RI. Below the LCST, the fluorescence lifetime increased linearly (r^2>0.95, Table 4.5) with %RH for the entire emission wavelength sampled (Figure 4.5a). The fit data (Table 4.5) showed that the slope was approximately the same at each RH. This would again suggest that the lifetime change was caused by RI changes. Above the LCST (Figure 4.5b), the situation was reversed and the lifetime decreased reasonably linearly with increasing water content.

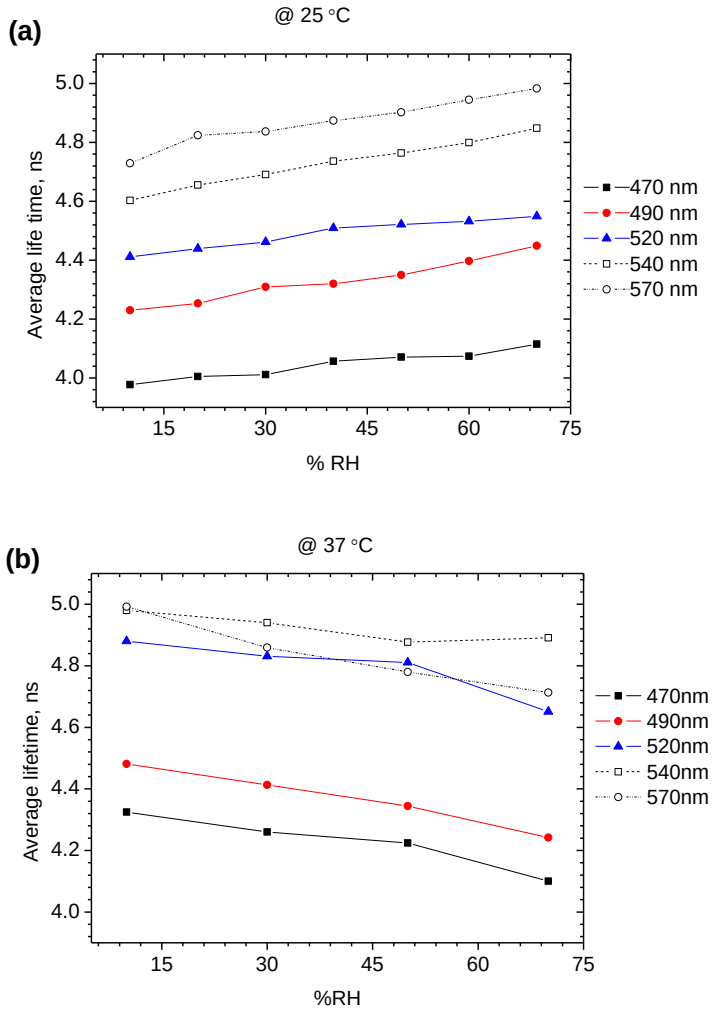

Figure 4.5: Plots showing the humidity-induced changes in average lifetime, $\langle\tau\rangle_f$ of pTr-PNIPAm thin films at 25 °C (a), and at 37 °C (b) (at different emission wavelengths).

The humidity-induced lifetime change of pTr-PNIPAm thin films can be explained by the fact that at 25 °C PNIPAm is soluble in water. Philipp *et al*. reported the RI of amorphous PNIPAm to be 1.495 at room temperature and ~1.3775 for a 25 mass% aqueous solution at 26 °C [251]. Therefore as the water content increased, water diluted the polymer and decreased its density (and thus RI) leading to increase lifetimes. Above 32 °C however, the situation was different as the fluorophore was located in hydrophobic domains and as water ingress occurred, these were squeezed tighter, and this increased the density and thus decreased the lifetime. This RI related lifetime behaviour was also observed for the individual lifetime components (Figure 4.7, and also see Appendix IV) but changes in $\langle\tau\rangle_f$ caused by humidity changes were small but significant. (Figure 4.5, and Table 4.5).

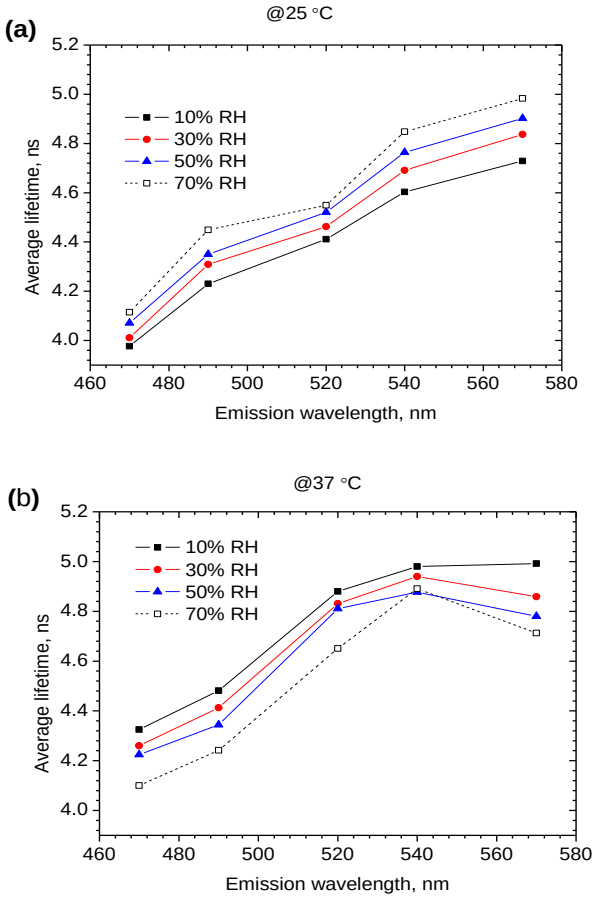

Figure 4.6: Plot showing the changes in average lifetime, $\langle\tau\rangle_f$ as a function of emission wavelengths for pTr-PNIPAm thin films at 25 (a) and 37 °C (b).

Table 4.5: Linear fit of average lifetime, $\langle\tau\rangle_f$ of pTr-PNIPAm thin film and total % changes (from its initial value, *i.e.* 10% RH) of pTr lifetime as a function of humidity (in right column) both at 25 and 37 °C.

Wavelengths	Fitted equation		Total % changes of lifetime	
	25 °C	37 °C	25 °C	37 °C
470 nm	y=0.0021x+3.95, r^2=0.95	y= –0.003x+4.39, r^2=0.91	+ 3.46	–5.20
490 nm	y=0.003x+4.18, r^2=0.97	y= –0.004x+4.52, r^2=0.98	+ 5.17	– 5.33
520 nm	y=0.002x+4.39, r^2=0.95	y= –0.003x+4.93, r^2=0.77	+ 3.12	–4.69
540 nm	y=0.003x+4.57, r^2=0.99	y= –0.001x+4.98, r^2=0.72	+ 5.32	–1.78
570 nm	y=0.003x+4.71, r^2=0.95	y= –0.004x+5.01, r^2=0.95	+ 5.37	–5.58

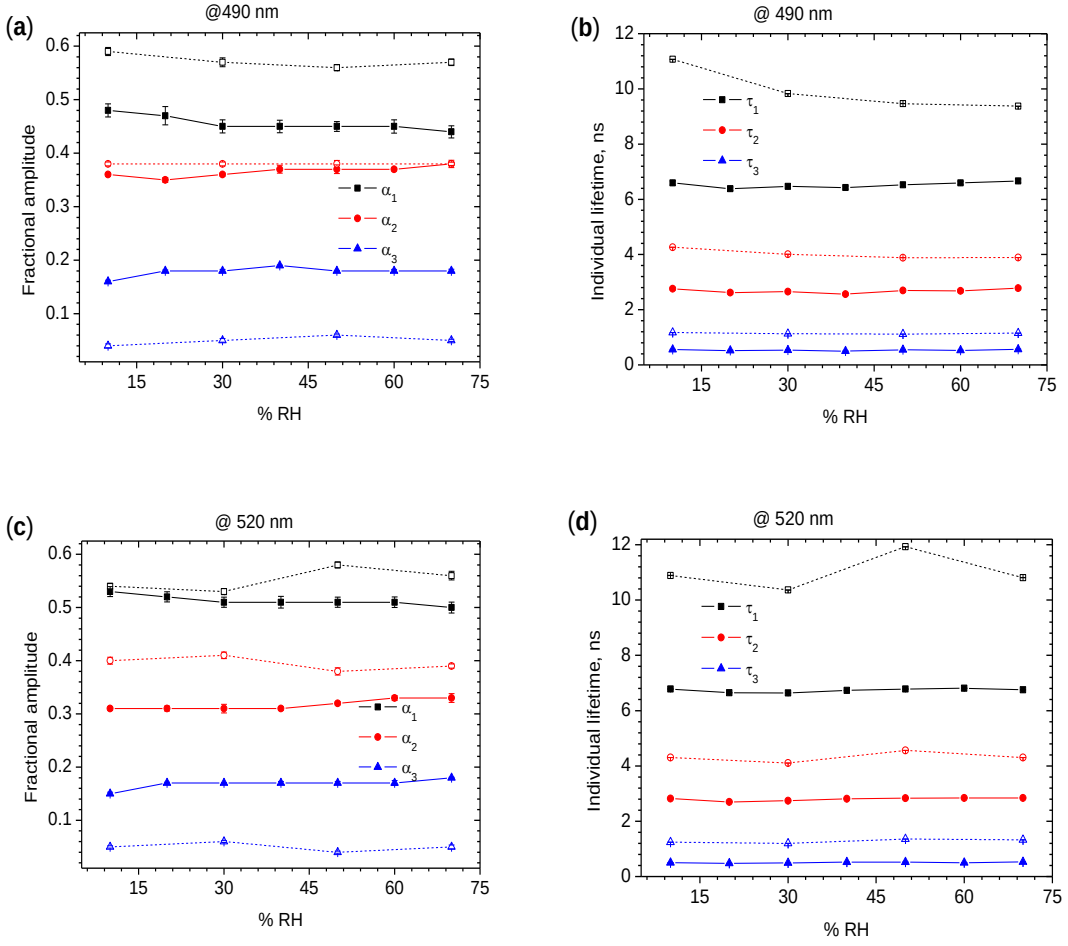

Figure 4.7: Plot of fractional amplitude and individual lifetime versus increasing humidity for a pTr-PNIPAm thin film at 25 and 37 °C at 490 and 520 nm emission wavelengths (for 470, 540, and 570 nm emission wavelengths, see Appendix IV). Symbols represent the measurement temperature where solid (at 25 °C), and open (at 37 °C). All data were fitted to a tri-exponential model. Where αi = fractional amplitudes/pre-exponential factors. Amplitudes have been normalised such that Σ|αi| = 1. Errors calculated using support plane analysis.

The pTr's average lifetime was significantly shorter in PNIPAm thin films compared to PS. For example, at 470 nm, 10% RH, and 25 °C, the pTr's lifetime was 3.97 ns in PNIPAm, whereas it was 6.95 ns in PS thin films. This shorter pTr's lifetime in PNIPAm thin films (compared to PS) might be related with the rigidity of local domain. This kind of local rigidity related changes in lifetime was also reported for dicyanodihydrofuran derivatives fluorophores in different polymers [254]. The PNIPAm films provided a comparatively less rigid /more flexible environment (than PS film) which allowed for more thermal motion (*i.e.* intramolecular vibration, rotation etc.) of the fluorophore and facilitated non-radiative decay pathways of pTr in the excited state and leading to a comparatively shorter lifetime in PNIPAm thin films.

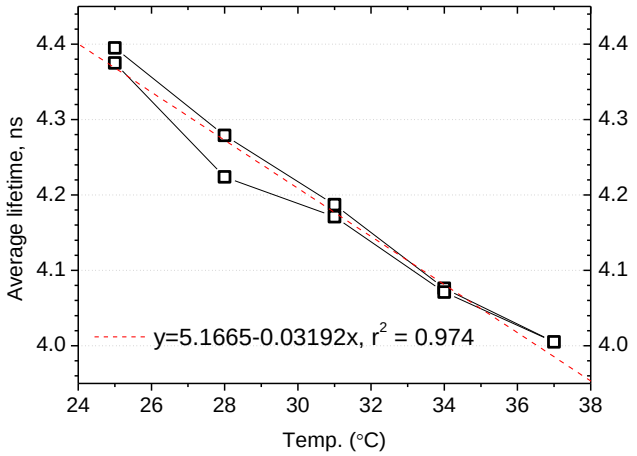

Figure 4.8: Temperature cycling plot showing pTr-PNIPAm thin film's lifetime variation with temperature, starting and ending at 25 °C (λ_{ex}=405 nm, λ_{em}=490 nm and at 50% RH).

The water saturated films at 25 and 37 °C were physically different matrixes as far as the fluorophores were concerned, which was why lifetimes were not identical at 70% RH. There were two aspects to consider, one the polarity, or rather the dielectric constant, ε, was lower above the LCST [250, 253, 255] and second the RI was higher. For every % RH, the average lifetime was longer above the LCST at every emission wavelength tested, which supports our view that above the LCST the fluorophore was located in a more dense hydrophobic domain, where the RI was closer to the bulk value of ~1.495 [251]. What was even more surprising was that when we measured the lifetime change with temperature (Figure 4.8) the change was linear at 50% RH. This indicated that the pTr molecule does not experience a major change in RI across the LCST, which seems to contradict the clearly observed behaviour of PNIPAm. The small differences between the lifetime data on the way up and down are well within the experimental error indicating that hysteresis was not significant. This measurement indicates that the RI of the pTr's microenvironment was changing linearly which again indicates that the probe was located away from any polymer domains that contained water.

4.5. Photostability study

A long term photostability study for pTr-PNIPAm thin films at 50% RH was then undertaken in order to observe the intensity drop over time and also with an aim to determine the suitability of pTr for imaging-based applications in the presence of

some water *i.e.* their suitability for *in-situ* measurements of polymer film thickness in biomedical applications.

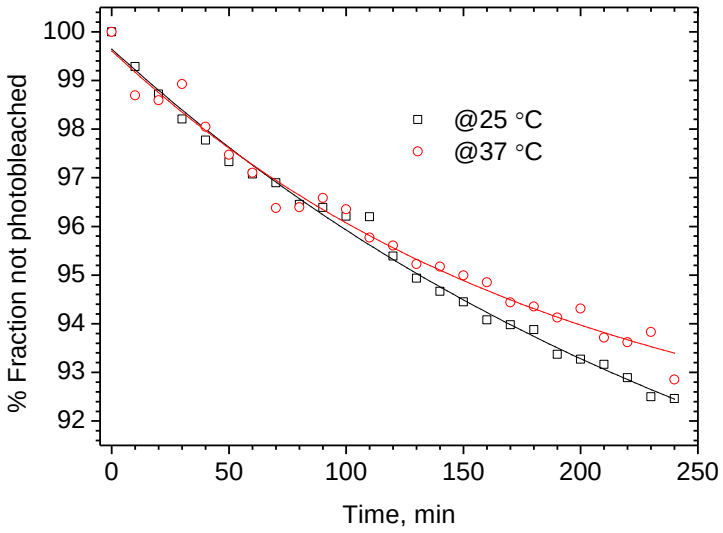

Figure 4.9: Plot represents the photodegradation of pTr-PNIPAm thin films as a % fraction not photobleached vs time both at 25 and 37 °C. The equation for the best mono-exponential fitting at 25 °C was y = 12.84 exp(-x/292.40) + 86.79 and at 37 °C was y = 8.69 exp(-x/191.62) + 90.91. The film was continuously irradiated by the 405 nm light over 4 hours where the power of incident light was 10 µW, the spot size was 1 mm, and the RH was 50%.

The pTr-PNIPAm photobleaching study showed a significant difference (compared to PS films, Chapter 3) which was, at 50% RH, the degree of photobleaching was very small (Figure 4.9) with only a 7% drop in intensity over 4 hours at both 25 and 37 °C.

Again, no H-bonding interactions were observed, as it was obvious from the unchanged overall emission (see Appendix IV). The smaller pTr photobleaching rate in PNIPAm compared to PS was probably due to shorter lifetime which reduces the probability of irreversible bleaching process.

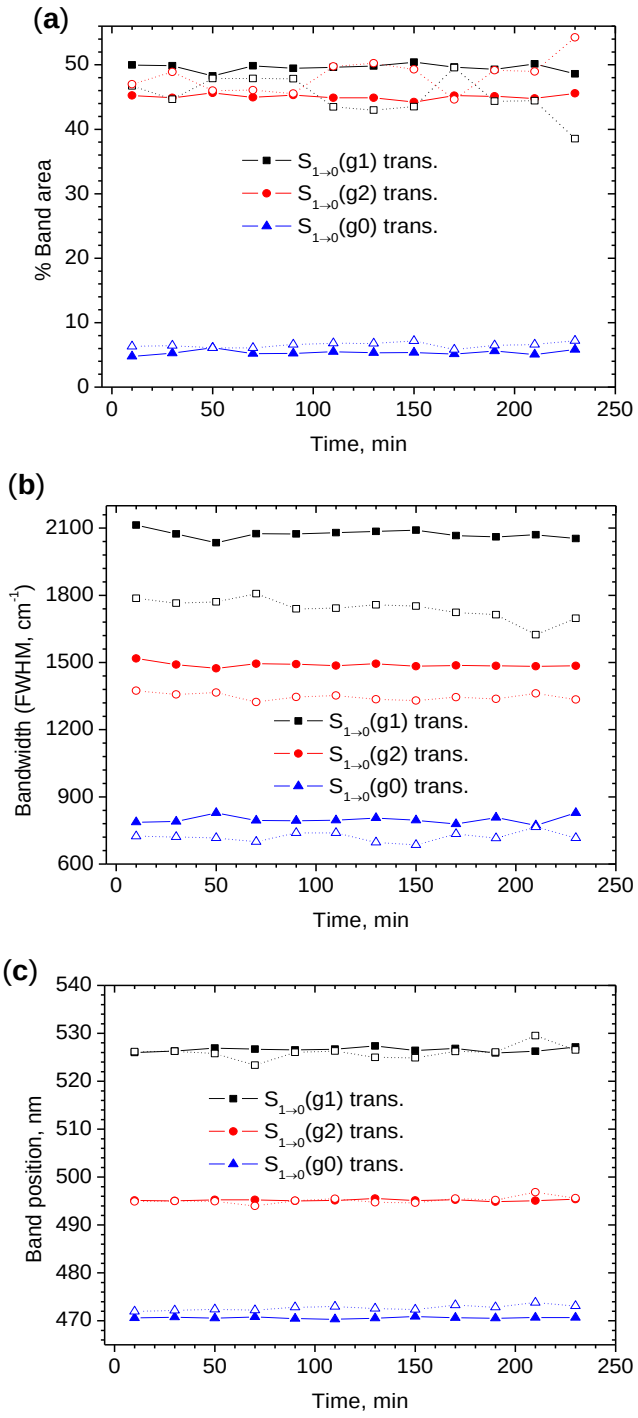

Figure 4.10: Photobleaching effect on emission properties of pTr-PNIPAm thin films, where plot of variation of % band area (a), bandwidth (FWHM, cm^{-1}) (b), and band position (c) at 25 and 37 °C. The symbol represents the measurement temperature, solid (at 25 °C) and open (at 37 °C). The humidity was 50 % and λ_{max} was 405 nm.

The photobleaching kinetics were the same (mono-exponentially fitted, for statistical parameters see Appendix IV) at 25 and 37 °C indicating the phase changes of PNIPAm had no effect on the homogeneity of the pTr domain and which thus leads to nearly the same degree of photobleaching. The photobleached samples did not show any significant variation in emission properties over the time (Figure 4.10). This indicates that all the bands were equally affected by the photobleaching process. It also proved that the variation shown in Figure 4.3a, was due to the changing fluorophore environment as water was incorporated, and not photobleaching.

4.6. Conclusions

The interaction of this pTr fluorophore with PNIPAm was largely governed by its hydrophobic nature with a significant hypsochromic shift being induced on incorporation into PNIPAm. The S-S emission properties (intensity and spectral shape) showed very little change as water was incorporated into the thin films, and there was no evidence for any H-bonding effects. As humidity increased, the overall fluorescence intensity decreased only by a small amount and that was due to photobleaching. The major changes in relative population for the emission from g1 and g2 excited state as an effect of humidity was due to IVR from g2 conformer into g1.

The hydrophobic pTr fluorophore had a very strong hydrophobic interaction with the backbone of PNIPAm. In EtOH solution, PNIPAm chains wrapped around pTr effectively solubilising the fluorophore. In the thin films, below the LCST something similar happened, with pTr being "wrapped up" by the hydrophobic parts of the polymer chains. This also explained the differences in lifetime change with increasing water content above and below the LCST. Below the LCST, PNIPAm and water were miscible so during water absorption the thin film remained homogeneous and the main environmental change sensed by the fluorophore was a reduction in the RI, leading to increased lifetimes. Above the LCST, the hydrophobic domains of PNIPAm became more dense as water was introduced, leading to an increase in local RI and a consequent decrease in lifetime.

The behaviour of pTr was very different to the polarity sensitive 3-HF fluorophores which located in the more hydrophilic domains and essentially only

reported on changes in the hydrophobic domains [4]. Since, this fluorophore also showed no evidence for aggregation, despite the relatively high concentration used here, and good photostability, it could potentially be used as a probe for studying heterogeneous polymer thin films.

Chapter 5 : Effect of %RH on the emission properties of hTr-PNIPAm thin films

This chapter will describe an investigation of the humidity-dependant photophysical properties of another Tr fluorophore (hTr, Figure 5.1, a hydrolysed form of pTr which has a blue shifted overall emission compared to pTr and does not show any major solvatochromic effects similar to pTr) that has been incorporated into a PNIPAm thin film. The impact of physicochemical changes above and below the LCST was assessed and so were the effects of water absorption on its emission properties.

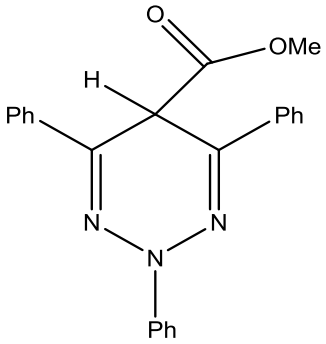

Figure 5.1: Structure of hTr

5.1. Photophysical properties of hTr in solution

pTr's photophysical properties in PNIPAm solution (in EtOH) were governed by the significant hydrophobic interactions (Chapter 4), whereas hTr did not show any interaction with the PNIPAm in solution. No major differences in absorption properties (Figure 5.2a) or in emission properties (Figure 5.2b) were found when comparing hTr in pure solvent (EtOH) solution to a PNIPAm solution. This indicated that hTr might be relatively less hydrophobic than pTr.

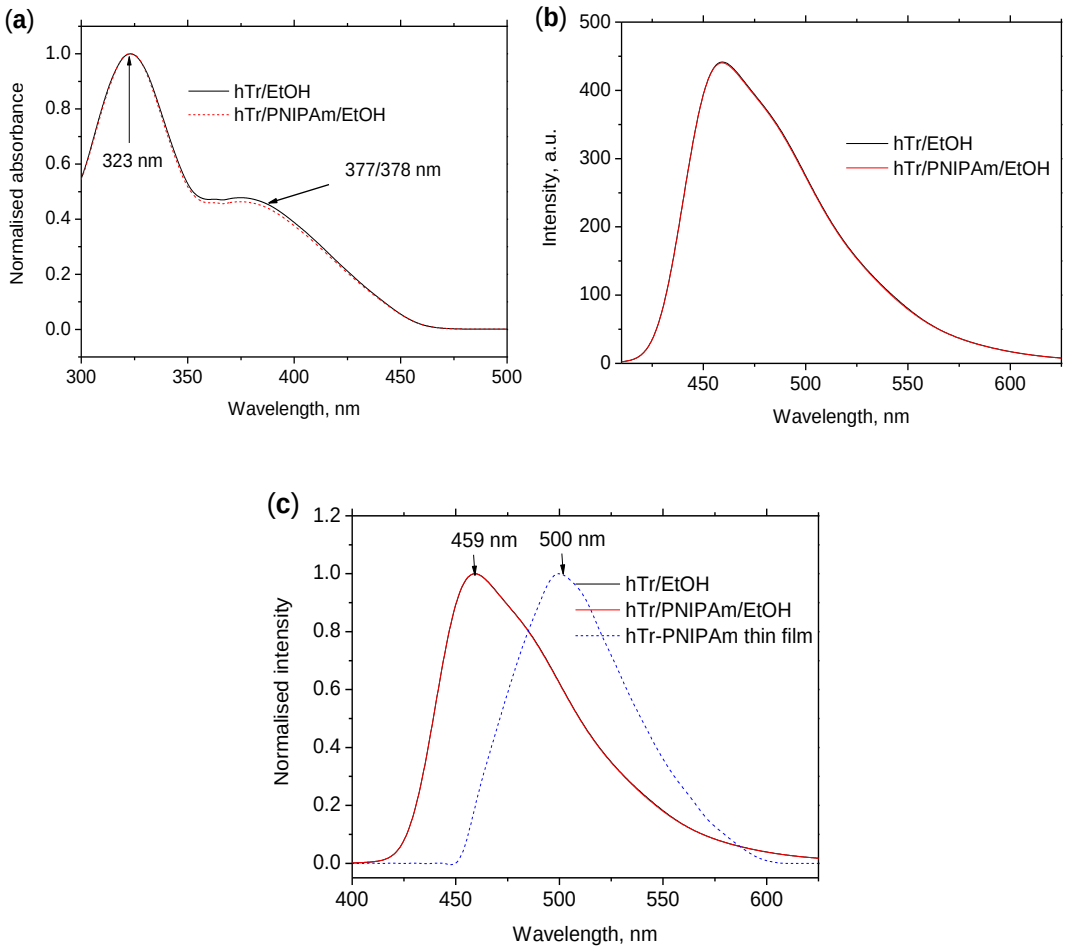

Figure 5.2: (a) Normalised absorption spectra of hTr/ EtOH and hTr/PNIPAm/EtOH solution (b) Smoothed fluorescence emission spectra of hTr/EtOH and hTr/PNIPAm/EtOH solution. (c) A comparative normalised emission spectra of hTr/EtOH, hTr/PNIPAm/EtOH and hTr-PNIPAm thin films (at dry condition). The concentration of hTr in solutions was 7×10^{-5} M and PNIPAm was 5% w/w. The λ_{ex} was 405 nm.

As the hTr emission bands also fit to a tri-band system similar to pTr (Table 5.1), we can assume that it has a similar set of conformers associated with the various excited states. The individual emission properties of these three conformers showed relatively unchanged behaviour (Table 5.1) demonstrating the absence of any interaction between hTr and PNIPAm in solution. However, when hTr was incorporated into a PNIPAm thin film, a large bathochromic shift (~41 nm) for the overall emission (Figure 5.2c), and the individual conformers (Table 5.1) were observed. This spectral change was indicative of a change in fluorophore environment. This was very different to pTr, and suggests that hTr was located in a different, less hydrophobic environment when incorporated into PNIPAm thin films.

Table 5.1: The emission properties of 3 conformers of hTr in three different media (hTr/EtOH, hTr/PNIPAm/EtOH and hTr-PNIPAm thin film). The concentration of hTr in solutions was 7 × 10^{-5} M and PNIPAm conc. was 5% w/w. The data acquired by using 405 nm λ_{ex} and at 25 °C.

hTr (in different media)	Transition for 3 emission bands	Emission properties		
		% Band area	FWHM (cm^{-1})	Band position (nm)
hTr/EtOH	$S_{1\rightarrow0}$ (g1) trans.	36 ± 0.57	3011 ± 19.7	507 ± 1.52
	$S_{1\rightarrow0}$ (g2) trans.	39 ± 0.57	1938 ± 14.0	475 ± 0.57
	$S_{1\rightarrow0}$ (g0) trans.	24 ±1.09	1242 ± 7.1	451 ± 0.57
hTr/PNIPAm/ EtOH	$S_{1\rightarrow0}$ (g1) trans.	34 ± 0.89	3082 ± 21.3	505 ± 0.85
	$S_{1\rightarrow0}$ (g2) trans.	41 ± 1.01	2048 ± 18.2	475 ± 1.45
	$S_{1\rightarrow0}$ (g0) trans.	25 ± 0.58	1361 ± 9.1	452 ± 1.19
hTr-PNIPAm film (dry)	$S_{1\rightarrow0}$ (g1) trans.	37 ± 0.57	1795 ± 23.3	530 ± 0.57
	$S_{1\rightarrow0}$ (g2) trans.	55 ± 1.0	1502 ± 7.1	496 ± 1.15
	$S_{1\rightarrow0}$ (g0) trans.	7 ± 0.87	806 ± 5.5	470 ± 0.57

The spectral change might be due to a large decrease in g0 emission and a correlated large increase in emission from the g2 state. The significant reduction in FWHM of individual conformers (Table 5.1) was an effect of the more rigid environment [61] and was previously described in Chapter 4.

5.2. S-S properties (Below and above LCST): a humidity study

The humidity-induced S-S emission properties of hTr differed from those of pTr (Chapter 4). First, the decrease in overall emission intensity was comparatively larger (Figure 5.3a) and different when the open and sealed films were compared which probably indicated the presence of hTr in a different environment (which was accessible to more water) leading to a higher rate of water-induced photophysical processes. The photobleaching contribution to the overall intensity drop was assessed by sealing the hTr thin films (Mylar wrapped) and repeating the wet-film experiment. Figure 5.3a shows that the intensity drop for Mylar wrapped film was 4-5% or about half of wet film which was obviously due to photobleaching. The remainder of the hTr's intensity drop in the wet films (Figure 5.3a) was due to: 1) a higher rate of water-induced photobleaching in wet films, 2) presence of water-induced quenching, and/or 3) the significant change in g1/g2 relative populations caused by interaction with the

polymer-water matrix. At present, it is not possible to discriminate between the effects using the S-S data and thus must look at the time-resolved measurements. Details will be provided in Section 5.3.

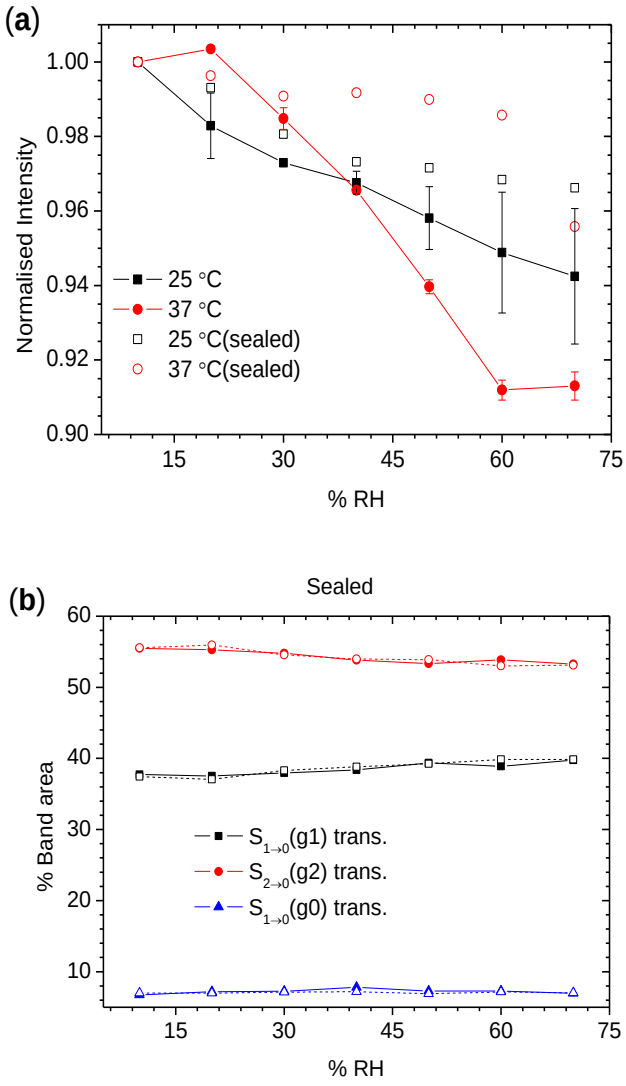

Figure 5.3: (a) Plot of variation of overall fluorescence intensity (normalised to 10% RH data) with increasing % RH for the hTr-PNIPAm thin films (wet and Mylar wrapped) both at 25 and 37 °C. (b) Changes in band area of individual emission conformers of Mylar wrapped films both at 25 and 37 °C, where symbol represents the measurement temperature, solid (at 25 °C) and open (at 37°C). For changes in FWHM and band position of wrapped films see Appendix V. The $\lambda_{ex.}$ was 405 nm. Since the accumulation of water droplet was observed in the humidity chamber window at ≥70% RH and at 37 °C, the intensity drop is presented up to 70% RH both for 25 and 37 °C. The thickness of the films was 10 µm.

Second, the larger changes in band area related to the population of g1/g2 conformers (Figure 5.4a) indicated that there was a higher rate of IVR from the g2 state to g1. The presence of humidity-induced IVR for hTr in PNIPAm thin films was

manifested by the almost unchanged $S_{1\rightarrow0}$ (g0) transition and similar (but opposite in sign) rates of changes in g1/g2 conformers (Table 5.3). The rate of change in g1/g2 conformer (through IVR process) was higher in hTr (than in pTr). For example, only ~4% changes in relative population for pTr were observed for g1 and g2 conformer, whereas ~7% changes were reported for hTr as a function of humidity at 25 °C (Figure 5.4a).

Table 5.2: Band position of the emission maximum of hTr-PNIPAm thin films both at 25 and 37 °C. SD were calculated from the average of three replicate measurements. The $\lambda_{ex.}$ was 405 nm.

% RH	Band position, nm	
	hTr	
	25 °C	37 °C
10	500±0.21	500±0.42
20	500±0.20	500±0.20
30	500±0.36	500±0.42
40	500±0.20	500±0.21
50	500±0.41	500±0.20
60	500±0.55	500±0.44
70	501±0.42	500±0.20

Table 5.3: Rate of changes in the relative population of the two excited states, S_1 (g1) and S_1 (g2) of hTr- PNIPAm thin films as a function of humidity.

Tr	Transition	25 °C			37 °C		
		Slope	Intercept	r^2	Slope	intercept	r^2
hTr	$S_{1\rightarrow0}$(g1) trans.	0.12±0.015	34.01±0.59	0.92	0.13±0.016	34.60±0.65	0.97
	$S_{1\rightarrow0}$(g2) trans.	-0.11±0.015	58.71±0.60	0.90	-0.12±0.015	58.41±0.59	0.97
	$S_{1\rightarrow0}$(g0) trans.	-0.01±0.002	7.27±0.097	0.82	-0.01±0.002	6.98±0.09	0.89

This higher rate of IVR for hTr (compared to pTr) might be due to; 1) hTr being located in a relatively less hydrophobic domain in PNIPAm which was more accessible to water, and/or 2) different vibrational modes being available to facilitate IVR.

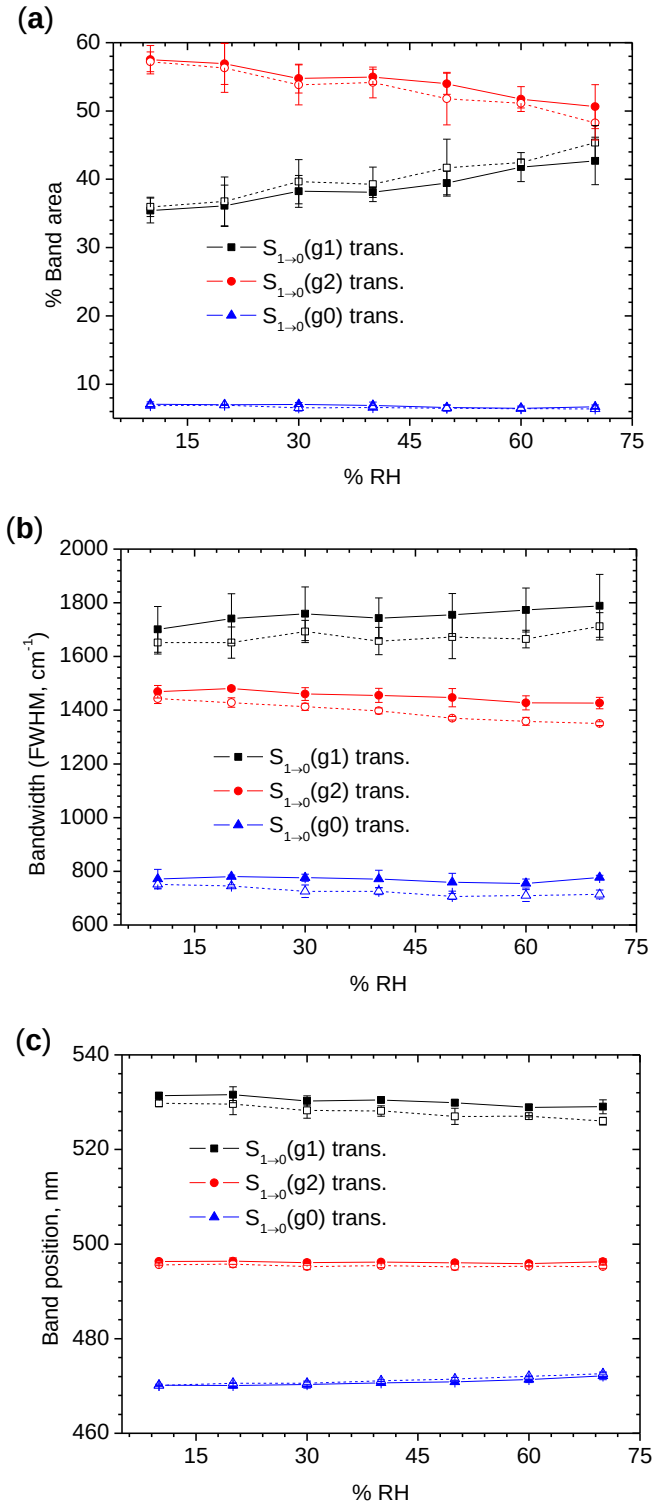

Figure 5.4: Plot of changes in (a) % band area, (b) bandwidth (FWHM, cm^{-1}), and (c) band position with increasing humidity for the hTr doped PNIPAm thin films. Symbols designate the measurement temperature, solid (at 25 °C) and open (at 37 °C). For every case, error bar represents the SD from the average of three replicate measurements.

According to Tamai *et al.*, the number of adsorbed water molecules in the hydrophilic and hydrophobic parts of PNIPAm is different at different levels of water

content (wt%) [82]. The hTr might be located in a micro-domain where a higher number of water molecules were adsorbed and the changes in micro-polarity were comparatively high. This ultimately facilitates a higher population of the g1 conformer (compared to pTr) and thus an increased rate of IVR (from g2 to g1 conformer) by the presence of higher polymer-water interaction.

Third, the humidity-induced changes in the relative population of the g1 conformer were also accompanied by a small change in the FWHM both at 25 and 37 °C (Figure 5.4b). These changes in FWHM provide information about the micro-heterogeneity of the polymer matrixes because the wider the bandwidth, the more heterogeneous the microenvironment. Generally, the FWHM for S_1 (g1) excited states increased, which indicated that the g1 excited state, experienced an increased micro-heterogeneity with increased humidity.

The band position (Figure 5.4c, Table 5.2, and Appendix V) was relatively unchanged indicating no major humidity-induced changes of excited states energies and no H-bonding with the absorbed water.

At ~32 °C, the phase transition occurs and PNIPAm absorbs less water (Chapter 4 and ref. [4]). Therefore, one could expect a smaller change in emission properties at 37 °C (compared to 25 °C). However, we observed a comparatively higher drop of overall intensity (Figure 5.3a) and the slope of the changes in relative population of g1/g2 conformer was slightly higher after the phase-change (Table 5.3). It indicates that at 37 °C, hTr might be located in a different environment which was more accessible to water leading to comparatively a higher rate of water-induced photobleaching at Figure 5.3a (more details will be in section 5.4) and a higher rate of IVR in Figure 5.4a.

Overall, the replacement of phenyl imine by an H atom at C-5 of the Tr ring had a significant effect on the humidity-induced changes of the hTr emission. There was some uncertainty however over the cause of the effects, and whether or not part of the drop in overall intensity was due to static or dynamic quenching. To get a better insight, the effect of humidity on hTr's average lifetime was then investigated.

5.3. Lifetime at different emission wavelengths

Since we know that the hTr was located in a different environment (e.g. S-S data) compared to pTr, it might be expected that the lifetime behaviour will also be different. In Figure 5.5 we saw that average lifetime did not change as dramatically as for pTr-PNIPAm for there are two possible explanations:

1. The hTr was located in an environment where the RI was not changing dramatically.
2. It was in the same environment as hTr but, the lifetime changes caused by changing RI were obscured due to some form of quenching by the incoming water.

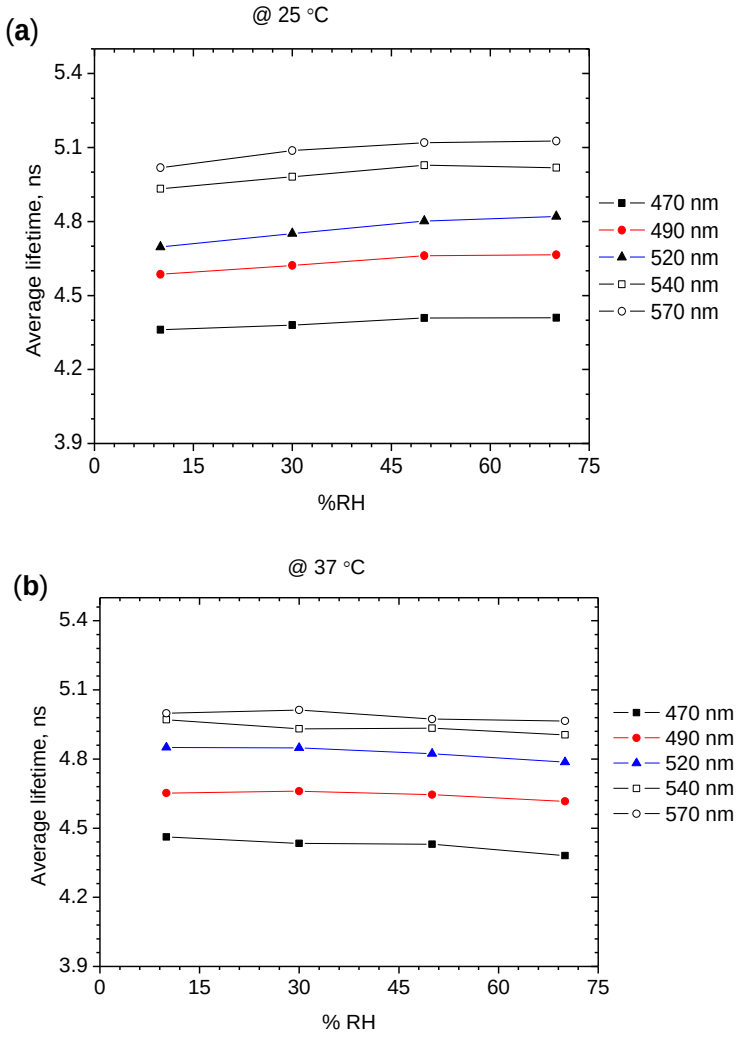

Figure 5.5: Plots showing the humidity-induced changes in average lifetime, $\langle\tau\rangle_f$ of hTr-PNIPAm thin films at 25 °C (a) and at 37 °C (b) at different emission wavelengths.

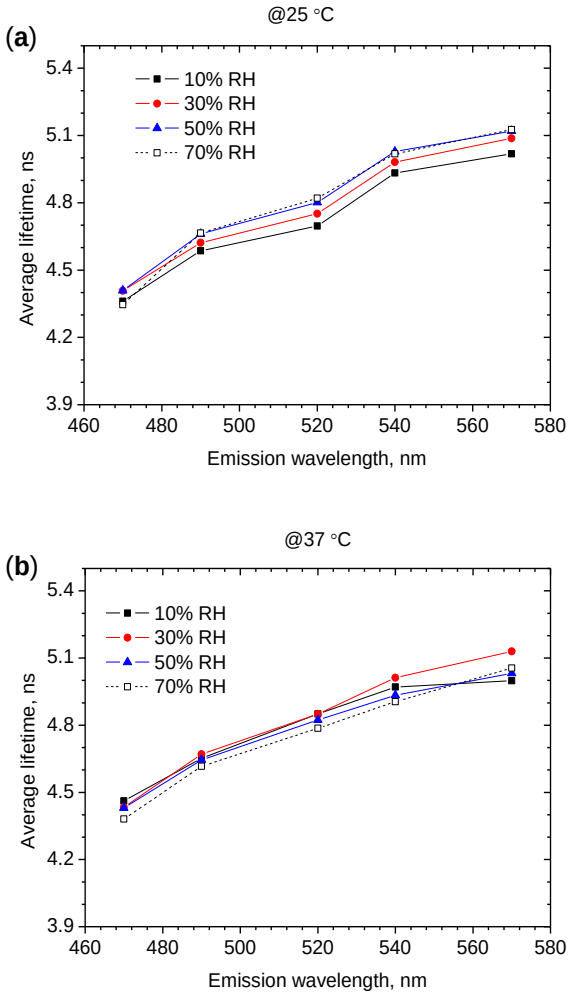

Figure 5.6: Plot showing the changes in average lifetime, $\langle\tau\rangle_f$ as a function of emission wavelength for hTr fluorophores (a) at 25 °C, and (b) at 37 °C.

If pure dynamic quenching was present in the humidity study, then one would expect average lifetime to drop, if pure static then lifetime should stay the same. However, there was a problem with the fact that any change in RI will also induce a lifetime change.

Measuring the RI of the films at a specific humidity was beyond the scope of the present work. Therefore, humidity-induced changes in average lifetime could not be corrected for, and it was difficult to conclusively differentiate the presence of any form of humidity-induced quenching in hTr-PNIPAm thin films systems.

Table 5.4: Rate of changes in average lifetime, $\langle\tau\rangle_f$ of hTr-PNIPAm thin film as a function of humidity to examine the linearity of the changes in lifetime with the humidity. The fitted data was reasonably linear (r^2>0.80) indicated that humidity-induced lifetime changes of hTr-PNIPAm thin films were due to changes of RI of the micro-domain. Total % changes in $\langle\tau\rangle_f$ from its initial value (*i.e.* at 10%) of hTr- PNIPAm thin films up to 70% RH are also presented in right-hand column.

Wavelength	Fitted equation		Total % changes of lifetime	
	25 °C	37 °C	25 °C	37 °C
470 nm	y=0.0008x+4, r^2= 0.95	y= –0.0012+4.8, r^2=0.94	+ 1.10	- 1.81
490 nm	y=0.0013x+4.5, r^2=0.88	y= –6.1E-4+5, r^2=0.82	+ 1.72	- 0.71
520 nm	y=0.0021x+4.7, r^2=0.94	y= –0.0015x+5, r^2=0.93	+ 2.64	- 1.31
540 nm	y=0.0015x+4.9, r^2=0.83	y= –0.0009x+5, r^2=0.92	+ 1.72	- 1.32
570 nm	y=0.0018x+5.0, r^2=0.80	y= –0.0006x+5, r^2=0.80	+ 2.15	- 1.14

The wavelength-related lifetime changes (Figure 5.6) was also observed for hTr in PNIPAm thin film which was mostly an RI issue (Chapter 3).

5.4. Photobleaching study

The hTr-PNIPAm photobleaching process was also different to a certain degree compared to pTr. Firstly, a higher degree of photobleaching was observed both at 25 and 37 °C (Figure 5.7) indicating water induced a higher rate of photobleaching. Secondly, the photobleaching kinetics were different at 37 °C which might be indicated the presence of different mechanism/pathways.

The hTr domain in PNIPAm thin films was more accessible to water (S-S study). This higher water content might be responsible for greater reactivity of the three emission conformers in their first excited singlet state. It cannot be discussed further without a complete emission model of hTr. This larger degree of hTr's photobleaching might also be responsible large variation in the results obtained from replicate measurements (Figure 5.4).

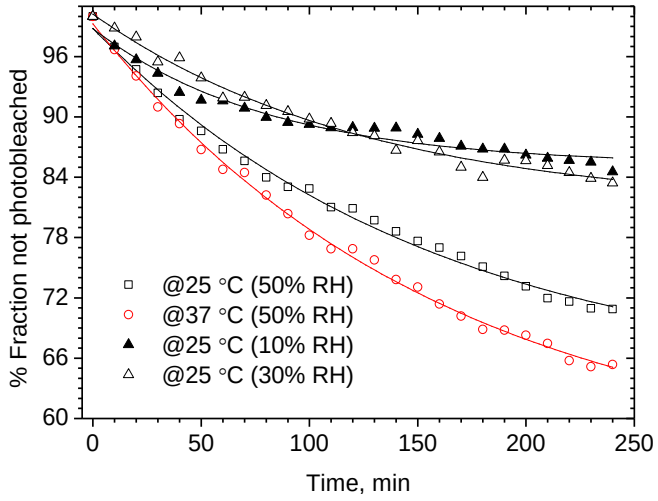

Figure 5.7: Plot represents the photodegradation of hTr-PNIPAm thin films as a % fraction not photobleached vs time both at 25 and 37 °C. At 50% RH, the fitted equation was y = 55.34 + 43.94exp(–x/159.71) at 25 °C (r^2 = 0.993) and at 37 °C it was y= –4.43 + 95.59exp (–x/973.30) + 9.02 exp(–x/34.52) and r^2 = 0.997. At 10% RH, y= 13.57 exp(-x/81.62) + 85.20, r^2 = 0.981 and at 30% RH, y = 19.31 exp(-x/126.09) + 80.91 r^2 = 0.984. The film was continuously irradiated by 405 nm light over 4 hours where the power of incident light was ~10 µW, the spot size was 1 mm.

To understand the contribution of the level of water absorption to the photobleaching rate, studies were also conducted at 10% and 30% RH (and at 25 °C). When the % fraction not photobleached of hTr intensity were plotted against irradiation time (Figure 5.7) for lower water levels (*i.e.* at 10% and 30% RH) it was clear that water had a significant effect. For example, at 10% and 30% RH the total intensity was reduced by 15.47% and 16.56% respectively. This finding was in agreement with other observation [35, 83] that water plays an important role in photobleaching.

Table 5.5: Different statistical parameters from the decay kinetic model of photobleaching process of hTr-PNIPAm thin films at 25 and 37 °C.

Parameter	**Temperature**			
	25 °C		**37 °C**	
	Mono-exponential	Bi-exponential	Mono-exponential	Bi-exponential
r^2	0.99	0.99	0.99	0.99
χ^2	0.32	0.36	0.47	0.14
$\sqrt{(\sum \text{Residual}^2)}$	0.28	0.28	0.41	0.11

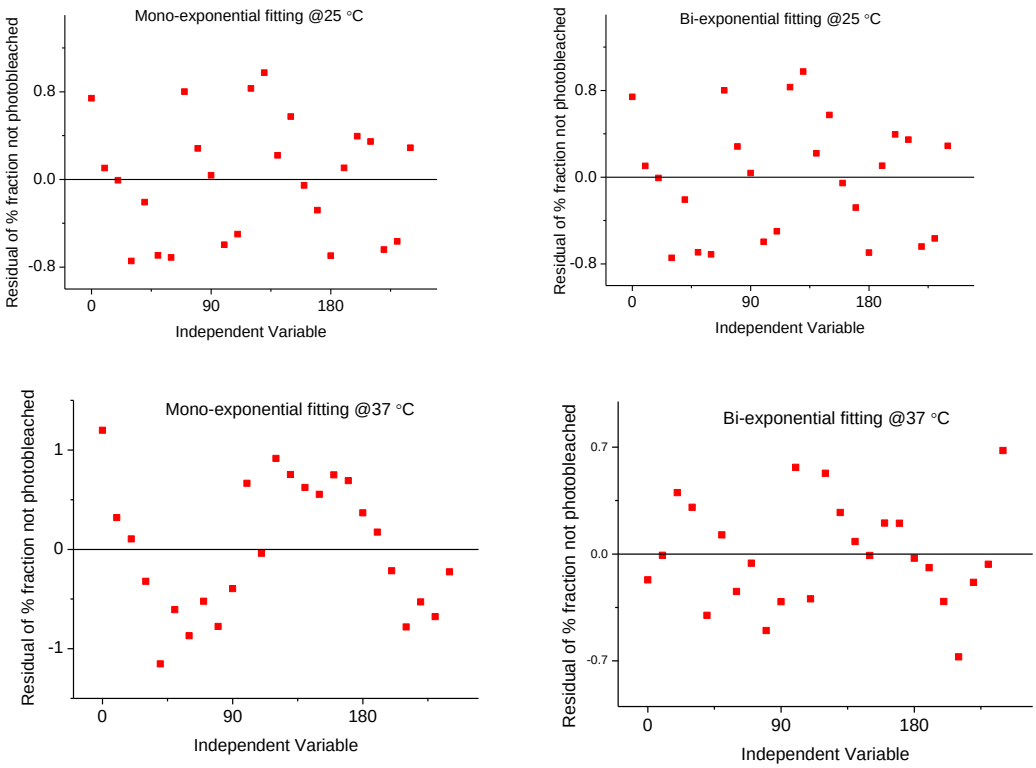

Figure 5.8: Plot of comparative residuals from different decay kinetic model of photobleaching process of hTr-PNIPAm thin films: mono and bi-exponential fitting at 25 and 37 °C.

When the decay kinetics of photobleaching reactions of hTr were investigated (Figure 5.7, Figure 5.8, and Table 5.5) to understand better the hTr environment, a mono-exponential at 25 °C and a bi-exponential decay function at 37 °C were confirmed. Below the LCST, all the fluorophores (within the illumination spot) were equally affected (due to uniform environment) by the photobleaching process and thus at 25 °C, the photobleaching kinetic were mono-exponential in nature. However, above the LCST, a heterogeneous environment might be created due to the phase changes in PNIPAm and then hTr could be located in two domains. One more accessible to water than the other and a bi-exponential photobleaching rate was the consequence.

Since, we expected a more water accessible hTr domain and the molar ratio of hTr: H_2O was ~1:1000 (since 4.3% w/w water was absorbed at 37 °C, chapter 4); a higher rate of photobleaching at 37 °C (compared to 25 °C, Figure 5.7) might be the consequence. The rate constant for faster photobleaching process was significantly higher than the slower process which thus led to a greater degree of photobleaching at 37 °C (compared to 25 °C).

No major changes in the band shape were observed (see Appendix V) indicating the absence of any H-bonding interaction at 50% RH. Small changes in the individual emission conformers (*i.e.* % band area, FWHM, and band position) were also observed in photobleaching experiment (Appendix V) which indicates that all parameters were equally affected by the photobleaching process.

5.5. Conclusions

For hTr, it was clear that it behaved significantly different compared to pTr. For one, there was no evidence (UV-vis or fluorescence) for any interaction with PNIPAm indicating that it was probably much less hydrophobic. When incorporated into PNIPAm thin films there was a relatively large bathochromic shift indicating that it was probably located in a very different environment to pTr. We suspect that hTr locates in a significantly more hydrophilic domain in PNIPAm. The evidence for this also lies in the fact that it's photobleaching rate was much more sensitive to the presence of water, and, the relative changes in lifetime with increasing %RH is much lower (Table 4.5 compared to Table 5.4). Overall, it can be concluded that hTr is a poorer potential imaging fluorophore because of its increased water-sensitive photobleaching rate.

Chapter 6 : kpTr fluorophore in PNIPAm polymer: A study of photophysics

The impact of physicochemical changes in the PNIPAm thin films above and below its LCST and with water absorption on the spectral properties of another triazine derivative, kpTr, (Figure 6.1, which has a red shifted emission and a significant longer average lifetime compared to pTr/hTr and also its absorption/emission properties are relatively unaffected by solvent variation (like as pTr/hTr)) will be investigated in this chapter. This investigation involves the study of the photophysics of kpTr in different media at 25 °C followed by the humidity-induced changes in emission properties.

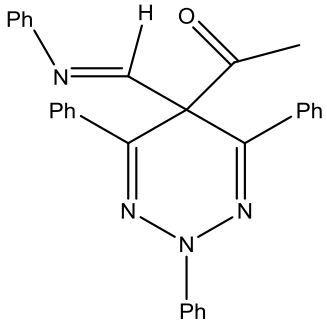

Figure 6.1: Structure of kpTr

6.1. kpTr photophysics in different media

For kpTr in PNIPAm solution, a significant difference compared to the kpTr-EtOH solution (Figure 6.2a) was observed which clearly indicated some form of interaction with PNIPAm, similar to the pTr case. However, unlike pTr, there was only a very small effect on the fluorescence emission, a small decrease in intensity (Figure 6.2b) but no changes in the fitted parameters (Table 6.1).

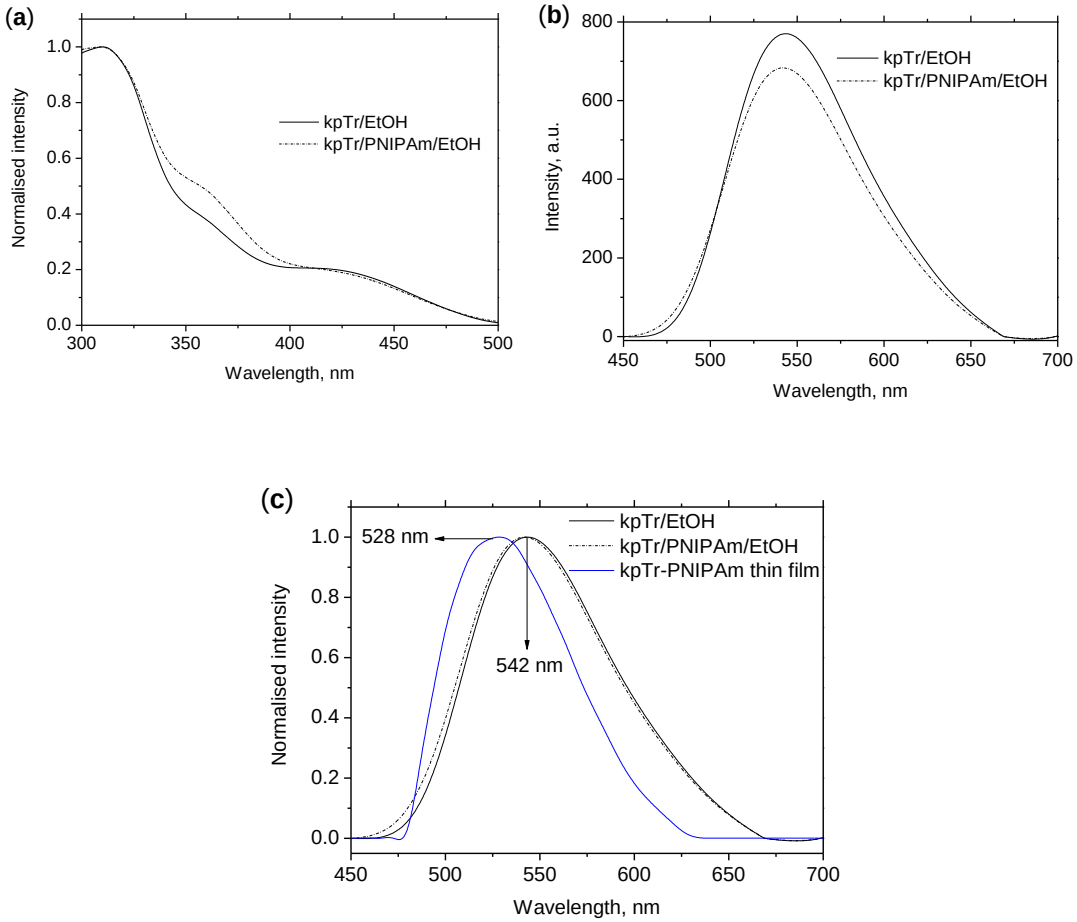

Figure 6.2: (a) Normalised absorption spectra of kpTr/EtOH and kpTr/PNIPAm/EtOH solution (b) Smoothed fluorescence emission spectra of kpTr /EtOH and PNIPAm /kpTr/EtOH solution. (c) Normalised emission spectra of kpTr/EtOH and kpTr/PNIPAm/EtOH and kpTr-PNIPAm thin films. The concentration of kpTr in solutions was 7×10^{-5} M and PNIPAm was 5% w/w. All data were acquired using λ_{ex} = 405 nm at 25 °C.

Table 6.1: Summary of emission properties (3 bands) of kpTr fluorophore in different environments. The concentration of kpTr in solutions was 7×10^{-5} M and PNIPAm was 5% w/w. The data were acquired at λ_{ex} = 405 nm and at 25 °C.

kpTr in diff. media	Transitions for 3 emission band	Emission properties		
		% band area	FWHM (cm^{-1})	Band position, nm
kpTr/EtOH	$S_{1\rightarrow0}$ (g1) trans.	49±1.52	3036±40.73	577±0.57
	$S_{1\rightarrow0}$ (g2) trans.	35±3.51	1771±14.41	549±2.08
	$S_{1\rightarrow0}$ (g0) trans.	15±2.08	1419±13.63	521±0.57
kpTr/PNIPAm/EtOH	$S_{1\rightarrow0}$ (g1) trans.	49±1.52	3070±75.12	576±1.52
	$S_{1\rightarrow0}$ (g2) trans.	35±3.51	1768±48.85	546±2.0
	$S_{1\rightarrow0}$ (g0) trans.	15±2.64	1498±08.90	521±1.0
kpTr-PNIPAm thin film (dry)	$S_{1\rightarrow0}$ (g1) trans.	49±2.43	1735±43.78	553±2.12
	$S_{1\rightarrow0}$ (g2) trans.	38±2.97	1284±27.12	521±1.32
	$S_{1\rightarrow0}$ (g0) trans.	13±1.89	828±15.14	499±1.45

Once the kpTr was cast into a thin film and the EtOH solvent removed, a large and significant change in the overall emission was observed. The large blue shift (~20 nm) was nearly the same for each band (Table 6.1) and was accompanied by a large decrease (~30-40%) in bandwidths. It is interesting to note that the % band areas did not change significantly indicating that IVR was not affected by the changing environment.

6.2. Effect of humidity on kpTr-PNIPAm photophysics

kpTr's emission properties were highly insensitive to change in the micro-environment (in humidity-induced study) compared to other two Tr fluorophores (*i.e.* pTr and hTr). A very small change in overall intensity (Figure 6.3a) and no major changes in individual emission properties (*i.e.* % band area, FWHM, and band position) of the three conformers (Figure 6.4) were observed both at 25 and 37 °C. The phase transition of PNIPAm had very little effect on the humidity-induced changes in kpTr's emission properties.

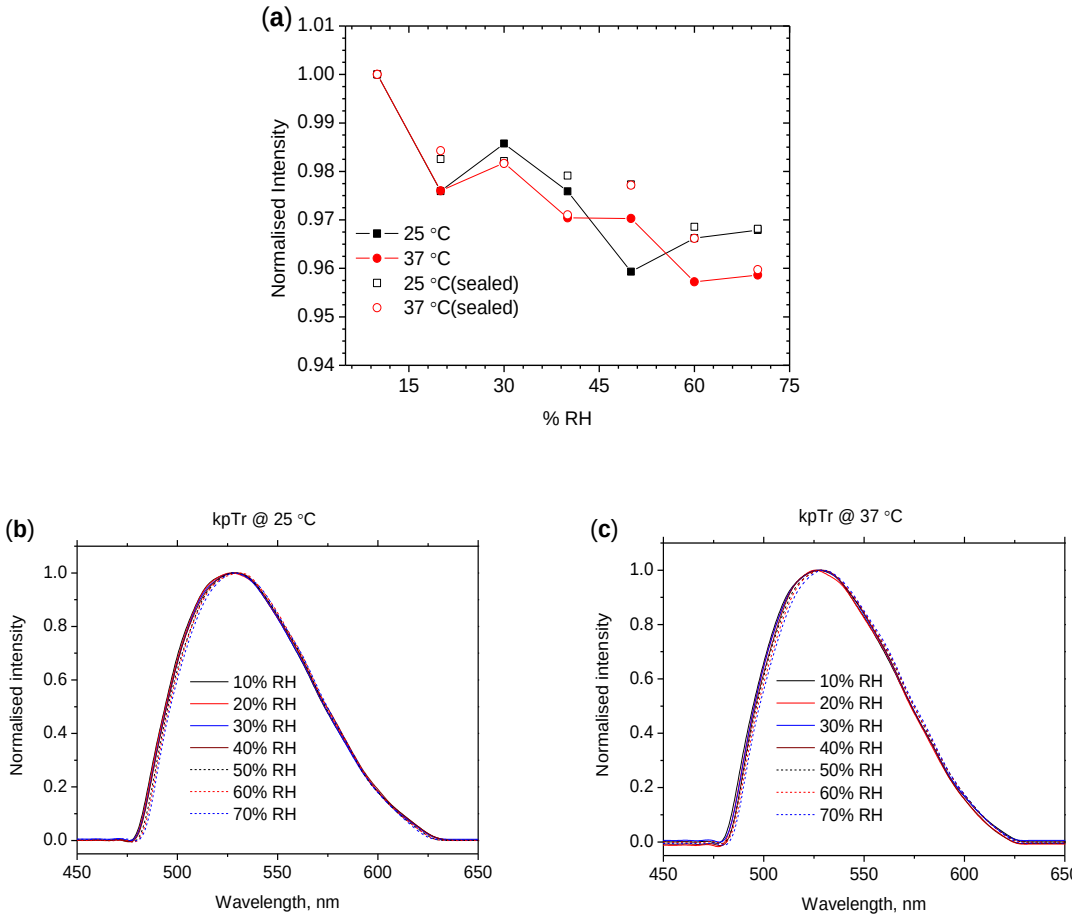

Figure 6.3: (a) Plot showing the humidity-induced drop in kpTr overall emission intensity for wet (solid symbol), and sealed (open symbol) film both at 25 and 37 °C, where intensity maximum at different humidities was normalised to 10% RH. Normalised, smoothed, fluorescence emission spectra of kpTr-PNIPAm thin films as an effect of humidity at 25 °C (b) and 37 °C (c) . The $\lambda_{ex.}$ was 405 nm. Since, the accumulation of water droplet was observed in the humidity chamber window at ≥70%RH and at 37 °C, the intensity drop of kpTr-PNIPAm thin films is presented up to 70% RH both for 25 and 37 °C. The thickness of the films was 10 µm.

The small drop in kpTr's overall intensity (~4%) caused by water ingress would suggest that the only process being observed was a small amount of photobleaching and that the fluorophore was either very environmentally insensitive or was located in a microenvironment which was not changing. A Mylar sealed film study also confirmed this hypothesis, since the intensity drop was nearly similar both for Mylar wrapped film and wet films (Figure 6.3a). There was also no major changes in the individual emission conformers of Mylar wrapped film (see Appendix VI) indicating no contribution of this photobleaching to individual emission property changes in Figure 6.4.

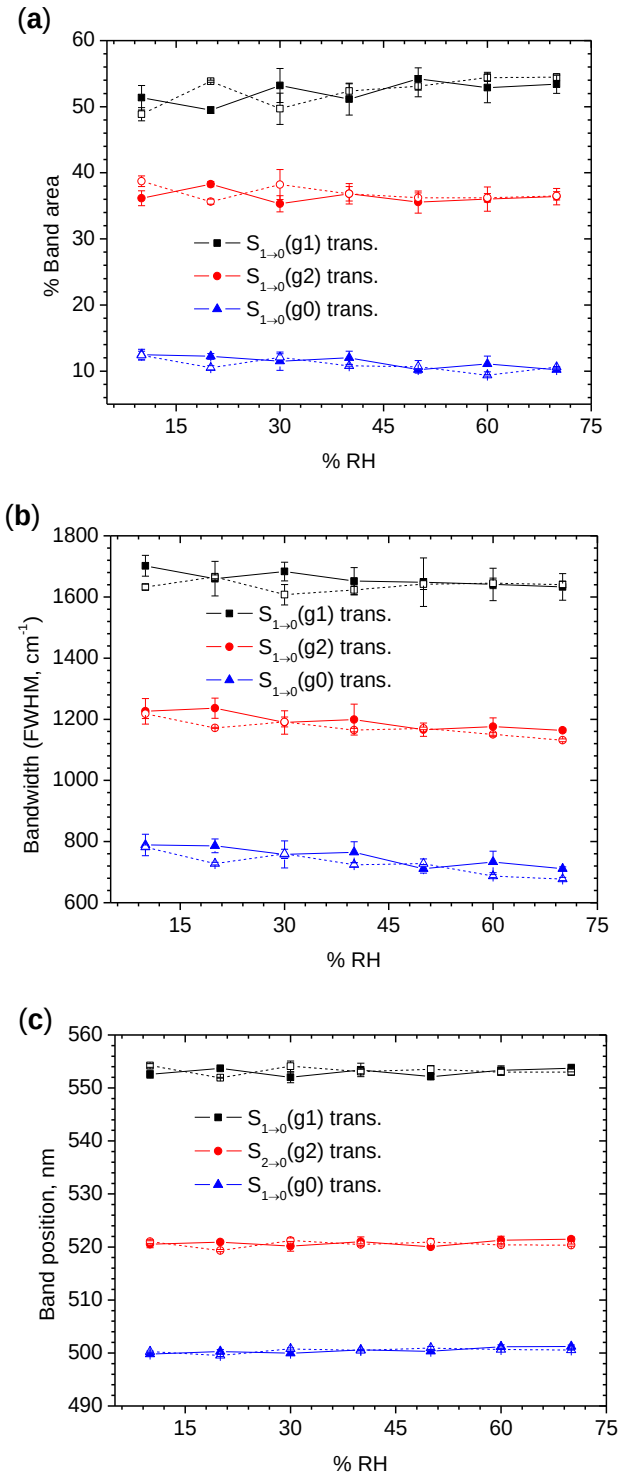

Figure 6.4: Plot of variation of (a) % band area, (b) bandwidth (FWHM, cm^{-1}), and (c) band position with increasing % relative humidity for the kpTr-PNIPAm thin films. Symbol designates the measurement temperature, solid (25 °C), and open (37 °C). For every case, error bar represents the SD from the average of three replicate measurements.

The overall changes in kpTr's S-S emission properties as a function of humidity were very small. But, there had no clear evidence where the probe was located in PNIPAm thin films (was it in pTr/hTr domain or in a different domain?); to get a clarification the humidity-induced changes in kpTr lifetime were then investigated.

Plotting the humidity-induced changes in kpTr's average lifetime, some significant differences were observed (compared to pTr/hTr, Chapter 4 and 5). First, the RI related lifetime changes were not seen and second the changes in kpTr's lifetime were very small <4% (Figure 6.5, Table 6.2). The PNIPAm phase change also had very little effect on the humidity-lifetime plot.

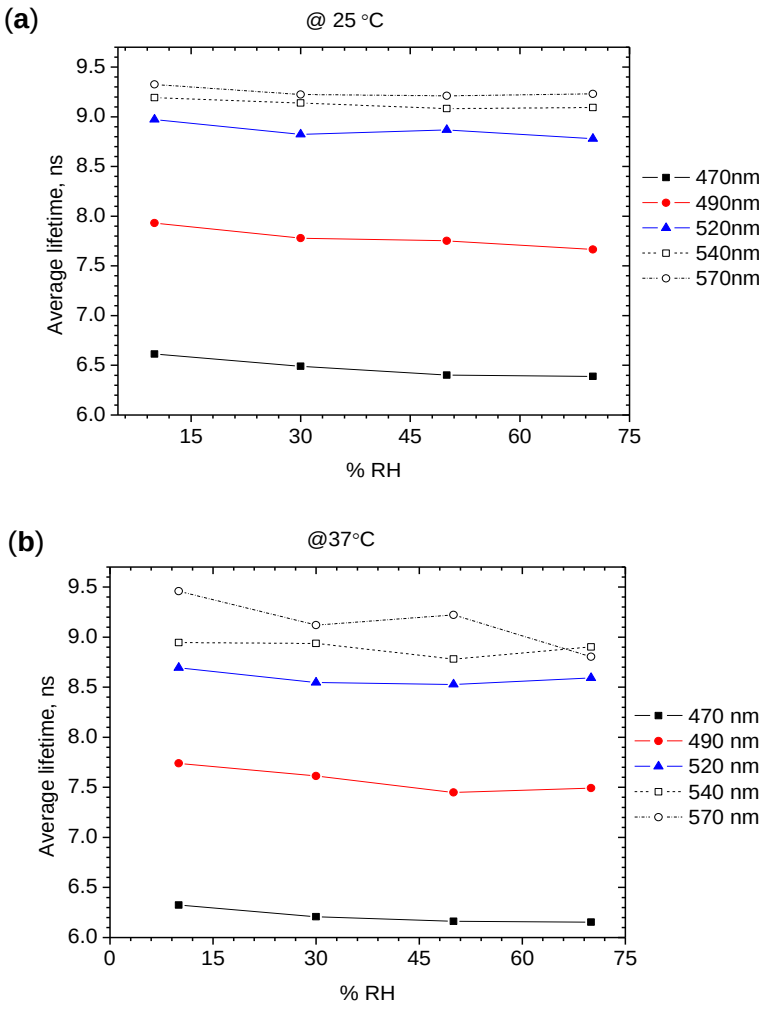

Figure 6.5: Plots showing the humidity-induced changes in average lifetime, $\langle\tau\rangle_f$ of kpTr-PNIPAm thin films at 25 °C (a)/ at 37 °C (b) and at different emission wavelengths.

Table 6.2: Total average lifetime, $\langle\tau\rangle_f$ changes from its initial value (*i.e.* at 10%) of kpTr-PNIPAm thin films up to 70% RH (as percentage). (–) denotes a decrease in lifetime.

Wavelengths	Total % changes in kpTr's lifetime	
	25 °C (%)	37 °C (%)
470 nm	–3.40	–2.70
490 nm	–3.35	–3.19
520 nm	–2.15	–1.16
540 nm	–1.07	–1.82
570 nm	–1.01	–6.92

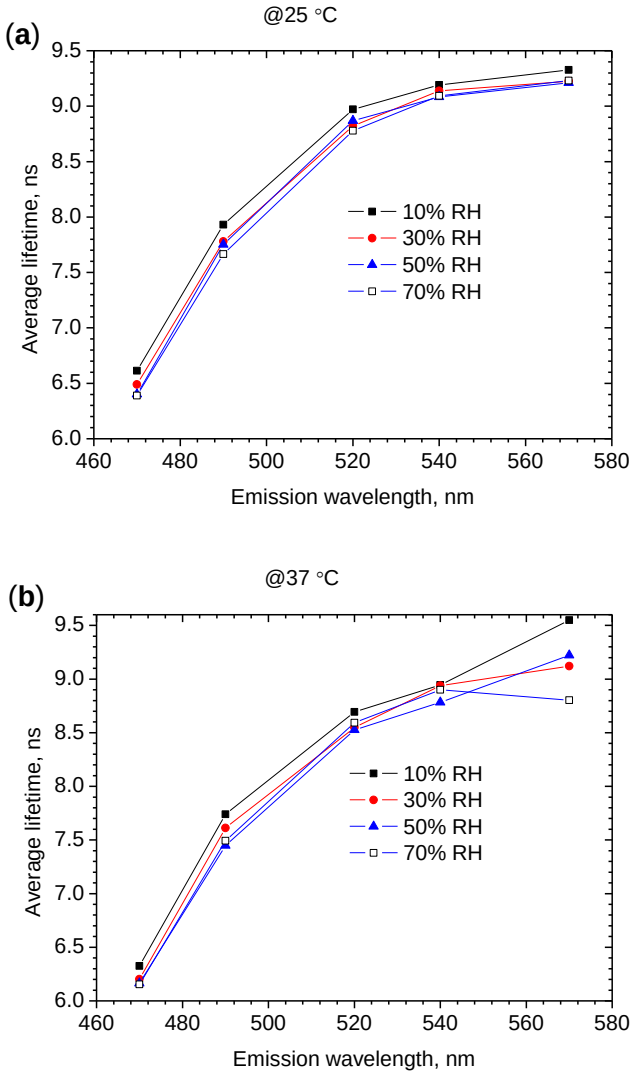

Figure 6.6: Plot showing the changes in average lifetime, $\langle\tau\rangle_f$ of kpTr-PNIPAm thin films vs emission wavelength at 25 (a)/37 °C (b) and at different %RH.

This lack of change in lifetime with changing water content indicated that: 1) kpTr was located in a domain, where the water absorption cannot change the micro-polarity or RI and/or 2) the kpTr's emission was very insensitive to the changes in micro-environment.

6.3. Photobleaching study

The photobleaching curves for kpTr fitted to a mono-exponential at 25 °C and a bi-exponential decay at 37 °C were similar to that observed for hTr (Figure 6.7). The degree of photobleaching for kpTr's emission at 50% RH was significantly larger compared to pTr (both at 25 and 37 °C). On other hand, kpTr's degree of photobleaching was nearly same at 25 °C, whereas it was slightly higher at 37 °C (compared to hTr).

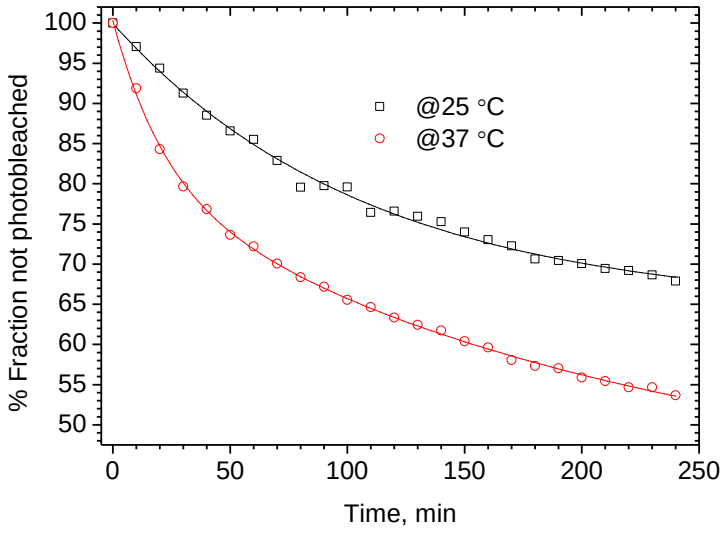

Figure 6.7: Plot represents the photodegradation of kpTr-PNIPAm thin films as a % fraction not photobleached vs time both at 25 and 37 °C. The corresponding fitting equation was y = 35.44 exp(–x/108.69) + 64.49, r^2 = 0.995 at 25 °C and at 37 °C the equation was y = 39.61 exp (–x/211.08) + 19.82 exp (–x/21.36) + 40.86, r^2 = 0.999. The film was continuously irradiated by the 405 nm light over 4 hours where the power of incident light was 10 µW, the spot size was 1 mm, and the RH was 50%.

The greater decrease in kpTr's intensity (compared to pTr) might be related to significant changes in dipole moment during excitation ([241]) together with its longer lifetime (Figure 6.5 and Chapter 4) which thus leads to an increased chance of photoinduced destruction (in presence of water). Since it was not confirmed where

exactly the kpTr was located in the PNIPAm thin films and we do not have any computational modelling of kpTr photophysics, it cannot be described any further. At 37 °C, photobleaching kinetics were different (compared to pTr) and two kpTr's domains were confirmed (due to phase changes of PNIPAm) by the bi-exponential fitting (for fitting statistics see Appendix VI). Photobleaching reaction rate might be somehow increased (at 37 °C) leading to a greater decrease of kpTr's overall intensity.

Compared to hTr (Chapter 5), the decay rate constant was slightly larger for kpTr but the amplitude was smaller at 25 °C, which ultimately leads to an approximately similar degree of (in magnitude) intensity drop after 4 hours illumination (Figure 6.7). On the other hand, at 37 °C, the rate constant and the fractional contribution were both larger for kpTr (compared to hTr) which was responsible for higher degree of intensity drop.

6.4. Conclusions

kpTr behaves similarly to pTr and was probably in the same environment and/or was probably just as hydrophobic. The insensitivity of the fluorescence emission to changes to environment when water was introduced was probably due to changes in energy levels and dipole moments of the kpTr molecule compared to pTr. It cannot be however discussed any further because of the unavailable computational data of kpTr's emission. In this study, no evidence of H-bonding between the kpTr and the incoming water (similar to pTr/hTr) was observed. Its higher degree of photobleaching is the limitation to use further for imaging applications.

Chapter 7 : Effect of %RH on Tr emission in PVA thin films: A photophysical study

7.1. Introduction

This chapter describes a detailed study of Tr emission properties in PVA, as a function of humidity. It also describes an investigation of the fluorophores' sensitivity to changes in micro-environment polarity. The PVA thin films are more hydrophilic than PNIPAm films and this greater hydrophilicity allows the PVA film to absorb larger amounts of water, [83, 256] the water absorption rate of PVA thin films also increases with temperature [257]. The humidity-induced photophysical properties of the films were investigated by looking at S-S and TRF data at 25 °C and 37 °C.

7.2. Mass of water absorption

The method for calculating the maximum water absorption by the PVA thin films was the same as that for PNIPAm. The results are given as average (increase from original dry weight ± SD), the average and SD were obtained using three replicate measurements.

The 20 µm Tr-PVA thick films absorbed 20.01 ± 2.07 w/w % water at 25 °C, and 22.45 ± 2.21 % at 37 °C. This degree of water absorption was greater than that measured for the PNIPAm 10 µm thick films (11.45 ± 0.67 % at 25 °C, and 4.29 ± 0.29 % at 37 °C, see Chapter 4).

7.3. S-S properties: a humidity study

It was found that humidity had very little effect on the emission properties of the pTr in PS/PNIPAm (Chapters 3 and 4), however, in PVA, humidity had a major effect. A large drop in the overall intensity of pTr emission (Figure 7.1a), a large change in the relative populations (Figure 7.2a) and a large change in the FWHM (Figure 7.3a) of individual emission conformers was observed at 25 and 37 °C. This indicates that a different photophysical/chemical process may have dominated in the PVA matrix. On the other hand, for hTr, the changes were small at 25 °C (Figure 7.1b, Figure 7.3b, and Figure 7.4b) indicating a little effect on humidity-induced changes in hTr's emission. There was a greater drop in overall intensity for both fluorophores at 37 °C (compared to 25 °C). These significant intensity drops were not accompanied

with any major shifts in emission, except for pTr at 37 °C (Figure 7.1, Table 7.1, and Figure 7.4) indicating the absence of H-bonding with incoming water. A significant blue shift in the emission from S_1(g1) was observed which increased with % RH (Figure 7.4a).

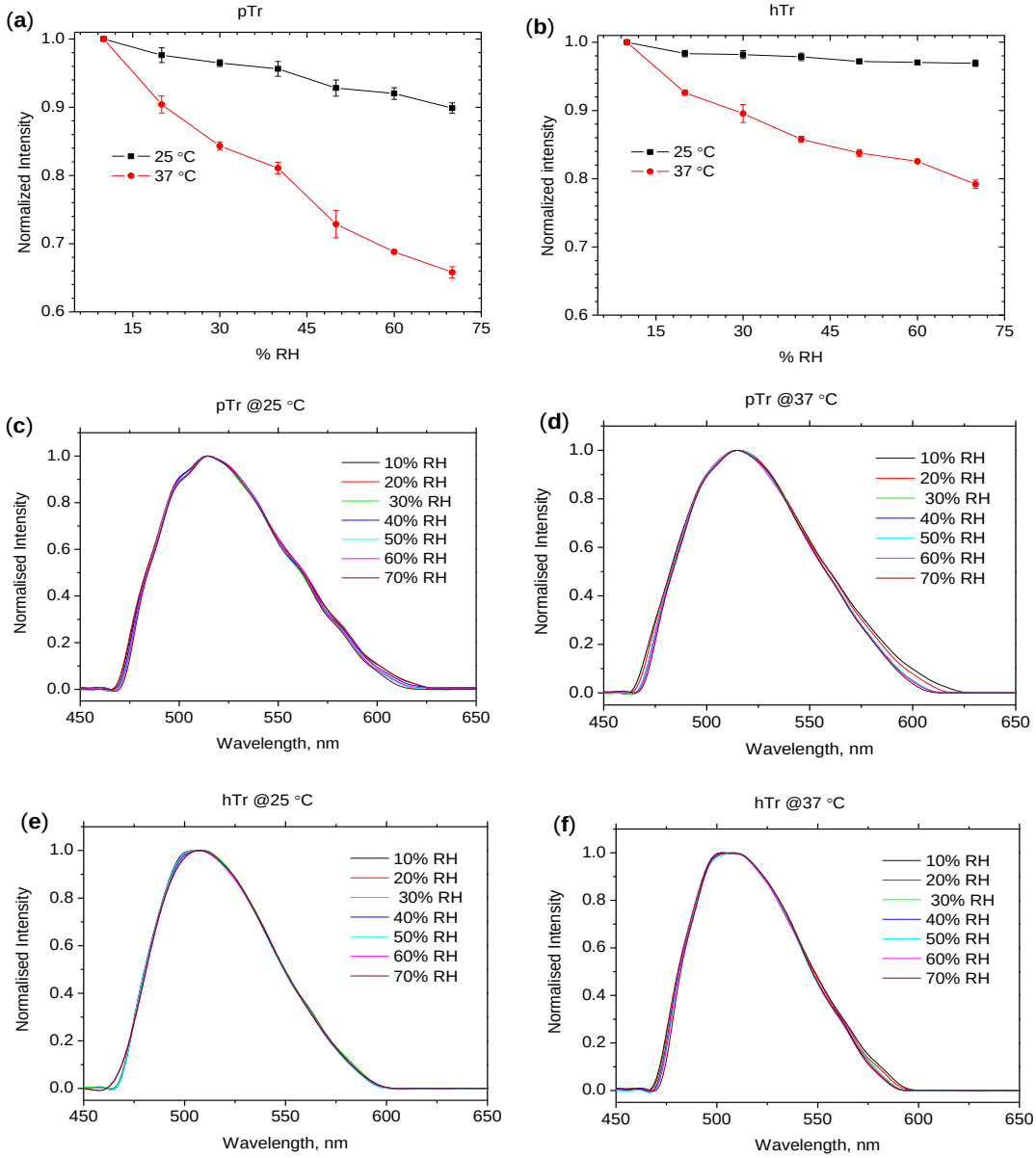

Figure 7.1: Intensity maximum changes of emission band (normalised to 10% RH) as an effect of humidity of Tr-PVA thin films, where, (a) is for pTr at 25 / 37 °C and (b) is for hTr both at 25/ 37 °C. Overlaid normalised, smoothed fluorescence emission spectra of Tr-PVA thin films where (c) is for pTr at 25 °C/ (d) 37 °C and for hTr at 25 °C (e)/37 °C(f) . Since, the accumulation of water droplet was observed in the humidity chamber window at ≥70%RH and at 37 °C, the intensity drop is presented up to 70% RH both for 25 and 37 °C. The λ_{ex} was 405 nm.

Table 7.1: Changes in overall emission band position of Tr-PVA thin films at different %RH both at 25 and 37 °C. The SD was calculated from three replicate measurements.

% RH	Band position, nm (±SD)			
	pTr		hTr	
	25 °C	37 °C	25 °C	37 °C
10	514±0.20	515±0.36	507±0.21	508±0.42
20	514±0.18	515±0.00	507±0.20	509±0.20
30	514±0.21	516±0.25	507±0.36	509±0.42
40	514±0.00	515±0.25	507±0.20	509±0.21
50	514±0.00	516±0.36	507±0.41	509±0.20
60	515±0.20	515±0.42	508±0.55	509±0.44
70	515±0.20	516±0.01	508±0.42	509±0.20

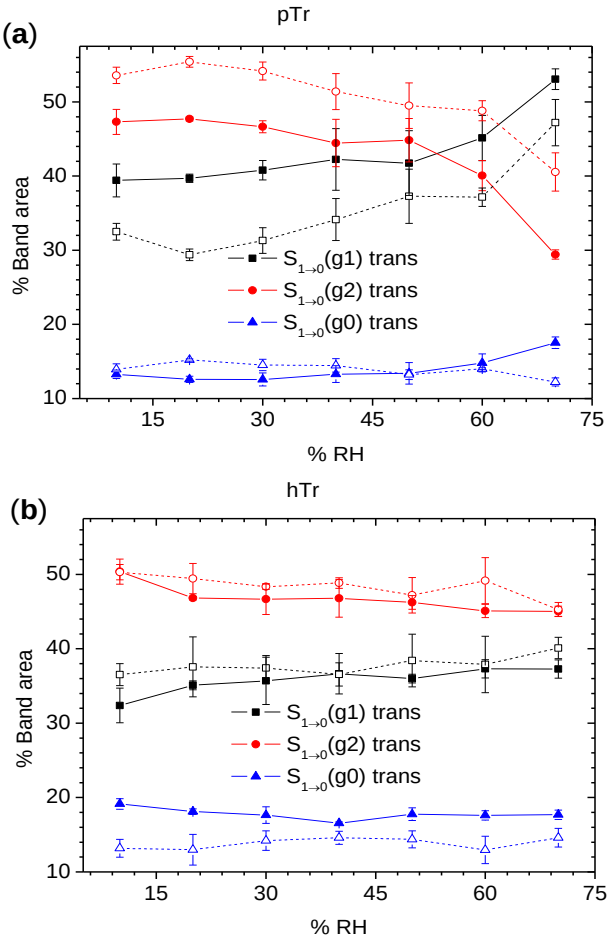

Figure 7.2: Plot of changes in relative population of three excited states of Tr-PVA thin films as a function of humidity, where, (a) is for pTr at 25 and 37 °C (b) is for hTr at 25 and 37 °C. Error bars represent the SD from the average value of three replicate measurements. Symbols designate the measurement temperature, solid (at 25 °C), and open (at 37 °C).

The large drop in intensity and changes in relative population of g1 and g2 conformers were more likely due to: 1) acidic hydrolysis (AH) and/or 2) water/anion (acetate residue)-induced quenching.

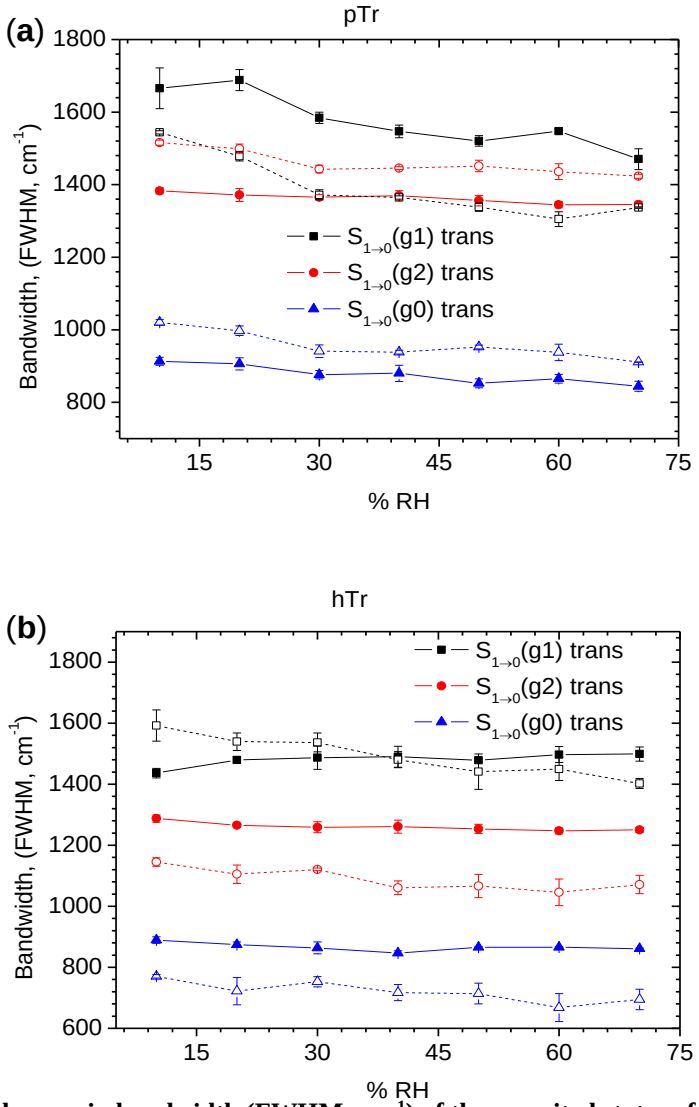

Figure 7.3: Plot of changes in bandwidth (FWHM, cm^{-1}) of three excited states of Tr-PVA thin films as a function of humidity, where, (a) is for pTr at 25 and 37 °C (b) is for hTr at 25 and 37 °C. Symbols designate the measurement temperature, solid (at 25 °C), and open (at 37 °C). Error bars represent the SD from the average value of three replicate measurements.

The pTr is susceptible to AH and produces hTr which has a lower quantum yield [241]. We did not have the ability to measure the pH *in-situ* for the thin polymer films to see if the AH theory could be confirmed. The best we could do was measure the pH of water-PVA solutions and see if there was a significant drop in pH.

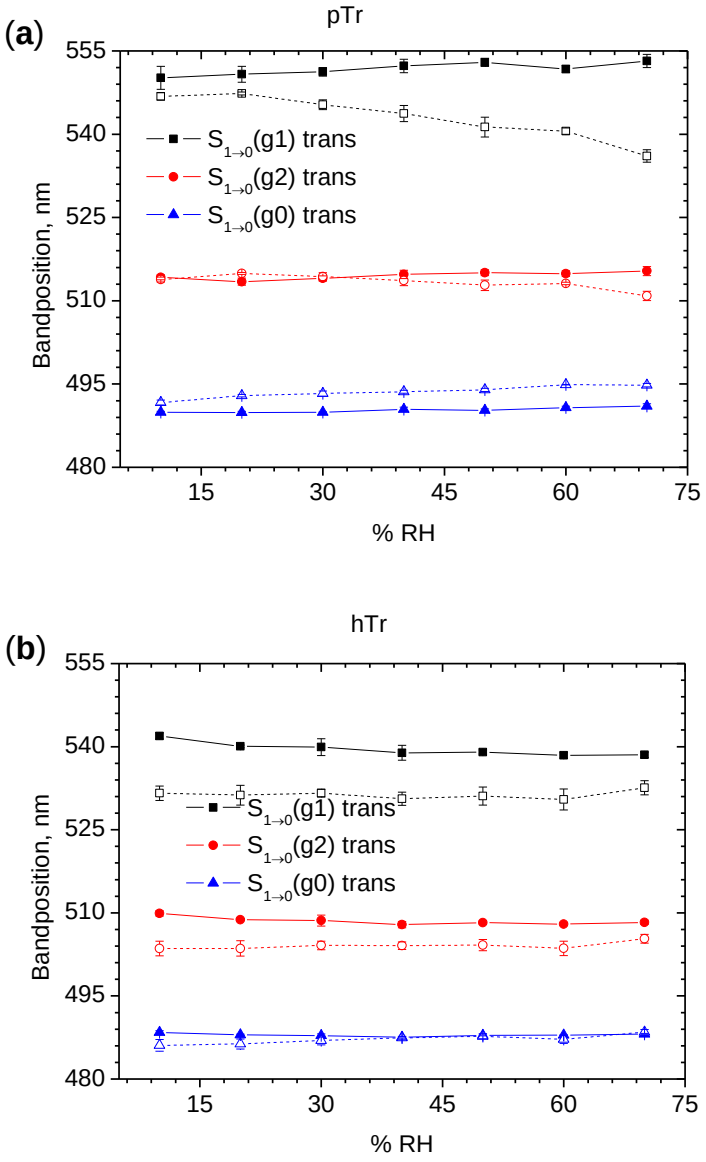

Figure 7.4: Plot showing the changes in band position of three excited states of Tr-PVA thin films as a function of humidity, where, (a) is for pTr at 25 and 37 °C (b) is for hTr at 25 and 37 °C. Error bar represent the SD from the average value of three replicate measurements. Symbols designate the measurement temperature, solid (25 °C), and open (37 °C).

As an attempt to prove the AH of pTr in PVA aqueous solution, a range of PVA (% w/w) solutions in water were prepared and the pH measured. The PVA aqueous solutions demonstrated the acidic environment (pH was ~ 6 for all of the solutions prepared up to 25% w/w, see Appendix VII) but no hydrolysis reaction was observed (this was demonstrated by the almost unchanged emission of pTr, usually the emission of hTr is at shorter wavelength compared to pTr in water, Figure 7.5).

Even after, leaving the pTr/PVA/H_2O solution in a dark place for more than 2 months, no significant changes in size and shape of overall emission bands (Figure 7.5c) were observed. A small shift of emission towards shorter wavelength was seen however, this was due to a small hydrophobic interaction between pTr and water (which has been discussed in Chapter 3).

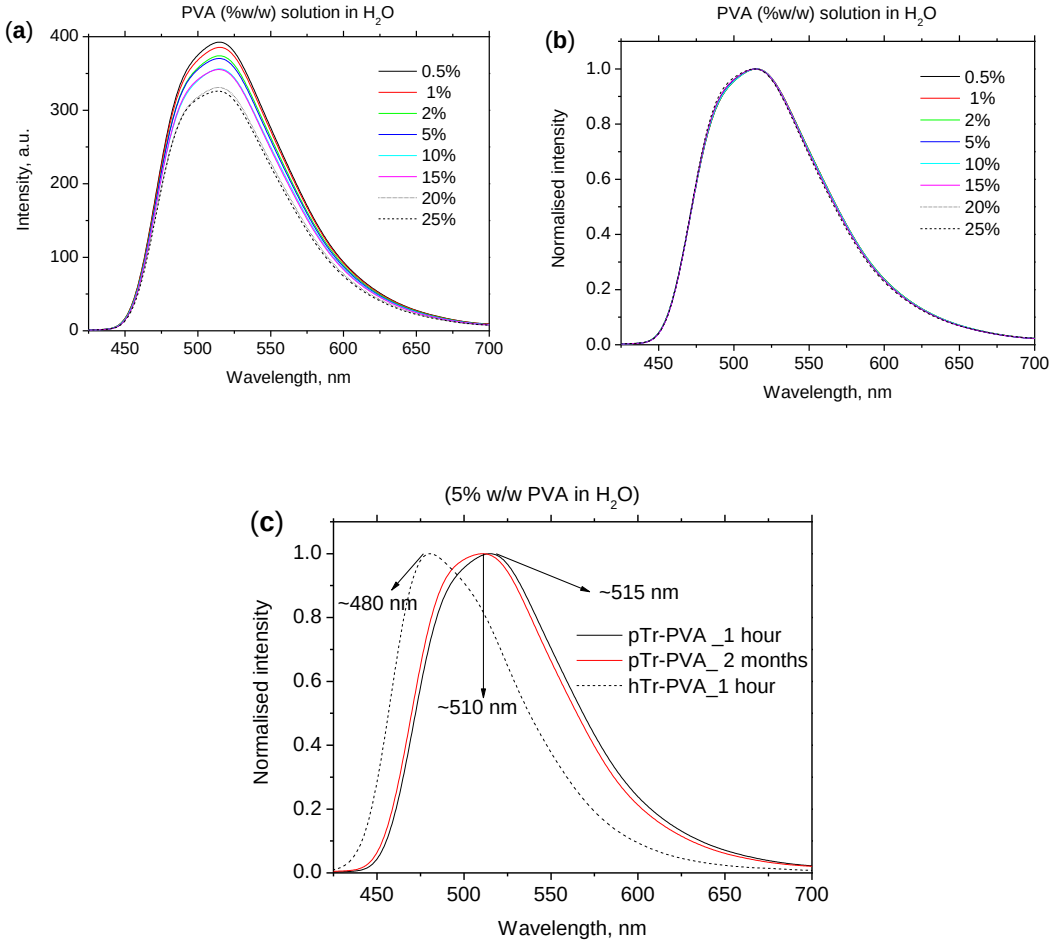

Figure 7.5: Testing for acid hydrolysis of pTr in different aqueous PVA solutions, where (a) is smoothed overlaid emission spectra, (b) is for smoothed and normalised emission spectra, and (c) represents the comparative normalised emission spectra for hTr and pTr. The Tr fluorophores concentration was 7.5 × 10^{-5} M, and λ_{ex} was 405 nm.

The second phenomenon hypothesized to cause the humidity-induced intensity drop (Figure 7.1a) was water-induced quenching. To investigate this quenching process, Equation 1.9 is rearranged by considering water as a quencher:

$$I_0/I_i \text{ or } \tau_0/\tau_i = 1 + K_{SV}\,[Q]_{H2O}$$

Where, I_0 and τ_0 are the fluorescence intensity and the decay time in the dry films and I_i and τ_i are the intensity maximum and decay time at corresponding humidity respectively. K_{SV} is the Stern-Volmer constant (slope of the plot and equal to $k_q\tau_0$, where k_q is the bimolecular quenching constant) and $[Q]_{H2O}$ is the concentration of quencher (in terms of %RH).

The S-S emission intensity and lifetimes of pTr-PVA thin films were collected both for presence and absence of quencher (*i.e.* water). When the intensity or lifetime ratio as a function of water was plotted (Figure 7.6), a linear relationship ($r^2 > 0.98$) of Stern-Volmer plot was observed both at 25 and 37 °C. This indicates that there was some form of humidity related quenching of emission present at this temperature. In addition, the slope of plot was about twice at 37 °C compared to 25 °C, indicating a higher rate.

The Stern-Volmer quenching constants were very small (0.002 and 0.004 M^{-1} at 25 and 37 °C respectively) and a pure collisional quenching was not observed because $I_0/I \neq \tau_0/\tau$. On the other hand, the presence of a combined static and dynamic quenching was also not observed, as any curvature of intensity/ lifetime ratio towards y-axis was not observed [13].

It was then decided to investigate if the large humidity-induced intensity drop could have been caused by anion-induced quenching (the PVA used in this analysis was 98–99% hydrolysed and it may have contained a significant amount of acetate (sodium/methyl) as an impurity [258]). To investigate this hypothesis, pTr (1×10^{-5} M) doped PVA aqueous solutions (0.5% w/w) were prepared and then pure sodium acetate (tri hydrate, AcONa) with different concentrations was added as a quencher. Plotting the Stern-Volmer plot (Figure 7.8), showed a strong linear correlation (r^2 >0.98) between intensity and quencher concentration, and lifetime ratio and quencher concentration, was observed.

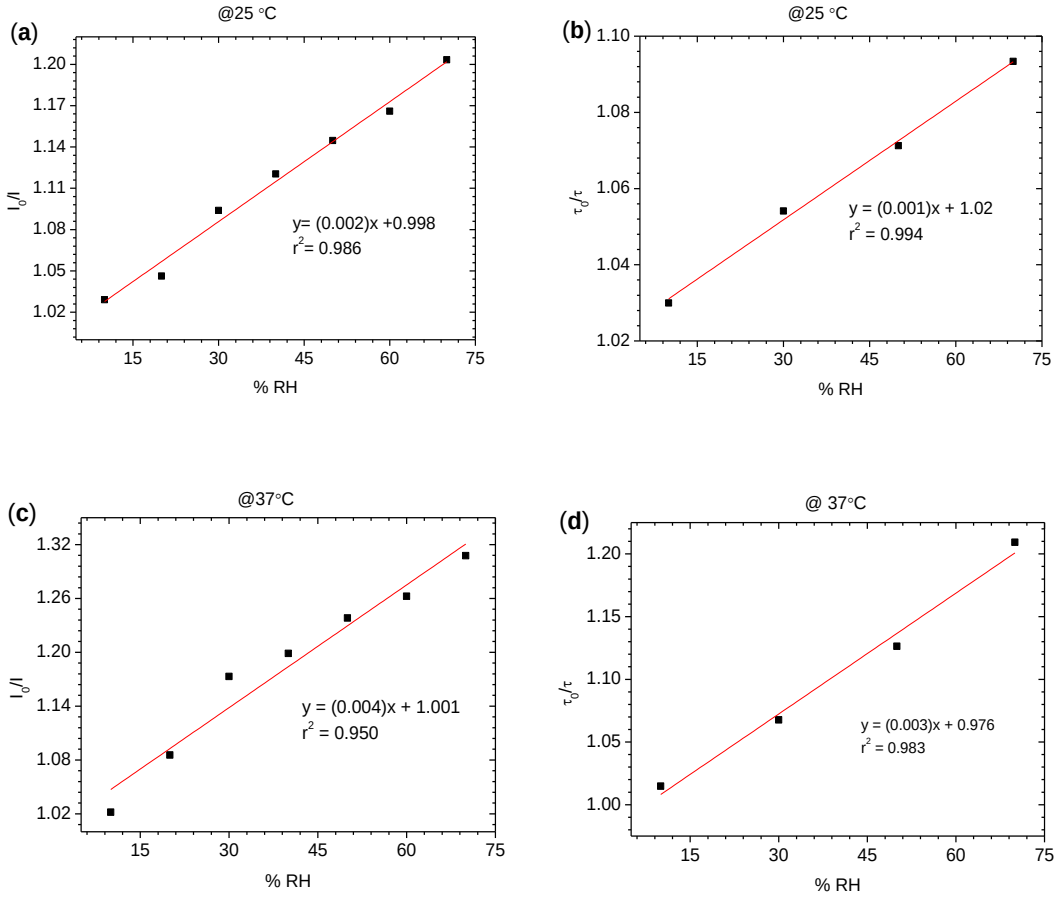

Figure 7.6: Stern-Volmer plot for pTr-PVA thin film as a function of %RH. The intensity ratio is presented on (a) at 25 °C and (c) at 37 °C where, I_0 and I are the intensity maximum of emission at absence and presence of quencher (water) respectively. The lifetime ratio as a function of humidity is presented on (b) at 25 °C and (d) at 37 °C, where, τ_0 and τ are the pTr lifetimes at absence and presence of quencher (water) respectively. The lifetime data were collected at only 520 nm emission wavelengths and λ_{ex} was 405 nm.

Several authors have reported a decrease in emission intensity for organic fluorophores caused by the acetate anion [259-261]. For example, at 0.2 M concentration and pH 7.4, the fluorescence intensity of m-tyramine was decreased by 69%, this was attributed to the formation of complex H-bond between the acetate and mono/di-hydroxyphenethylamines [259]. These ground-state complex formations were evident by the changes in the absorption spectra. However, in this study no changes in the absorption spectra were observed (see Appendix VII). There was also no shift in the overall emission band (see Appendix VII); this indicates that the drop in intensity was not due to a proton transfer reaction in the excited state.

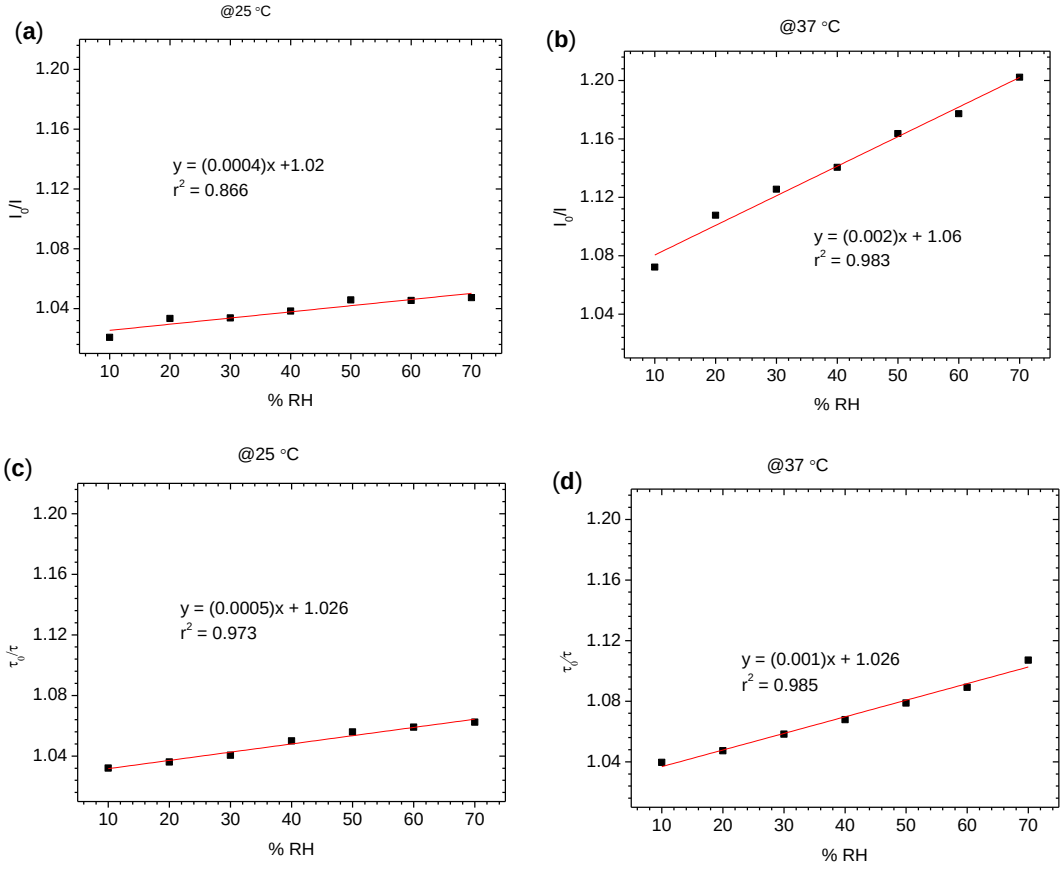

Figure 7.7: Stern-Volmer plot for hTr-PVA thin film as a function of %RH. The intensity ratio is presented on (a) at 25 °C and (b) at 37 °C where, I_0 and I are the intensity maximum of emission at dry condition and at a specific humidity respectively. The lifetime ratio as a function of humidity is presented on (c) at 25 °C and (d) at 37 °C where, τ_0 and τ are the hTr lifetime under dry conditions and at a specific humidity respectively. The lifetime data were collected at only 520 nm emission wavelengths and λ_{ex} was 405 nm.

The calculated bimolecular quenching constant (k_q) was 2.33×10^8 $M^{-1}sec^{-1}$ at 520 nm emission (longer emission band, g1 conformer). Generally, diffusion controlled quenching by small molecules should have a k_q value near to 1×10^{10} $M^{-1}sec^{-1}$ [13]. However, in the case of macromolecules, generally fluorophores are shielded by the macromolecules; the quenchers need to diffuse in a specific direction to execute this quenching and the maximum k_q value is expected to be about 50% of the diffusion-controlled value.

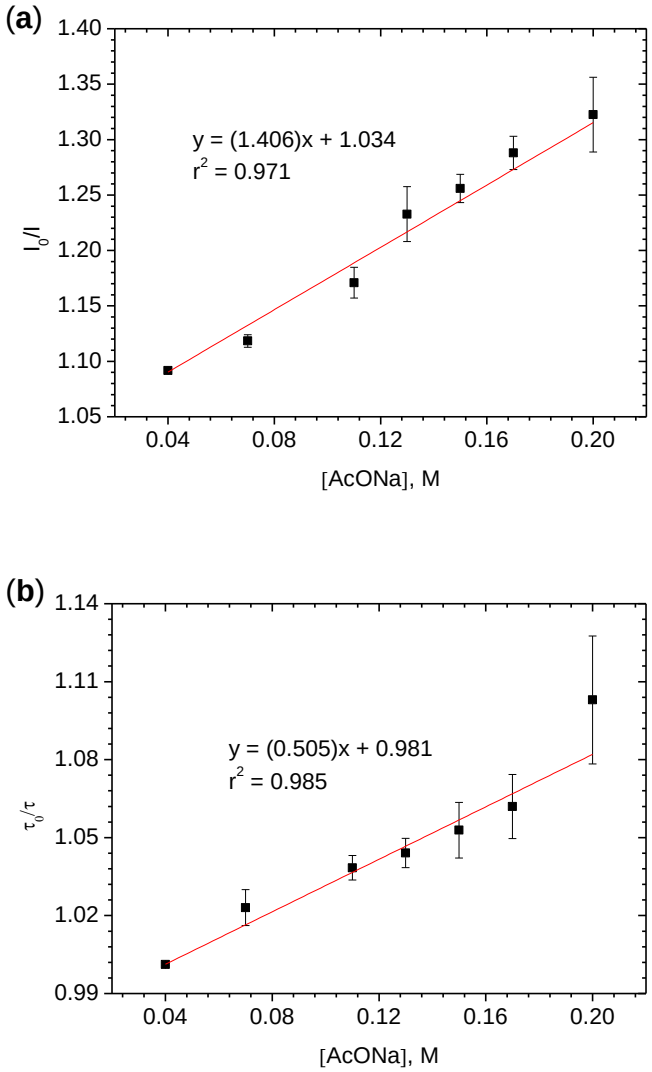

Figure 7.8: Stern-Volmer plot as an intensity ratio (a) and lifetime ratio (b) for pTr doped PVA aqueous solution where AcONa at different concentration is used as a quencher. Where, I_0 and I are the intensity maximum of emission in the absence and presence of quencher respectively. The λ_{ex} was 405 nm and temperature was 25 °C. The τ_0 and τ are the pTr lifetime at the absence and presence of quencher respectively. The lifetime data were presented at only 520 nm emission wavelengths. See Appendix for the lifetime ratio at 470 and 490 nm wavelengths vs quencher's concentration.

To determine the PVA polymer effect on k_q value (Figure 7.8), a quenching study with AcONa only (no PVA) was undertaken and the Stern-Volmer plot generated (Figure 7.9) and in this case, a larger k_q value (compared to Figure 7.8) was observed. This was attributable to the absence of macromolecules *i.e.* PVA and reduction of viscosity of medium leading to diffusion-controlled quenching.

In presence of PVA (*e.g.* 0.5% w/w PVA concentration), one could expect that the pTr became shielded by the PVA strands. Therefore, the experimental k_q values obtained tended to support quenching by acetate anion through a dynamic mechanism.

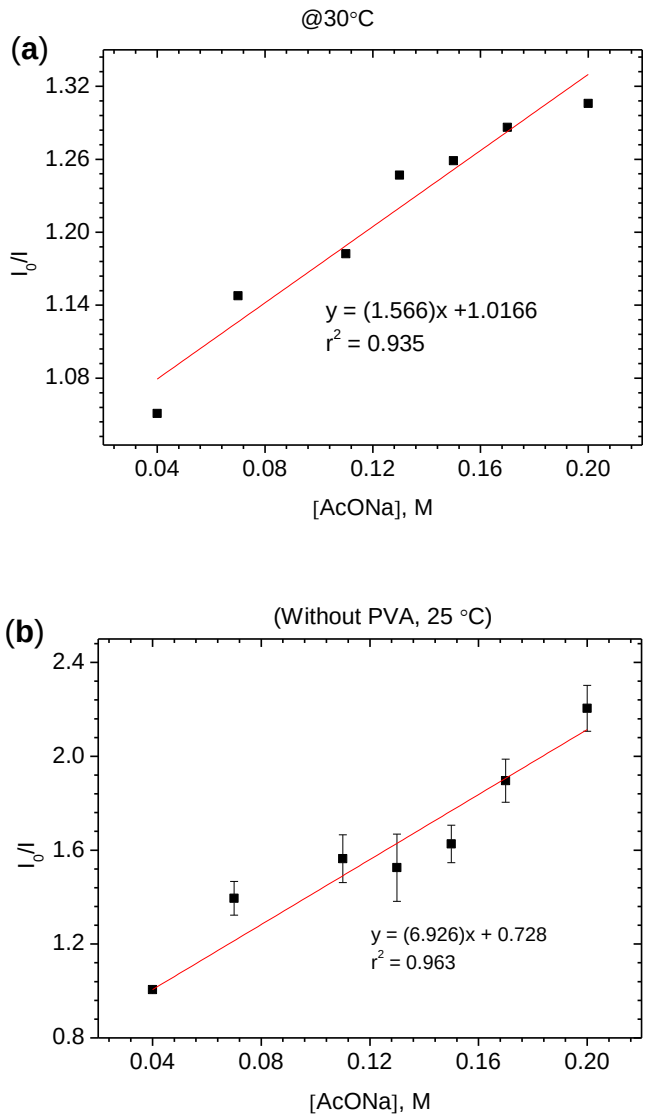

Figure 7.9: Stern-Volmer plot of (as intensity ratio) pTr as a function of acetate anion's concentration in PVA aqueous solution at 30 °C (a)/ without PVA at 25 °C (b). Where, I_0 and I are the fluorescence overall intensity in the absence and presence of quencher respectively.

And finally, the possible explanation for this humidity-induced collisional quenching of pTr overall intensity by AcONa (Figure 7.1a) is: since the absorption of water was generally a function of % RH and temperature of the system [4, 262], with an increase in humidity, the amount of water absorbed into polymer thin films increased. The film thickness also affects the amount of water absorption and diffusion of absorbed water molecules into the thin films [263]. Therefore, at higher humidity

one would expect a higher amount of water diffusion in 20 µm thick PVA films. This higher content of water was also evidenced by the higher % water absorption (compared to PNIPAm thin film, see Chapter 4 and Section 7.2). Since, PVA is a water soluble polymer; a relatively large volume of water penetrates into the films leading to loss of crystallinity of PVA. Eventually, the films swell [264, 265] and produce a more homogeneous environment similar to PVA solution. Therefore as water content increases in the PVA films (as a function of humidity), AcONa mobility increases leading to a greater quenching of overall fluorescence emission intensity (Figure 7.1). As temperature increases, AcONa mobility was also increased which leads to a greater rate of quenching at 37 °C (Figure 7.1a). This was also proved by the higher K_{SV} value at 30 °C compared to 25 °C (Figure 7.9).

In addition, the swelling of the films leads to an increase in the volume and thus decreases the concentration of pTr which ultimately decreases the fluorescence overall intensity according to Mishra *et al.* [84].

When the individual emission properties of each conformer were analysed (see Appendix VII), major changes as a function of [AcONa] were not found (the minor changes that were observed were most probably due to dilution effects). So, the humidity-induced changes in the relative populations of the various conformer (Figure 7.2a) might be related either 1) IVR, 2) water-induced quenching and/or 3) photobleaching.

Interestingly, at 37 °C, the g1 and g2 excited states were blue shifted with the increase of water absorption (Figure 7.4a) indicating: 1) the pTr might be located in different domain (*i.e.* more hydrophobic domain compared to 25 °C) and the presence of hydrophobic-hydrophobic interaction. This might be possible for segmental motion of PVA (more will be provided in section 7.6), and or 2) effect of photobleaching (will be discussed in section 7.6).

The humidity-induced drop in hTr's overall intensity were small at 25 °C in PVA thin films (like as PNIPAm) indicating the anion-induced quenching had very little effect on Figure 7.1b. The water related quenching and/or photobleaching might be responsible for this small intensity drop. This statement was also supported by the very lower Stern-Volmer quenching constant (humidity-induced) for hTr compared to

pTr (Figure 7.7 compared to Figure 7.6). But, at 37 °C, this drop was larger in PVA (compared to PNIPAm). It could be expected that at higher temperatures (*e.g.* 37 °C) the mobility of polymer chain would be increased which would ease the diffusion of water and AcONa molecules into the PVA polymer matrices (compared to 25 °C) [60] leading to a diffusion controlled anion-induced quenching.

The hTr in PNIPAm thin films showed a significant change in g1 and g2 conformer emission intensity due to water-induced IVR with increase in humidity (Chapter 5). Since the amount of absorbed water is two times higher than for PNIPAm, it was expected that for PVA films, the changes of g1 conformer should be larger (due to water sensitive hTr emission). However, only a small change was observed (Figure 7.2b). This might be due to the increased rate of g1 population (as a function of humidity) was reduced by the counteraction of quenching (anion/water-induced).

Table 7.2: Emission properties changes of Tr-PVA thin film as a function of humidity both at 25 and 37 °C. Since, the accumulation of water droplets were observed in the humidity chamber window at ≥70% RH, the water induced emission properties changes are considered from 10-70% RH both at 25 and 37 °C. Where A_1, A_2, and A_3 are the relative population; W_1, W_2, and W_3 are the FWHM; and BP_1, BP_2, and BP_3 are the band position of S_1 (g1), S_1 (g2) and S_1 (g0) excited state respectively. (+) indicate the increase and (-) indicate decrease.

Tr	Temp.	% Band area (%)			Bandwidth (FWHM, cm^{-1})			Band position, nm		
		ΔA_1	ΔA_2	ΔA_3	ΔW_1	ΔW_2	ΔW_3	ΔBP_1	ΔBP_2	ΔBP_3
pTr	25 °C	+14%	-18%	+4%	-195	-39	-69	+3	+1	+1
	37 °C	+15%	-13%	-2%	-238	-92	-110	-8	-3	+3
hTr	25 °C	+5%	-5%	-2%	+62	-37	-29	-3	-2	+1
	37 °C	+5%	-5%	~2%	-190	-100	-102	-1	-2	+2

A continuous decrease in bandwidth for all emission conformers of pTr was observed as an effect of humidity both at 25 and 37 °C (Figure 7.3a). This indicated that pTr was experiencing a more homogeneous micro-environment. On the other hand, no humidity-induced major changes in FWHM at 25 °C was observed for hTr, whereas humidity-induced significant decrease in FWHM was observed at 37 °C indicating a narrower range of environment (Figure 7.3b).

Overall, there was no evidence of H-bonding interaction between the Tr fluorophores (Tr-PVA thin films) and incoming water in the humidity studies. Instead, some form of quenching (water-induced and/or anion-induced) was responsible for the

changes in emission intensity. The next section describes an investigation of the humidity-induced changes in the fluorescence lifetime of Tr-PVA thin films. These experiments were undertaken to get a better insight about the effect of anion-induced quenching into the humidity-induced Tr photophysics.

7.4. Lifetime at different emission wavelengths

The RI related humidity-induced changes in Tr fluorophore's lifetime (Chapter 3, 4, and 5) were not present in the PVA polymer matrix. A major change in Tr fluorophore's average lifetime was observed as an effect of humidity (both at 25 and 37 °C, Figure 7.10) indicating again the presence of dominating anion-induced quenching (like as humidity-induced S-S study of Tr-PVA thin films).

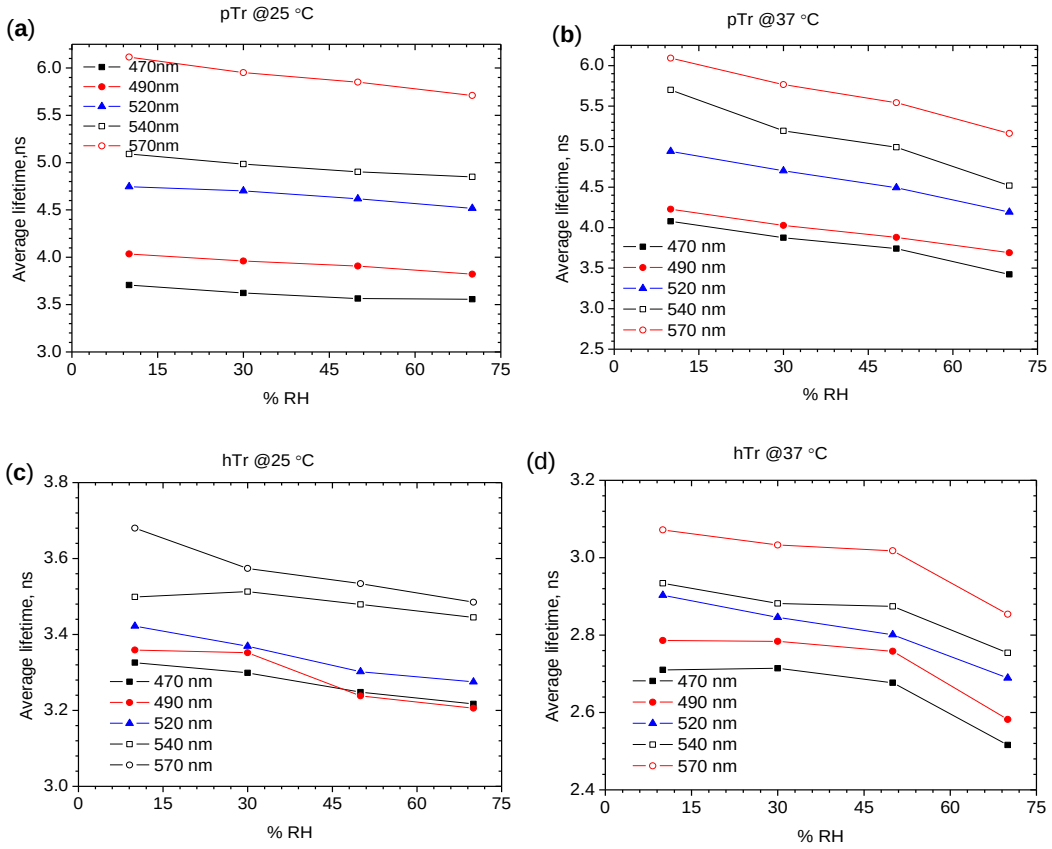

Figure 7.10: Plot showing the average lifetime, $\langle\tau\rangle_f$ changes of Tr-PVA thin films as an effect of humidity at different emission wavelengths, where (a) is for pTr at 25 °C, (b) is for pTr at 37 °C (c) is for hTr at 25 °C, and (d) is for hTr at 37 °C. The λ_{ex} was 405 nm.

Plotting the pTr-PVA thin film lifetime changes versus humidity showed that the lifetime decreased with increasing humidity (Figure 7.10a/b). As it was obvious from the S-S data, these humidity-induced lifetime changes were consistent with

anion-induced quenching. These drops in lifetime were larger at 37 compared to 25 °C (Figure 7.10b and Table 7.3) indicating a higher rate of diffusion based anion-induced quenching.

Compared to pTr, the lifetime changes were small for hTr indicates the anion-induced quenching did not have much effect on hTr emission, which was also supported by the S-S emission properties.

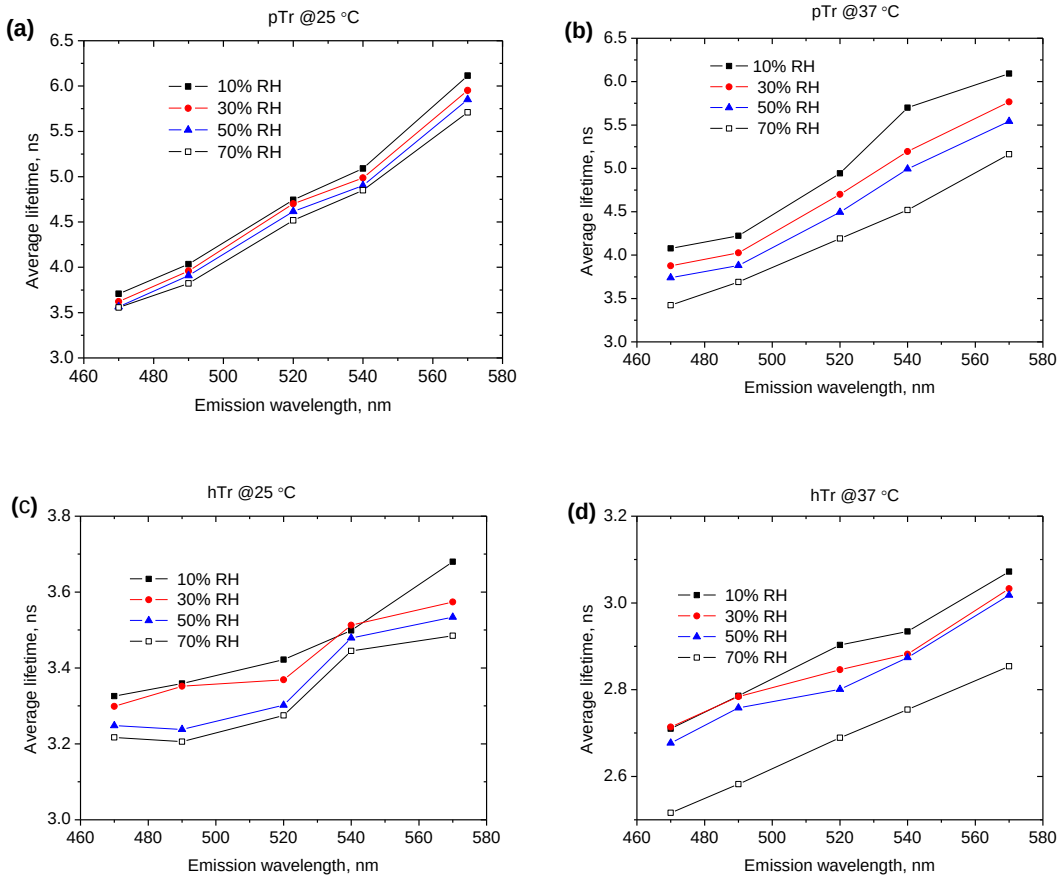

Figure 7.11: Plots show the average lifetime, $\langle\tau\rangle_f$ changes of pTr-PVA thin film as a function of emission wavelengths both at 25 °C (a)/37 °C (b). Plot show the $\langle\tau\rangle_f$ changes of hTr-PVA thin films with different emission wavelengths at 25 °C (c)/37 °C(d).

A linear relationship (For pTr, r^2>0.98, except for 470 nm where r^2 = 0.94, and for hTr the plots were very nearly linear[11]) was observed (Table 7.4) for the change in

[11] The fitted plots of humidity-induced hTr's lifetime changes were nearly linear, where r^2>0.93 for 3 plots and r^2>0.70 for 9 plots. A small deviation from the linearity might be originated from relatively a long accumulation time (due to very low emission intensity) and within this time, hTr might be photobleached.

lifetime with increasing humidity both at 25 and 37 °C which indicated that only dynamic quenching was responsible.

Table 7.3: Total drops in average lifetime $\langle\tau\rangle_f$ from its initial value (*i.e.* at 10%) of Tr- PVA thin films up to 70% RH both at 25 °C and 37 °C. The λ_{ex} was 405 nm.

Wavelengths	pTr		hTr	
	25 °C	37 °C	25 °C	37 °C
470 nm	3.69%	16.13%	3.27%	7.15%
490 nm	5.30%	12.68%	4.50%	7.32%
520 nm	4.78%	15.19%	4.29%	7.37%
540 nm	4.73%	20.71%	1.54%	6.13%
570 nm	6.62%	15.26%	5.29%	7.07%

Table 7.4: Rate of changes in humidity induced lifetime of Tr-PVA thin films at different emission wavelengths, where λ_{ex} was 405 nm

Wavelengths	pTr		hTr	
	25 °C	37 °C	25 °C	37 °C
470 nm	y= –0.002x+3.71 r^2=0.94	y= –0.01x+4.19 r^2=0.98	y= –0.0002x+4 r^2=0.45	y= –0.0012x+4.8 r^2=0.94
490 nm	y= –0.003x+4.07 r^2=0.99	y= –0.009x+4.3 r^2=0.99	y= –0.0013x+4.5 r^2=0.88	y= –0.006x+5 r^2=0.76
520 nm	y= –0.004x+4.79 r^2=0.98	y= –0.012x+5.07 r^2=0.99	y= –0.0021x+4.7 r^2=0.94	y= –0.015x+5 r^2=0.93
540 nm	y= –0.004x+5.11 r^2=0.99	y= –0.018x+5.85 r^2=0.99	y= –0.0015x+4.9 r^2=0.73	y= –0.0014x+5 r^2=0.76
570 nm	y= –0.006x+6.16 r^2=0.99	y= –0.015x+6.24 r^2=0.99	y= –0.0018x+5.0 r^2=0.80	y=.0004x+5 r^2=0.76

The average lifetime of Tr in PVA thin films was increased (Figure 7.11) with emission wavelengths and already has been discussed in Chapter 3. It was increased total by ~2 ns for pTr and ~0.5 ns for hTr within the emission wavelength range from 470–570 nm both for 25/37 °C.

7.5. Study of temperature effect

The effect of temperature on the fluorescence emission properties of pTr-PVA thin films was investigated to elucidate the relationship between temperature and

emission properties. This was achieved by placing the sample into the humidity chamber and varying the temperature by 1 °C increments. The S-S data and lifetime decay curves were then collected.

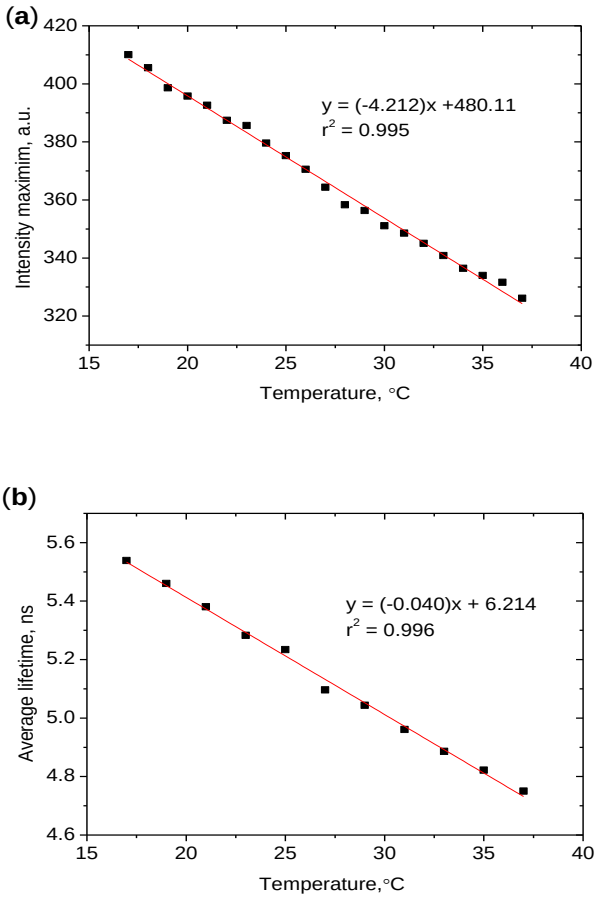

Figure 7.12: Plot of emission properties variation as a function of temperature of pTr-PVA thin film at 50% RH where (a) is for emission intensity drop as a function of temperature, and (b) decrease of lifetime as a function of temperature. The lifetime data were collected at only 520 nm emission wavelengths and λ_{ex} was 405 nm.

Figure 7.12 shows that with increasing temperature a linear (r^2>0.99) decrease of fluorescence intensity and lifetime were observed. However, the band positions were not shifted (Appendix VII) as a function of temperature which implies that the energy difference between the ground state and the excited state of pTr-PVA thin film was unaltered. The linear relationship (r^2 >0.99) between the emission intensity and lifetime (Figure 7.12a/b) is an indication of the presence of a single quenching process (*i.e.* anion-induced quenching).

7.6. Photobleaching study of Tr-PVA thin films

It is now clear from the variable humidity S-S study that a large drop of pTr's overall intensity was due to collisional based anion-induced quenching and only partly related to water content. The pTr-PVA film photobleaching study also showed that this effect led to a dramatic intensity drop (total ~58%, Figure 7.13) without changes in band position (see Appendix VII) at 25 °C. The photobleaching study was conducted at 50% RH and thus it could be possible that the presence of a considerable amount of absorbed water leads to a diffusion controlled anion-induced quenching. This quenching rate was higher at 37 °C and responsible for a greater drop in overall emission (total ~83%, Figure 7.13).

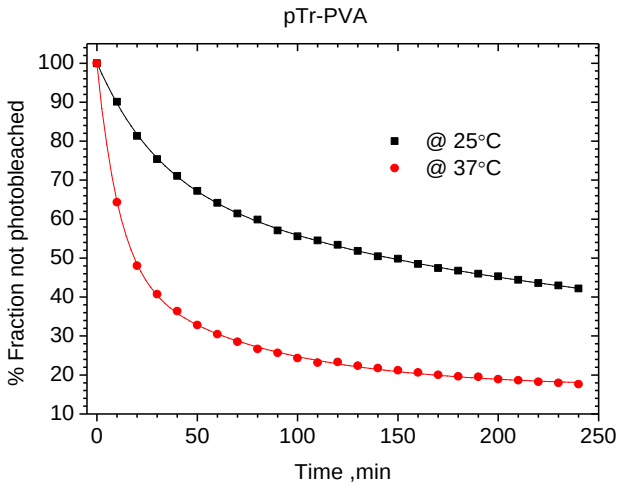

Figure 7.13: Plot represents the photodegradation of pTr-PVA thin films as a fraction not photobleached with time at 25 and 37 °C. The bi-exponential fitting equation at 25 °C is y = 29.55 exp(-x/29.08) + 42.16 exp(-x/215) + 28.42, r^2 = 0.999 and at 37 °C is y = 52.70 exp(-x/10.84) + 30.36 exp(-x/73.60) + 19.91, r^2 = 0.999. The films were continuously irradiated by the 405 nm light over 4 hours where the power of incident light was 10 µW, the spot size was 1 mm, λ_{ex} was 405 nm, and the humidity was 50%.

By careful analysis of the statistical parameters (Appendix VII), it was found that a bi-exponential function was required to describe the photobleaching processes at 25 and 37 °C. This might indicate the presence of two different photobleaching processes. One might be linked to the presence of AcONa and the other to water.

PVA is a semi-crystalline polymer and can provide two sorption sites for fluorophores (*e.g.* one was isolated by the PVA leading to a slower rate and other was in close proximity to each other, leading to a faster rate of photobleaching by D-D interaction) which thus leads to two photobleaching rate according to Talhavini *et al.*

[30]. Although, the pTr-PVA photobleaching kinetics were bi-exponential and the concentration of pTr (0.09% w/w) was similar to that used in ref. [30, 37], it was not expected to occur in pTr's photobleaching by using this hypothesis. Because, the studied probe (fluorescein) in ref. [27, 34] was very different (structure is flat and very reactive to form dimer) to our present study. In the previous photophysical study (Chapter 3 and 4) or the pTr aggregation study in EtOH solution (see Appendix VII) also showed the absence of any D-D interaction or dimer formation.

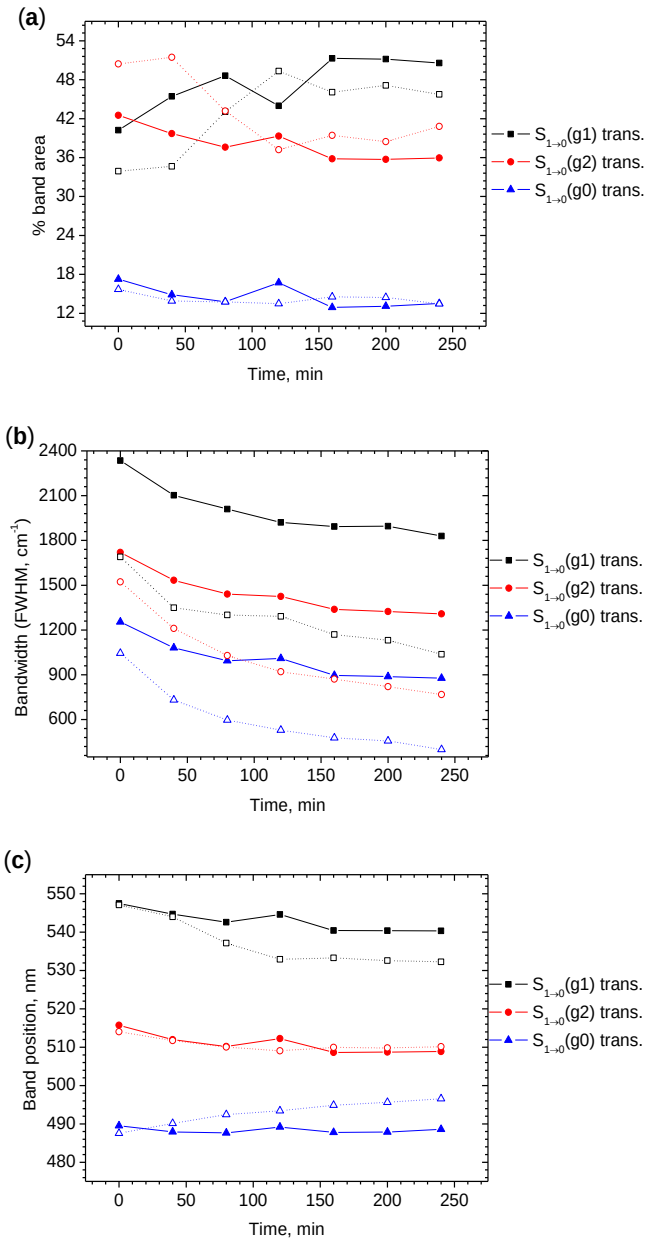

Figure 7.14: Photobleaching effect on emission properties of pTr-PVA thin films both at 25 and 37 °C, where changes in % band area (a), bandwidth, FWHM (b), and band position (c). Symbol designate the measurement temperature where solid is at 25 and open is at 37 °C.

To compare the photobleaching bi-exponential fits at 25 and 37 °C (Figure 7.13), the weight factor of amplitude (for each decay rate constant) was considered. The contribution of the normalised weight factor for these two rates is mostly dependent on temperature [37]. This hypothesis was also in agreement with the present study. At 25 °C, the slower process dominates, whereas, at 37 °C, the photobleaching process was dominated by the faster process. For example, at 25 °C, the slower rate contributes 59% but at 37 °C, the faster rate contributes 63%.

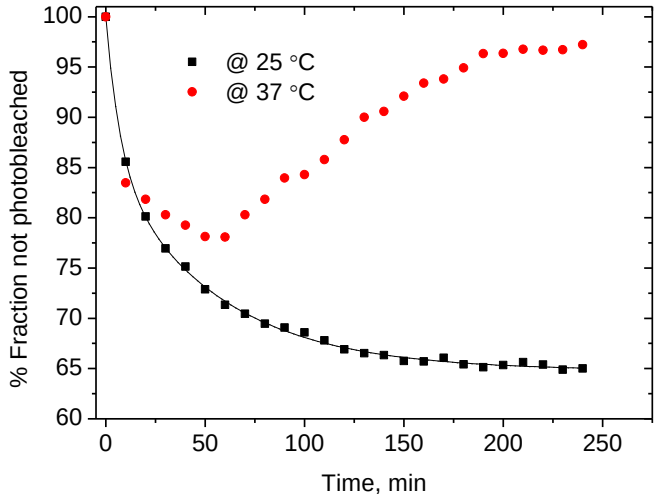

Figure 7.15: Plot represents the photodegradation of hTr-PVA thin films as % fraction not photobleached with time both at 25 /37 °C. The bi-exponential fitting equation at 25 °C is y = 14.31 exp(-x/7.02) + 20.88 exp(-x/54.11) + 64.80, r^2 = 0.999. The film was continuously irradiated by the 405 nm light over 4 hours where the power of incident light was 10 µW, the spot size was 1 mm, and the humidity was 50%.

A major change in the relative populations and energies of the excited states was observed which indicated that all conformers were not equally affected by this photobleaching process (Figure 7.14).

The overall emission band was ~3 nm blue shifted after 4 hours exposure to excitation light (see Appendix VII). The individual emission from g1 state was shifted to higher energy (~25 nm blue shifted) and g0 state was shifted to lower energy (~9 nm red shifted) at 37 °C (Figure 7.14). This was indicating that the energy of transition from S_1 (g1) and S_1 (g0) excited states was changed due to photobleaching. Once again, this was due to significant changes in dipole moment during excitation (more details in Chapter 4).

On the other hand, at 25 °C, the degree of photobleaching was slightly higher for hTr in PVA thin films (compared to PNIPAm, Chapter 5) and in both cases these occurred without changes in band position. This indicates that, at 25 °C, probably AcONa had an effect (but very small) together with water on the photobleaching process of hTr in PVA thin films. The presence of anion-induced quenching in hTr-PVA photobleaching process was also confirmed by the bi-exponential fitting in PVA (whereas photobleaching kinetics was mono-exponential in PNIPAm, see appendix VII for fitting statistics).

This emission intensity however increased after certain time exposure to 405 nm excitation light at 37 °C (Figure 7.15). This unusual behaviour of the hTr-PVA thin films at 37 °C was reproducible when the experiment was repeated several times (by using different films fabricated by maintaining same condition). It was not accompanied by any significant shift in emission wavelengths or changes in individual emission bands (Appendix VII) which implies that the emitter was still hTr.

The photobleaching behaviour at 37 °C was definitely odd but might be explained by a combination of water assisted aggregation of hTr in hydrophobic domains induced by increased thermal motion at the higher temperature.

It was suspected that breaking of the intermolecular H-bonding between PVA polymers at higher temperature (*i.e.* at 37 °C) leads to an increase the side chain mobility of the polymer [82]. A relaxation in PVA sidechain was observed which involves segmental movement of the macromolecules which were not H-bonded and this could enhance the diffusion of both water and the hTr fluorophore. This increase in diffusion, coupled with the hydrophobic nature of hTr could drive the hTr molecules to aggregate in the more hydrophobic domains and changing the photophysical behaviour. Why the hTr behaves so very differently from pTr is still unknown, but recent evidence from single molecule FCS studies in the laboratory (unpublished results) have indicated that when pTr fluorophores are co-located in micelles we get unusually bright and stable emission. Since we have seen no evidence for aggregate formation in the ensemble bulk measurements, we will have to await the outcome of further more detailed FCS studies to validate this hypothesis. This FCS work is outside the scope of my thesis research but will be communicated at a later date when these PVA studies are submitted for publication.

7.7. Conclusions

The humidity-induced changes in the photophysical properties of Tr fluorophores in PVA films were different than PNIPAm (*e.g.* large changes in emission properties were observed). It was clear that in PVA, a greater quenching of emission occurred as % RH increases. This quenching was collisional based and was due to AcONa impurities and only partly related to water content. As water increases in the PVA films as a function of humidity, AcONa mobility also increases leading to a greater quenching. As temperature increases, AcONa mobility also increases and responsible for a higher rate of quenching. This dominating anion-induced quenching was also lies in the evidence of photobleaching study of pTr-PVA thin films. The photobleaching kinetics was bi-exponential indicating the presence of both anion and water induced quenching. H-bonding interactions between the Tr fluorophores and incoming water molecules were not observed.

For hTr (compared to pTr), this anion-induced quenching had a small effect in PVA thin films. This was manifested by the humidity-induced small changes in overall intensity, average lifetime, and also in the photobleaching. At 37 °C, an unusual behaviour of hTr-PVA thin films was observed where photobleaching rate was decreased after 60 minutes continuous illumination of light. This might be due to an increased diffusion rate of water and hTr at 37 °C could initiate an aggregation of hydrophobic hTr in a more hydrophobic PVA domain.

Chapter 8 : Conclusions and future work

The photophysics of Tr-polymer thin films were studied with the goal of looking for a potential application in the characterisation of thermoresponsive polymer thin films (*e.g.* film thickness) used in biomedical applications. A variety of spectroscopic methods and a controlled humidity chamber were used for this investigation. The photophysics of the Tr was governed by the interplay between the three conformers and the emission was relatively insensitive to environmental factors. In addition, pTr is uniquely photostable in PNIPAm (compared to hTr, and kpTr) thin films which makes it suitable for imaging applications. The insensitivity towards changes in water content, together with its photostability, mean fluorophore concentration could be correlated accurately with polymer thickness *in-situ*.

The first goal of this research was to make a correlation between the lifetimes of Tr-polymer thin films and the RI of the polymer matrix. The wavelength dependent lifetime change of Tr-polymer thin films was determined to be a purely RI effect.

Water incorporation into fluorophore doped PNIPAm thin films can have a significant effect on emission properties [4]. However, when the humidity-induced effect on emission properties of Tr-polymer thin films were studied, only a slight intensity drop (due to photobleaching) was observed and other properties were left relatively unchanged. The photobleaching contribution in hTr-PNIPAm thin film's overall intensity drop was large (compared to pTr). hTr was less hydrophobic than pTr and tended to be located in a more hydrophilic part of PNIPAm in thin films. Therefore, it had a greater accessibility to water (as a function of humidity) which thus led to a more water-induced photobleaching.

Temperature or phase changes of PNIPAm had no major effect on the emission properties of all the Tr fluorophores studied. The changes in humidity had very small effect in changing the energy of transition. No H-bonding effect was observed throughout the humidity induced studies. The major changes in relative population of g1 and g2 conformers (both for pTr and hTr) as a function of humidity was due to IVR from the g2 excited state into g1. The humidity-induced this interconversion rate through IVR was higher for hTr (compared to pTr), again this was due to hTr being located in a different, more hydrophilic (*i.e.* more water accessible) environment.

The lifetime behaviour of Tr fluorophores in humidity-induced PNIPAm thin films was dominated by RI effects. The RI of the PNIPAm is smaller at 25 mass% aqueous solution (at 26 °C) compared to amorphous [252]. Therefore, the humidity-induced lifetime changes of pTr-PNIPAm thin films can be described as: below the LCST, water was miscible with PNIPAm and incorporation of water increases the volume of Tr micro-domain leading to a decrease of density (and thus RI). As a consequence the pTr lifetime was increased (as a function of humidity). On the other hand, above the LCST, the hydrophobic PNIPAm micro-domain was squeezed tighter which thus increases the RI (due to increase of PNIPAm density) leading to a decrease of lifetime with humidity. This RI related lifetime behaviour was also observed for hTr but the humidity-induced this lifetime changes were smaller than pTr. This indicated that, hTr domain's RI was not significantly changes with the humidity or the lifetime changes caused by the RI were counteract by some form of quenching with the water incorporation.

The behaviour of kpTr with respect to changes in environment was nearly identical to pTr and most likely they were in the same environment. The highly insensitive emission properties of kpTr (compared to pTr) might be related with different change in dipole moment during excitation and different energy states of three conformers.

When the long term photobleaching of Tr-PNIPAm thin films (at 50% RH, 405 nm λ_{ex}, 10 µW irradiation power, and 1 mm spot) were studied to justify its potential application in further imaging applications, a unique photostability was observed for pTr. Compared to pTr, the photobleaching degree was higher for hTr/kpTr indicating a higher rate of photobleaching. hTr domain was more accessible to water in PNIPAm thin films leading to a greater reactivity of three emission conformers and thus a higher rate of photobleaching. The higher kpTr's photobleaching rate (compared to pTr) might be related to its longer intensity average lifetime together with dipole moment changes during excitation. This higher rate of photobleaching is a limitation for the use of hTr/kpTr in imaging applications. The emission properties (*e.g.* relative population, FWHM, and band position) changes of three conformers during photobleaching study were very small indicated that all the conformers were equally affected by the photobleaching.

The humidity-induced changes in emission properties of pTr were studied in PVA in order to explore the photophysical behaviour of this other, more hydrophilic, medium. Unfortunately, in this experiment significant intensity drops of overall emission (compared to PNIPAm) were observed, this indicated the presence of a different photophysical process, induced quenching (*i.e.* anions were present as impurities (methyl or sodium ethanoate) in PVA [259]). This anion-induced quenching was diffusion controlled. At higher temperatures, the diffusion of water and AcONa was increased which led to a higher rate of anion-induced quenching and a greater drops in overall intensity at 37 °C (compared to 25 °C) was the consequence. This behaviour was also observed for humidity-induced TRF and in long term photobleaching studies of pTr-PVA thin films.

Compared to pTr, anion-induced quenching was not a major effect in hTr-PVA films. It caused only small drops of overall emission intensity and also a small change in humidity-induced lifetime properties. A peculiar behaviour was observed during the photobleaching study of hTr-PVA thin films at 37 °C. The overall intensity increased after a certain time exposure to 405 nm irradiation light. This was might be due to a water assisted aggregation of hTr fluorophore in more hydrophobic domain of PVA at higher temperature.

This thesis has opened many avenues to further interesting work on the application of these fluorophores in the measurement of biomedical polymer film thickness and also in the exploration of the unusual photobleaching behaviour of hTr-PVA thin films at 37 °C. One of the issues could be examine the imaging application of this exceptionally photostable pTr by doping it into polymer thin films and then correlate with the film thickness. Furthermore, a complete single molecule FCS study would be required to elucidate the unresolved hTr-PVA thin film's photobleaching behaviour at 37 °C.

List of publications and conference attendance

Publications:

1. Muhammad Zakarul Islam, Cheryl Morris, Alan G Ryder, *Study the photophysics of novel 1,2,3 triazine fluorophore in PNIPAm thin films (**in preparation**).*
2. Muhammad Zakarul Islam, Cheryl Morris, Alan G Ryder, *Anion-induced quenching study of 1, 2, 3 triazine fluorophore in PVA thin films (**in preparation).***

Poster presentations:

1. Muhammad Islam, Dr. Alan G Ryder, *Study the photophysics of 2, 5-di-hidro 1, 2, 3 triazine fluorophore.* Methods and application of Fluorescence, 13-15. 09.2015, Wurzburg, Germany.
2. Muhammad Islam, Dr. Alan G Ryder, *Photostable and environmentally insensitive dye: 2, 5-di-hidro 1, 2, 3 triazine fluorophore.* Research Day, 21.04.2015, NUI Galway Ireland.
3. Muhammad Islam, Dr. Alan G. Ryder, *Photostability of novel 2, 5-di-hidro 1, 2, 3 phenyl triazine fluorophore.* Research Day, 11.04.2013, NUI Galway Ireland.
4. Muhammad Islam, Dr. Alan G. Ryder, *Novel photostable fluorophore for polymer characterization.* Royal Academy of Medical in Ireland (Section of Biomedical Science), 14.06.2012, NUI Galway Ireland.
5. Muhammad Islam, Dr. Alan G. Ryder, *Fluorescence characterisation of biomedical polymers.* The Synergy Project, 30.04.2012, NUI Galway Ireland.

Appendices:

Appendix I:

1. Time correlated single photon counting (TCSPC):

One of the most widely used methods for lifetime measurements is TCSPC (time domain measurement). The TCSPC is a statistical method based on:

1. Fluorescence emission is random.
2. If detection rate is < ~1% , then detected photons should obey Poisson statistics.
3. The histogram of photon arrival time over intensity yields the true decay curve.

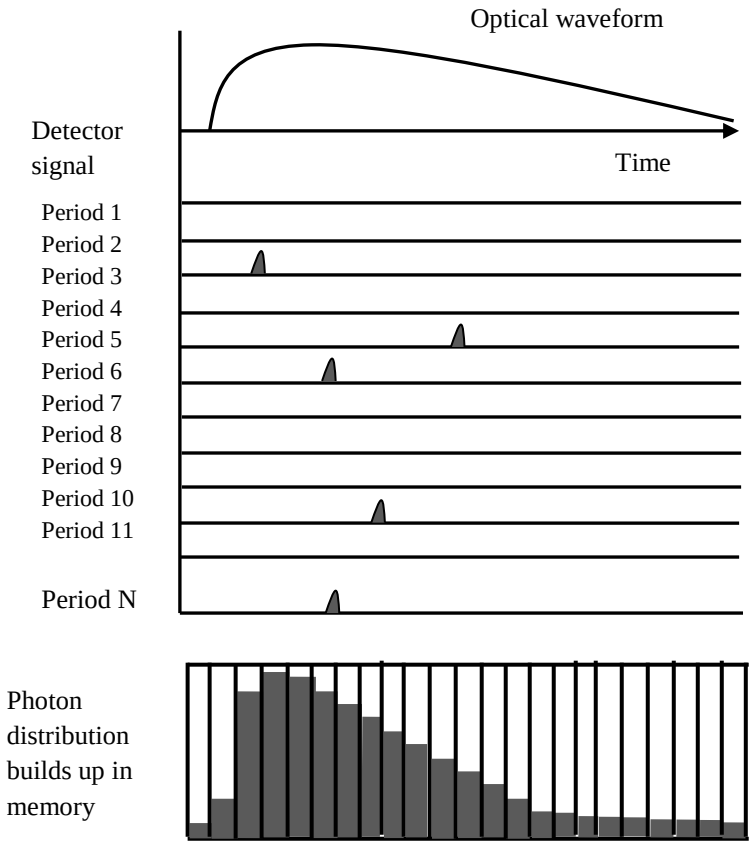

Figure A.I.1: Principle of TCSPC. The photon generated in each panel is represented over time as a pulse in the middle panel. Accumulation of required numbers of photons counts over arrival time build up the histogram, from where we can calculate the lifetime of the fluorophore. Reproduced from ref. [266]

The general working procedure of TCSPC is presented in Figure A.I.1. The heart of TCSPC is the time-to-amplitude converter (TAC) which is analogous to a fast stopwatch. It measures the elapsed time between a start pulse generated by the excitation light pulse and that of the stop pulse which is generated by first emitted photon detected. The measurement conditions are maintained in such a way that the photon detection rate is typically less than one photon per 100 excitation pulses. The start signal produced from the excitation pulse from the laser is used to trigger the voltage ramp of the TAC. After receiving the trigger pulse, the TAC then initiates the charging of a capacitor plate which is routed to the TAC start input via a discriminator.

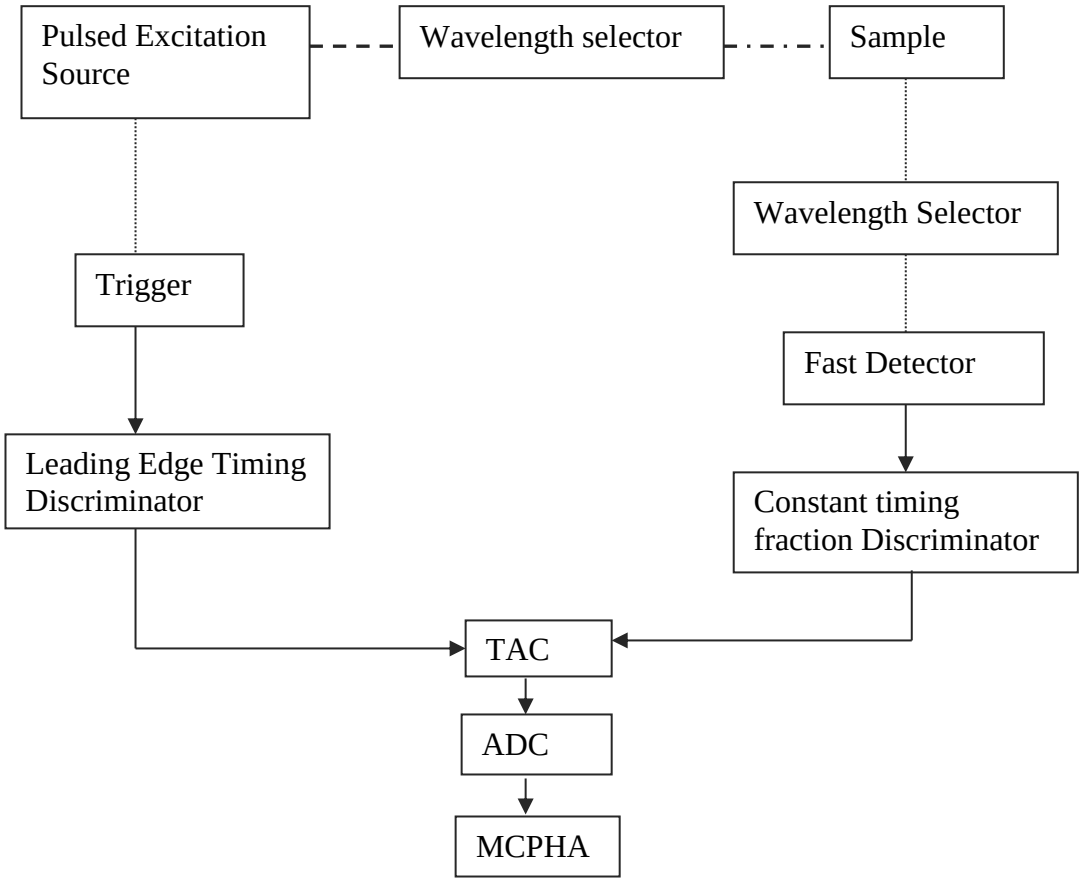

Figure A.I.2: A schematic diagram of a TCSPC. Reproduced from ref. [45].

When a photon reaches the detector, a pulse is generated whose amplitude is proportionally related to the charge of the capacitor, *i.e.* the time gap between the start and the stop pulse. The TAC output is then given a numerical value within the analog-to-digital converter (ADC), and is stored in data storage device (multichannel pulse height analyser (MCPHA)/Histogrammer,) in an address corresponding to that

number. This data is used to construct a histogram where the x-axis is the arrival time and y-axis is the number of photons detected at each time. The process of excitation and detection is repeated until the required number of counts to represent the decay curve of the samples is obtained.

Appendix II:

1. **Calculation, showing the mass/volume requirement of Tr-PNIPAm solution for the 10 µm thick films preparations:**

Volume of Tr fluorophore doped PNIPAm/PVP solutions needed for preparing a 10 µm thick films.

Mass = Density × thickness × area (quartz slide)

= (1 g/cm^3) (10 × 10^{-4} cm) (5.4 cm^2)

= 0.0054 g

= 5.4 mg

We prepared the thin films from 5% (w/w) PNIPAm/PVP solution

So, (Mass of polymer/Mass of solvent, EtOH) × 100% = 5% (w/w)

Mass of EtOH = 0.108 g

Volume of EtOH needed = 0.108 g / 0.789 g/cm^3 = ~138 µL EtOH

So, 5.4 mg PNIPAm/PVP dissolved in 138 µL EtOH fluorophore solution was used to give 10 µm thick films.

PS (10 µm thick films):

The volume of solvent needed for PS thin film was different as we used DCM solvent. As same 5% PS solution was used for film preparation, mass of solvent was same as PNIPAm for 10 µm thin film (0.108 g).

Volume of DCM needed: 0.108 g/1.33 g/cm^3 = ~81 µL

So, 5.4 mg PS dissolved in 81 µL DCM fluorophore solution to give 10 µm thick films.

To make 1mL stock solution of Tr doped PS solution in DCM, we need 5.4/0.081 × 1 mL = 66.25 mg = 0.06625 gm PS dissolved in 1mL DCM fluorophore solution.

PVA (20 µm thick films):

The volume of solvent needed for PVA thin film was also different as we used a mixture of EtOH and H_2O solvent. The ratio of EtOH and H_2O solvent was 200:800. As we prepared 20 µm thin films the mass of polymer needed 10.8 mg.

The density of solvent mixture: 0.949 g/cm^3

The PVA concentration: 4% w/w

So, (0.0108 / x) ×100% = 4%, (where x = mass of solvent mixture)

x = 0.27 g of solvent mixture

The volume of pTr-PVA solution needed: 0.27/0.949 g/cm^3 = 284 µL

2. Calculation the concentration of Tr (%w/w) in polymer thin films:

The film volume was = 12 mm × 45 mm × 10 µm

= 5.4 × 10^{-9} m^3 = 5.4 × 10^{-6} dm^3

Solution (PNIPAm/EtOH) volume was taken: 138 × 10^{-6} L

pTr concentration: 7.5 × 10^{-5} mol/dm^3

The mass of PNIPAm in 10 µm films: 0.0054 gm

The mass of pTr in PNIPAm films: 4.8906 × 10^{-6} gm

So, the concentration of pTr in PNIPAm films: 0.09% (w/w)

In the same way,

The concentration of pTr in 10 µm thick PS film (82 µL pTr/PS solution was used): 0.05% (w/w)

The concentration of hTr in 10 µm PNIPAm films: 0.07% (w/w)

And, the concentration of kpTr in 10 µm PNIPAm films: 0.08% (w/w)

3. **Calculation the concentration of Tr (%w/w) in 20 µm thick PVA thin films:**

The volume of polymer solution was taken: 284×10^{-6} L

pTr's concentration: 7.5×10^{-5} mol/dm^3

The weight of PVA was taken: 0.0108 gm (calculated weight for 20 µm PVA)

The mass of pTr in PVA thin films: 1.006×10^{-5} gm

So, the concentration of pTr in PVA films: 0.09% (w/w)

hTr's concentration (in solution): 8×10^{-5} mol/dm^3

The mass of hTr in PVA films: 8.39299×10^{-6} gm

So, the concentration of hTr in PVA films: 0.077% (w/w)

Appendix III:

1. **Changes in emission properties for Mylar sealed pTr-PS films:**

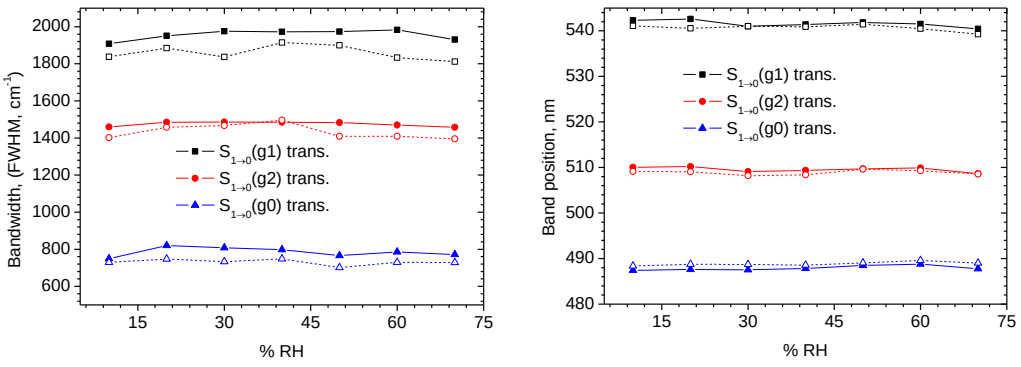

Figure A.III.1: Plot showing the changes in FWHM (left) and band position (right) for Mylar wrapped pTr-PS films, showing no major changes in micro-heterogeneity or energy of the excited state. Symbols represent the measurement temperature, solid (at 25 °C) and open (at 37 °C).

2. Humidity-induced Overlay spectra of pTr-PS thin films:

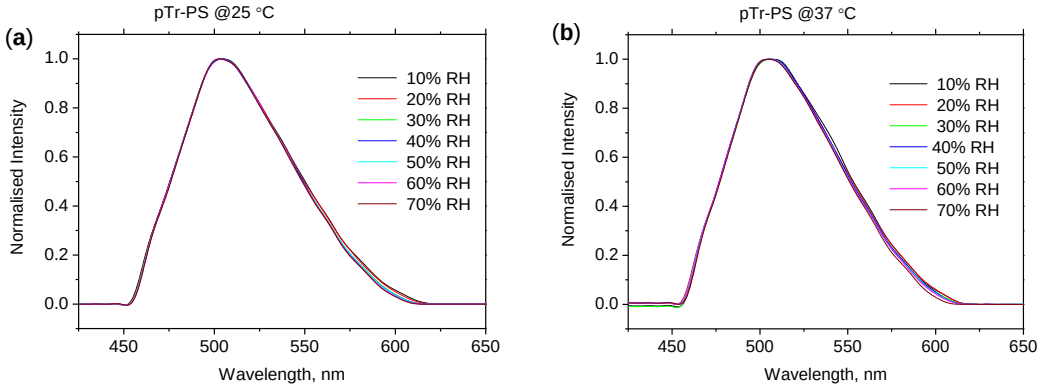

Figure A.III.2: Normalised, smoothed overlay emission spectra of pTr-PS thin films both at 25 (a) and 37 °C (b) as a function of humidity. It shows no humidity-induced spectral shift.

3. Humidity-induced changes in individual lifetime of pTr-PS thin films:

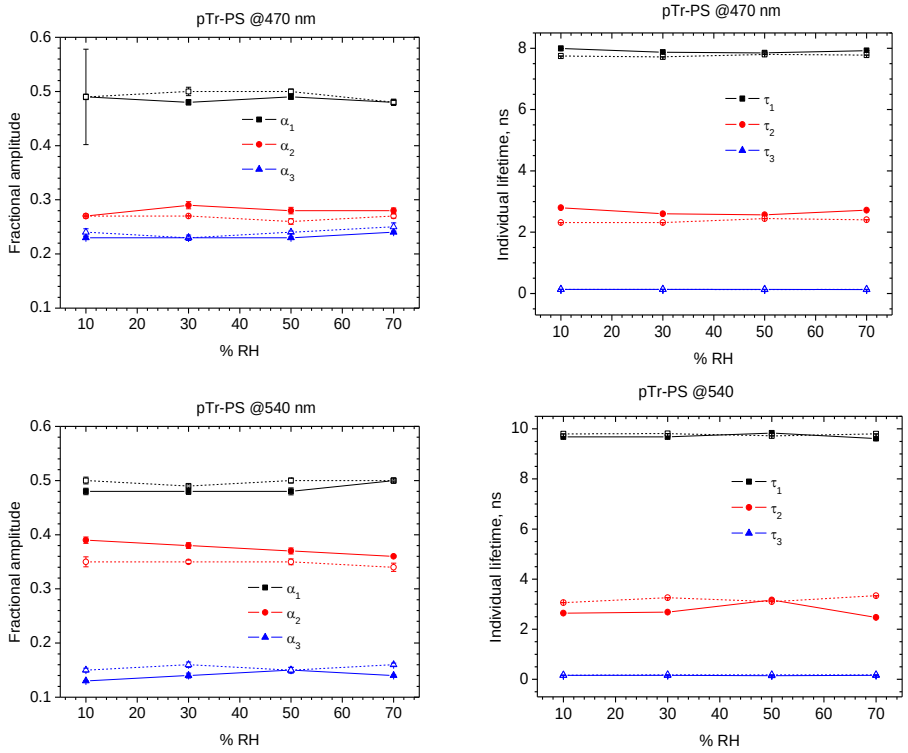

Figure A.III.3: Plots of fractional amplitude and individual lifetime vs increasing humidity for pTr-PS thin films at 25 and 37 °C (at 470 and 540 nm emission wavelengths). Symbols represent the measurement temperature, solid (25 °C) and open (37 °C). The figure shows relatively unchanged individual lifetime components as an effect of humidity. All data were fitted to a tri-exponential model. Where αi = fractional amplitudes/pre-exponential factors. Amplitudes have been normalised such that Σ|αi| = 1.Errors calculated using support plane analysis.

4. Overlay spectra of photobleaching of pTr-PS films:

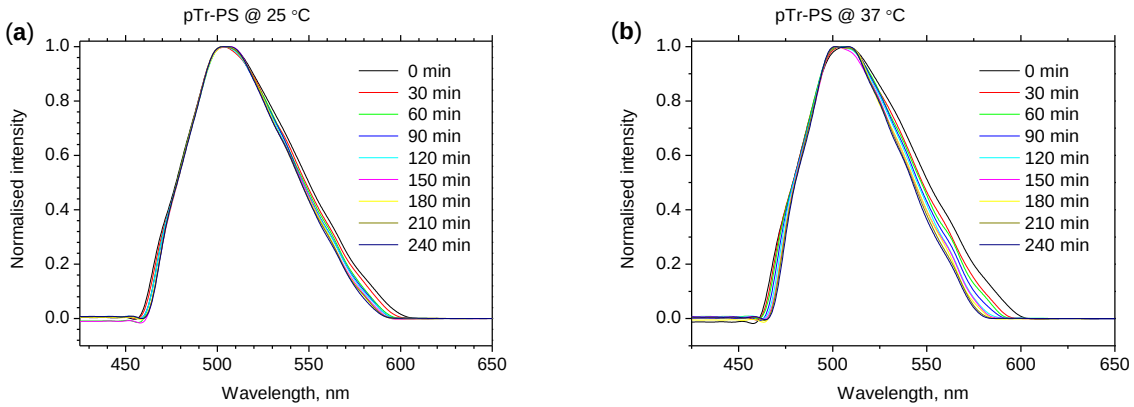

Figure A.III.4: Overlaid plots of pTr-PS thin film spectra (smoothed and normalised) collected during the photobleaching experiment which shows relatively un-shifted overall emission band both at 25 °C (a) and 37 °C (b).

Appendix IV:

1. Calculation of Orientation polarizability:

According to Lippert-Mataga equation the energy difference in cm^{-1}

$$\Delta\bar{\nu}\ (Stokes\ shift\ ) = \frac{2\Delta f}{hca^3}(\mu_E - \mu_G)^2$$

Where h is Planck's constant, c is velocity of light, a is the cavity radius in which the fluorophore resides.

μ_E and μ_G are the dipole moment in the excited and ground state of molecule respectively. Δf is the orientation polarizabilities which can be presented as:

$$\Delta f = \frac{\epsilon - 1}{2\epsilon + 1} - \frac{n^2 - 1}{2n^2 + 1}$$

Where ϵ the dielectric constant and n is the RI

For EtOH, the ε is 24.55 and n is 1.37 so Δf is 0.2856

And in case of PNIPAm/EtOH the ϵ is 63 at below LCST and n is 1.459, so Δf is 0.2624

2. Overlaid spectra of pTr-PNIPAm films: effect of humidity

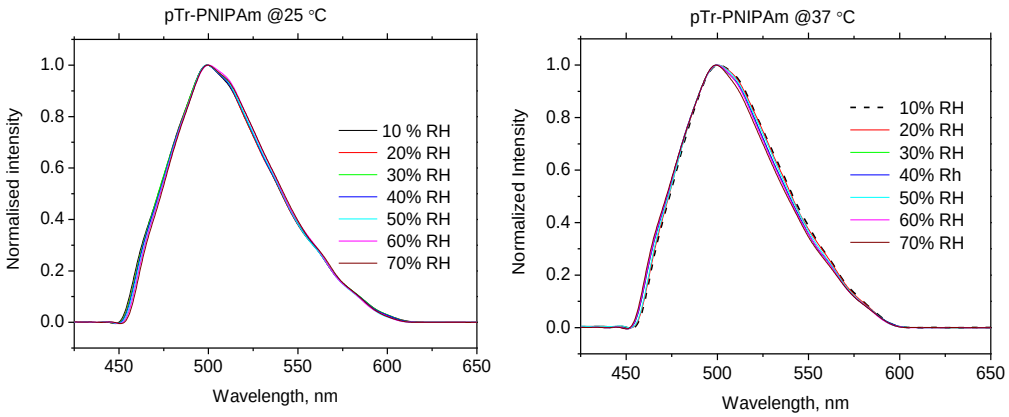

Figure A.IV.1: Smoothed, normalised overlay emision spectra of pTr-PNIPAm thin films both at 25 (left) and 37 °C (right), shows a unchanged size and shape as a function of humidity. The $\lambda_{ex.}$ was 405 nm and the thickness of the films were 10 µm.

Table A.IV.1: Band position of emission maximum of pTr-PNIPAm thin films both at 25 and 37 °C. SD were calculated from the average of three replicate measurements. The $\lambda_{ex.}$ was 405 nm. The thicknesses of the films were 10 µm.

% RH	Band position, nm	
	pTr	
	25 °C	37 °C
10	500 ± 0.20	499 ± 0.21
20	500 ± 0.56	499 ± 0.21
30	500 ± 0.56	499 ± 0.21
40	500 ± 0.56	500 ± 0.10
50	500 ± 0.36	499 ± 0.08
60	500 ± 0.83	499 ± 0.21
70	500 ± 1.05	500 ± 0.10

3. Emission properties of Mylar sealed pTr-PNIPAm films:

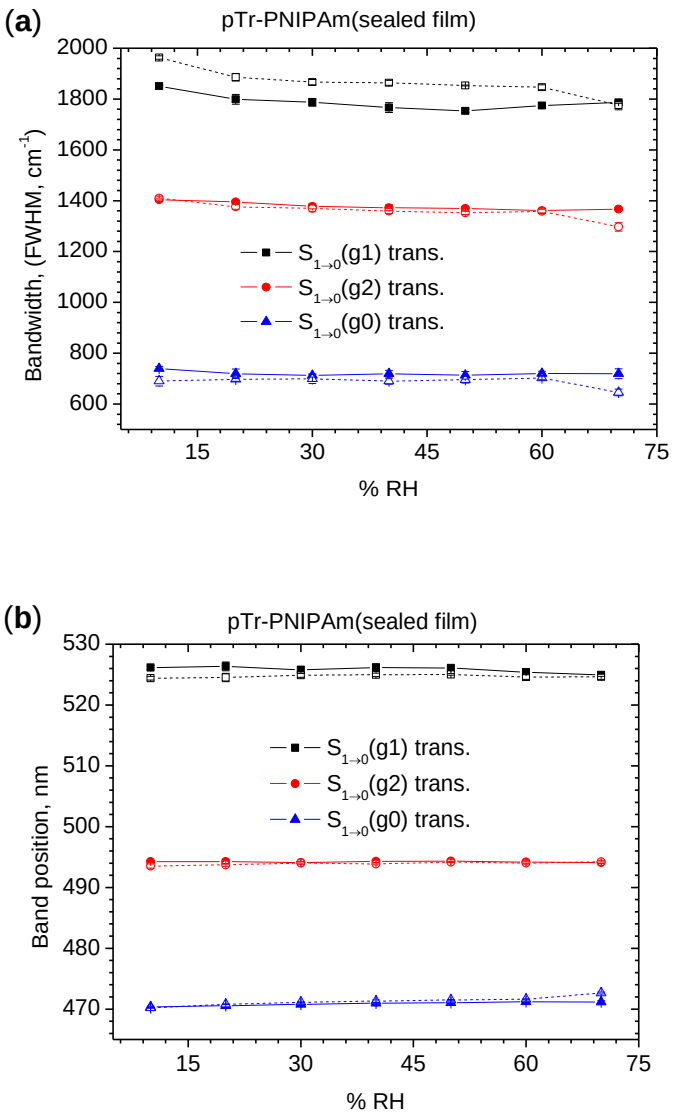

Figure A.IV.2: Plot of changes in FWHM (a) and band position (b) of Mylar wrapped pTr-PNIPAm thin films. It shows nearly unchanged emission properties with the increase of humidity. Symbol represents the measurement temperature solid (at 25 °C) and open (at 37 °C).

4. Individual lifetime of pTr-PNIPAm thin films:

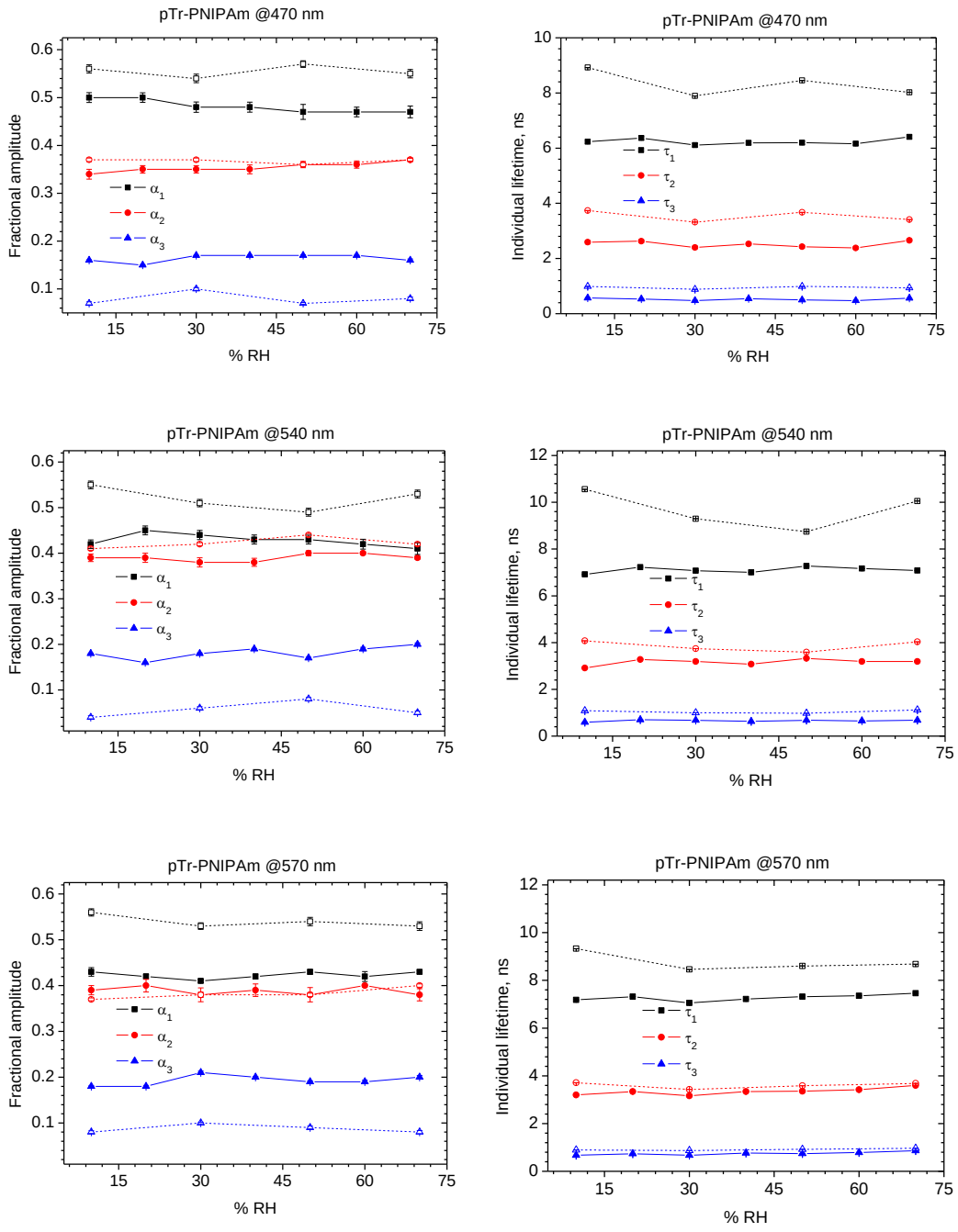

Figure A.IV.3: Plot of fractional amplitude and individual lifetime versus increasing humidity for a pTr-PNIPAm thin film at 25 and 37 °C at different emission wavelengths. Symbols represent the measurement temperature, solid (at 25 °C) and open (at 37 °C). The figure shows individual lifetime components were generally increased at 25 and decreased at 37 °C. All data were fitted to a tri-exponential model. Where αi = fractional amplitudes/pre-exponential factors. Amplitudes have been normalised such that Σ|αi| = 1. Errors calculated using support plane analysis.

5. Photobleaching study: pTr-PNIPAm

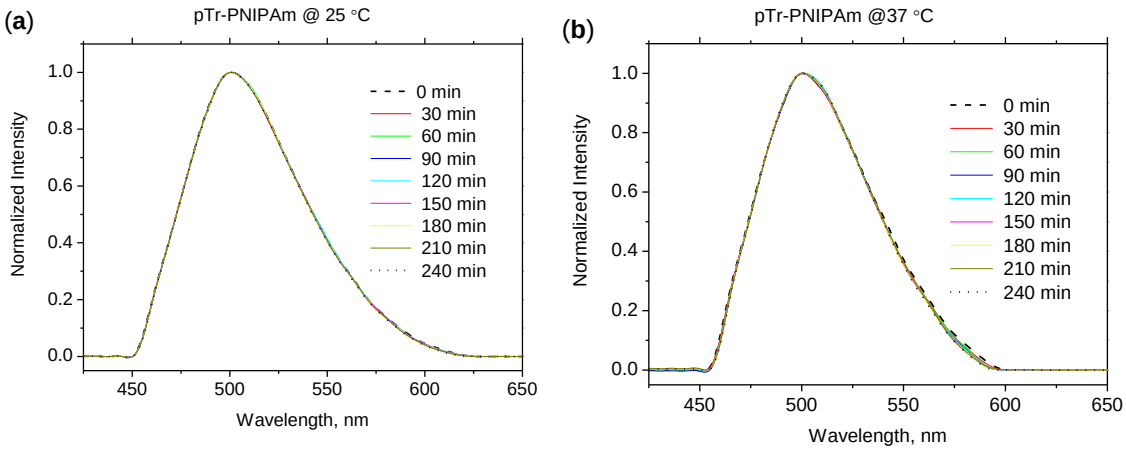

Figure A.IV.4: Overlaid normalised emission spectra of photobleaching of pTr-PNIPAm thin films (10 µm) with time both at 25 (a) and 37 °C (b) which shows that no shifted overall emission as an effect of photobleaching. The film was continuously irradiated by the 405 nm light over 4 hours where the power of incident light was 10 µW, the spot size was 1 mm, and the relative humidity was 50%.

Table A.IV.2: Different statistical parameters from the decay kinetic model of photobleaching process of pTr-PNIPAm thin films at 25 and 37 °C

Parameter	Temperature					
	25 °C			37 °C		
	Linear	Mono-expon.	Bi-expon.	Linear	Mono-expon.	Bi-expon.
r^2	0.979	0.997	0.990	0.951	0.976	0.976
χ^2	–	0.041	0.046	–	0.085	0.085
$\sqrt{(\sum \text{Residual}^2)}$	2.25	0.921	0.921	4.057	1.88	1.71

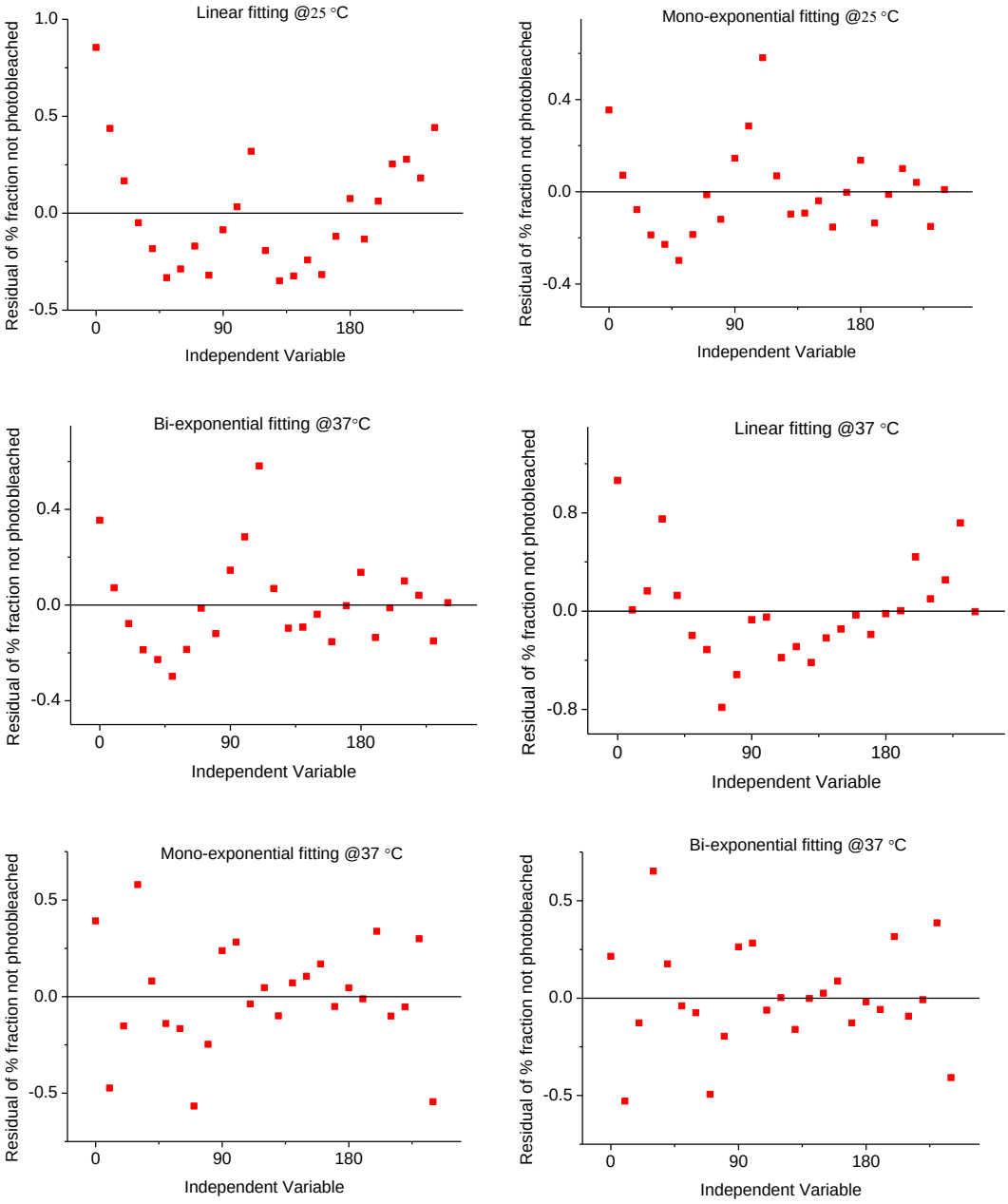

Figure A.IV.5: Comparative residual from different fitting of pTr-PNIPAm photobleaching curve both at 25 and 37 °C which shows that mono-exponential fit at 25 and 37 °C was the best fit of photobleaching curve.

Appendix V:

1. Humidity-induced overlay spectra of hTr-PNIPAm thin films:

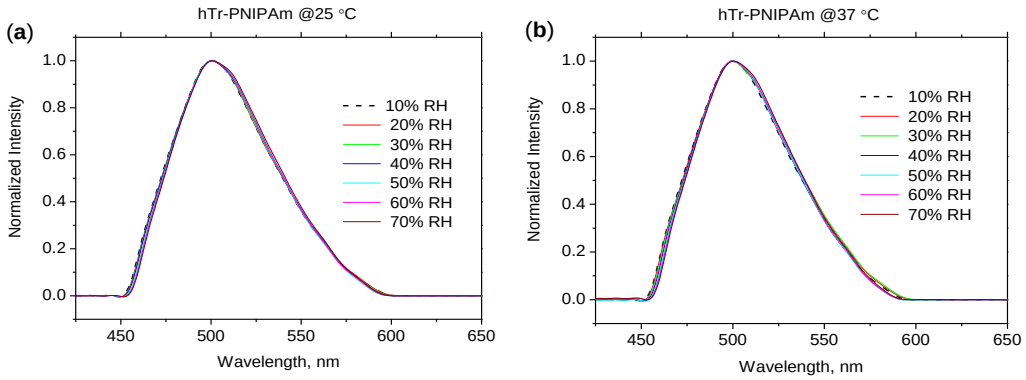

Figure A.V.1: Smoothed, normalised overlay spectra of hTr-PNIPAm thin films both at 25 (a) and 37 °C (b) which shows that no shifted overall emission as an effect of humidity. The film was continuously irradiated by the 405 nm light over 4 hours where the power of incident light was 10 µW, the spot size was 1 mm, and the relative humidity was 50%. The $\lambda_{ex.}$ was 405 nm and the thickness of the films were 10 µm.

2. Emission properties of Mylar wrapped hTr-PNIPAm films:

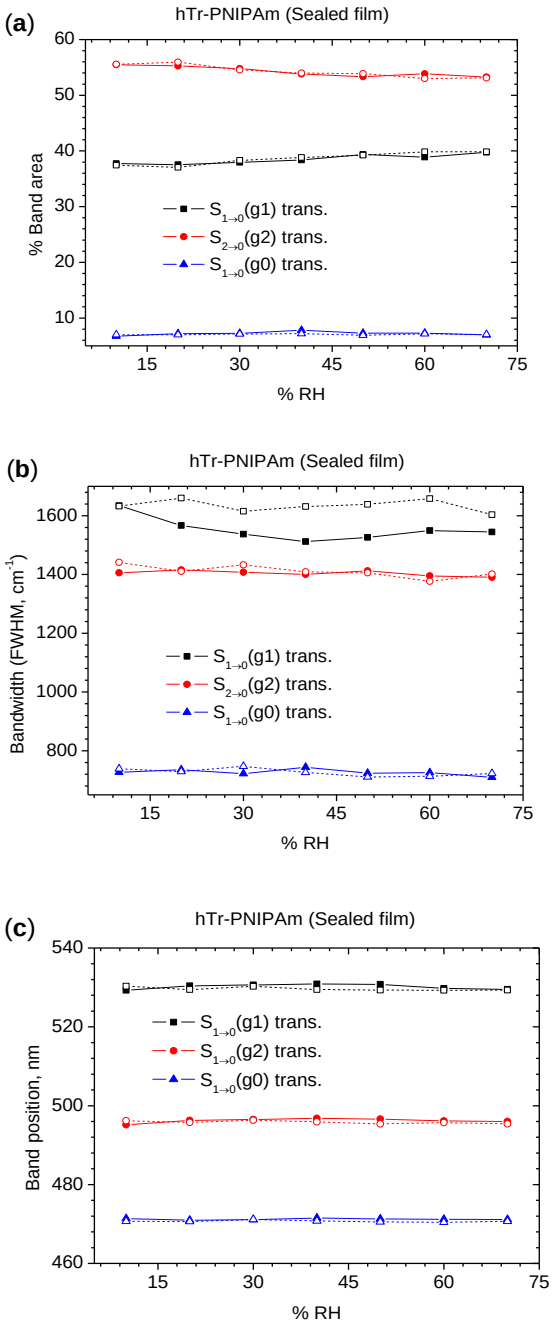

Figure A.V.2: Plot of changes in % band area (a), FWHM (b), and band position (c) of Mylar wrapped films of hTr-PNIPAm thin films. The emission properties changes as a function of humidity of Mylar wrapped hTr-PNIPAm films were very small. Symbols represent the measurement temperature, solid (at 25 °C) and open (at 37 °C).

3. Individual lifetime hTr-PNIPAm thin films:

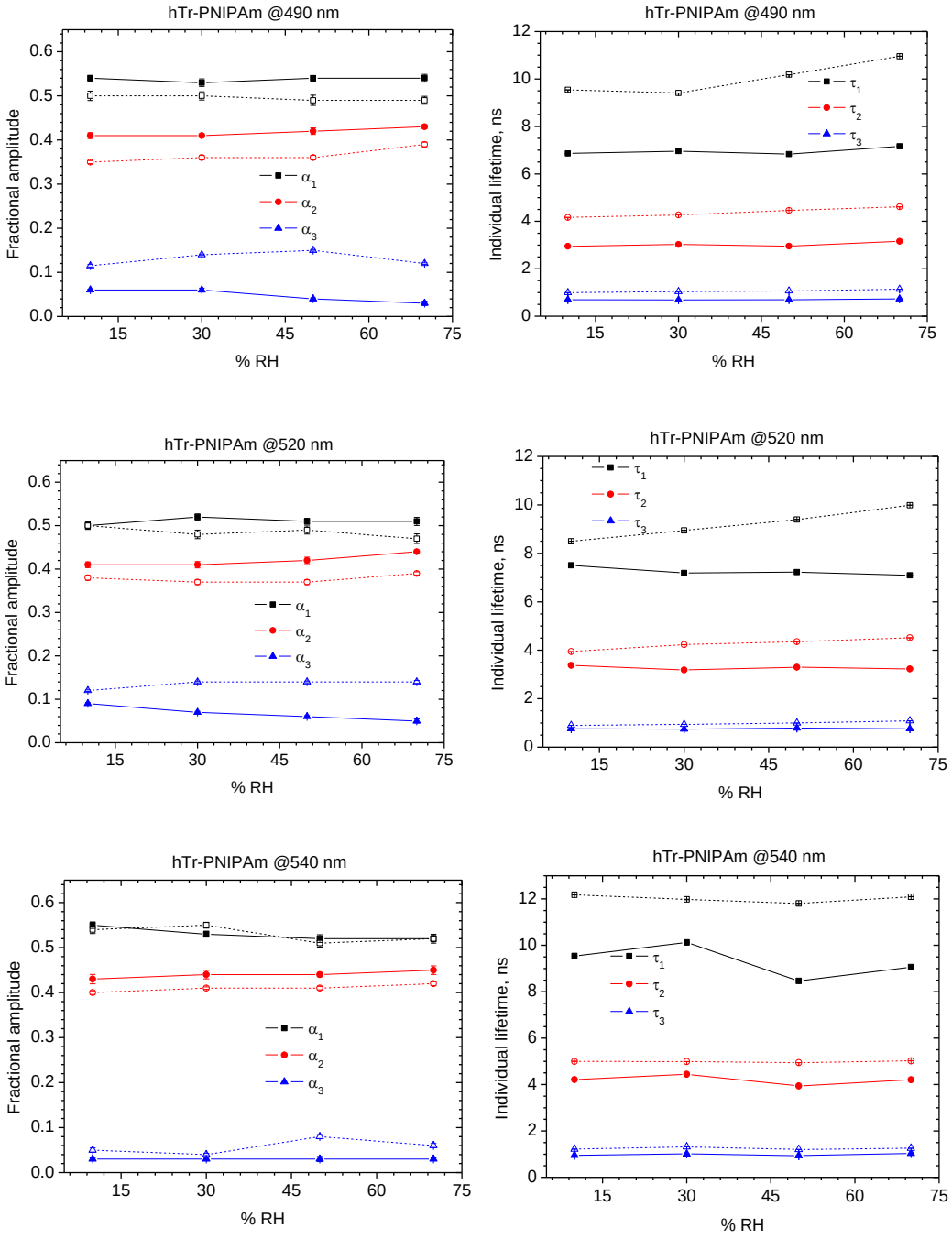

Figure A.V.3: Plot of fractional amplitude and individual lifetime versus increasing humidity for a hTr-PNIPAm thin film at 25 and 37 °C at different emission wavelengths. Symbols represent the measurement temperature, solid (at 25 °C) and open (at 37 °C). The data shows increase of individual lifetime at 25 and decrease at 37 °C. All data were fitted to a tri-exponential model. Where αi = fractional amplitudes/pre-exponential factors. Amplitudes had been normalised such that Σ|αi| = 1. Errors calculated using support plane analysis.

4. Photobleaching study of hTr-PNIPAm thin films: Overlaid spectra

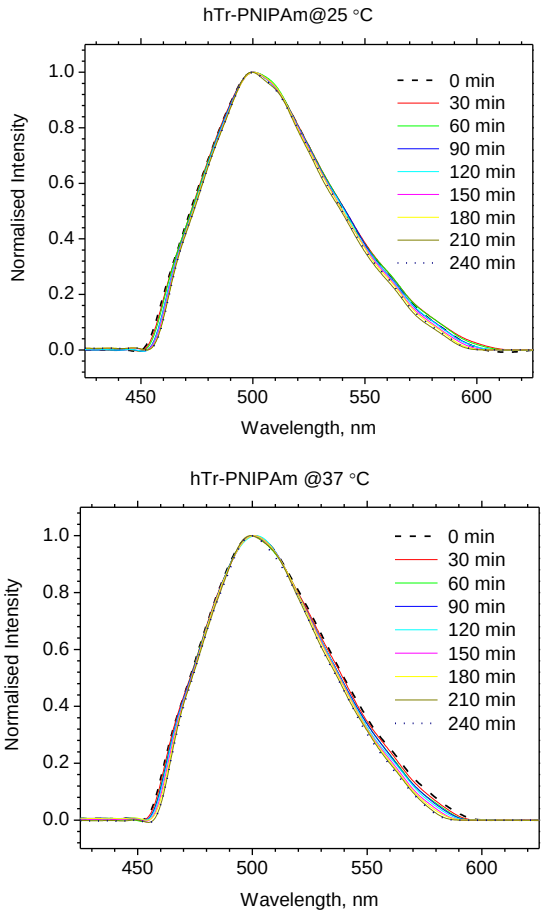

Figure A.V.4: Overlaid normalised emission spectra of photobleaching of hTr-PNIPAm thin films (10 µm) with time both at 25 (a) and 37 °C (b) (at 50% RH), shows an un-shifted emission during the entire photobleaching study. The film was continuously irradiated by 405 nm light over 4 hours where the power of incident light was ~10 µW and the spot size was 1 mm.

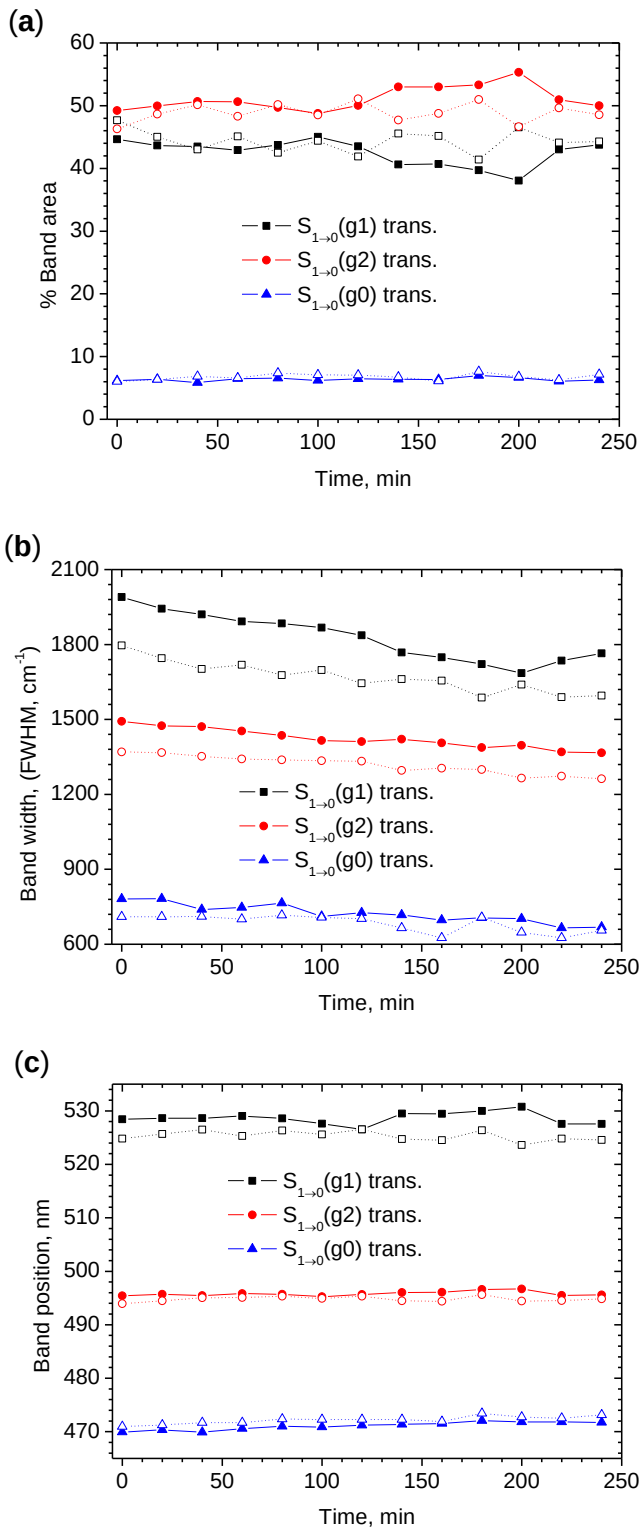

Figure A.V.5: Photobleaching effect on emission properties of hTr-PNIPAm thin films, where changes in % band area, (a) bandwidth (FWHM, cm^{-1}) (b), and band position (c). Symbol represents the measurement temperature, where solid is for 25 °C and open is for 37 °C.

Appendix VI:

1. Emission properties of Mylar wrapped film of kpTr-PNIPAm thin films:

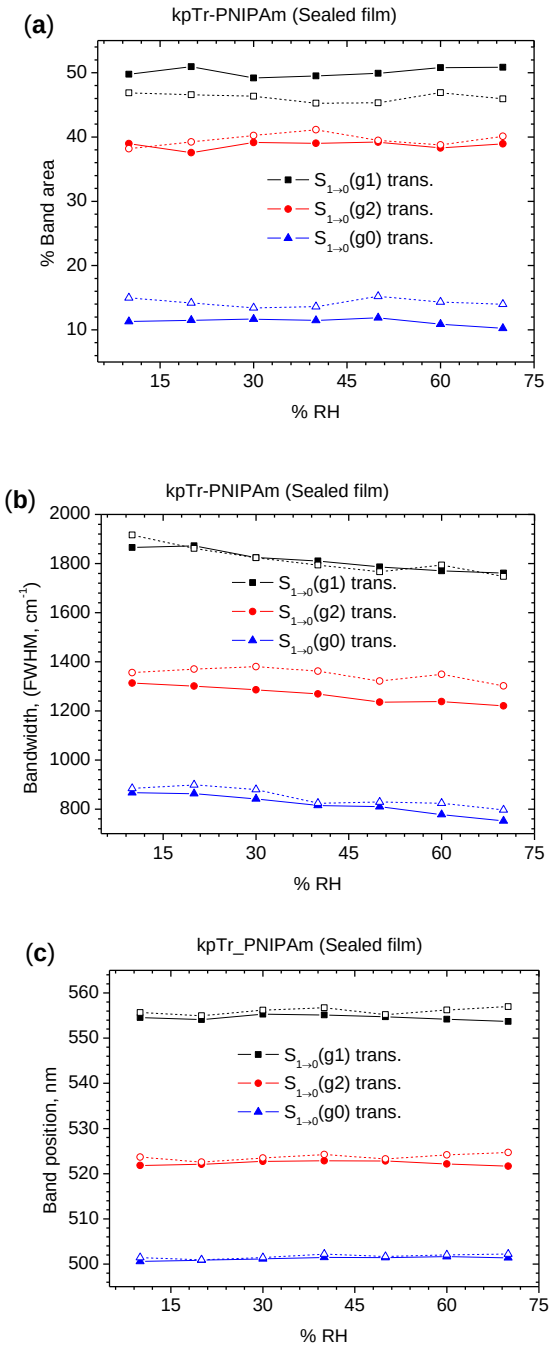

Figure A.VI.1: Plot of changes in % band area (a), bandwidth, FWHM (b), and band position (c) as a function of humidity for Mylar sealed film. Symbols represent the measurement temperature, solid (at 25 °C) and open (at 37 °C). No remarkable changes in the individual emission properties during the Mylar wrapped thin film study.

2. Individual lifetime kpTr-PNIPAm thin films

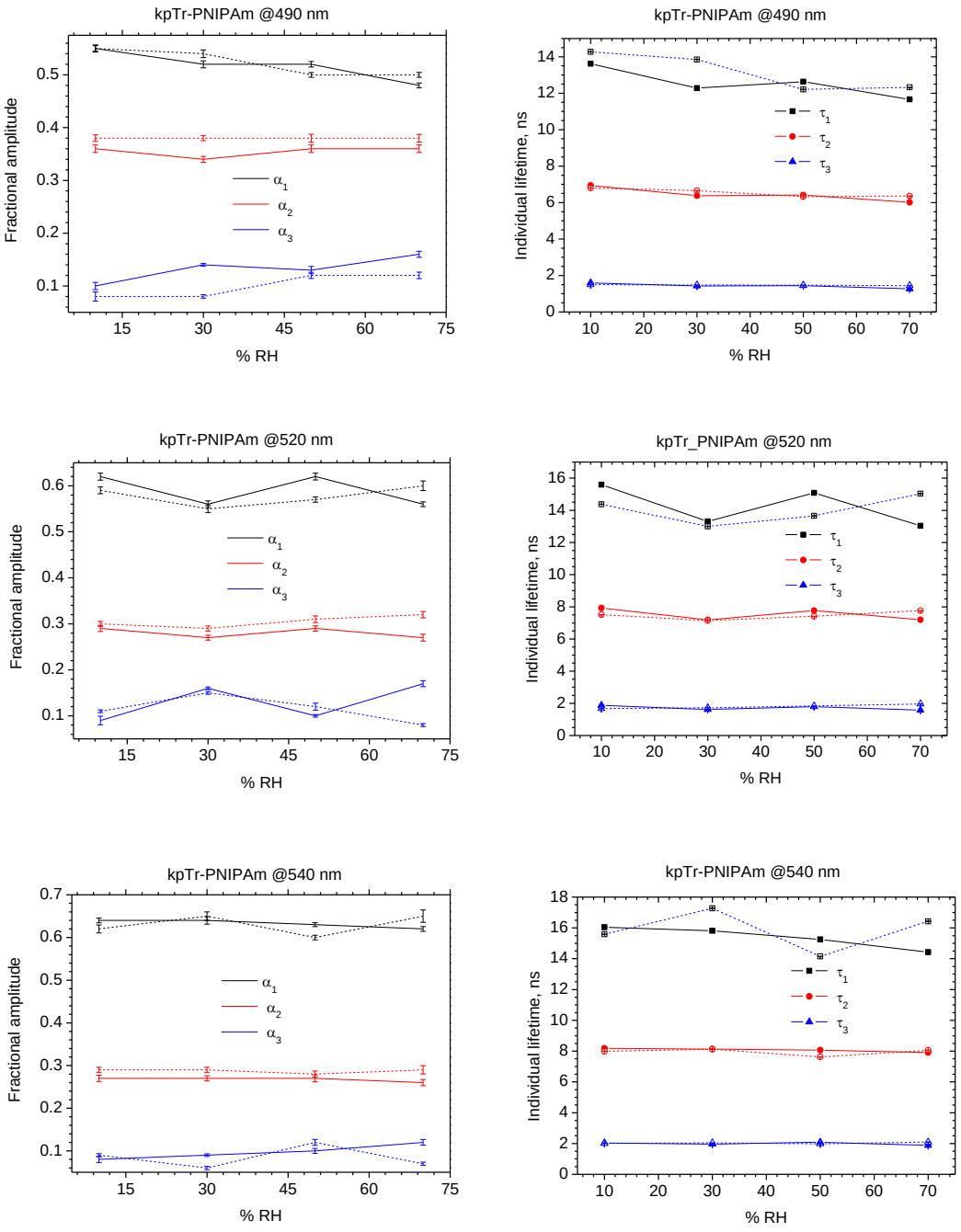

Figure A.VI.2: Plot of fractional amplitude and individual lifetime versus increasing humidity for a kpTr-PNIPAm thin film at 25 and 37 °C at different emission wavelengths. Symbols represent the measurement temperature, solid (at 25 °C) and open (at 37 °C). Relatively no humidity-induced changes in individual lifetime were observed. All data were fitted to a tri-exponential model. Where αi = fractional amplitudes/pre-exponential factors. Amplitudes have been normalised such that Σ|αi| = 1. Errors calculated using support plane analysis.

3. Photobleaching of kpTr-PNIPAm thin films: Overlaid spectra

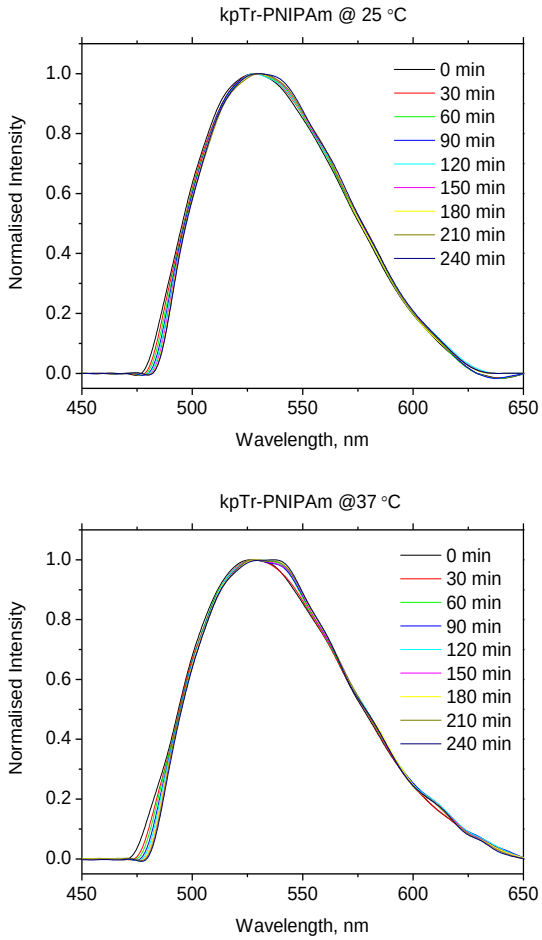

Figure A.VI.3: Overlay smoothed and normalised spectra of photobleaching of kpTr-PNIPAm thin films at 25 and 37 °C. The emission spectra were unchanged during the entire photobleaching study. The film was continuously irradiated by 405 nm light over 4 hours where the power of incident light was ~10 µW and the spot size was 1 mm.

Table A.VI.I: Rate of changes in relative population of the three excited state (S_1 (g1), S_1 (g2), and S_1 (g0)) of kpTr-PNIPAm thin films as a function of humidity. There was no correlation (*i.e.* the slope was not equal and oppositeTable) between the humidity-induced changes in g1 and g2 conformers. This indicated that humidity-induced IVR was absent. This also indicates incorporation of water had virtually no effect on kpTr's photophysics.

	25 °C			37 °C		
	Slope	**Intercept**	**r^2**	**Slope**	**intercept**	**r^2**
$S_{1\rightarrow0}$(g1) trans	0.07±0.016	49.61±0.93	0.68	0.08±0.04	49.23±1.76	0.66
$S_{1\rightarrow0}$(g2) trans	-0.03±0.012	37.32±0.69	0.31	-0.03±0.02	38.19±1.08	0.52
$S_{1\rightarrow0}$(g0) trans	-0.04±0.006	13.07±0.34	0.76	-0.05±0.02	12.56±0.74	0.77

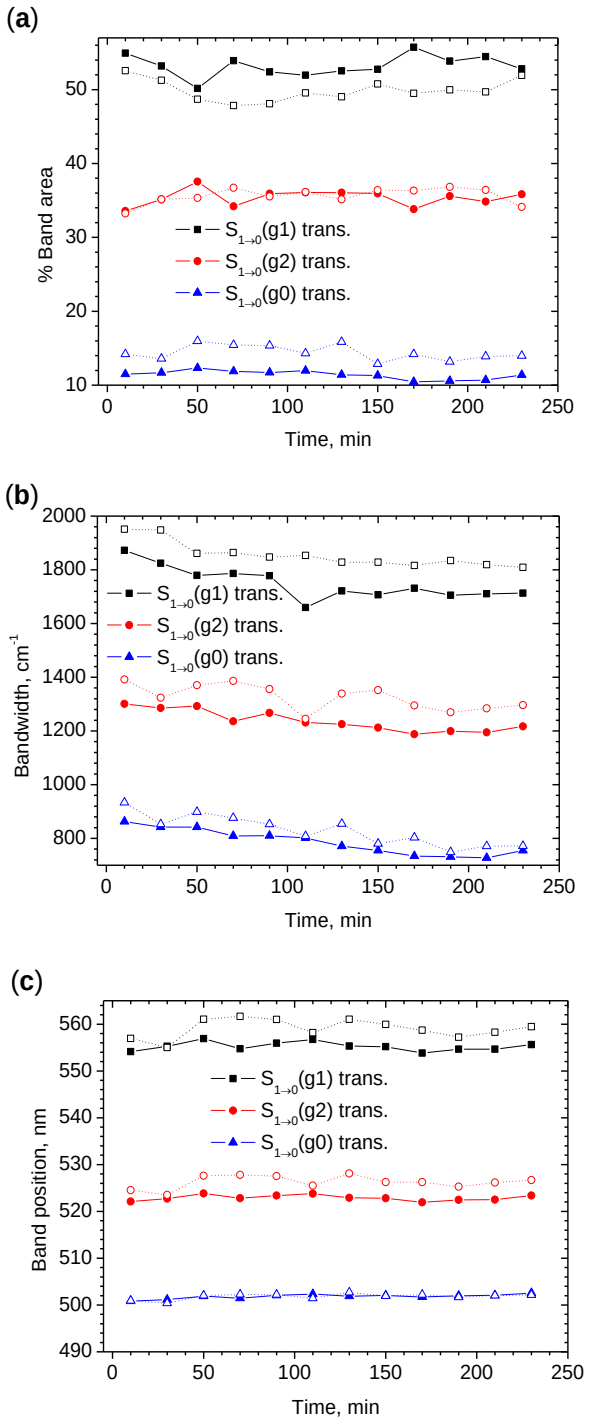

Figure A.VI. 4: Effect of Photobleaching on emission properties of kpTr-PNIPAm thin films, where changes in % band area (a), bandwidth (FWHM, cm^{-1}) (b), and band position (c). Symbol represents the measurement temperature, where solid is for 25 °C and open is for 37 °C.

4. Residual plots for photobleaching curve fitting: kpTr-PNIPAm

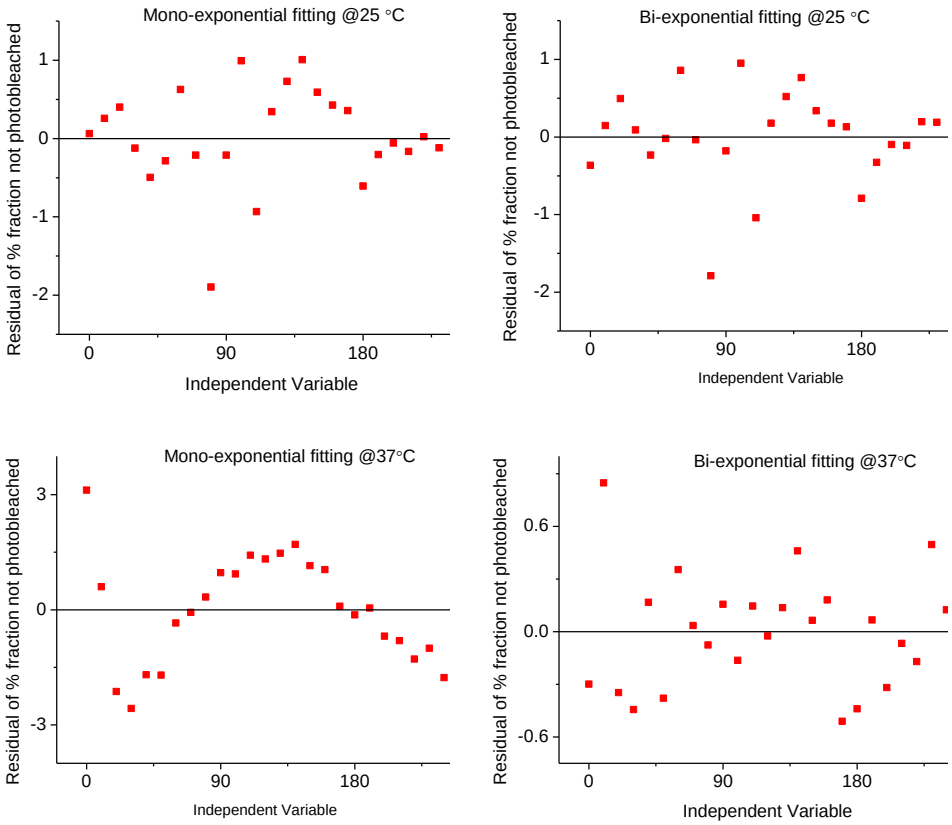

Figure A.VI.5: Comparative residual from different exponential fitting of kpTr-PNIPAm photobleaching curve both at 25 and 37 °C which shows that mono-exponential fit at 25 and bi-exponential fit at 37 °C was the best fit of photobleaching curve.

Table A.VI.II: Different statistical parameters from the decay kinetic model of photobleaching process of kpTr-PNIPAm thin films at 25 and 37 °C

Parameter	Temperature			
	25 °C		37 °C	
	Mono-expon.	Bi-expon.	Mono-expon.	Bi-expon.
R^2	0.995	0.995	0.985	0.999
χ^2	0.433	0.414	2.14	0.13
$\sqrt{(\sum \text{Residual}^2)}$	9.53	8.29	47.20	2.62

Appendix VII:

Table A.VII.1: pH of different concentrated aqueous PVA solution.

PVA solution (%w/w)	pH
0.5%	6.39
1%	6.07
2%	5.95
5%	5.92
10%	6.00
15%	6.01
20%	5.96
25%	6.03

Table A.VII.2: Rate of changes in relative population of the individual excited states, S_1 (g1), S_1 (g2), and S_1 (g0) of Tr- PVA thin films as a function of humidity. The changes in raltive population of g1 and g2 emitting states were not linearly correlated ($r^2 < 0.67$ for pTr and for hTr $r^2 < 0.73$) both at 25 and 37 °C.

Transition	pTr	
	25 °C	37 °C
$S_{1\rightarrow0}$(g1) trans.	y= 0.18x +35.6, r^2 = 0.67	y= 0.23x + 26.0, r^2 = 0.68
$S_{1\rightarrow0}$(g2) trans.	y= –0.25x + 53.0, r^2 = 0.64	y= –0.20x + 58.0, r^2 = 0.72
$S_{1\rightarrow0}$(g0) trans.	y= 0.06x + 11.35, r^2 = 0.55	y= –0.03x + 15.19, r^2 = 0.37
Transition	**hTr**	
	25 °C	**37 °C**
$S_{1\rightarrow0}$(g1) trans.	y= 0.07x +36.0, r^2 = 0.73	y= 0.04x + 36.0, r^2 = 0.52
$S_{1\rightarrow0}$(g2) trans.	y= –0.07x + 49.5, r^2 = 0.68	y= –0.05x + 50.7, r^2 = 0.52
$S_{1\rightarrow0}$(g0) trans.	y= –0.01x + 18.53, r^2 = 0.13	y= 0.01x + 13.2, r^2 = 0.03

Anion-induced quenching study:

One of the hypothesis for humidity-induced large drops in pTr's overall emission intensity (both at 25 and 37 °C) was anion (AcONa anion present as an impurity) induced quenching. To confirm this hypothesis different concentrated AcONa solutions were prepared and pTr solution was added to observe if there presence of any anion-induced quenching and was it diffusion controlled or static?

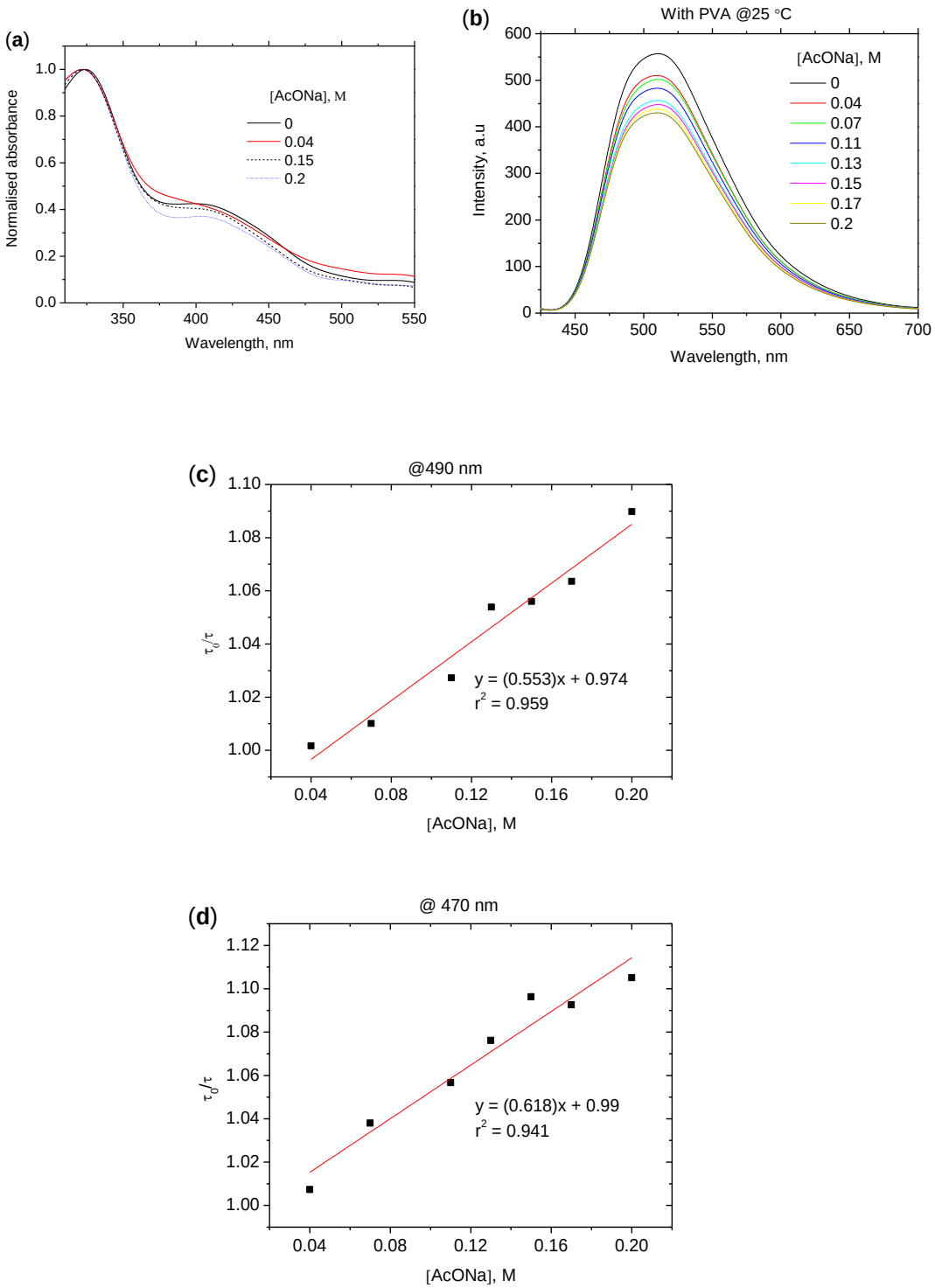

Figure A.VII.1: Anion-induced quenching study of pTr doped PVA aqueous solution. (a) Normalised and smoothed absorption spectra shows the absence of any ground state interaction (b) smoothed emission spectra at different concentrations of quencher (AcONa) of pTr doped PVA aqueous solution , shows a decrease of emission intensity with the quencher concentration, and (c) Stern-Volmer plot at 490 nm (c)/470 nm (d) emission wavelength.

Table A.VII.3: Changes in emission properties as a function of [AcONa] into a pTr (1×10^{-5} M) doped 0.05% w/w PVA aqueous solution. It shows no major changes in the individual emission properties as a function of quencher concentration. All data were acquired using λ_{ex} = 405 and at 25 °C.

[AcONa]	Transition	Emission properties		
		% Band area	FWHM, cm^{-1}	Band position
0 M	$S_{1\rightarrow0}$ (g1) trans.	36	3418	541
	$S_{1\rightarrow0}$ (g2) trans.	49	2358	514
	$S_{1\rightarrow0}$ (g0) trans.	15	1515	482
0.04 M	$S_{1\rightarrow0}$ (g1) trans.	37	3447	540
	$S_{1\rightarrow0}$ (g2) trans.	48	2359	514
	$S_{1\rightarrow0}$ (g0) trans.	15	1508	482
0.07 M	$S_{1\rightarrow0}$ (g1) trans.	37	3448	540
	$S_{1\rightarrow0}$ (g2) trans.	49	1388	513
	$S_{1\rightarrow0}$ (g0) trans.	13	1491	481
0.11 M	$S_{1\rightarrow0}$ (g1) trans.	35	3463	541
	$S_{1\rightarrow0}$ (g2) trans.	50	2407	513
	$S_{1\rightarrow0}$ (g0) trans.	13	1483	482
0.13 M	$S_{1\rightarrow0}$ (g1) trans.	37	3494	539
	$S_{1\rightarrow0}$ (g2) trans.	49	2382	514
	$S_{1\rightarrow0}$ (g0) trans.	13	1484	482
0.15 M	$S_{1\rightarrow0}$ (g1) trans.	38	3490	539
	$S_{1\rightarrow0}$ (g2) trans.	49	2390	513
	$S_{1\rightarrow0}$ (g0) trans.	13	1476	482
0.17 M	$S_{1\rightarrow0}$ (g1) trans.	37	3482	539
	$S_{1\rightarrow0}$ (g2) trans.	49	2384	513
	$S_{1\rightarrow0}$ (g0) trans.	14	1488	482
0.20 M	$S_{1\rightarrow0}$ (g1) trans.	37	3498	539
	$S_{1\rightarrow0}$ (g2) trans.	49	2358	513
	$S_{1\rightarrow0}$ (g0) trans.	14	1488	482

Conclusion: Get quenching by AcONa, but it affects all three states equally.

1. Humidity-induced changes in individual lifetime of Tr-PVA thin films:

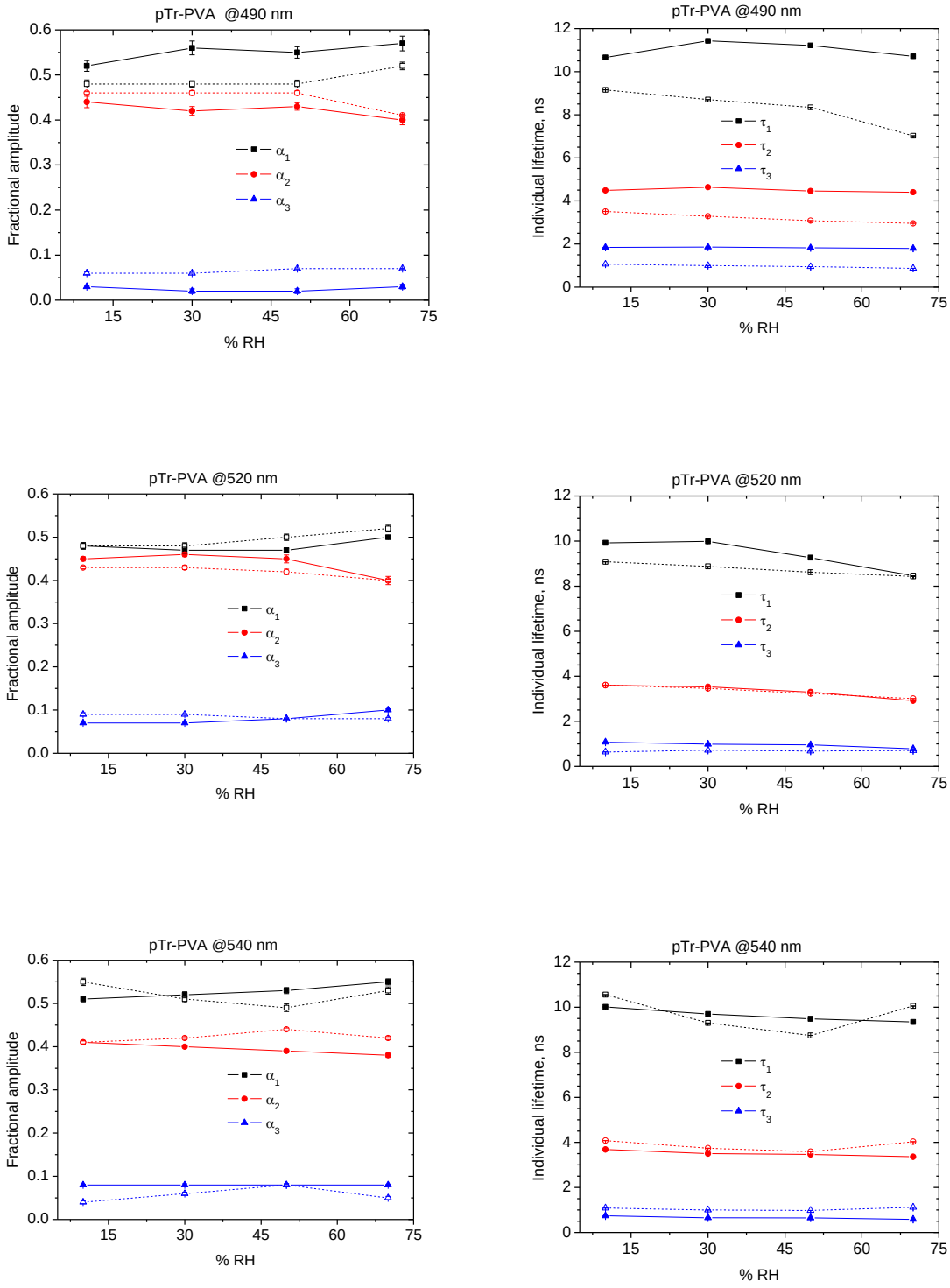

Figure A.VII.2: Plot of fractional amplitude and individual lifetime versus increasing humidity for a pTr-PVA thin film at 25 and 37 °C at different emission wavelength. Symbols designate the measurement temperature, solid (25 °C), and open (37 °C). All data were fitted to a tri-exponential model. Where αi = fractional amplitudes/pre-exponential factors. Amplitudes had been normalised such that Σ|αi| = 1. Errors calculated using support plane analysis.

Individual fluorescence lifetime of hTr-PVA thin film:

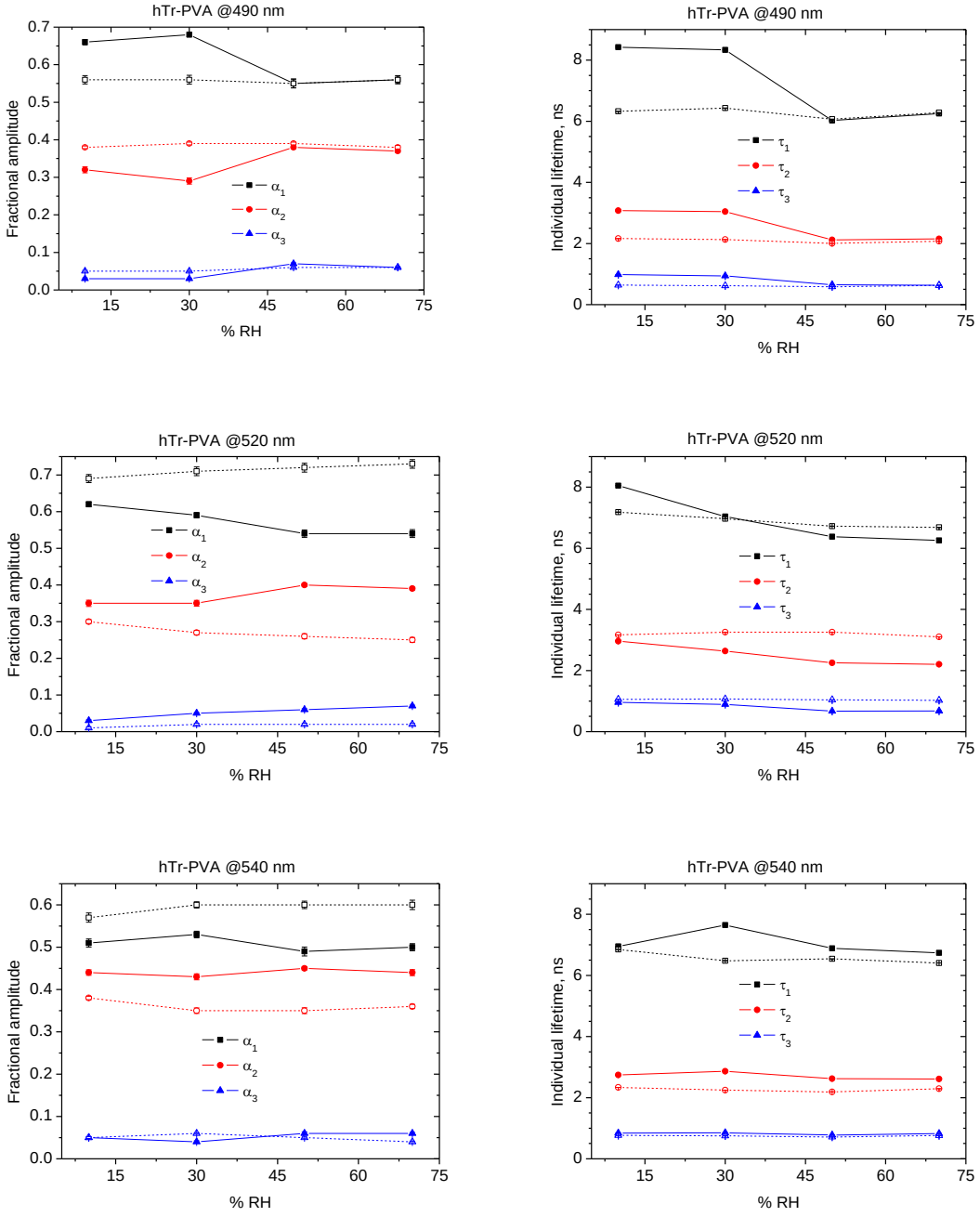

Figure A.VII.3: Plot of fractional amplitude and individual lifetime versus increasing humidity for a hTr-PVA thin film at 25 and 37 °C at different emission wavelengths. Symbols designate the measurement temperature, solid (25 °C), and open (37 °C). All data were fitted to a tri-exponential model. Where αi = fractional amplitudes/pre-exponential factors. Amplitudes had been normalised such that Σ|αi| = 1. Errors calculated using support plane analysis.

2. Temperature effect on pTr-PVA thin films:

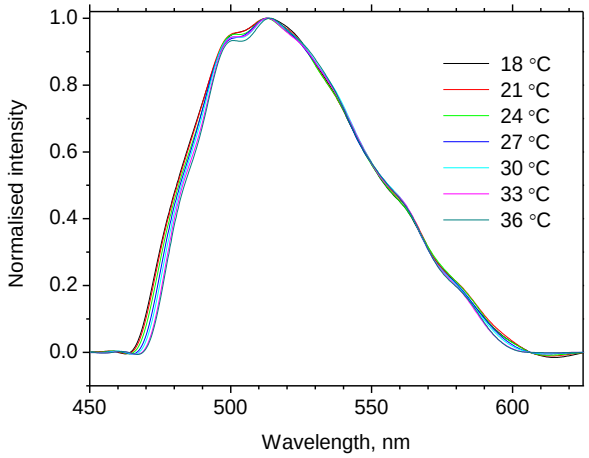

Figure A.VII.4: Overlay normalised emission spectra of pTr-PVA thin films at different temperatures and at 50% RH and shows relatively unchanged overall emission spectra.

3. Photobleaching study:

Table A.VII.4: Different statistical parameters from the decay kinetic model of photobleaching process of pTr-PVA thin films at 25 and 37 °C.

Parameter	Temperature			
	25 °C		37 °C	
	Mono-exp.	Bi-exp.	Mono-exp.	Bi-exp.
R^2	0.976	0.999	0.974	0.999
χ^2	1.79	0.070	8.49	0.119
$\sqrt{(\sum \text{Residual}^2)}$	1.79	0.056	0.34	0.094

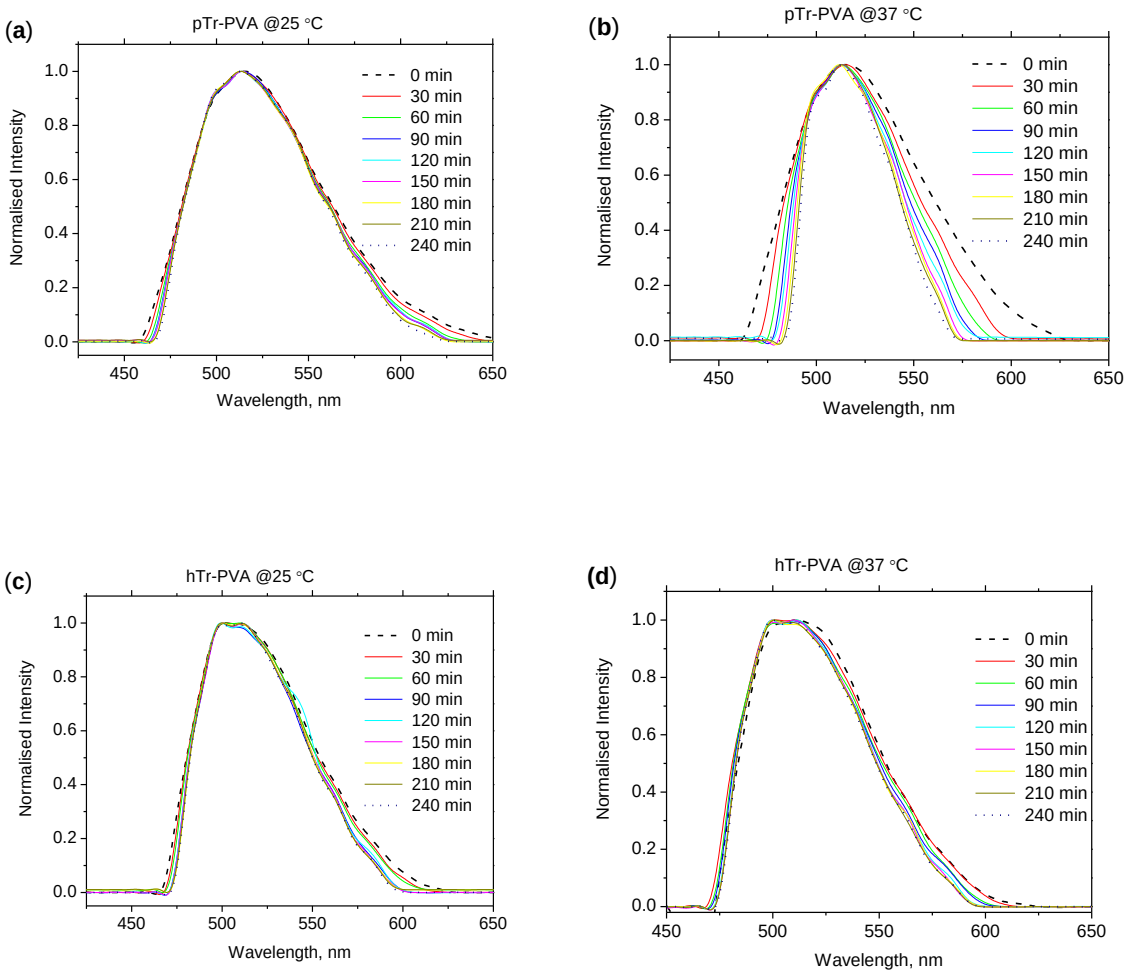

Figure A.VII.5: Overlaid normalised emission spectra of the photobleaching of pTr (a and b) and hTr (c and d) at 25 °C (left) and 37 °C (right). The film was continuously irradiated by the 405 nm light over 4 hours where the power of incident light was 10 µW, the spot size was 1 mm, λ_{ex} was 405 nm, and the humidity was 50%.

Statistical analysis of exponential fitting of photobleaching curve:

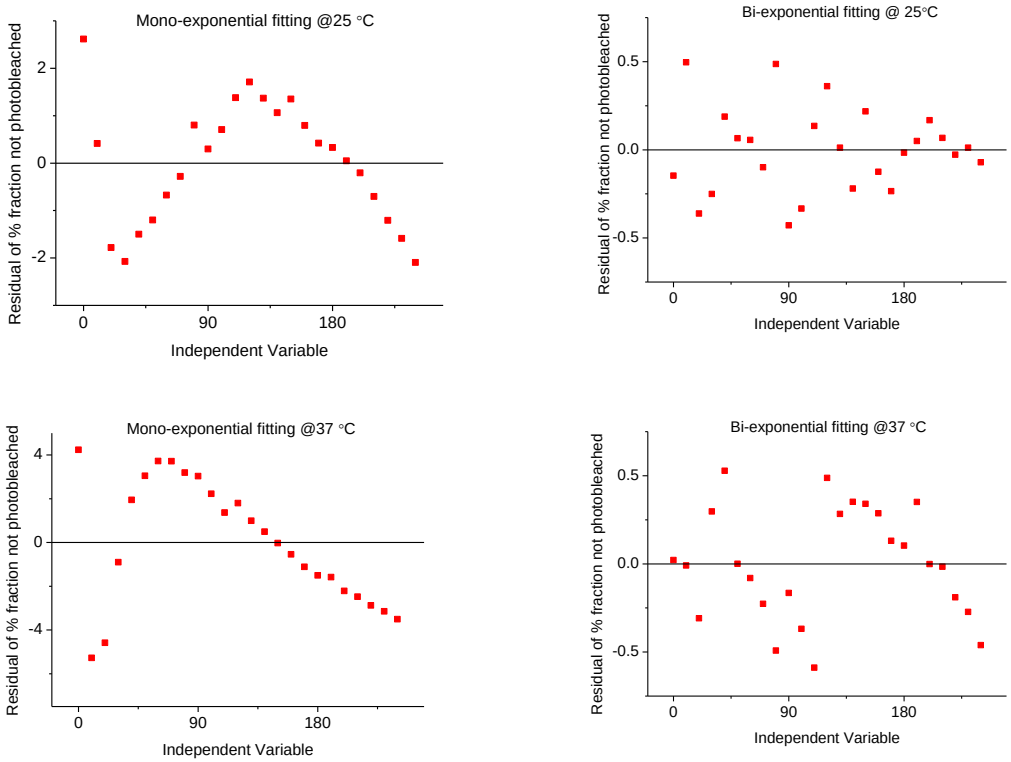

Figure A.VII.6: Comparative analysis of residual from different exponential fitting of photobleaching curve of pTr-PVA thin films at 25 and 37 °C.

Table A.VII.5: Different statistical parameters from the decay kinetic model of photobleaching process of hTr-PNIPAm thin films at 25 °C.

Parameter	Temperature	
	25 °C	
	Mono-exp.	Bi-exp.
R^2	0.972	0.993
χ^2	0.94	0.25
$\sqrt{(\sum \text{Residual}^2)}$	20.77	5.00

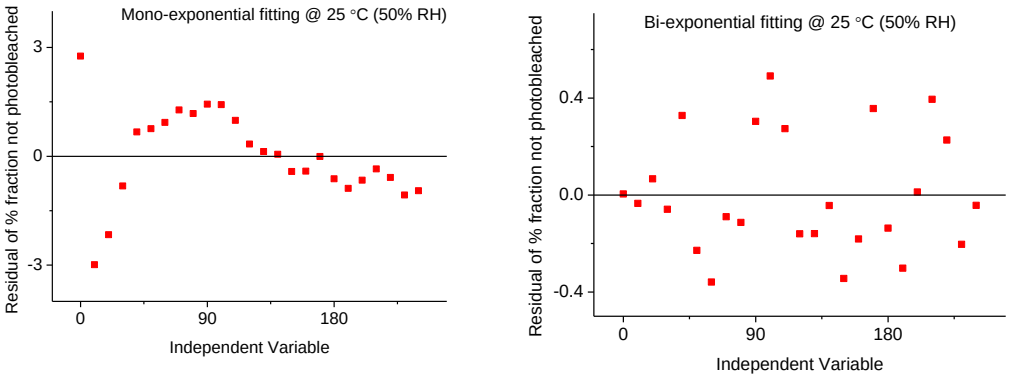

Figure A.VII.7: Comparative analysis of residuals from different exponential fitting of photobleaching curve of hTr-PVA thin films at 25 °C.

Table A.VII.6: Changes in band position during photobleaching study of pTr-PVA thin polymer films. The film was continuously irradiated by the 405 nm light over 4 hours where the power of incident light was 10 µW, the spot size was 1 mm, and the humidity was 50%.

Time, min	Band position, nm	
	25 °C	37 °C
0	516	515
30	514	515
60	514	513
90	514	513
120	514	513
150	514	513
180	513	512
210	513	513
240	513	512

Aggregation study of pTr fluorophore in solution:

To investigate if pTr aggregated in solution, five different concentrations *i.e.* 9 $\times 10^{-5}$ M, 7 $\times 10^{-5}$ M, 5 $\times 10^{-5}$ M, 1 $\times 10^{-5}$ M, and 8 $\times 10^{-6}$ M of pTr solution (in EtOH) were made and then the emission spectra collected. Apparently, No changes in the size and shape of the emission spectra (Figure A.VII.8) or very small changes in the

emission properties of three emission conformer (Table A.VII.7) were observed indicating the absence of aggregation of pTr in solution.

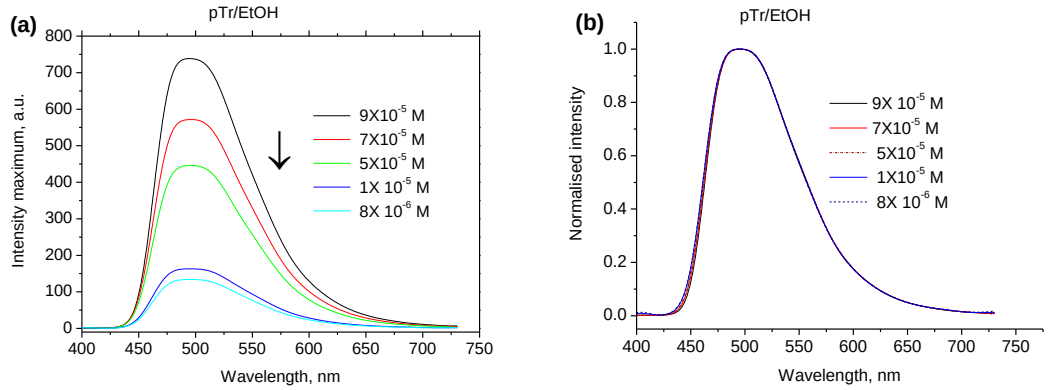

Figure A.VII.8: Smoothed (a)/ normalised (b) emission spectra of pTr at 5 different concentrations in EtOH. Data were acquired using 405 nm excitation and at 25 °C.

Table A.VII.7: Individual emission properties of pTr/ EtOH solution with varying pTr concentrations.

Dye/ media	Conc. of pTr (M)	Transition for 3 emission bands	Emission properties		
			% Band area	FWHM (cm^{-1})	Band position (nm)
pTr/ EtOH	$9x10^{-5}$	$S_{1\rightarrow0}$ (g1) trans.	37	3037	540
		$S_{1\rightarrow0}$ (g2) trans.	46	2114	504
		$S_{1\rightarrow0}$ (g0) trans.	17	1218	475
	$7x10^{-5}$	$S_{1\rightarrow0}$ (g1) trans.	36	3082	540
		$S_{1\rightarrow0}$ (g2) trans.	47	2180	504
		$S_{1\rightarrow0}$ (g0) trans.	17	1248	475
	$5x10^{-5}$	$S_{1\rightarrow0}$ (g1) trans.	36	3100	540
		$S_{1\rightarrow0}$ (g2) trans.	48	2201	504
		$S_{1\rightarrow0}$ (g0) trans.	17	1257	474
	$1x10^{-5}$	$S_{1\rightarrow0}$ (g1) trans.	34	3168	539
		$S_{1\rightarrow0}$ (g2) trans.	49	2269	504
		$S_{1\rightarrow0}$ (g0) trans.	17	1286	474
	$8x10^{-6}$	$S_{1\rightarrow0}$ (g1) trans.	33	3197	540
		$S_{1\rightarrow0}$ (g2) trans.	50	2282	504
		$S_{1\rightarrow0}$ (g0) trans.	17	1294	474

Changes in hTr's emission properties: as an effect of photobleaching

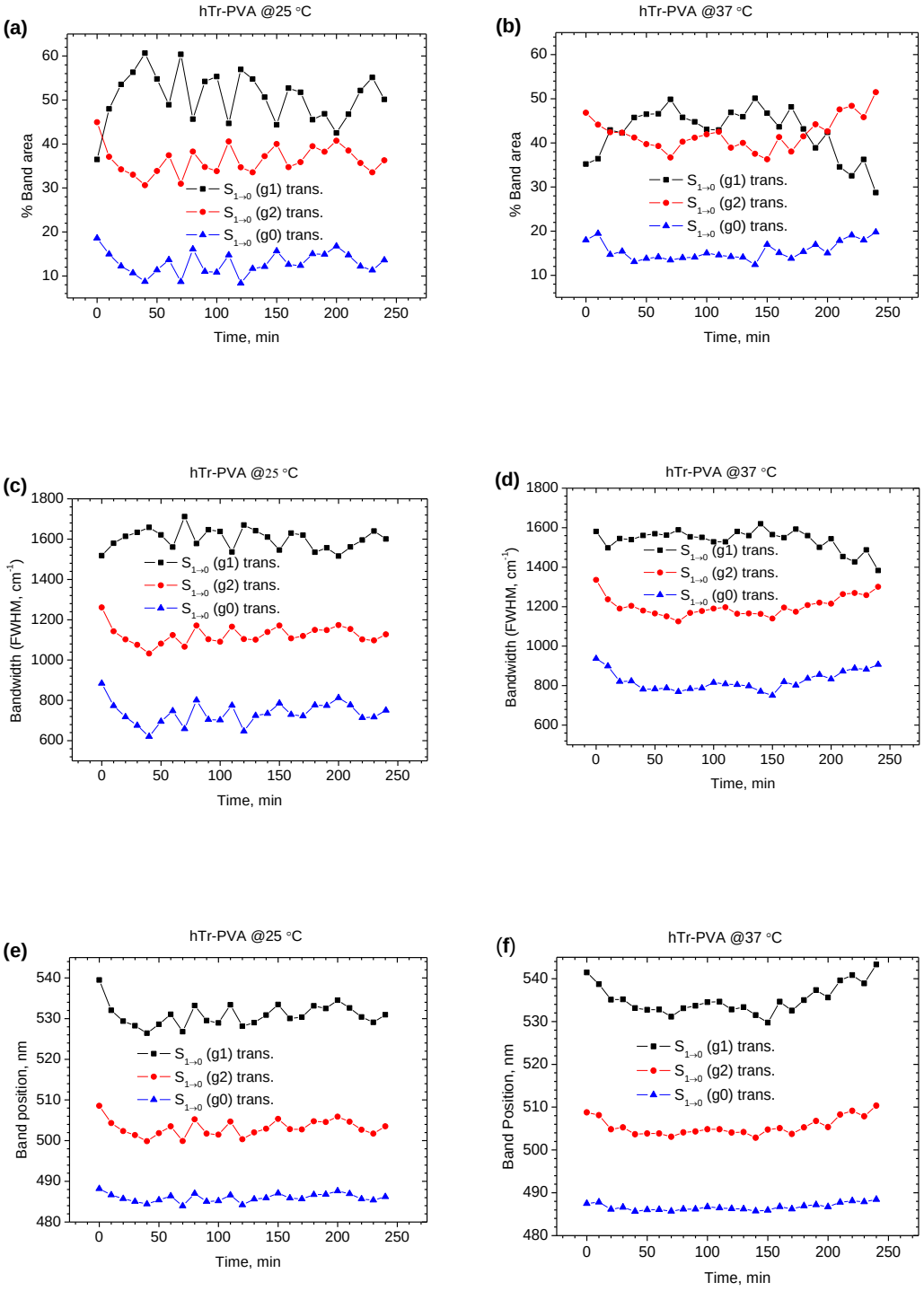

Figure A.VII.9: Photobleaching effect on emission properties of hTr-PVA thin films, where plot of variation of % band area at 25 °C (a) and 37 °C (b), bandwidth (FWHM, cm^{-1}) at 25 (c) and 37 °C (d), band position at 25 °C (e) and 37 °C (f). The humidity was 50 % and λ_{ex} was 405 nm.

References:

1. Bult, H., *Restenosis: a challenge for pharmacology.* Trends in Pharmacological Sciences, 2000. **21**(7): p. 274-279.
2. Lewis, A., Tolhurst, L., and Stratford, P., *Analysis of a phosphorylcholine-based polymer coating on a coronary stent pre-and post-implantation.* Biomaterials, 2002. **23**(7): p. 1697-1706.
3. da Silva, R.M.P., Mano, J.F., and Reis, R.L., *Smart thermoresponsive coatings and surfaces for tissue engineering: switching cell-material boundaries.* Trends in biotechnology, 2007. **25**(12): p. 577-583.
4. Morris, C., Szczupak, B., Klymchenko, A.S., and Ryder, A.G., *Study of water adsorption in poly(N-isopropylacrylamide) thin films using fluorescence emission of 3-hydroxyflavone probes.* Macromolecules, 2010. **43**(22): p. 9488-9494.
5. Butler, R.N., Fahy, A.M., Fox, A., Stephens, J.C., McArdle, P., Cunningham, D., and Ryder, A. G., *One-pot synthesis of fluorescent 2, 5-dihydro-1, 2, 3-triazine derivatives from a cascade rearrangement sequence in the reactions of 1, 2, 3-triazolium-1-aminide 1, 3-dipoles with propiolate esters.* Journal of organic chemistry, 2006. **71**(15): p. 5679-5687.
6. Mart, D. St., Togashi, D.M., Burke, L. A., Ryder, A. G. and Stephens, J. C., *Photophysical model of the 2,5-dihydro-1,2,3-triazine fluorophore (in preparation).*
7. Mart, D.St., Togashi, D.M., Burke, L. A., Ryder, A. G. and Stephens, J. C., *Solvatochromism of the 2,5-dihydro-1,2,3-triazine fluorophores (in preparation).*
8. Itagaki, H., *Chapter 3 - Fluorescence Spectroscopy*, in *Experimental Methods in Polymer Science*, T. Tanaka, Editor. 2000, Academic Press: Boston. p. 155-260.
9. Wehry, E.L., *Molecular fluorescence, phosphorescence, and chemiluminescence spectrometry.* Analytical Chemistry, 1986. **58**(5): p. 13R-33R.
10. Drummen, G.P., *Fluorescent probes and fluorescence (microscopy) techniques--illuminating biological and biomedical research.* Molecules (Basel, Switzerland), 2012. **17**(12): p. 14067-14090.
11. Valeur, B., *Molecular fluorescence: principles and applications*. 2013: John Wiley & Sons.
12. Mycek, M.A. and Pogue, B.W., *Handbook of biomedical fluorescence*. 2003: CRC Press.
13. Lakowicz, J.R., *Principles of fluorescence spectroscopy*. 2009: Springer.
14. Turro, N.J., *Modern molecular photochemistry*. 1991: University Science Books.
15. Stennett, E.M., Ciuba, M.A., and Levitus, M., *Photophysical processes in single molecule organic fluorescent probes.* Chemical Society Reviews, 2014. **43**(4): p. 1057-1075.
16. Kasha, M., *Characterization of electronic transitions in complex molecules.* Discussions of the Faraday Society., 1950. **9**: p. 14-19.
17. Yuster, P. and Weissman, S., *Effects of perturbations on phosphorescence: luminescence of metal organic complexes.* The Journal of Chemical Physics, 1949. **17**(12): p. 1182-1188.
18. Berberan-Santos, M.N. and Garcia, J.M., *Unusually strong delayed fluorescence of C70.* Journal of the American Chemical Society, 1996. **118**(39): p. 9391-9394.
19. Goltsev, V., Zaharieva, I., Chernev, P., and Strasser, R.J., *Delayed fluorescence in photosynthesis.* Photosynthesis research, 2009. **101**(2-3): p. 217-232.
20. de Oliveira, M. and Atvars, T., *Fluorescence Spectra of Anthracene Dissolved in Vinylic and Olefinic Polymers.* Journal of the Brazilian Chemical Society, 1995. **6**(2): p. l27-133.

21. Wu, P. and Brand, L., *Resonance energy transfer: methods and applications.* Analytical biochemistry, 1994. **218**(1): p. 1-13.
22. Andrews, D.L., *Mechanistic principles and applications of resonance energy transfer.* Canadian Journal of Chemistry, 2008. **86**(9): p. 855-870.
23. Hussain, S.A., Dey, D., Chakraborty, S., Saha, J., Roy, A.D., Chakraborty, S., Debnath, P., and Bhattacharjee, D., *Fluorescence Resonance Energy Transfer (FRET) sensor.* Journal of spectroscopy and dynamics, 2015, **5**: p. 7-23.
24. Uji-Ie, K., Kasama, K., Kikuchi, K., and Kokubun, H., *Temperature effect on the intersystem crossing of acridine in various solvents.* Chemistry Letters, 1978. **7**(3): p. 247-250.
25. Wang, B., Guan, X., Hu, Y., and Su, Z., *Preparation and fluorescent properties of poly(vinyl alcohol) bearing coumarin.* Polymers for Advanced Technologies, 2007. **18**(7): p. 529-534.
26. Talhavini, M. and Atvars, T.D.Z., *Dye-polymer interactions controlling the kinetics of fluorescein photobleaching reactions in poly(vinyl alcohol).* Journal of Photochemistry and Photobiology A: Chemistry, 1998. **114**(1): p. 65-73.
27. Rettig, W., Strehmel, B., Schrader, S., and Seifert, H., *Applied fluorescence in chemistry, biology and medicine*. 2012: Springer Science & Business Media.
28. Baugher, J. and Grossweiner, L., *Photolysis mechanism of aqueous tryptophan.* The Journal of Physical Chemistry, 1977. **81**(14): p. 1349-1354.
29. Gollnick, K., Franken, T., Fouda, M.F.R., Paur, H.R., and Held, S., *Merbromin (mercurochrome) and other xanthene dyes: Quantum yields of triplet sensitizer generation and singlet oxygen formation in alcoholic solutions.* Journal of Photochemistry and Photobiology B: Biology, 1992. **12**(1): p. 57-81.
30. Talhavini, M. and Atvars, T., *Photostability of xanthene molecules trapped in poly (vinyl alcohol)(PVA) matrices.* Journal of Photochemistry and Photobiology A: Chemistry, 1999. **120**(2): p. 141-149.
31. Zheng, Q., Juette, M.F., Jockusch, S., Wasserman, M.R., Zhou, Z., Altman, R.B., and Blanchard, S.C., *Ultra-stable organic fluorophores for single-molecule research.* Chemical Society Reviews, 2014. **43**(4): p. 1044-1056.
32. Song, L., Varma, C., Verhoeven, J., and Tanke, H.J., *Influence of the triplet excited state on the photobleaching kinetics of fluorescein in microscopy.* Biophysical journal, 1996. **70**(6): p. 2959.
33. Song, L., Van Gijlswijk, R., Young, I.T., and Tanke, H.J., *Influence of fluorochrome labeling density on the photobleaching kinetics of fluorescein in microscopy.* Cytometry, 1997. **27**(3): p. 213-223.
34. Hoebe, R., Van Oven, C., Gadella, T.W., Dhonukshe, P., Van Noorden, C., and Manders, E., *Controlled light-exposure microscopy reduces photobleaching and phototoxicity in fluorescence live-cell imaging.* Nature biotechnology, 2007. **25**(2): p. 249-253.
35. Zondervan, R., Kulzer, F., Kol'chenk, M.A., and Orrit, M., *Photobleaching of Rhodamine 6G in Poly(vinyl alcohol) at the Ensemble and Single-Molecule Levels.* The Journal of Physical Chemistry A, 2004. **108**(10): p. 1657-1665.
36. Dibbern-Brunelli, D., de Oliveira, M.G., and Atvars, T.D.Z., *Temperature dependence of the photobleaching process of fluorescein in poly(vinyl alcohol).* Journal of Photochemistry and Photobiology A: Chemistry, 1995. **85**(3): p. 285-289.
37. Talhavini, M., Corradini, W., and Atvars, T., *The role of the triplet state on the photobleaching processes of xanthene dyes in a poly (vinyl alcohol) matrix.* Journal of Photochemistry and Photobiology A: Chemistry, 2001. **139**(2): p. 187-197.
38. Dubois, A., Canva, M., Brun, A., Chaput, F., and Boilot, J.-P., *Photostability of dye molecules trapped in solid matrices.* Applied Optics, 1996. **35**(18): p. 3193-3199.

39. Hooker, J.C. and Torkelson, J.M., *Coupling of probe reorientation dynamics and rotor motions to polymer relaxation as sensed by second harmonic generation and fluorescence.* Macromolecules, 1995. **28**(23): p. 7683-7692.
40. Levitus, M., Talhavini, M., Negri, R.M., Atvars, T.D.Z., and Aramendía, P.F., *Novel kinetic model in amorphous polymers. Spiropyran-merocyanine system revisited.* The Journal of Physical Chemistry B, 1997. **101**(39): p. 7680-7686.
41. Fang, Y., Qiang, J.C., Hu, D.D., Wang, M.Z., and Cui, Y.L., *Effect of urea on the conformational behavior of poly (N-isopropylacrylamide).* Colloid and Polymer Science, 2001. **279**(1): p. 14-21.
42. Geddes, C., Lakowicz, J., and Rosenfeld, M., *Methods and Applications of Fluorescence.* Journal of Fluorescence, 2002. **12**(2): p. 119-119.
43. Gardecki, J.A. and Maroncelli, M., *Set of Secondary Emission Standards for Calibration of the Spectral Responsivity in Emission Spectroscopy.* Applied Spectroscopy, 1998. **52**(9): p. 1179-1189.
44. Winefordner, J., *Practical fluorescence: theory, methods, and techniques.* Journal of Chemical Education, 1974. **51**(1): p. A48.
45. Bright, F.V. and Munson, C.A., *Time-resolved fluorescence spectroscopy for illuminating complex systems.* Analytica chimica acta, 2003. **500**(1): p. 71-104.
46. Owens, P., *Time-Resolved Fluorescence Spectroscopy of Crude Petroleum oils.*, in Chemistry 2010, National University of Ireland, Galway, Ireland. p. 79.
47. Sillen, A. and Engelborghs, Y., *The correct use of "average" fluorescence parameters.* Photochemistry and photobiology, 1998. **67**(5): p. 475-486.
48. Tregidgo, C., Levitt, J.A., and Suhling, K., *Effect of refractive index on the fluorescence lifetime of green fluorescent protein.* Journal of biomedical optics, 2008. **13**(3): p. 031218-031218-8.
49. Magde, D., Wong, R., and Seybold, P.G., *Fluorescence Quantum Yields and Their Relation to Lifetimes of Rhodamine 6G and Fluorescein in Nine Solvents: Improved Absolute Standards for Quantum Yields.* Photochemistry and photobiology, 2002. **75**(4): p. 327-334.
50. Suhling, K., Siegel, J., Phillips, D., French, P.M., Leveque-Fort, S., Webb, S.E., and Davis, D.M., *Imaging the environment of green fluorescent protein.* Biophysical journal, 2002. **83**(6): p. 3589-3595.
51. Lavallard, P., Rosenbauer, M., and Gacoin, T., *Influence of surrounding dielectrics on the spontaneous emission of sulforhodamine B molecules.* Physical Review A, 1996. **54**(6): p. 5450.
52. Lamouche, G., Lavallard, P., and Gacoin, T., *Optical properties of dye molecules as a function of the surrounding dielectric medium.* Physical Review A, 1999. **59**(6): p. 4668.
53. Challa, G., *Polymer chemistry: an introduction*. 1993: Prentice Hall.
54. Sperling, L.H., *Introduction to physical polymer science*. 2005: Wiley. com.
55. Cowie, J.M.G. and Arrighi, V., *Polymers: chemistry and physics of modern materials*. 2007: CRC press.
56. Malcolm, P.S., *Polymer chemistry: an introduction.* Oxford University Press, New York, 1999: p. 87-91.
57. Bahadur, P. and Sastry, N., *Principles of polymer science*. 2005: Alpha Science Int'l Ltd.
58. Jagur-Grodzinski, J., *Biomedical application of functional polymers.* Reactive and Functional Polymers, 1999. **39**(2): p. 99-138.
59. Brash, J.L., *Hydrophobic Polymers as Materials for Interfacing with Blood*, in *Assisted Circulation*, F. Unger, Editor. 1979, Springer Berlin Heidelberg. p. 506-519.
60. Ellis, B. and Smith, R., *Polymers: a property database*. 2008: CRC Press.

61. Ooyama, H.E., Hayashi, A., Mamura, T., Ide, T., Hino, T., Tanigami, T., and Yoshida, K., *Photophysical properties and photostability of novel unsymmetric polycyclicphenazine-type D-π-A fluorescent dyes and the dye-doped films.* Journal of Photochemistry and Photobiology A: Chemistry, 2012. **230**(1): p. 38-46.
62. Mark, H.F., Bikales, N., Overberger, C.G., and Menges, G., *Encyclopedia of polymer science and engineering, Vol. 11: Photographic applications to polyesters, elastomeric.* 1987.
63. LaPorte, R.J., *Hydrophilic polymer coatings for medical devices*. 1997: CRC Press.
64. Blecher, L., Lorenz, D., Lowd, H., Wood, A., Wyman, D., and Davidson, R., *Handbook of water-soluble gums and resins.* McGraw-Hill, New York, 1980.
65. Sen, S., Sukul, D., Dutta, P., and Bhattacharyya, K., *Solvation dynamics in aqueous polymer solution and in polymer-surfactant aggregate.* The Journal of Physical Chemistry B, 2002. **106**(15): p. 3763-3769.
66. Finch, C.A., *Polyvinyl alcohol: properties and applications*. 1973: Wiley London.
67. Hassan, C.M. and Peppas, N.A., *Structure and applications of poly (vinyl alcohol) hydrogels produced by conventional crosslinking or by freezing/thawing methods*, in *Biopolymers· PVA Hydrogels, Anionic Polymerisation Nanocomposites*. 2000, Springer. p. 37-65.
68. *Vinyl Alcohol Polymers*, in *Van Nostrand's Scientific Encyclopedia*. 2005, John Wiley & Sons, Inc.
69. Paradossi, G., Cavalieri, F., Chiessi, E., Spagnoli, C., and Cowman, M.K., *Poly (vinyl alcohol) as versatile biomaterial for potential biomedical applications.* Journal of Materials Science: Materials in Medicine, 2003. **14**(8): p. 687-691.
70. Kamoun, E.A., Chen, X., Mohy Eldin, M.S., and Kenawy, E.-R.S., *Crosslinked poly(vinyl alcohol) hydrogels for wound dressing applications: A review of remarkably blended polymers.* Arabian Journal of Chemistry, 2015. **8**(1): p. 1-14.
71. Azarbayjani, A.F., Venugopal J.R., Ramakrishna S., Lim P.F., Chan Y.W., and Chan, S.Y., *Smart Polymeric Nanofibers for Topical Delivery of Levothyroxine.* Journal of Pharmacy and Pharmaceutical Science, 2010. **13**(3): p. 400 - 410.
72. Taepaiboon, P., Rungsardthong U., Supaphol, P., *Drug-loaded electrospun mats of poly(vinyl alcohol) fibres and their release characteristics of four model drugs.* Nanotechnology, 2006. **17**: p. 2317-2329.
73. Peppas, N. and Kim, B., *Stimuli-sensitive protein delivery systems.* Journal of drug delivery science and technology, 2006. **16**(1): p. 11.
74. Marin, E., Rojas, J., and Ciro, Y., *A review of polyvinyl alcohol derivatives: Promising materials for pharmaceutical and biomedical applications.* African Journal of Pharmacy and Pharmacology, 2014. **8**(24): p. 674-684.
75. Fujii, T., Noami, M., Tomita, K., and Furuya, Y., *PVA copolymer: the new coating agent.* Pharmaceutical Technology Europe, 2008. **20**(10).
76. Xu, M., Zhang, C., Luo, Y., Xu, L., Tao, X., Wang, Y., He, H., and Tang, X., *Application and functional characterization of POVACOAT, a hydrophilic co-polymer poly (vinyl alcohol/acrylic acid/methyl methacrylate) as a hot-melt extrusion carrier.* Drug development and industrial pharmacy, 2014. **40**(1): p. 126-135.
77. Matsuguchi, M., Sadaoka, Y., Mizuguchi, H., Umeda, K., and Sakai, Y., *Solvatochromic study of water sorption in polymer films.* Journal of applied polymer science, 1997. **63**(12): p. 1681-1691.
78. Zhang, W.Z., Satoh, M., and Komiyama, J., *A differential scanning calorimetry study of the states of water in swollen poly(vinyl alcohol) membranes containing nonvolatile additives.* Journal of Membrane Science, 1989. **42**(3): p. 303-314.

79. Cha, W.I., Hyon, S.H., and Ikada, Y., *Microstructure of poly(vinyl alcohol) hydrogels investigated with differential scanning calorimetry.* Die Makromolekulare Chemie, 1993. **194**(9): p. 2433-2441.
80. Hodge, R., Edward, G.H., and Simon, G.P., *Water absorption and states of water in semicrystalline poly (vinyl alcohol) films.* Polymer, 1996. **37**(8): p. 1371-1376.
81. Ping, Z.H., Nguyen, Q.T., Chen, S.M., Zhou, J.Q., and Ding, Y.D., *States of water in different hydrophilic polymers — DSC and FTIR studies.* Polymer, 2001. **42**(20): p. 8461-8467.
82. Tamai, Y., Tanaka, H., and Nakanishi, K., *Molecular Dynamics Study of Polymer−Water Interaction in Hydrogels. 2. Hydrogen-Bond Dynamics.* Macromolecules, 1996. **29**(21): p. 6761-6769.
83. Hou, Y. and Higgins, D.A., *Single molecule studies of dynamics in polymer thin films and at surfaces: effect of ambient relative humidity.* The Journal of Physical Chemistry B, 2002. **106**(40): p. 10306-10315.
84. Mishra, H., Misra, V., Mehata, M.S., Pant, T.C., and Tripathi, H.B., *Fluorescence Studies of Salicylic Acid Doped Poly(vinyl alcohol) Film as a Water/Humidity Sensor.* The Journal of Physical Chemistry A, 2004. **108**(12): p. 2346-2352.
85. Shimizu, K., Fujita, H., and Nagamori, E., *Oxygen plasma-treated thermoresponsive polymer surfaces for cell sheet engineering.* Biotechnology and Bioengineering, 2010. **106**(2): p. 303-310.
86. Doorty, K.B., Golubeva, T.A., Gorelov, A.V., Rochev, Y.A., Allen, L.T., Dawson, K.A., Gallagher, W.M., and Keenan, A.K., *Poly(N-isopropylacrylamide) co-polymer films as potential vehicles for delivery of an antimitotic agent to vascular smooth muscle cells.* Cardiovascular Pathology, 2003. **12**(2): p. 105-110.
87. Stile, R.A. and Healy, K.E., *Thermo-Responsive Peptide-Modified Hydrogels for Tissue Regeneration.* Biomacromolecules, 2001. **2**(1): p. 185-194.
88. Hacker, M.C., Klouda, L., Ma, B.B., Kretlow, J.D., and Mikos, A.G., *Synthesis and Characterization of Injectable, Thermally and Chemically Gelable, Amphiphilic Poly(N-isopropylacrylamide)-Based Macromers.* Biomacromolecules, 2008. **9**(6): p. 1558-1570.
89. Feil, H., Bae, Y.H., Feijen, J., and Kim, S.W., *Effect of comonomer hydrophilicity and ionization on the lower critical solution temperature of N-isopropylacrylamide copolymers.* Macromolecules, 1993. **26**(10): p. 2496-2500.
90. Vihola, H., Laukkanen, A., Tenhu, H., and Hirvonen, J., *Drug release characteristics of physically cross-linked thermosensitive poly(N-vinylcaprolactam) hydrogel particles.* Journal of Pharmaceutical Sciences, 2008. **97**(11): p. 4783-4793.
91. Vihola, H., Marttila, A.K., Pakkanen, J.S., Andersson, M., Laukkanen, A., Kaukonen, A.M., Tenhu, H., and Hirvonen, J., *Cell–polymer interactions of fluorescent polystyrene latex particles coated with thermosensitive poly(N-isopropylacrylamide) and poly(N-vinylcaprolactam) or grafted with poly(ethylene oxide)-macromonomer.* International Journal of Pharmaceutics, 2007. **343**(1–2): p. 238-246.
92. Pasparakis, G. and Vamvakaki, M., *Multiresponsive polymers: nano-sized assemblies, stimuli-sensitive gels and smart surfaces.* Polymer Chemistry, 2011. **2**(6): p. 1234-1248.
93. Liu, F. and Urban, M.W., *Recent advances and challenges in designing stimuli-responsive polymers.* Progress in Polymer Science, 2010. **35**(1–2): p. 3-23.
94. Jeong, B. and Gutowska, A., *Lessons from nature: stimuli-responsive polymers and their biomedical applications.* Trends in biotechnology, 2002. **20**(7): p. 305-311.
95. Park, T.G. and Hoffman, A.S., *Synthesis and characterization of pH- and/or temperature-sensitive hydrogels.* Journal of Applied Polymer Science, 1992. **46**(4): p. 659-671.

96. Zhang, X., Wu, D., and Chu, C.C., *Synthesis and characterization of partially biodegradable, temperature and pH sensitive Dex–MA/PNIPAAm hydrogels.* Biomaterials, 2004. **25**(19): p. 4719-4730.
97. Murray, M.J., Snowden, M.J., *The preparation, characterisation and applications of colloidal microgels*. *Advances in Colloid and Interface Science*, 1995. **54**: p. 73-91.
98. Jeong, B.a.A.G., *Trends in Biotechnology* Vol. 20. 2002: Elsevier.
99. Kumar, A., Srivastava, A., Galaev, I.Y., and Mattiasson, B., *Smart polymers: physical forms and bioengineering applications.* Progress in Polymer Science, 2007. **32**(10): p. 1205-1237.
100. Aguilar, M., Elvira, C., Gallardo, A., Vázquez, B., and Román, J., *Smart polymers and their applications as biomaterials.* Topics in tissue engineering, 2007. **3**(6).
101. Schild, H.G. and Tirrell, D.A., *Microcalorimetric detection of lower critical solution temperatures in aqueous polymer solutions.* The Journal of Physical Chemistry, 1990. **94**(10): p. 4352-4356.
102. Schild, H., *Poly (N-isopropylacrylamide): experiment, theory and application.* Progress in polymer science, 1992. **17**(2): p. 163-249.
103. Ottaviani, M.F., Winnik, F.M., Bossmann, S.H., and Turro, N.J., *Phase separation of poly (N-isopropylacrylamide) in mixtures of water and methanol: A spectroscopic study of the phase-transition process with a polymer tagged with a fluorescent dye and a spin label.* Helvetica Chimica Acta, 2001. **84**(9): p. 2476-2492.
104. Ward, M.A. and Georgiou, T.K., *Thermoresponsive polymers for biomedical applications.* Polymers, 2011. **3**(3): p. 1215-1242.
105. Seuring, J. and Agarwal, S., *Polymers with upper critical solution temperature in aqueous solution: unexpected properties from known building blocks.* ACS Macro Letters, 2013. **2**(7): p. 597-600.
106. Chee, C.K., Ghiggino, K.P., Smith, T.A., Rimmer, S., Soutar, I., and Swanson, L., *Time-resolved fluorescence studies of the interactions between the thermoresponsive polymer host, poly(N-isopropylacrylamide), and a hydrophobic guest, pyrene.* Polymer, 2001. **42**(5): p. 2235-2240.
107. Kolaric, B., Sliwa, M., Vallée, R., and Van der Auweraer, M., *Polymer–dye interactions as a tool for studying phase transitions.* Colloids and Surfaces A: Physicochemical and Engineering Aspects, 2009. **338**(1): p. 61-67.
108. Heskins, M. and Guillet, J.E., *Solution properties of poly (N-isopropylacrylamide).* Journal of Macromolecular Science—Chemistry, 1968. **2**(8): p. 1441-1455.
109. Gorelov, A., Du Chesne, A., and Dawson, K., *Phase separation in dilute solutions of poly (N-isopropylacrylamide).* Physica A: Statistical Mechanics and its Applications, 1997. **240**(3): p. 443-452.
110. Winnik, F.M., *Fluorescence studies of aqueous solutions of poly (N-isopropylacrylamide) below and above their LCST.* Macromolecules, 1990. **23**(1): p. 233-242.
111. Ringsdorf, H., Venzmer, J., and Winnik, F., *Fluorescence studies of hydrophobically modified poly (N-isopropylacrylamides).* Macromolecules, 1991. **24**(7): p. 1678-1686.
112. Tamai, Y., Tanaka, H., and Nakanishi, K., *Molecular Dynamics Study of Polymer−Water Interaction in Hydrogels. 1. Hydrogen-Bond Structure.* Macromolecules, 1996. **29**(21): p. 6750-6760.
113. Von Recum, H., Kikuchi, A., Okuhara, M., Sakurai, Y., Okano, T., and Sung Wan, K., *Retinal pigmented epithelium cultures on thermally responsive polymer porous substrates.* Journal of Biomaterials Science, Polymer Edition, 1998. **9**(11): p. 1241-1253.

114. Lee, E.L. and von Recum, H.A., *Cell culture platform with mechanical conditioning and nondamaging cellular detachment.* Journal of Biomedical Materials Research Part A, 2010. **93A**(2): p. 411-418.
115. Chung, J.E., Yokoyama, M., Yamato, M., Aoyagi, T., Sakurai, Y., and Okano, T., *Thermo-responsive drug delivery from polymeric micelles constructed using block copolymers of poly(N-isopropylacrylamide) and poly(butylmethacrylate).* Journal of Controlled Release, 1999. **62**(1–2): p. 115-127.
116. Yan, H. and Tsujii, K., *Potential application of poly(N-isopropylacrylamide) gel containing polymeric micelles to drug delivery systems.* Colloids and Surfaces B: Biointerfaces, 2005. **46**(3): p. 142-146.
117. Tiera, M.J., dos Santos, G.R., de Oliveira Tiera, V.A., Vieira, N.A.B., Frolini, E., da Silva, R.C., and Loh, W., *Aqueous solution behavior of thermosensitive (N-isopropylacrylamide-acrylic acid-ethyl methacrylate) terpolymers.* Colloid and Polymer Science, 2005. **283**(6): p. 662-670.
118. Nykänen, A., Nuopponen, M., Laukkanen, A., Hirvonen, S.P., Rytelä, M., Turunen, O., Tenhu, H., Mezzenga, R., Ikkala, O., and Ruokolainen, J., *Phase Behavior and Temperature-Responsive Molecular Filters Based on Self-Assembly of Polystyrene-block-poly(N-isopropylacrylamide)-block-polystyrene.* Macromolecules, 2007. **40**(16): p. 5827-5834.
119. Fundueanu, G., Constantin, M., and Ascenzi, P., *Poly (N-isopropylacrylamide-co-acrylamide) cross-linked thermoresponsive microspheres obtained from preformed polymers: Influence of the physico-chemical characteristics of drugs on their release profiles.* Acta Biomaterialia, 2009. **5**(1): p. 363-373.
120. Kavanagh, C.A., Rochev, Y.A., Gallagher, W.M., Dawson, K.A., and Keenan, A.K., *Local drug delivery in restenosis injury: thermoresponsive co-polymers as potential drug delivery systems.* Pharmacology & therapeutics, 2004. **102**(1): p. 1-15.
121. Peppas, N., Huang, Y., Torres-Lugo, M., Ward, J., and Zhang, J., *Physicochemical foundations and structural design of hydrogels in medicine and biology.* Annual Review of Biomedical Engineering, 2000. **2**(1): p. 9-29.
122. Gil, E.S. and Hudson, S.M., *Stimuli-reponsive polymers and their bioconjugates.* Progress in Polymer Science, 2004. **29**(12): p. 1173-1222.
123. Lin, C.C. and Metters, A.T., *Hydrogels in controlled release formulations: network design and mathematical modeling.* Advanced drug delivery reviews, 2006. **58**(12): p. 1379-1408.
124. Moran, M.T., Carroll, W.M., Selezneva, I., Gorelov, A., and Rochev, Y., *Cell growth and detachment from protein-coated PNIPAm-based copolymers.* Journal of Biomedical Materials Research Part A, 2007. **81**(4): p. 870-876.
125. Peterson, S.L., McDonald, A., Gourley, P.L., and Sasaki, D.Y., *Poly(dimethylsiloxane) thin films as biocompatible coatings for microfluidic devices: Cell culture and flow studies with glial cells.* Journal of Biomedical Materials Research Part A, 2005. **72A**(1): p. 10-18.
126. Lahann, J.B., Mercedes; Rodon, Teresa; Lee, Jinwook; Choi, Insung S.; Jensen, Klavs F.; Langer, Robert, *Reactive polymer coatings: A platform for patterning proteins and mammalian cells onto a broad range of materials.* Langmuir., 2002. 18: p. 3632–3638.
127. Soper, S.A., Henry, A.C., Vaidya, B., Galloway, M., Wabuyele, M., and McCarley, R.L., *Surface modification of polymer-based microfluidic devices.* Analytica Chimica Acta, 2002. **470**(1): p. 87-99.
128. Prabhakar, B., Roy, S.K., *Bioadhesive Polymeric Platforms for Transmucosal Drug Delivery Systems – a Review.* Tropical Journal of Pharmaceutical Research, 2010. **9**(1): p. 91-104.

129. Song, J. and Vancso, G.J., *Responsive Organometallic Polymer Grafts: Electrochemical Switching of Surface Properties and Current Mediation Behavior.* Langmuir, 2011. **27**(11): p. 6822-6829.
130. Rajeswari Ravichandran, S.S., Venugopal, J.R., Mukherjee, S., and Ramakrishna, A.S., *Applications of conducting polymers and their issues in biomedical engineering.* Journal of the Royal Society Interface, 2010. **7** (5): p. S559-S579.
131. Yoshitake A., Iwabuchi, K., Yuji, F., and Keisuke, M., *Long-term and room temperature operable bioactuator powered by insect dorsal vessel tissue.* Lab on a Chip, 2009. **9** (1): p. 140-44.
132. Suchaneck, G., Guenther, M., Sorber, J., Gerlach, G., Arndt, K.F., Deyneka, A., and Jastrabik, L., *Plasma surface modification of hydrogel thin films.* Surface and Coatings Technology, 2003. **174–175**(0): p. 816-820.
133. Drachman, D.E., *Clinical experience with drug-eluting stents.* Reviews in cardiovascular medicine, 2001. **3**: p. S31-7.
134. Szczupak, B., Ryder, A.G., Togashi, D.M., Klymchenko, A.S., Rochev, Y.A., Gorelov, A., and Glynn, T.J., *Polarity assessment of thermoresponsive poly (NIPAM-co-NtBA) copolymer films using fluorescence methods.* Journal of Fluorescence, 2010. **20**(3): p. 719-731.
135. Koynov, K., Bahtiar, A., Ahn, T., Cordeiro, R.M., Hörhold, H.H., and Bubeck, C., *Molecular weight dependence of chain orientation and optical constants of thin films of the conjugated polymer MEH-PPV.* Macromolecules, 2006. **39**(25): p. 8692-8698.
136. Demir, M.M., Koynov, K., Akbey, Ü., Bubeck, C., Park, I., Lieberwirth, I., and Wegner, G., *Optical properties of composites of PMMA and surface-modified zincite nanoparticles.* Macromolecules, 2007. **40**(4): p. 1089-1100.
137. Reichardt, C., *Solvatochromic dyes as solvent polarity indicators.* Chemical Reviews, 1994. **94**(8): p. 2319-2358.
138. Nigam, S. and Rutan, S., *Principles and applications of solvatochromism.* Applied Spectroscopy, 2001. **55**(11): p. 362A-362A.
139. DeBolt, S.E. and Kollman, P.A., *A theoretical examination of solvatochromism and solute-solvent structuring in simple alkyl carbonyl compounds. Simulations using statistical mechanical free energy perturbation methods.* Journal of the American Chemical Society, 1990. **112**(21): p. 7515-7524.
140. Karelson, M. and Zerner, M.C., *On the n-.pi.* blue shift accompanying solvation.* Journal of the American Chemical Society, 1990. **112**(25): p. 9405-9406.
141. Kosower, E.M., *The Effect of Solvent on Spectra. I. A New Empirical Measure of Solvent Polarity: Z-Values.* Journal of the American Chemical Society, 1958. **80**(13): p. 3253-3260.
142. Kamlet, M.J., Abboud, J.L., and Taft, R.W., *The solvatochromic comparison method. 6. The .pi.* scale of solvent polarities.* Journal of the American Chemical Society, 1977. **99**(18): p. 6027-6038.
143. Buncel, E. and Rajagopal, S., *Solvatochromism and solvent polarity scales.* Accounts of Chemical Research, 1990. **23**(7): p. 226-231.
144. Tunuli, M.S., Rauf, M.A., and Farhataziz, *Dimroth's $E_T(30)$ as parameters of solvent polarity: a caveat.* Journal of Photochemistry, 1984. **24**(4): p. 411-413.
145. Dong, D.C. and Winnik, M.A., *The py scale of solvent polarities. solvent effects on the vibronic fine structure of pyrene fluorescence and empirical correlations with et and y values.* Photochemistry and Photobiology, 1982. **35**(1): p. 17-21.
146. Szczupak, B., Ryder, A.G., Togashi, D.M., Rochev, Y.A., Gorelov, A.V., and Glynn, T.J., *Measuring the micro-Polarity and hydrogen-bond donor/acceptor ability of*

thermoresponsive N-isopropylacrylamide/N-tert-butylacrylamide copolymer films using solvatochromic indicators. Applied Spectroscopy, 2009. **63**(4): p. 442-449.
147. Abboud, J.L. and Notari, R., *Critical compilation of scales of solvent parameters. Part I. Pure, non-hydrogen bond donor solvents.* Pure and Applied Chemistry, 1999. **71**(4): p. 645-718.
148. Bosch, P., Catalina, F., Corrales, T., and Peinado, C., *Fluorescent probes for sensing processes in polymers.* Chemistry-A European Journal, 2005. **11**(15): p. 4314-4325.
149. Demchenko, A.P., *The red-edge effects: 30 years of exploration.* Luminescence, 2002. **17**(1): p. 19-42.
150. Yang, J. S. and Swager, T.M., *Porous shape persistent fluorescent polymer films: an approach to TNT sensory materials.* Journal of the American Chemical Society, 1998. **120**(21): p. 5321-5322.
151. Liu, J., Yan, J., Chen, X., and Fang, Y., *Studies on the conformational behavior of acenaphthylene-labeled poly (acrylamide-co-acryloyl-6-deoxy-6-amino-β-cyclodextrin).* Colloid and Polymer Science, 2007. **285**(8): p. 881-889.
152. Fritzsche, M., Barreiro, C., Hitzmann, B., and Scheper, T., *Optical pH sensing using spectral analysis.* Sensors and Actuators B: Chemical, 2007. **128**(1): p. 133-137.
153. Kalyanasundaram, K. and Thomas, J., *Environmental effects on vibronic band intensities in pyrene monomer fluorescence and their application in studies of micellar systems.* Journal of the American Chemical Society, 1977. **99**(7): p. 2039-2044.
154. Weber, G. and Farris, F.J., *Synthesis and spectral properties of a hydrophobic fluorescent probe: 6-propionyl-2-(dimethylamino) naphthalene.* Biochemistry, 1979. **18**(14): p. 3075-3078.
155. Chong, P.L.G., *Effects of hydrostatic pressure on the location of PRODAN in lipid bilayers and cellular membranes.* Biochemistry, 1988. **27**(1): p. 399-404.
156. Catalan, J., Perez, P., Laynez, J., and Blanco, F.G., *Analysis of the solvent effect on the photophysics properties of 6-propionyl-2-(dimethylamino) naphthalene (PRODAN).* Journal of Fluorescence, 1991. **1**(4): p. 215-223.
157. Hiratsuka, T., *ATP-induced opposite changes in the local environments around Cys697 (SH2) and Cys707 (SH1) of the myosin motor domain revealed by the prodan fluorescence.* Journal of Biological Chemistry, 1999. **274**(41): p. 29156-29163.
158. Karukstis, K.K., Frazier, A.A., Loftus, C.T., and Tuan, A.S., *Fluorescence investigation of multiple partitioning sites in aqueous and reverse micelles.* The Journal of Physical Chemistry B, 1998. **102**(42): p. 8163-8169.
159. Lissi, E., Abuin, E., Rubio, M., and Ceron, A., *Fluorescence of Prodan and Laurdan in AOT/heptane/water microemulsions: partitioning of the probes and characterization of microenvironments.* Langmuir, 2000. **16**(1): p. 178-181.
160. Prendergast, F.G., Meyer, M., Carlson, G.L., Iida, S., and Potter, J.D., *Synthesis, spectral properties, and use of 6-acryloyl-2-dimethylaminonaphthalene (Acrylodan). A thiol-selective, polarity-sensitive fluorescent probe.* Journal of Biological Chemistry, 1983. **258**(12): p. 7541-7544.
161. Samanta, A. and Fessenden, R., *Excited state dipole moment of PRODAN as determined from transient dielectric loss measurements.* The Journal of Physical Chemistry A, 2000. **104**(39): p. 8972-8975.
162. Haugland, R.P., *Handbook of fluorescent probes and research products*. 2002: Molecular Probes.
163. Wagner, B.D., *The use of coumarins as environmentally-sensitive fluorescent probes of heterogeneous inclusion systems.* Molecules, 2009. **14**(1): p. 210-237.

164. Nad, S., Kumbhakar, M., and Pal, H., *Photophysical Properties of Coumarin-152 and Coumarin-481 Dyes: Unusual Behavior in Nonpolar and in Higher Polarity Solvents.* The Journal of Physical Chemistry A, 2003. **107**(24): p. 4808-4816.
165. Jones, G., Jackson, W.R., Kanoktanaporn, S., and Halpern, A.M., *Solvent effects on photophysical parameters for coumarin laser dyes.* Optics Communications, 1980. **33**(3): p. 315-320.
166. Jones, G., Jackson, W.R., Choi, C.Y., and Bergmark, W.R., *Solvent effects on emission yield and lifetime for coumarin laser dyes. Requirements for a rotatory decay mechanism.* The Journal of Physical Chemistry, 1985. **89**(2): p. 294-300.
167. Abdel-Mottaleb, M., Loutfy, R.O., and Lapouyade, R., *Non-radiative deactivation channels of molecular rotors.* Journal of Photochemistry and Photobiology A: Chemistry, 1989. **48**(1): p. 87-93.
168. Haidekker, M.A. and Theodorakis, E.A., *Molecular rotors—fluorescent biosensors for viscosity and flow.* Organic & Biomolecular Chemistry, 2007. **5**(11): p. 1669-1678.
169. Lee, C.H., Miyaji, H., Yoon, D. W., and Sessler, J.L., *Strapped and other topographically nonplanar calixpyrrole analogues. Improved anion receptors.* Chemical Communications, 2008(1): p. 24-34.
170. Vincetini, L.M. and Villereal, M.L., *Inositol phosphates turnover, cytosolic Ca^{++} and pH: putative signals for the control of cell growth.* Life sciences, 1986. **38**(25): p. 2269-2276.
171. Kubohara, Y. and Okamoto, K., *Cytoplasmic Ca^{2+} and H^{+} concentrations determine cell fate in Dictyostelium discoideum.* The FASEB journal, 1994. **8**(11): p. 869-874.
172. Ronnie, M., Kjell, C., and Anders, L., *Characterization of probe binding and comparison of its influence on fluorescence lifetime of two pH-sensitive benzo.* xanthene dyes using intensity-modulated multiple-wavelength scanning technique, 2000. **283**(1): p. 104-110.
173. Niu, C.G., Gui, X.Q., Zeng, G.M., and Yuan, X.Z., *A ratiometric fluorescence sensor with broad dynamic range based on two pH-sensitive fluorophores.* Analyst, 2005. **130**(11): p. 1551-1556.
174. Ellison, C.J., Miller, K.E., and Torkelson, J.M., *In situ monitoring of sorption and drying of polymer films and coatings: self-referencing, nearly temperature-independent fluorescence sensors.* Polymer, 2004. **45**(8): p. 2623-2632.
175. Goodelle, J.P., Pearson, R.A., and Santore, M.M., *Water-uptake kinetics in poly(methyl methacrylate) films with a fluorescent rotor probe.* Journal of Applied Polymer Science, 2002. **86**(10): p. 2463-2471.
176. Olmos, D., López-Morón, R., and González-Benito, J., *The nature of the glass fibre surface and its effect in the water absorption of glass fibre/epoxy composites. The use of fluorescence to obtain information at the interface.* Composites Science and Technology, 2006. **66**(15): p. 2758-2768.
177. Demchenko, A.P., Klymchenko, A.S., Pivovarenko, V.G., and Ercelen, S., *Ratiometric Probes: Design and Applications*, in *Fluorescence Spectroscopy, Imaging and Probes*, R. Kraayenhof, A.W.G. Visser, and H. Gerritsen, Editors. 2002, Springer Berlin Heidelberg. p. 101-110.
178. Lakowicz, J.R., *Emerging biomedical application of time-resolved florescence spectroscopy.* Topics in Fluorescence spectroscopy, 1994. **4**: p. 1-19.
179. Demchenko, A.P., *Optimization of fluorescence response in the design of molecular biosensors.* Analytical biochemistry, 2005. **343**(1): p. 1-22.
180. Létard, J.F., Delmond, S., Lapouyade, R., Braun, D., Rettig, W., and Kreissler, M., *New intrinsic fluoroionophores with dual fluorescence: DMABN-Crown4 and DMABN-Crown5.* Recueil des Travaux Chimiques des Pays-Bas, 1995. **114**(11-12): p. 517-527.

181. Shynkar, V.V., Klymchenko, A.S., Duportail, G., Demchenko, A.P., and Mély, Y., *Two-color fluorescent probes for imaging the dipole potential of cell plasma membranes.* Biochimica et Biophysica Acta (BBA)-Biomembranes, 2005. **1712**(2): p. 128-136.
182. Turkmen, Z., Klymchenko, A.S., Oncul, S., Duportail, G., Topcu, G., and Demchenko, A.P., *A triterpene oleanolic acid conjugate with 3-hydroxyflavone derivative as a new membrane probe with two-color ratiometric response.* Journal of biochemical and biophysical methods, 2005. **64**(1): p. 1-18.
183. Demchenko, A.P., Klymchenko, A.S., Pivovarenko, V.G., Ercelen, S., Duportail, G., and Mely, Y., *Multiparametric color-changing fluorescence probes.* Journal of Fluorescence, 2003. **13**(4): p. 291-295.
184. Klymchenko, A.S. and Demchenko, A.P., *Multiparametric probing of intermolecular interactions with fluorescent dye exhibiting excited state intramolecular proton transfer.* Physical Chemistry Chemical Physics, 2003. **5**(3): p. 461-468.
185. Klymchenko, A.S. and Demchenko, A.P., *3-Hydroxychromone dyes exhibiting excited-state intramolecular proton transfer in water with efficient two-band fluorescence.* New journal of chemistry, 2004. **28**(6): p. 687-692.
186. Klymchenko, A.S., Mély, Y., Demchenko, A.P., and Duportail, G., *Simultaneous probing of hydration and polarity of lipid bilayers with 3-hydroxyflavone fluorescent dyes.* Biochimica et Biophysica Acta (BBA)-Biomembranes, 2004. **1665**(1): p. 6-19.
187. Barbara, P.F., Walsh, P.K., and Brus, L.E., *Picosecond kinetic and vibrationally resolved spectroscopic studies of intramolecular excited-state hydrogen atom transfer.* The Journal of Physical Chemistry, 1989. **93**(1): p. 29-34.
188. Douhal, A., Lahmani, F., and Zewail, A.H., *Proton-transfer reaction dynamics.* Chemical physics, 1996. **207**(2): p. 477-498.
189. Formosinho, S.J. and Arnaut, L.G., *Excited-state proton transfer reactions II. Intramolecular reactions.* Journal of Photochemistry and Photobiology A: Chemistry, 1993. **75**(1): p. 21-48.
190. LeGourriérec, D., Kharlanov, V.A., Brown, R.G., and Rettig, W., *Excited-state intramolecular proton transfer (ESIPT) in 2-(2'-hydroxyphenyl)-oxazole and-thiazole.* Journal of Photochemistry and Photobiology A: Chemistry, 2000. **130**(2): p. 101-111.
191. Santra, S., Krishnamoorthy, G., and Dogra, S.K., *Excited state intramolecular proton transfer in 2-(2'-benzamidophenyl) benzimidazole: effect of solvents.* Chemical physics letters, 1999. **311**(1): p. 55-61.
192. Shynkar, V.V., Klymchenko, A.S., Mély, Y., Duportail, G., and Pivovarenko, V.G., *Anion formation of 4'-(dimethylamino)-3-hydroxyflavone in phosphatidylglycerol vesicles induced by HEPES buffer: A steady-state and time-resolved fluorescence investigation.* The Journal of Physical Chemistry B, 2004. **108**(48): p. 18750-18755.
193. Smoluch, M., Joshi, H., Gerssen, A., Gooijer, C., and van der Zwan, G., *Fast excited-state intramolecular proton transfer and subnanosecond dynamic stokes shift of time-resolved fluorescence spectra of the 5-methoxysalicylic acid/diethyl ether complex.* The Journal of Physical Chemistry A, 2005. **109**(4): p. 535-541.
194. Ameer-Beg, S., Ormson, S.M., Brown, R.G., Matousek, P., Towrie, M., Nibbering, E.T., Foggi, P., and Neuwahl, F.V., *Ultrafast measurements of excited state intramolecular proton transfer (ESIPT) in room temperature solutions of 3-hydroxyflavone and derivatives.* The Journal of Physical Chemistry A, 2001. **105**(15): p. 3709-3718.
195. Bader, A.N., Ariese, F., and Gooijer, C., *Proton transfer in 3-hydroxyflavone studied by high-resolution 10 K laser-excited Shpol'skii spectroscopy.* The Journal of Physical Chemistry A, 2002. **106**(12): p. 2844-2849.
196. Bader, A.N., Pivovarenko, V.G., Demchenko, A.P., Ariese, F., and Gooijer, C., *Excited state and ground state proton transfer rates of 3-hydroxyflavone and its derivatives*

studied by shpol'skii spectroscopy: The influence of redistribution of electron density. The Journal of Physical Chemistry B, 2004. **108**(29): p. 10589-10595.
197. Brewer, W.E., Studer, S.L., Standiford, M., and Chou, P.T., *Dynamics of the triplet state and the reverse proton transfer of 3-hydroxyflavone.* The Journal of Physical Chemistry, 1989. **93**(16): p. 6088-6094.
198. Brucker, G. and Kelley, D., *Proton transfer in matrix-isolated 3-hydroxyflavone and 3-hydroxyflavone complexes.* Journal of Physical Chemistry, 1987. **91**(11): p. 2856-2861.
199. Brucker, G., Kelley, D., and Swinney, T., *Proton-transfer and solvent polarization dynamics in 3-hydroxyflavone.* The Journal of Physical Chemistry, 1991. **95**(8): p. 3190-3195.
200. Carturan, S., Quaranta, A., Maggioni, G., Bonafini, M., and Della Mea, G., *3-Hydroxyflavone-based wavelength shifting systems for near UV optical sensors.* Sensors and Actuators A: Physical, 2004. **113**(3): p. 288-292.
201. Cornard, J., Vrielynck, L., Merlin, J., and Wallet, J., *Structural and vibrational study of 3-hydroxyflavone and 3-methoxyflavone.* Spectrochimica Acta Part A: Molecular and Biomolecular Spectroscopy, 1995. **51**(5): p. 913-923.
202. Dharia, J.R., Johnson, K.F., and Schlenoff, J.B., *Synthesis and characterization of wavelength-shifting monomers and polymers based on 3-hydroxyflavone.* Macromolecules, 1994. **27**(18): p. 5167-5172.
203. Dick, B. and Ernsting, N.P., *Excited-state intramolecular proton transfer in 3-hydroxylflavone isolated in solid argon: fluoroescence and fluorescence-excitation spectra and tautomer fluorescence rise time.* Journal of Physical Chemistry, 1987. **91**(16): p. 4261-4265.
204. Guharay, J., Chaudhuri, R., Chakrabarti, A., and Sengupta, P.K., *Excited state proton transfer fluorescence of 3-hydroxyflavone in model membranes.* Spectrochimica Acta Part A: Molecular and Biomolecular Spectroscopy, 1997. **53**(3): p. 457-462.
205. Itoh, M., Tokumura, K., Tanimoto, Y., Okada, Y., Takeuchi, H., Obi, K., and Tanaka, I., *Time-resolved and steady-state fluorescence studies of the excited-state proton transfer in 3-hydroxyflavone and 3-hydroxychromone.* Journal of the American Chemical Society, 1982. **104**(15): p. 4146-4150.
206. Mandal, P.K. and Samanta, A., *Evidence of ground-state proton-transfer reaction of 3-hydroxyflavone in neutral alcoholic solvents.* The Journal of Physical Chemistry A, 2003. **107**(32): p. 6334-6339.
207. Martinez, M.L., Studer, S.L., and Chou, P.T., *Direct evidence of the triplet-state origin of the slow reverse proton transfer reaction of 3-hydroxyflavone.* Journal of the American Chemical Society, 1990. **112**(6): p. 2427-2429.
208. McMorrow, D. and Kasha, M., *Proton-transfer spectroscopy of 3-hydroxychromones. Extreme sensitivity to hydrogen-bonding perturbations.* Journal of the American Chemical Society, 1983. **105**(15): p. 5133-5134.
209. McMorrow, D. and Kasha, M., *Intramolecular excited-state proton transfer in 3-hydroxyflavone. Hydrogen-bonding solvent perturbations.* The Journal of Physical Chemistry, 1984. **88**(11): p. 2235-2243.
210. Oncul, S. and Demchenko, A.P., *The effects of thermal quenching on the excited-state intramolecular proton transfer reaction in 3-hydroxyflavones.* Spectrochimica Acta Part A: Molecular and Biomolecular Spectroscopy, 2006. **65**(1): p. 179-183.
211. Premvardhan, L.L. and Peteanu, L.A., *Dipolar properties of and temperature effects on the electronic states of 3-hydroxyflavone (3HF) determined using Stark-effect spectroscopy and compared to electronic structure calculations.* The Journal of Physical Chemistry A, 1999. **103**(37): p. 7506-7514.

212. Quaranta, A., Carturan, S., Maggioni, G., Ceccato, R., and Della Mea, G., *Probing the chemical environment of 3-hydroxyflavone doped ormosils by a spectroscopic study of excited state intramolecular proton transfer.* Journal of non-crystalline solids, 2003. **322**(1): p. 1-6.
213. Sarkar, M., Guha Ray, J., and Sengupta, P.K., *Effect of reverse micelles on the intramolecular excited state proton transfer (ESPT) and dual luminescence behaviour of 3-hydroxyflavone.* Spectrochimica Acta Part A: Molecular and Biomolecular Spectroscopy, 1996. **52**(2): p. 275-278.
214. Sarkar, M. and Sengupta, P.K., *Influence of different micellar environments on the excited-state proton-transfer luminescence of 3-hydroxyflavone.* Chemical physics letters, 1991. **179**(1): p. 68-72.
215. Schwartz, B.J., Peteanu, L.A., and Harris, C.B., *Direct observation of fast proton transfer: femtosecond photophysics of 3-hydroxyflavone.* The Journal of Physical Chemistry, 1992. **96**(9): p. 3591-3598.
216. Sengupta, P.K. and Kasha, M., *Excited state proton-transfer spectroscopy of 3-hytdroxyflavone and quercetin.* Chemical physics letters, 1979. **68**(2): p. 382-385.
217. Strandjord, A. and Barbara, P.F., *Hydrogen/deuterium isotope effects on the excited-state proton transfer kinetics of 3-hydroxyflavone.* Chemical physics letters, 1983. **98**(1): p. 21-26.
218. Strandjord, A.J. and Barbara, P. F., *The proton-transfer kinetics of 3-hydroxyflavone: solvent effects.* The Journal of Physical Chemistry, 1985. **89**(11): p. 2355-2361.
219. Strandjord, A.J., Smith, D.E., and Barbara, P.F., *Structural effects on the proton-transfer kinetics of 3-hydroxyflavones.* The Journal of Physical Chemistry, 1985. **89**(11): p. 2362-2366.
220. Studer, S.L., Brewer, W.E., Martinez, M.L., and Chou, P.T., *Time-resolved study of the photooxygenation of 3-hydroxyflavone.* Journal of the American Chemical Society, 1989. **111**(19): p. 7643-7644.
221. Swinney, T. and Kelley, D., *Proton-transfer and solvent polarization dynamics in 3-hydroxyflavone. 2. Mixed solvents.* The Journal of Physical Chemistry, 1991. **95**(25): p. 10369-10373.
222. Tokumura, K., Kurauchi, M., Yagata, N., and Itoh, M., *Phototautomerization of 3-hydroxyflavone in the lowest triplet state.* Chemical physics letters, 1996. **258**(3): p. 495-500.
223. Tommasini, S., Calabro, M., Donato, P., Raneri, D., Guglielmo, G., Ficarra, P., and Ficarra, R., *Comparative photodegradation studies on 3-hydroxyflavone: influence of different media, pH and light sources.* Journal of pharmaceutical and biomedical analysis, 2004. **35**(2): p. 389-397.
224. Woolfe, G. and Thistlethwaite, P., *Direct observation of excited state intramolecular proton transfer kinetics in 3-hydroxyflavone.* Journal of the American Chemical Society, 1981. **103**(23): p. 6916-6923.
225. Zhu, A., Wang, B., White, J., and Drickamer, H., *Effect of pressure on the excited-state proton transfer of 3-hydroxyflavone.* The Journal of Physical Chemistry B, 2003. **107**(37): p. 9973-9976.
226. Klymchenko, A.S., Pivovarenko, V.G., Ozturk, T., and Demchenko, A.P., *Modulation of the solvent-dependent dual emission in 3-hydroxychromones by substituents.* New journal of chemistry, 2003. **27**(9): p. 1336-1343.
227. Klymchenko, A.S., Duportail, G., Demchenko, A.P., and Mély, Y., *Bimodal distribution and fluorescence response of environment-sensitive probes in lipid bilayers.* Biophysical journal, 2004. **86**(5): p. 2929-2941.

228. Ercelen, S., Klymchenko, A.S., and Demchenko, A.P., *Ultrasensitive fluorescent probe for the hydrophobic range of solvent polarities.* Analytica Chimica Acta, 2002. **464**(2): p. 273-287.
229. Klymchenko, A.S., Pivovarenko, V.G., and Demchenko, A.P., *Elimination of the hydrogen bonding effect on the solvatochromism of 3-hydroxyflavones.* The Journal of Physical Chemistry A, 2003. **107**(21): p. 4211-4216.
230. Ha, T. and Tinnefeld, P., *Photophysics of fluorescent probes for single-molecule biophysics and super-resolution imaging.* Annual Review of Physical Chemistry, 2012. **63**: p. 595-617.
231. Chou, P.T., Pu, S.C., Cheng, Y.M., Yu, W.S., Yu, Y.C., Hung, F.T., and Hu, W.P., *Femtosecond dynamics on excited-state proton/charge-transfer reaction in 4'-N, N-diethylamino-3-hydroxyflavone. The role of dipolar vectors in constructing a rational mechanism.* The Journal of Physical Chemistry A, 2005. **109**(17): p. 3777-3787.
232. Swinney, T. and Kelley, D., *Proton transfer dynamics in substituted 3-hydroxyflavones: Solvent polarization effects.* The Journal of chemical physics, 1993. **99**: p. 211.
233. Nemkovich, N., Baumann, W., and Pivovarenko, V., *Dipole moments of 4'-aminoflavonols determined using electro-optical absorption measurements or molecular Stark-effect spectroscopy.* Journal of Photochemistry and Photobiology A: Chemistry, 2002. **153**(1): p. 19-24.
234. Chou, P.T., Martinez, M.L., and Clements, J.H., *Reversal of excitation behavior of proton-transfer vs. charge-transfer by dielectric perturbation of electronic manifolds.* The Journal of Physical Chemistry, 1993. **97**(11): p. 2618-2622.
235. Cheng, Y.M., Pu, S.C., Yu, Y.C., Chou, P.T., Huang, C.H., Chen, C.T., Li, T.H., and Hu, W.P., *Spectroscopy and femtosecond dynamics of 7-N, N-diethylamino-3-hydroxyflavone. The correlation of dipole moments among various states to rationalize the excited-state proton transfer reaction.* The Journal of Physical Chemistry A, 2005. **109**(51): p. 11696-11706.
236. Chou, P.T., Martinez, M.L., and Clements, J.H., *The observation of solvent-dependent proton-transfer/charge-transfer lasers from 4'-diethylamino-3-hydroxyflavone.* Chemical physics letters, 1993. **204**(5): p. 395-399.
237. Ormson, S.M., Brown, R.G., Vollmer, F., and Rettig, W., *Switching between charge- and proton-transfer emission in the excited state of a substituted 3-hydroxyflavone.* Journal of Photochemistry and Photobiology A: Chemistry, 1994. **81**(2): p. 65-72.
238. Zhang, W., Shi, B., and Shi, J., *Time-dependent density functional investigation on electronic spectra of 4'-N-dimethylamino-3-hydroxyflavone.* Journal of Molecular Structure: THEOCHEM, 2005. **731**(1): p. 219-224.
239. Yushchenko, D.A., Bilokin, M.D., Pyvovarenko, O.V., Duportail, G., Mély, Y., and Pivovarenko, V.G., *Synthesis and fluorescence properties of 2-aryl-3-hydroxyquinolones, a new class of dyes displaying dual fluorescence.* Tetrahedron letters, 2006. **47**(6): p. 905-908.
240. Ragnarsson, G. and Johansson, M.O., *Coated drug cores in multiple unit preparations influence of particle size.* Drug Development and Industrial Pharmacy, 1988. **14**(15-17): p. 2285-2297.
241. Mart, D. St., *Design, synthesis and fluorescent characterisation of 2,5-dihydro-1,2,3-triazines.*, in *Chemistry*. 2013, National University of Ireland Maynooth, Maynooth, Co. Kildare, Ireland. p. 366.
242. Kang, W., Kitamura, M., Kamura, M., Aomori, S., and Arakawa, Y., *Solvent Dependence of Vacuum-Dried C60 Thin-Film Transistors.* Japanese Journal of Applied Physics, 2012. **51**(2S): p. 02BK10.

243. Song, S., Jin, Y., Park, S.H., Kim, S.H., Kim, I., Lee, K., and Suh, H., *Syntheses and characterization of the alternating polymers based on cyclopenta [def] phenanthrene backbone with spiro group.* Polymer journal, 2009. **41**(12): p. 1105-1110.
244. Campoy-Quiles, M., Nelson, J., Etchegoin, P.G., Bradley, D.D.C., Zhokhavets, V., Gobsch, G., Vaughan, H., Monkman, A., Ingänas, O., Persson, N.K., Arwin, H., Garriga, M., Alonso, M.I., Herrmann, G., Becker, M., Scholdei, W., Jahja, M., and Bubeck, C., *On the determination of anisotropy in polymer thin films: A comparative study of optical techniques.* physica status solidi (c), 2008. **5**(5): p. 1270-1273.
245. Sultanova, N., Kasarova, S., and Nikolov, I., *Dispersion Proper ties of Optical Polymers.* Acta Physica Polonica-Series A General Physics, 2009. **19**(4): p. 585.
246. Magde, D., Rojas, G.E., and Seybold, P.G., *Solvent dependence of the fluorescence lifetimes of xanthene dyes.* Photochemistry and Photobiology, 1999. **70**: p. 737-744.
247. Mohanty, J. and Nau, W.M., *Refractive index effects on the oscillator strength and radiative decay rate of 2, 3-diazabicyclo [2.2. 2] oct-2-ene.* Photochemical & Photobiological Sciences, 2004. **3**(11-12): p. 1026-1031.
248. Borst, J.W., Hink, M.A., van Hoek, A., and Visser, A.J., *Effects of refractive index and viscosity on fluorescence and anisotropy decays of enhanced cyan and yellow fluorescent proteins.* Journal of fluorescence, 2005. **15**(2): p. 153-160.
249. Iwai, K., Matsumura, Y., Uchiyama, S., and de Silva, A.P., *Development of fluorescent microgel thermometers based on thermo-responsive polymers and their modulation of sensitivity range.* Journal of Materials Chemistry, 2005. **15**(27-28): p. 2796-2800.
250. Uchiyama, S., Matsumura, Y., de Silva, A.P., and Iwai, K., *Fluorescent Molecular Thermometers Based on Polymers Showing Temperature-Induced Phase Transitions and Labeled with Polarity-Responsive Benzofurazans.* Analytical Chemistry, 2003. **75**(21): p. 5926-5935.
251. Philipp, M., Aleksandrova, R., Muller, U., Ostermeyer, M., Sanctuary, R., Muller-Buschbaum, P., and Kruger, J.K., *Molecular versus macroscopic perspective on the demixing transition of aqueous PNIPAM solutions by studying the dual character of the refractive index.* Soft Matter, 2014. **10**(37): p. 7297-7305.
252. Thijs, H.M.L., Becer, C.R., Guerrero-Sanchez, C., Fournier, D., Hoogenboom, R., and Schubert, U.S., *Water uptake of hydrophilic polymers determined by a thermal gravimetric analyzer with a controlled humidity chamber.* Journal of Materials Chemistry, 2007. **17**(46): p. 4864-4871.
253. Iwai, K., Hanasaki, K., and Yamamoto, M., *Fluorescence label studies of thermo-responsive poly(N-isopropylacrylamide) hydrogels.* Journal of Luminescence, 2000. **87–89**: p. 1289-1291.
254. Willets, K.A., Ostroverkhova, O., He, M., Twieg, R.J., and Moerner, W., *Novel fluorophores for single-molecule imaging.* Journal of the American Chemical Society, 2003. **125**(5): p. 1174-1175.
255. Ahmed, Z., Gooding, E.A., Pimenov, K.V., Wang, L., and Asher, S.A., *UV resonance Raman determination of molecular mechanism of poly (N-isopropylacrylamide) volume phase transition.* The Journal of Physical Chemistry B, 2009. **113**(13): p. 4248-4256.
256. Pritchard, J.G., *Poly (vinyl alcohol): basic properties and uses*. 1970: Gordon and Breach London.
257. Patra, D. and Mishra, A., *Fluorescence quenching of benzo [k] fluoranthene in poly (vinyl alcohol) film: a possible optical sensor for nitro aromatic compounds.* Sensors and Actuators B: Chemical, 2001. **80**(3): p. 278-282.
258. Egginger, M., Irimia-Vladu, M., Schwödiauer, R., Tanda, A., Bauer, S., and Sariciftci, S.N., *Ionic Impurities in Poly(vinyl alcohol) Gate Dielectrics and Hysteresis Effects in*

Organic Field Effect Transistors. MRS Online Proceedings Library Archive, 2008. **1091**: p. 1091-AA11-46 (6 pages).
259. De Vente, J., Bruyn, P.J.M., and Zaagsma, J., *Fluorescence spectroscopic analysis of the hydrogen bonding properties of catecholamines, resorcinolamines, and related compounds with phosphate and other anionic species in aqueous solution.* Journal of Pharmacy and Pharmacology, 1981. **33**(5): p. 290-296.
260. Willis, K.J. and Szabo, A.G., *Fluorescence decay kinetics of tyrosinate and tyrosine hydrogen-bonded complexes.* The Journal of Physical Chemistry, 1991. **95**(4): p. 1585-1589.
261. Szabo, A.G., Lynn, K.R., Krajcarski, D.T., and Rayner, D.M., *Tyrosinate fluorescence maxima at 345 nm in proteins lacking tryptophan at pH 7.* FEBS Letters, 1978. **94**(2): p. 249-252.
262. McGill, R.A., Paley, M.S., and Harris, J.M., *Solvatochromic characterization of polymers. Effects of relative humidity.* Macromolecules, 1992. **25**(12): p. 3015-3019.
263. Yang, M.R. and Chen, K.S., *Humidity sensors using polyvinyl alcohol mixed with electrolytes.* Sensors and Actuators B: Chemical, 1998. **49**(3): p. 240-247.
264. Chen, W.L., Shull, K.R., Papatheodorou, T., Styrkas, D.A., and Keddie, J.L., *Equilibrium Swelling of Hydrophilic Polyacrylates in Humid Environments.* Macromolecules, 1998. **32**(1): p. 136-144.
265. Ebrahimzadeh, P. and Kubat, J., *Mechanosorptive effects in cellophane, polyamide 6 and some other polymers studied by dynamic mechanical analysis.* Journal of materials science, 1997. **32**(16): p. 4227-4235.
266. Becker, W., *Advanced time-correlated single photon counting techniques (Series in chemical physics, Vol. 81)*. 2005: Springer-Verlag.